MODEL ATMOSPHERE STUDIES OF EARLY TYPE STARS

Thesis by

Dimitri Manuel Mihalas

In Partial Fulfillment of the Requirements

For the Degree of

Doctor of Philosophy

California Institute of Technology

Pasadena, California

1964

ACKNOWLEDGEMENTS

With great pleasure I thank Dr. J. B. Oke for originally suggesting the helium abundance problem as a thesis project; for offering me continuous encouragement; for persistently indicating the necessity of connecting theory with observation, and to this end, for teaching me the use of the coudé scanner. I wish also to thank Dr. J. L. Greenstein for allowing me to use the great amount of computer time required to develop programs and to obtain the results given here as well as for numerous helpful discussions and suggestions. Thanks are also due to Dr. G. Münch for suggestions and for reading the first draft of my thesis. Many very helpful discussions and useful comparisons of independent results were offered by Mr. R. H. Norton. Suggestions regarding various phases of the completed and planned work have been offered by Drs. L. Searle and B. Baschek. Finally, thanks is due to the continued assistance and special privileges offered by the staff of the computing center, and to Mr. Gene Hancock and Mr. Al Olmstead for their patience as night assistants to an inexperienced and sometimes naive observer.

This work was started during tenure of an N. S. F. Pre-doctoral Fellowship, continued during tenure of the Van Maanen Fellowship administered by the California Institute of Technology, and completed during tenure of an N. S. F. Summer Fellowship. For this support I am most grateful.

Finally, I wish to dedicate this thesis to my parents in thanks for their years of work and care on my behalf, and out of my respect

for a man great both as a man and an astrophysicist, to the memory of Otto Struve, who, among other things, pioneered the study of the Stark broadening of hydrogen and helium lines in stellar spectra.

ABSTRACT

Model atmospheres have been constructed over a wide range of temperature and gravities. The condition of radiative equilibrium is enforced using a variation of the temperature correction scheme devised by M. Krook, thus extending the work of Gingerich to the realm of higher temperatures; flux constancy is attained to within ±1% to a depth of $\tau_{STD} = 10$ or more, the standard wavelength being either λ4000 or λ5050. The source function is determined from the Milne-Eddington equation allowing for coherent scattering in the continuum. The properties of the atmospheres are described and given in detailed tabular form, and data of rather general use is presented.

For each model we have computed Hβ and Hγ profiles and equivalent widths, and for the hotter models, profiles and equivalent widths of λ4686, λ4200, λ4542, λ5412 of He II and λ5876, λ4713, λ4438, and λ4121 of He I. Interpolating formulae are devised to describe the temperature and gravity variations of the line strengths.

A fit is carried out between theory and observations made with the 100" coude scanner of six O-type stars, yielding the effective temperature, gravity, and an estimate of the helium abundance for these stars. It is found that the computed hydrogen and ionized helium lines appear consistent with observation whereas the computed neutral helium lines seem to be incorrect for these spectral types.

The results indicate that a typical O9 star has the following properties: $\theta_e = 0.146$, $\log g = 4.2$, $N(He)/N(H) \sim 0.15$ or 0.2, and from an assumed mass-luminosity law we find: $R/R_\odot = 10$, $\mathcal{M}/\mathcal{M}_\odot = 60$,

and $L/L_{\odot} = 1.4 \times 10^5$. The helium abundance derived here is in substantial agreement with that found by the Kiel group but in disagreement with nebular studies. The masses and radii are probably quite doubtful because of the possible incorrectness of the assumed mass-luminosity law.

ADDENDUM

Since completion of this thesis we have found a regrettable error in the input routine which causes the fluxes to be computed incorrectly by a few percent. Not all of the models are affected, nor have we determined yet the magnitude of the error. The numerical results will be corrected at the first possible opportunity; the methodology is sound.

TABLE OF CONTENTS

Chapter I

INTRODUCTION

Our knowledge of the helium abundance in early type stars follows from the spectroscopic analysis of their atmospheres. In the late to middle B stars we observe the lines of neutral helium, while in the early B and O type stars we observe both neutral and ionized helium lines. As astrophysical theory has become more sophisticated, more and more detailed techniques have been applied to the analysis of these spectra, so that today we attempt to construct detailed models of the atmospheric structure of these objects and predict line profiles which may be compared with observation. The procedure has been demonstrated well by the studies of Traving (1955, 1956), Miss Underhill (1948, 1951a, b, 1956, 1957, 1961), and Jugaku (1959). These studies suffered most from inadequate line broadening theories for the hydrogen and helium lines; furthermore, no quickly convergent systematic method of enforcing the condition of flux constancy throughout the model had yet been devised, and the enormous amount of labor involved in constructing a model precluded making a large number of them. Also, the observational data available was often less accurate than one would wish.

Recently the situation has improved in practically every respect. In the first place, the development of very high speed electronic computers allows the construction of a large number of quite accurate models with an amount of work that is not prohibitive. These computers also allow more accurate numerical treatment of the line profile

problem; indeed potentially much more accurate than given here. Secondly, the line broadening theories have been markedly improved so that while the older theory could give results wrong by a factor of two, there are several indications that the newer theory is reliable to about 10%. Thirdly, the problem of insuring flux constancy throughout the model may now be considered solved as the result of the fundamental improvement made by Krook (1963) over all previous techniques. This method has afforded us an objective way of correcting the temperature distribution of a model to obtain constant flux in a fairly small number of iterations. Finally, but by no means least important, the recent development of the coudé photoelectric spectrum scanner by Dr. J. B. Oke offered promise of allowing observations to be gathered without the necessity of the tedious calibration process which represents one of the fundamental limitations to the accuracy of photographic spectroscopy. The photographic process still has some advantages over the scanner, but if we are content to study a few spectral features in detail rather than surveying the entire spectrum, the scanner is superior.

Thus in every sense the time seemed opportune to restudy the helium abundance problem and to attempt to redetermine the atmospheric properties of the early spectral types. To this end we observed the O stars (to have access to both ionized and neutral helium lines), and developed a set of computer programs to construct constant-flux models, using a slight modification of Krook's procedure; curves of growth; and the hydrogen and helium line profiles. We have of course not solved the problem, but progress has been made. The models

necessarily remain uncertain insofar as the largest portion of the flux emerges in the presently unobservable ultraviolet. We found that because we neglected the effects of the hydrogen line blanketing the boundary temperatures of our models are too high, and as a consequence, we cannot correctly predict neutral helium line intensities. We can, however, obtain T_e, log g, and an estimate of the helium abundance from the hydrogen lines and ionized helium lines, which we appear to predict correctly.

We still need more observations and more models in the important high-temperature regions. We were unable to obtain models forming a tight enough grid at high temperatures because we were forced to inch our way up the temperature scale step by step; to fill in the grid more tightly will be easier and can be done more quickly. It is to be hoped that further observations will be obtained with slower scan rates, paying closer attention to fewer spectral regions. And eventually, we may hope that the models will be revised to allow for blanketing by hydrogen lines with the consequent revision of the boundary temperatures.

The form of this thesis is somewhat of a hybrid. It can scarcely be considered of a theoretical nature in the usual sense, since the number of new formal developments given here is small, and yet to call it an observational thesis would be an affront to many an observer. It is instead a computational work in which we attempt to find numerically the fit between theory and observation. The procedure is not particularly elegant, but it is probably the soundest approach to making the connection.

In chapter II we discuss the method of computation of the models and give results in chapter III. Chapter IV discusses the computed hydrogen and helium line profiles, and chapter V gives the comparison between theory and observation.

Chapter II

THE COMPUTATION OF THE MODELS

1. Introduction

In this chapter we will describe in detail the method of computation of the model atmospheres used in the present study. A discussion of the actual results will be deferred until the next chapter. One of the main purposes of the present set of computations is to achieve model atmospheres in a high degree of radiative equilibrium. This goal is attained by constructing a sequence of models and iterating to obtain constancy of the flux throughout the atmosphere. The deviations from flux constancy are used to correct the model so that the next iterate more fully satisfies this condition. The number of actual numerical calculations required is enormous, and the solution of the problem was carried out using an IBM 7090 computer.

Needless to say, a number of approximations and idealizations have necessarily been made; in general these approximations affect the physics of the situation since these problems are more fundamentally difficult to cope with than are numerical difficulties. The latter of course can be very troublesome, as is shown by the long time required to convert the computer program from a series of flow diagrams to a working system. But in the final analysis, almost any numerical problem can be solved satisfactorily if one is willing to spend sufficient time in the computations while physical problems often require theoretical or experimental information not at hand, or insight and understanding beyond the capabilities of the investigator.

This is unfortunate since ultimately we are not interested in numerical accuracy for its own sake, but we wish to deal with real entities: the stars. The problem is complicated by limitations in the observations as well (see the very instructive remarks of A. Unsöld, 1958). Thus at the outset we should emphasize the assumptions that have been made and the physical restrictions that have been imposed.

2. Assumptions and discussion of general equations

In this section we will write down the principal equations to be solved and discuss the assumptions made. For a derivation of these equations, see Aller's textbook (1953) and Chandrasekhar's monograph (1950), as well as the review article by Münch (1960).

(a) The atmospheres are assumed to be plane parallel. This assumption is valid (Gingerich, 1961) for all but the most distended stellar envelopes. This assumption allows us to write the equation of transfer as:

$$\mu \frac{\partial I_\nu(\mu, \tau)}{\partial \tau_\nu} = I_\nu - S_\nu \qquad (2.1)$$

In equation 2.1, $\mu = \cos\theta$, θ being the angle between the pencil of radiation under consideration and the outward normal; I_ν = specific intensity at frequency ν, S_ν = the "source function," that is, the emissivity per unit mass, j_ν, divided by the extinction coefficient $(\kappa_\nu + \sigma_\nu)$; κ_ν = the true absorption coefficient; σ_ν = the scattering coefficient; $\tau_\nu = -\int (\kappa_\nu + \sigma_\nu)\rho \, dx$, the optical depth; and ρ = the density of stellar material in gm/cm^3. κ_ν and σ_ν are per gram of stellar material, and dx is an element of physical length along the normal to the atmosphere.

With the assumption of this equation of transfer, we are led to formal solutions for the mean intensity $J_\nu \equiv \frac{1}{2}\int_{-1}^{+1} I_\nu(\mu)\, d\mu$ and the flux $F_\nu \equiv 2\int_{-1}^{+1} I_\nu(\mu)\, \mu\, d\mu$. These definitions of J_ν and F_ν assume the radiation field does not depend upon the azimuthal angle about the normal to the atmosphere. Note further that F_ν is the "astrophysical flux"; the actual "physical flux" in ergs/cm^2-sec is given by $\mathfrak{F}_\nu = \pi F_\nu$. These definitions are all quite standard. The formal solutions for J_ν and F_ν are then

$$J_\nu(\tau_\nu) = \frac{1}{2}\int_0^\infty \mathbb{S}_\nu(t_\nu) E_1 |t_\nu - \tau_\nu| \, dt_\nu \qquad (2.2)$$

$$F_\nu(\tau_\nu) = 2\int_{\tau_\nu}^\infty \mathbb{S}_\nu(t_\nu) E_2(t_\nu - \tau_\nu) dt_\nu - \int_0^{\tau_\nu} S_\nu(t_\nu) E_2(\tau_\nu - t_\nu) dt_\nu \qquad (2.3)$$

where $E_1(x)$ and $E_2(x)$ are the exponential integrals $E_n(x) = \int_1^\infty \frac{e^{-xt}}{t^n} dt$.

The problem is thus to determine the run of the physical variables as a function of depth in the atmosphere, from this to determine the source function at each point, and then perform the integrations indicated by equations 2.2 and 2.3. Since the absorption and scattering coefficients are strongly dependent upon frequency, the optical depth scale and source functions must be established as functions of frequency at each depth. In the present computations we consider 30 frequencies and 50 depths. The distribution of points in frequency has been chosen to characterize the features of the continuous energy distribution while the depth points are chosen so as to specify the run of physical variables, completely enough not only for the atmospheric computations, but also

for line strength computations. Since the calculations have been carried out over the temperature range of 7,000 ^{o}K to 50,000 ^{o}K, it was necessary to change the frequency points at temperatures greater than 24,000 ^{o}K in order to account for the radiation beyond the Lyman limit and also the absorption edges due to Helium.

(b) The atmosphere is assumed to be in hydrostatic equilibrium. Thus if p is the total pressure, we have

$$\frac{dp}{dx} = - \rho g \qquad (2.4)$$

where g is the surface gravity of the star, GM/R^2, assumed to be constant throughout the atmosphere. Now since $d\tau_\nu = - (\kappa_\nu + \sigma_\nu)\rho\, dx$ we have

$$\frac{dp}{d\tau_\nu} = \frac{g}{\kappa_\nu + \sigma_\nu} \qquad (2.5)$$

This equation is valid so long as the physical conditions of the atmosphere allow it to be quiescent. In view of the dramatic dynamical phenomena observed in such an ordinary star as the sun, we may well wonder about the validity of this simple equation; but for the moment it is the best we can do. We shall in fact find cases where the assumption of this equation leads to results which clearly indicate that it is invalid, as is already known from observations in the case of supergiants.

The total pressure p is the sum of the partial pressures p_g and p_r, where p_r is the radiation pressure and p_g is the gas pressure. In turn we regard the gas pressure as the sum of the partial pressures p_e and p_A where p_e is due to free electrons and p_A is due to atoms and ions. Since it is convenient to consider p_g as the

dependent variable and p_r as distinct from it, we will write:

$$\frac{dp_g}{d\tau_\nu} = \frac{g}{(\kappa_\nu + \sigma_\nu)} - \frac{dp_r}{d\tau_\nu} \tag{2.6}$$

Now the amount of momentum transferred per unit time per unit area by the radiation field to a slab of material in the atmosphere is $-\rho\, dx \cdot \frac{\pi}{c}\int_0^\infty F_\nu(\kappa_\nu+\sigma_\nu)d\nu$, the minus sign being due to the fact that F_ν is taken positive outward while x is measured positive inward. Thus we have:

$$\frac{dp_g}{d\tau_\nu} = \frac{g}{(\kappa_\nu + \sigma_\nu)} - \frac{\pi}{c}\frac{\int_0^\infty F_\nu(\kappa_\nu+\sigma_\nu)d\nu}{(\kappa_\nu+\sigma_\nu)} \tag{2.7}$$

It will be noted that thus far we have assumed the equation of hydrostatic equilibrium is integrated in terms of the monochromatic optical depth at some definite frequency (which we shall usually call the "standard frequency"). This frequency may be arbitrary, but as the classical analyses of the "grey" transfer problem have shown, it is often advantageous to use a mean opacity defined in one of many possible ways. One of the most satisfactory of these means is the flux-weighted mean $\overline{\kappa} = \int_0^\infty \kappa_\nu F_\nu d\nu / F$ and a good approximation to it is the Rosseland mean $\frac{1}{\overline{\kappa}} = \int_0^\infty \frac{1}{\kappa_\nu}\frac{\partial B_\nu}{\partial T}d\nu \Big/ \int_0^\infty \frac{\partial B_\nu}{\partial T}d\nu$ (see for example, the discussions by Chandrasekhar, 1950; Kourganoff, 1952; Michard, 1949; and Saito, 1959). While the integrations in the present computations have been carried out monochromatically, the standard frequency used for the integration was usually chosen to correspond as

is convenient to the Rosseland mean; as we shall note below, the results are quite independent of the actual frequency used.

This procedure allows the following simplification: in the first integration for a given model we have no a priori knowledge of the fluxes F_ν. Thus we cannot calculate $dp_r/d\tau_\nu$. If, however, our standard frequency is chosen so that roughly $(\kappa_\nu+\sigma_\nu)_{STD} = \overline{(\kappa+\sigma)}$ then we have

$$\frac{\pi}{c}\frac{\int F_\nu(\kappa_\nu+\sigma_\nu)d\nu}{(\kappa_\nu+\sigma_\nu)_{STD}} \sim \frac{\pi}{c}\frac{\int F_\nu(\kappa_\nu+\sigma_\nu)d\nu}{\overline{(\kappa+\sigma)}} = \frac{\pi}{c}F = \frac{\sigma T_e^4}{c} \qquad (2.8)$$

This approximate value for $dp_r/d\tau_\nu$ is used in the initial integration and is replaced in each subsequent iteration by the actual value found using the fluxes predicted by the preceeding model. Once some accurate models have been constructed in this way, we may interpolate the initial guess more accurately from these previous results.

We might state here some reasons for having not used a mean absorption coefficient. First, the main use of a mean absorption coefficient is to allow the use of the grey body temperature distribution. But this temperature distribution implies a unique relationship between the boundary temperature and the effective temperature. We shall see below that this relationship is in fact a function of the effective temperature of the model. Second, it is computationally more expedient to use a monochromatic absorption coefficient since either the mean must be computed at each point (which in the present case would be roughly 30 times as time-consuming) or vast tables must be precomputed and interpolated (a tricky and dangerous procedure in the case of the

opacity). Furthermore, if the latter alternative be followed, these tables must be re-computed whenever an additional opacity source is considered. Since we have access to high-speed computers today, it is relatively pointless to try to reduce the problem of stellar atmospheres to the grey problem, since they are in fact extremely non-grey, and modern techniques allow us to consider the temperature distribution as a functional relationship to be found a posteriori.

(c) The atmosphere is assumed to be in strict radiative equilibrium. This implies that the transfer of energy by convection is ignored. Indeed, all dynamical effects are ignored. This represents a rather severe limitation to the range of applicability of the computations in regions where the hydrogen and helium ionization zones are important. On the other hand, no entirely satisfactory theory of convection is available at present, and indications are that probably in the atmosphere the radiative gradient lies closer to the true temperature gradient in some cases than does the adiabatic gradient commonly used in the interior. To help evaluate how serious are the potential effects of convection both the radiative and adiabatic temperature-pressure gradients have been computed, and in some models an estimate was made of the magnitude of the convection flux by use of a mixing length theory. It was found in some models that the convection flux computed in this way exceeds the total flux assumed to be passing through the atmosphere, while in other models it was only a negligible fraction of the flux. In the latter case the radiative gradient is the correct one to use. In the former case the models presented here have questionable validity.

(d) The opacities considered are limited. Because the continuous absorption coefficients are unknown for most atoms and ions, the present computations include only the true absorption coefficients of H, H^-, H_2^+, He I, and He II, and the scattering coefficients from free electrons and from Rayleigh scattering by neutral H. While this list probably includes most of the more important sources of opacity, many possibly important sources are not included, and this should be recognized as potentially a rather severe limitation of the accuracy of the results. In fact, evidence has been presented recently that there are serious discrepancies between the theoretical predictions of model atmospheres and actual observations in the rocket ultraviolet (Stecher and Milligan, 1962) which show a profound ultraviolet deficiency below λ2400A in the radiation of early type stars, when compared to models. A less pronounced discrepancy of this nature had been noticed some time ago in the sun, and Varsavsky (1957) suggested that it was due to additional absorption by a transition of collisionally produced H_2 from its unstable $(1s\sigma)(2p\sigma)\,{}^3\Sigma_U^+$ level to its $(1s\sigma)(2s\sigma)\,{}^3\Sigma_g^+$ level. This same mechanism has been reviewed by Stecher (1962) and Zwaan (1962) based on recent calculations of the absorption coefficient of the transition by Erkovich (1960). For the early type stars, Stecher and Milligan proposed that high opacities might result from combinations of H and He atoms and ions; in particular they suggest opacity due to H_3^+, HeH^+ and HeH^{++}, however, no opacity formulae are yet available, and the problem is under study by Mr. R. H. Norton.

An alternative suggested by Meinel (1963) is that in general temperatures for the B stars are much lower than previously thought

and we observe not a deficiency of the flux at $\lambda 2000$, but an excess at $\lambda 2400$ due to a recombination of excited H atoms yielding ultimately the unstable $^3\sum_g^+$ molecule which dissociates and emits a photon. The implications of this mechanism are most interesting as Meinel shows. The Meinel mechanism probably will not cause as large a change in the results as would the absorption at $\lambda 2000$, but serious modifications of the results given here may be necessary in the future. Certainly as information becomes available on other sources of opacity they will be included in the computations, and the results revised accordingly.

(e) The effects of the spectrum lines is not included. These effects will drastically alter the temperature distribution near the surface of the star (Traving, 1956). In particular, for the A type stars one would expect the Blamer lines to be important, and for earlier types the Lyman lines become important. Ultimately it is hoped to include the Hydrogen lines in the transfer problem in a rigorous way at the outset, and in fact this seems quite feasible with present computers.

(f) Probably the most difficult problem with the present computations is that the populations of the levels and the ionization fractions are assumed to be given by the Boltzmann distribution and the Saha equation respectively, while the Kirchoff-Planck law is assumed to hold for that part of the source function dominated by absorption terms. The fact is that important deviations from these distributions occur near the surface of the photosphere. This represents a serious defect if, for example, very precise line profiles are required

for strong lines, although this is certainly not the only difficulty here. On the other hand, indications are that this presents no important trouble if the atmospheres are used to study the continuum energy distribution or used to find starting values for stellar interiors computations (Lecar, 1963). As will be described below, we have computed a quantity which allows assessment of these deviations.

In summary it should be recognized that we are still dealing with fairly high order idealizations of stellar atmospheres. Perhaps the principal gain made in the present computations is that we now have a fairly homogeneous set of models over a wide range of temperatures and gravities in which the flux constancy is of the order of ± 1 per cent and in some cases better.

3. Computation of the physical variables

The solution of the pressure equation is carried out in logarithmic form so that we actually integrate:

$$\frac{d \log_{10} p_g}{d\tau_\nu} = \frac{1}{2.3025851 \cdot p_g} \left[\frac{g}{\kappa_\nu + \sigma_\nu} - \frac{dp_r}{d\tau_\nu} \right] \qquad (2.9)$$

The starting value procedure will be given below. At each step, using an initially assumed $T(\tau_\nu)$ relationship we have p_g and T. Log p_e is found by interpolating in a table of $\log p_g(p_e, \theta)$. Having p_e we evaluate and then evaluate $dp_r/d\tau_\nu$ either using the grey approximation or by interpolation in a table from the previous model. Thus we can evaluate the derivative and proceed with the integration by standard numerical methods. We will give the details of the computation of all

relevant physical quantities in Appendix IV, and merely outline the procedures here. Numerical results for 28 models are given in Appendix I.

(a) Gas pressures

The table of gas pressures is computed at the beginning of a series of integrations for a given model. The table is made large enough so that it generally suffices for not only the initial model but the successive iterates as well; if, however, the boundary conditions are revised outside the range of the table by one of the later iterates, the table is automatically recomputed. Uniform steps are taken in the arguments $\log p_e$ and θ, and $\log p_g$ is computed at each of these points; this mesh of points is chosen sufficiently fine that accurate interpolation may be done. Here

$$p_g = p_A + p_e = N_A kT + N_e kT \tag{2.10}$$

(b) Density

The density of stellar material in grams/cm^3 is

$$\rho = \sum_i \left[(m_A N_A)_i + M_{ION} N_{ION})_i \right] + m_e N_e$$

$$= \sum_i \left[m_{ATOM} (N_{ATOM} + N_{ION}) \right]_i \tag{2.11}$$

since obviously the mass equivalent of the ionization energies is entirely negligible. But

$$\sum_i \left[m_{ATOM}(N_{ATOM} + N_{ION}) \right]_i = N_H m_H \frac{\sum a_i A_i}{A_H}$$

$$= N m_H \frac{\sum a_i A_i}{A_H \sum a_i} \qquad (2.12)$$

since $N_H = N/\sum a_i$. Thus defining

$$\mu = \frac{\sum a_i A_i}{A_H \sum a_i} \qquad (2.13)$$

and recognizing $N = (p_g - p_e)/kT$, we have

$$\rho = \mu m_H \frac{(p_g - p_e)}{kT} \qquad (2.14)$$

(c) Geometrical depth

The geometrical depth follows from "inverting" the hydrostatic equilibrium equation and using the known run of the pressure, density, and opacity to find the depth h. Thus

$$- \frac{dp_g}{(\kappa_\nu + \sigma_\nu)\rho\, dh} = \left[\frac{g}{(\kappa_\nu + \sigma_\nu)} - \frac{dp_r}{d\tau_\nu} \right] \qquad (2.15)$$

so that

$$dh = \frac{-2.3025851 (p_g/\rho) d \log_{10} p_g}{[g - (\kappa_\nu + \sigma_\nu) dp_r/d\tau_\nu]} \qquad (2.16)$$

Finally,

$$h(b) - h(a) = \int_a^b (2.3025851) \frac{p_g}{\rho} \frac{d(\log_{10} p_g)}{[g - (\kappa_\nu + \sigma_\nu) dp_r/d\tau_\nu]} \qquad (2.17)$$

The quadrature is performed using the trapezoidal rule.

(d) Radiative and adiabatic gradients

The radiative gradient is defined as

$$\nabla_R = \frac{d \log T}{d \log p_g}\bigg|_{\text{Radiative}} = \frac{p}{T}\frac{dT}{dp} = \frac{p}{T}\left(\frac{dT}{d\tau}\right)\left(\frac{d\tau}{dp}\right) \qquad (2.18)$$

$\left(\frac{dT}{d\tau}\right)$ is found by direct numerical differentiation of the $T(\tau)$ relationship. As is always the case, numerical differentiation is delicate and unstable. In some cases noticeable oscillations occur in the values of the radiative gradient. These are due primarily to the fact that the final $T(\tau)$ represents many interpolated and integrated correction terms, each of which may not be completely smooth. If this is troublesome, graphical smoothing of the points helps, or a low order differentiation formula can be used to enhance stability. This is not an important problem at present, but certainly will be if the convection problem is treated. $\left(\frac{dp}{d\tau}\right)$ is found from the equations above. This gradient is to be compared to the adiabatic gradient which we have computed using the results of Krishna-swamy (1961); his expression accounts fully for the effects of ionization and radiation pressure. Since helium is fairly abundant relative to hydrogen, and can still be present after most of the hydrogen is ionized, it is important to account for the fact that it has two ionization potentials. This complicates the problem, but the complication can be avoided if we note that since the two ionization potentials are so widely separated, helium can for all practical purposes be considered as two distinct atoms, and the contribution of each added separately to the ionization terms. Of

course the contribution to N_{ATOMS} is to be added in only once. This treatment assumes no overlap of the three ionization states, and is not strictly correct, but certainly is adequate for present purposes.

(e) The opacity

The total opacity is considered to consist of a pure absorption term κ_ν and a coherent isotropic scattering term σ_ν. These quantities are very sensitive functions of the temperature, electron pressure, and frequency, so they are computed directly in each case instead of attempting to interpolate them from tables. Let:

$\alpha_\nu(H)$ = absorption coefficient per neutral atom of H

$\alpha_\nu(H^-) \cdot P_e$ = absorption coefficient of H^- per neutral atom of H

$\alpha_\nu(H_2^+)$ = absorption coefficient of H_2^+ per neutral atom of H and per H ion

$\alpha_\nu(He)$ = absorption coefficient per neutral atom of He

$\alpha_\nu(He^+)$ = absorption coefficient per singly ionized atom of He.

Then, letting

$$\mu' = \frac{\sum \alpha_i A_i}{\alpha_H A_H} = \frac{\text{grams of stellar material}}{\text{gram of H}} \qquad (2.19)$$

$$Y = \frac{N_{He}}{N_H} \qquad (2.20)$$

$$f_1 = \frac{N_H}{N_H + N_{H^-} + N_{H^+} + 2(N_{H_2} + N_{H_2^+})} \qquad (2.21)$$

$$f_2 = \frac{N_{H^+}}{N_H + N_{H^-} + N_{H^+} + 2(N_{H_2} + N_{H_2^+})} \qquad (2.22)$$

$$f_3 = \frac{N_{He}}{N_{He} + N_{He^+} + N_{He^{++}}} \tag{2.23}$$

$$f_4 = \frac{N_{He^+}}{N_{He} + N_{He^+} + N_{He^{++}}} \tag{2.24}$$

we have for κ_ν in cm^2[gram of stellar material:

$$\kappa_\nu = \frac{1}{\mu' m_H}\left[f_1(a_\nu(H) + P_e a_\nu(H^-) + \rho f_2 a_\nu(H_2^+) \right.$$

$$\left. + Y(f_3 a_\nu(He) + f_4 a_\nu(He^+)) \right] \tag{2.25}$$

Each of the absorption coefficients includes the effects of stimulated emission.

We should remark here that although the partition functions used in this study differ greatly at high temperatures from previous calculations, the opacities are not appreciably affected. This comes about because while the absorption coefficient contains a factor of $1/B_o$, the fraction of Neutral H atoms is proportional to B_o (when the hydrogen is mostly ionized--which is also when B_o becomes large); so to first order the terms in B_o cancel.

The six contributors to the total extinction coefficient are of varying importance for different temperature-pressure-wavelength regions. Through most of the range of models to be presented H is the dominant source of opacity. For the hottest models He II and σ_e are important. For the very hottest models, we have dominance by electron scattering alone in the outermost layers (where the ionization

is very high because of the very low pressures) and in the very deepest layers (where the ionization is high due to high temperature despite high pressures). This sometimes makes the solution of the equation of transfer difficult, especially near the long wavelength side of the Lyman edge where all other opacity sources are quite small. At low gravities, the scattering terms become increasingly important, and the equation of transfer increasingly difficult to solve. At lower temperatures the negative hydrogen ion begins to become important for high gravity models. Rayleigh scattering becomes important for low temperatures as hydrogen is mostly in its ground state, and is increasingly important for low gravity models where the decrease in electron pressure causes the contribution of H^- to the opacity to greatly diminish. In such cases, we have essentially pure scattering at wavelengths near the long wavelength edge of the Lyman limit, and the solution of the equation of transfer may fail completely. Typically the scattering terms decrease very rapidly inward for most models (the highest temperature cases being the exceptions). In the regions near the Lyman edge where the Rayleigh scattering terms are important, the opacity may very rapidly diminish at some point as the relatively sudden excitation of hydrogen atoms from the ground state and ionization of hydrogen begin. This is reflected quite strikingly in a plot of the monochromatic optical depth versus the standard depth; the curve rises very steeply at first, and suddenly rolls over and becomes very nearly flat. This behavior is quite reminiscent of the behavior of the hydrogen ionization edge in the well-known Strömgren-sphere problem of planetary nebulae. We shall show some of these features graphically below.

(f) The optical depth

Once we have integrated the equation of hydrostatic equilibrium we have the information required to calculate tables of monochromatic opacities as a function of depth. We may then directly perform the numerical quadrature

$$\tau_\nu(\tau) = \int_0^\tau \frac{\kappa_\nu(t)}{\kappa_{STD}(t)}\, dt \qquad (2.26)$$

to find the monochromatic optical depths, as well as

$$\bar{\tau}(\tau) = \int_0^\tau \frac{\bar{\kappa}(t)}{\kappa_{STD}(t)}\, dt \qquad (2.27)$$

to find the mean optical depth (which in fact is never used in these calculations). In the computations given later, we have found the Planck mean opacity and depth, although the flux-weighted mean follows immediately from the tables of $dp_r/d\tau_\nu$, as is evident from equations 2.6 and 2.7.

(g) The integration procedure

To obtain a starting value for the integration of the hydrostatic equilibrium equation, we set $\theta = \theta_o$, which is determined either from the grey solution or from a preceeding model. A first guess at $\log p_e$ is obtained from $(\log p_e)_o \sim \theta_o(0.13 \log g - 3.06) + 0.72 + 0.34 \log g$. We then form tables of $\log p_g(p_e, \theta_o)$ and $\kappa_{STD}(p_e, \theta_o)$ starting from $(\log p_e)_o - 0.5$, and taking steps of 0.025 in $\log p_e$. We may then find $\tau_\nu(p_g)$ by direct integration of the hydrostatic equation, now regarding p_g as the independent variable, by Simpson's rule. This integration

is continued until either $\tau_\nu \geq 0.001$ or until 20 steps have been taken. If the latter occurs and τ_ν is still less than 0.001, $(\log p_e)_o$ is stepped by 0.3, and another attempt is made. If, on the other hand, $\tau_\nu \geq 0.001$ and less than ten steps have been taken in the integration, $(\log p_c)_o$ is decreased by 0.4 and another attempt is made. This is done up to 8 times; if no satisfactory result is found by then, it is assumed that something has gone wrong with the computations, and they are automatically terminated. If both criteria are satisfied, we obtain $(\log p_g)$ and $(\log p_e)$ at $\tau_\nu = 0.0005$ by backwards interpolation; these values are adopted as the starting values. This procedure is quite uniform, and has the advantage of making no restrictive assumptions about the functional behavior of the physical variables other than assuming the temperature gradient is negligible at the very boundary when measured on an optical depth scale. In the results quoted below, any results quoted at the surface or at $\tau_\nu = 0$ strictly speaking refer to $\tau_\nu = 0.0005$.

From these starting values, the integration is continued taking first $\log p_g$ as the independent variable, and finding $\tau_\nu(\log p_g)$ in steps of $\Delta \log p_g = 0.05$. This procedure is advantageous because of the very steep pressure gradients encountered near the surface when p_g is measured on a τ_ν scale. The first step is made using a four point Runge-Kutta formula, and the integration is continued using a Milne predictor-corrector formula. This procedure is amenable to automatic truncation error control, which is set so that the relative truncation error in each step is $\leq 10^{-5}$. The Milne formula is:

$$\dot{Y} = f(x, y)$$

$$Y_{n+1}^{\text{Predicted}} = Y_n + \frac{\Delta x}{24}\left[55f_n - 59f_{n-1} + 37f_{n-2} - 9f_{n-3} \right]$$

$$Y_{n+1}^{\text{Corrected}} = Y_n + \frac{\Delta x}{24}\left[9f_{n+1} + 19f_n - 9f_{n-1} + f_{n-2} \right] \qquad (2.28)$$

where f_{n+1} is computed using $y_{n+1}^{\text{Predicted}}$. The evaluation of the derivatives is carried out in single precision arithmetic, and the ordinates are kept in double precision. This greatly reduces the problem of round-off errors.

The integration is continued in this manner until $\frac{d\tau_\nu}{d \log p_g} > 1$. At this time, $\log p_g$ at the standard depths is found by backwards interpolation, and the integration is continued now using τ_ν as the independent variable using equations 2.28; again the relative truncation error is held at $\leq 10^{-5}$. From the resulting table of $\log p_g$ as a function of τ_ν we find $\log p_e$ by backwards interpolation in the gas pressure table and then evaluate all the other physical quantities described above. Figures 1 and 2 show the final run of gas, electron, and radiation pressure for a model with $\theta_e = 0.14$, $\log G = 4.0$, and $N(HE)/N(H) = 0.15$. The run of the radiation pressure was obtained by integrating the known run of $dp_r/d\tau$; p_r was set = 0 at the boundary, and it merges with the black body value, $\frac{1}{3} aT^4$, at $\tau \approx 10$. At much greater depths it deviates from this value due to unsatisfactory numerical extrapolation. These graphs show the (typically) steep pressure gradient at the surface. Figure 3 shows a comparison of the radiative and adiabatic gradients; this model is stable against convection.

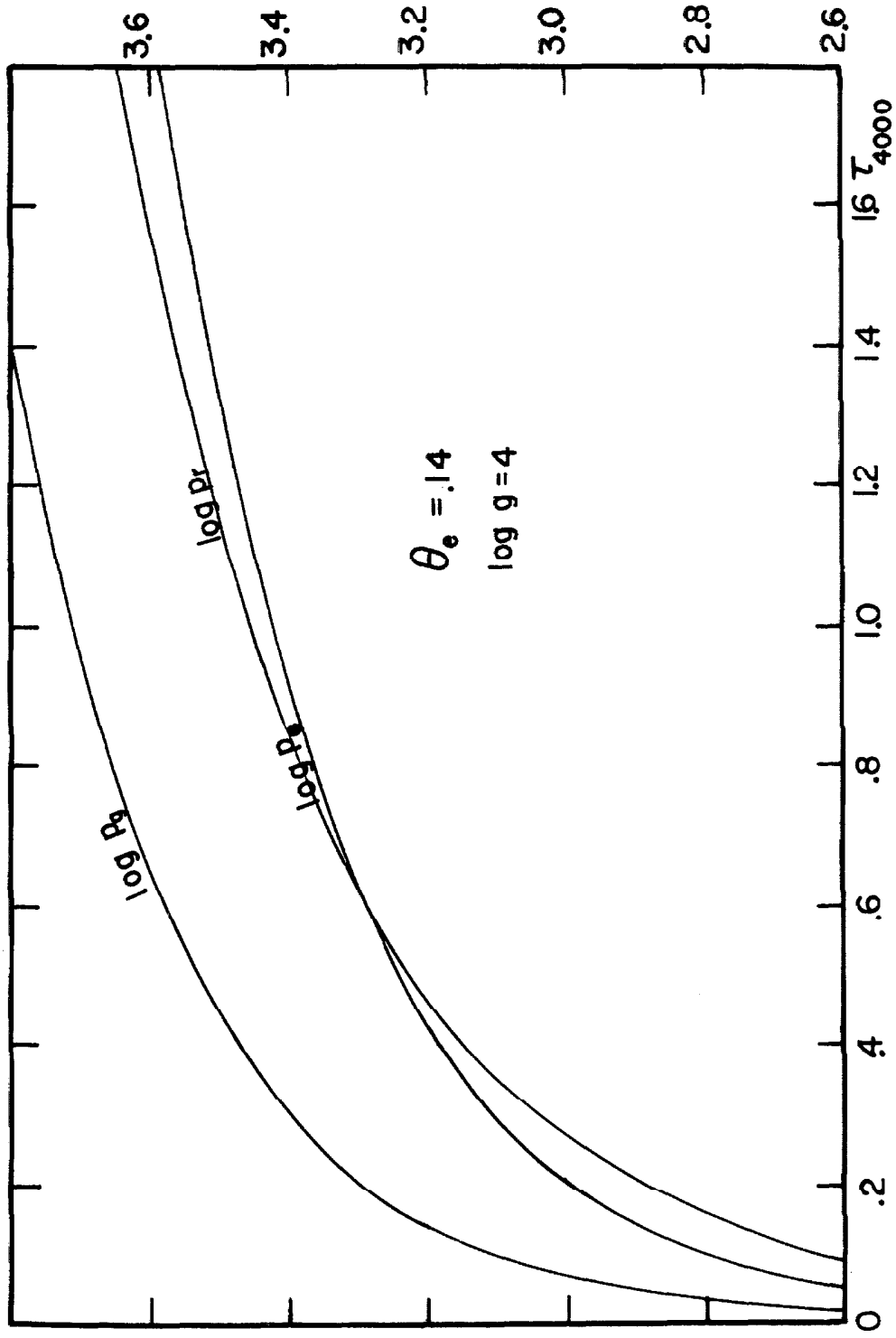
3.6
3.4
3.2
3.0
2.8
2.6
16 τ4000
0
.2
.4
.6
.8
1.0
1.2
1.4
log Pg
log Pr
log Pe
θe = .14
log g = 4

Fig. 1

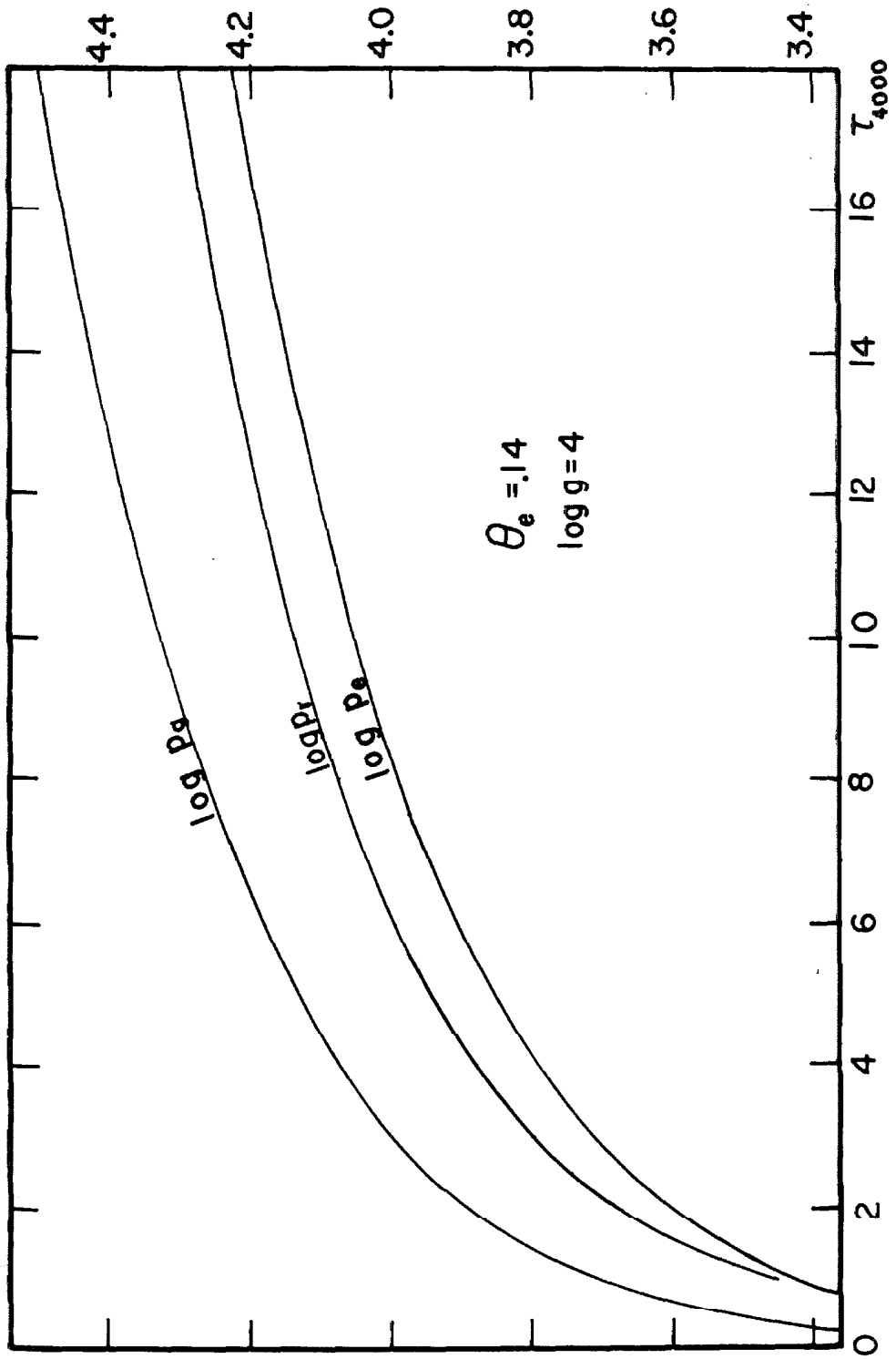
4.4
4.2
4.0
3.8
3.6
3.4
τ_{4000}
0
2
4
6
8
10
12
14
16
log P_g
log P_r
log P_e
θ_e =.14
log g=4

Fig. 2

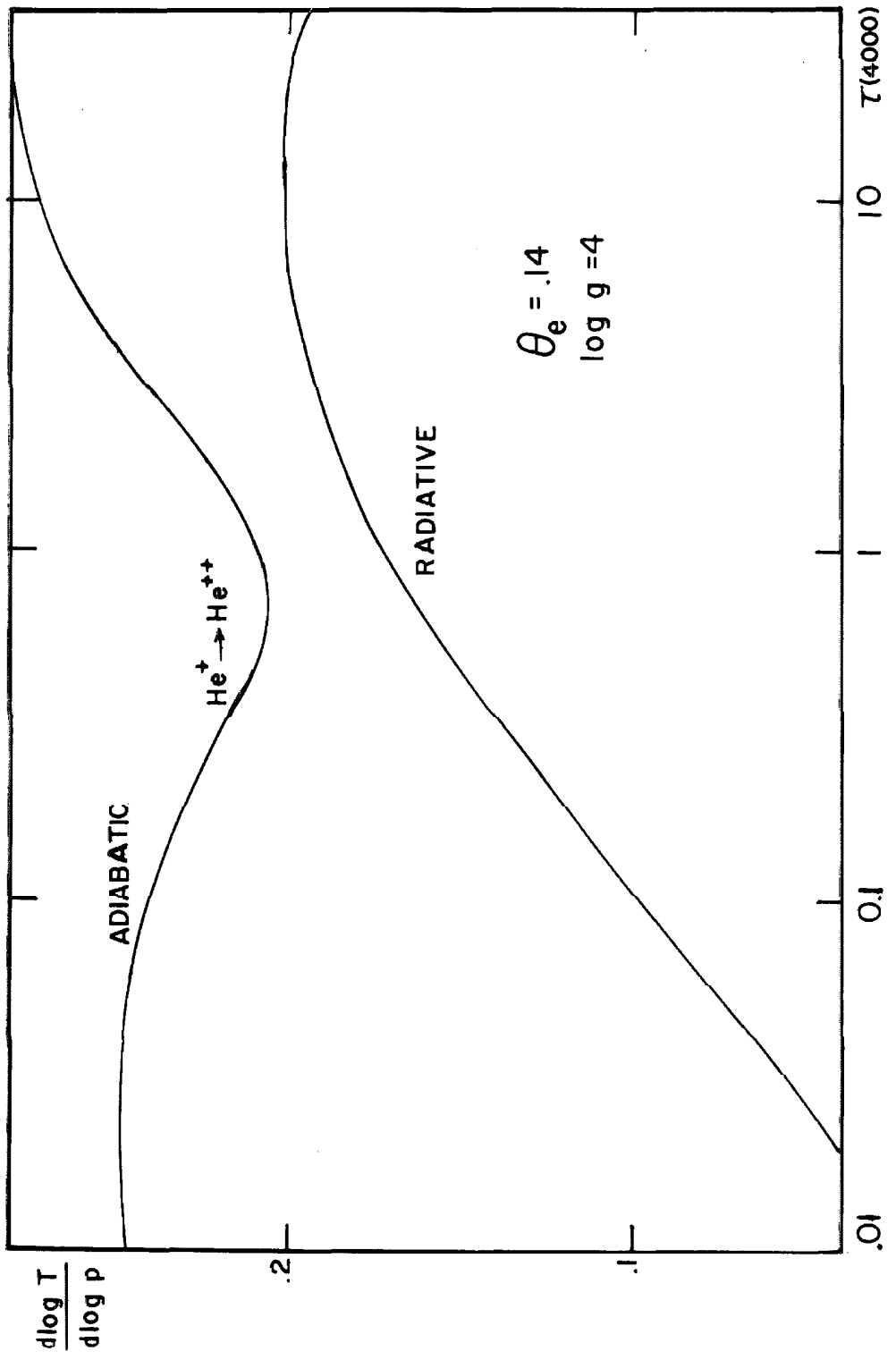
dlog T / dlog p
.2
.1
.01
0.1
1
10
τ(4000)
ADIABATIC
He+ → He++
RADIATIVE
θe = .14
log g =4

Fig. 3

4. Solution of the transfer equation

If scattering can be neglected, and we assume LTE, then we simply set $S_\nu = B_\nu$ and perform the integrations indicated in equations 2.2 and 2.3 to determine the mean intensities and fluxes. This is done at each frequency for the chosen set of optical depths. The details of the quadrature will be given below. As mentioned previously, the frequencies are chosen so as to account for the ionization edges of H, He, and He^+ since these are the most important opacity sources. In this calculation we simply lump σ_ν with κ_ν; such a procedure is unsound, however, since the radiation scattered depends upon the local mean intensity, and is largely independent of the local temperature. This decoupling of the local radiation field from the local temperature distribution can drastically alter the frequency distribution of the radiation and causes large changes in the emergent flux whenever the scattering terms are large. The source function which most simply accounts for the presence of scattering is:

$$S_\nu(t_\nu) = \frac{\kappa_\nu}{\sigma_\nu + \kappa_\nu} B_\nu(t_\nu) + \frac{\sigma_\nu}{\sigma_\nu + \kappa_\nu} J_\nu(t_\nu) \qquad (2.29)$$

This yields the well-known Milne-Eddington integral equation since the mean intensity is in turn dependent upon the source function as shown in equation 2.2.

The question of "When is scattering important?" is difficult to answer; it depends upon the physical conditions encountered in the model. As mentioned above, for hotter stars electron scattering is important while for cooler stars Rayleigh scattering is important.

The problem is worst on the long wavelength side of an absorption edge, where the true absorption terms are generally smallest, though for some temperatures and gravities, Rayleigh scattering can dominate over a large range into the visual part of the spectrum. Further, very dramatic changes can occur in the nature of the source function near the surface as is shown in figure 4; the case illustrated is by no means the most extreme case encountered. To anticipate a bit, we might mention that the dominance of scattering near the surface can be troublesome in attempting to obtain a temperature correction to make the model satisfy the flux constancy condition, since the integrals used in the computations are sometimes heavily biased by scattering terms, which as noted are uncoupled from the temperature distribution, and peculiarities such as temperature inversions may result.

It is this writer's opinion that the effects of scattering have generally been under-rated, and that in the most accurate work one should solve the Milne-Eddington equation in most cases. It should be remembered that while F_ν may be small in wavelength regions in which scattering dominates, this is frequently compensated by the large frequency range over which this condition occurs. In particular, the range $912\,A < \lambda < 3646\,A$ is a large frequency interval, and the integrated effects of F_ν and of scattering upon this F_ν are non-negligible for almost any star.

Let us now turn to the problem of solving equation 2.29. The basic procedure is that of using an iterative solution suggested by Strömgren (see, e.g., Aller's book, 1933, p. 267 ff.). Let us form the difference $J_\nu - B_\nu$. Now:

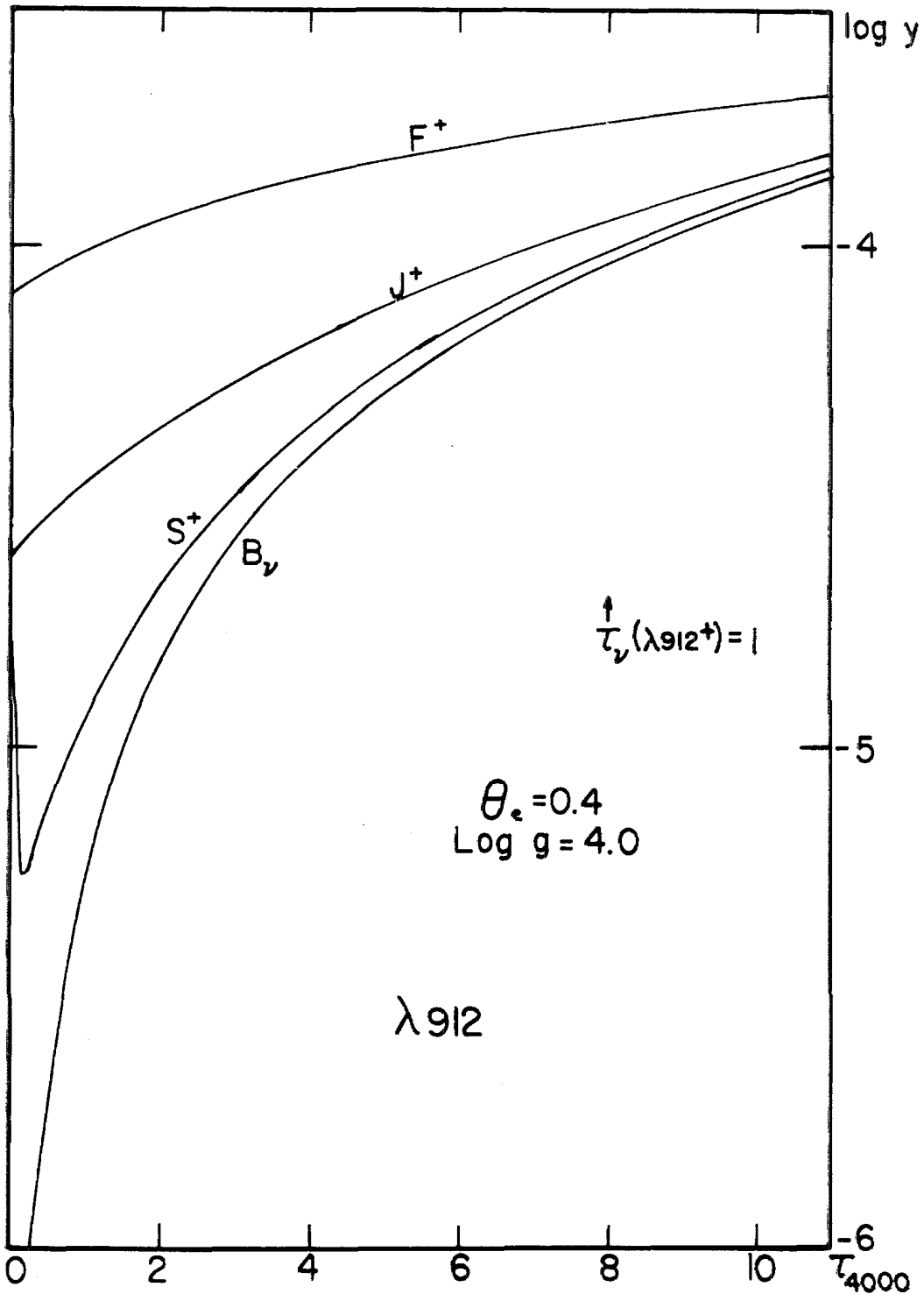

Fig. 4

$$J_\nu(\tau_\nu) = \frac{1}{2}\int_o^\infty S_\nu(t_\nu)E_1|t_\nu-\tau_\nu|dt_\nu$$

$$= \frac{1}{2}\int_o^\infty \left\{\frac{\kappa_\nu}{\kappa_\nu+\sigma_\nu} B_\nu(t_\nu) + \frac{\sigma_\nu}{\kappa_\nu+\sigma_\nu} J_\nu(t_\nu)\right\} E_1|\tau_\nu-t_\nu|dt_\nu$$

$$= \frac{1}{2}\int_o^\infty \left\{B_\nu(t_\nu) + \frac{\sigma_\nu}{\kappa_\nu+\sigma_\nu} (J_\nu-B_\nu)\right\} E_1|\tau_\nu-t_\nu|dt_\nu$$

$$= \overline{B}_\nu(\tau_\nu) + \frac{1}{2}\int_o^\infty \rho_\nu(J_\nu-B_\nu)E_1|\tau_\nu-t_\nu|dt_\nu$$

where

$$\rho_\nu = \frac{\sigma_\nu}{\sigma_\nu+\kappa_\nu} \tag{2.30}$$

and

$$\overline{B}_\nu(\tau_\nu) = \frac{1}{2}\int_o^\infty B_\nu(t_\nu)E_1|t_\nu-\tau_\nu|dt_\nu \tag{2.31}$$

Thus finally

$$(J_\nu(\tau_\nu) - B_\nu(\tau_\nu)) = [\overline{B}_\nu(\tau_\nu) - B_\nu(\tau_\nu)] + \frac{1}{2}\int_o^\infty \rho_\nu(J_\nu-B_\nu)E_1|\tau_\nu-t_\nu|dt_\nu \tag{2.32}$$

Equation 2.32 is solved by iteration as follows: as a first estimate guess, let us take $J_\nu \approx \overline{B}_\nu$ so that substituting back into the equation we have

$$(J_\nu - B_\nu)_1 = (J_\nu - B_\nu)_o + \Delta_1 = (\overline{B}_\nu - B_\nu) + \Delta_1$$

$$= (\overline{B}_\nu - B_\nu) + \frac{1}{2}\int_o^\infty \rho_\nu(\overline{B}_\nu - B_\nu)E_1|\tau_\nu-t_\nu|dt_\nu$$

Now using $(J_\nu - B_\nu)_1$ in the integral of equation 2.32 it is clear that

the new estimate of $(J_\nu - B_\nu)$ is the same as the old plus an additional term of the form $\frac{1}{2}\int_0^\infty \rho_\nu \Delta_1 E_1 |\tau_\nu - t_\nu| dt_\nu$. Thus we will have

$$(J_\nu - B_\nu) = (\overline{B}_\nu - B_\nu) + \sum_{m=1} \Delta m \tag{2.33}$$

and

$$\Delta m = \frac{1}{2}\int_0^\infty \rho_\nu \Delta_{m-1} E_1 |t_\nu - \tau_\nu| dt_\nu \tag{2.34}$$

This procedure is straightforward, although very time consuming, and converges well so long as the scattering terms are not overwhelming. In practice we have considered convergence complete when $\Delta S/S < 0.001$. Since the solution of the Milne equation is the lengthiest part of the computation, we have attempted to speed convergence by two means, namely, by attempting to make a better first guess for the solution and by trying to estimate a better correction between successive iterates.

To make a better first guess we argue that when scattering terms are dominant, the solution for the source function is formally the same as solving the classical "grey body" problem which is in fact a pure scattering problem. The only thing lacking is a suitable normalization for the mean intensity. Thus we must have at least approximately

$$J_\nu(\tau) \approx J_\nu^*(\tau + q(\tau)) \tag{2.35}$$

where J^* is a suitable normalization factor. Experience has shown that when $\rho_\nu \sim 0.85$ or $\rho_\nu \sim 0.9$, on the one hand the grey solution is roughly valid while on the other hand a decent estimate of J_ν^* is given by $\overline{B}_\nu$ from the lower layers. Thus if τ_ν^* is the depth at which

$\rho_\nu \sim 0.9$ we write

$$J_\nu(\tau_\nu) = \overline{B}_\nu(\tau_\nu) \qquad \text{for } \tau_\nu \geq \tau_\nu^* \qquad (2.36)$$

and

$$J_\nu(\tau_\nu) = \frac{\overline{B}_\nu(\tau_\nu^*)}{(\tau_\nu^* + q(\tau_\nu^*))} \cdot (\tau + q(\tau)) \qquad \text{for } \tau_\nu \leq \tau_\nu^* \qquad (2.37)$$

This first guess is sometimes quite superior to the estimate of $J_\nu \equiv \overline{B}_\nu$. However, as Mr. R. H. Norton has shown, the normalization constant J^* as described here is still essentially arbitrary, and this first guess can be quite badly in error relative to the true solution; in such cases convergence is never obtained either by the usual Strömgren procedure or by using equations 2.36 and 2.37. These cases occur in practice when the redward edge of the Lyman limit is dominated by Rayleigh scattering terms to great depth. The fundamental difficulty is that the kernel of the equation is singular, so that "information" propagates only very slowly in the solution when $\rho_\nu \sim 1$. Then the same correction term is repeated over and over, so that even though at a given stage $\Delta S/S < 0.01$, the final solution may differ by an order of magnitude! When this failure has occurred in the results to be given later, specific mention will be made.

To obtain a better estimate of the correction to be applied between successive iterates, let us call Δ the correction term predicted between two successive iterates. Then the next estimate of $J_\nu - B_\nu$ will be

$$(J_\nu - B_\nu)_{New} = (J_\nu - B_\nu)_{Old} + \int_0^\infty \Delta \cdot \rho \cdot E_1 |\tau_\nu - t_\nu| dt_\nu \qquad (2.38)$$

But the kernel of the integral is singular, so that to at least a rough

approximation, we can write

$$\int_o^\infty \Delta(t_\nu)\rho_\nu(t_\nu)E_1|\tau_\nu - t_\nu|\,dt_\nu \sim \Delta(\tau_\nu)\rho_\nu(\tau_\nu)\int_o^\infty E_1|\tau_\nu - t_\nu|\,dt_\nu \qquad (2.39)$$

where

$$\int_o^\infty E_1|\tau_\nu - t_\nu|\,dt_\nu = 1 - \frac{1}{2}E_2(\tau_\nu) \qquad (2.40)$$

Thus we derive an improved estimate of the correction term to be applied, namely:

$$\Delta^* = \Delta[1 + (1 - \tfrac{1}{2}E_2(\tau_\nu)) \cdot \rho_\nu(\tau_\nu)] \qquad (2.41)$$

Note that when using this procedure we do not form explicitly the sequence of terms and sum them as in equation 2.33 but instead work directly with each successive $J_\nu - B_\nu$. Test cases have shown a saving of around 40% in the number of iterates required to obtain convergence when we use equations 2.36, 2.37 and 2.41.

Having solved the Milne equation at each frequency we perform the integrations of equations 2.2 and 2.3 to find J_ν and F_ν. The detailed behavior of $\sigma_\nu/(\sigma_\nu+\kappa_\nu)$ and of S_ν, J_ν and F_ν relative to B_ν are among the more interesting results of the computations, and may best be studied graphically. To reproduce all of the results obtained would, however, be prohibitively laborious at present, so we will offer the following generalities and illustrate them with a few diagrams.

1. For most stars, ρ_ν is a very sharply monotone decreasing function of depth at most frequencies. On the long wavelength side of the Lyman limit the effects of scattering are the greatest and persist

to large optical depths (see figure 5). For the hottest stars, ρ_ν may increase at the greatest depths considered, showing the overwhelming importance of electron scattering. Small plateaus or "bumps" are sometimes evident on plots of ρ_ν as a function of depth; it is interesting to speculate whether these may be places where a sudden small increase in σ_e occurs because of the rapid ionization of some element at that depth, but it would be hard to prove that they are not in fact small numerical errors due to non-smooth table interpolation for $\log p_g(p_e, \theta)$ or for the partition functions.

2. If the monochromatic opacity of the wavelength under consideration is larger than the mean, J_ν is less than B_ν at the surface because J_ν includes an empty hemisphere in which there is no radiation. At depth, J_ν tends toward B_ν, the more rapidly when ρ_ν decreases rapidly. These features show in figures 6-11 for $\lambda 912^-$, $\lambda 3647^-$ and $\lambda 5050$.

3. If the monochromatic opacity is small relative to the mean, J_ν at the surface may be either greater or less than B_ν. The former follows if the fact that J_ν includes an empty hemisphere is more than compensated by the increased transparency which allows radiation from greater depths to reach the surface and/or if scattering provides a radiation leak from the interior independent of the local temperature. This case is well illustrated by the $\lambda 912^+$ solution in figure 6. The reverse case obviously occurs when the empty hemisphere prevails; this is well illustrated by the $\lambda 3647^+$ solution in figure 8.

4. Because of the general dominance of σ_ν over κ_ν for high temperature models at the boundary, S_ν approaches J_ν very closely

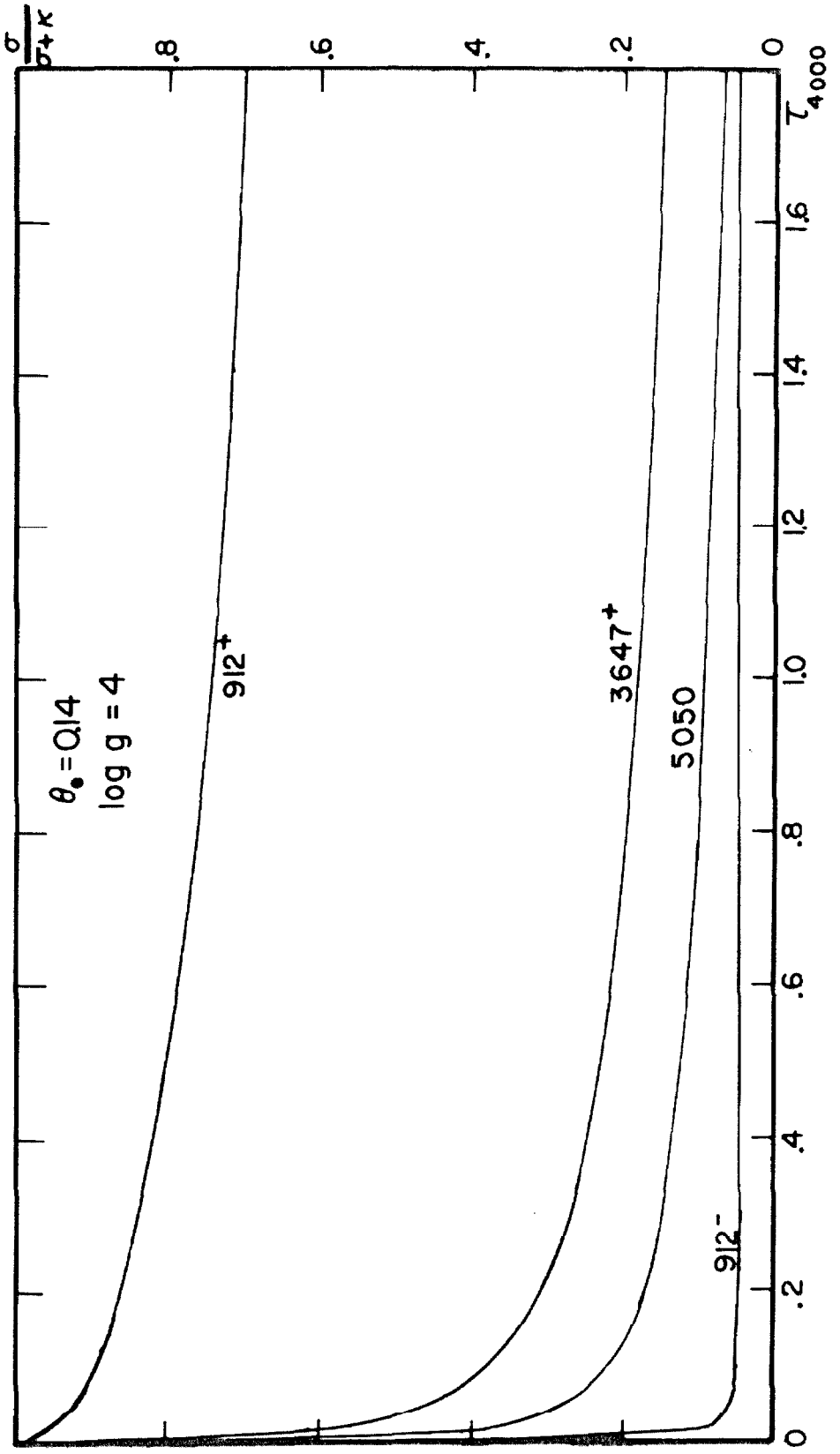

Fig. 5

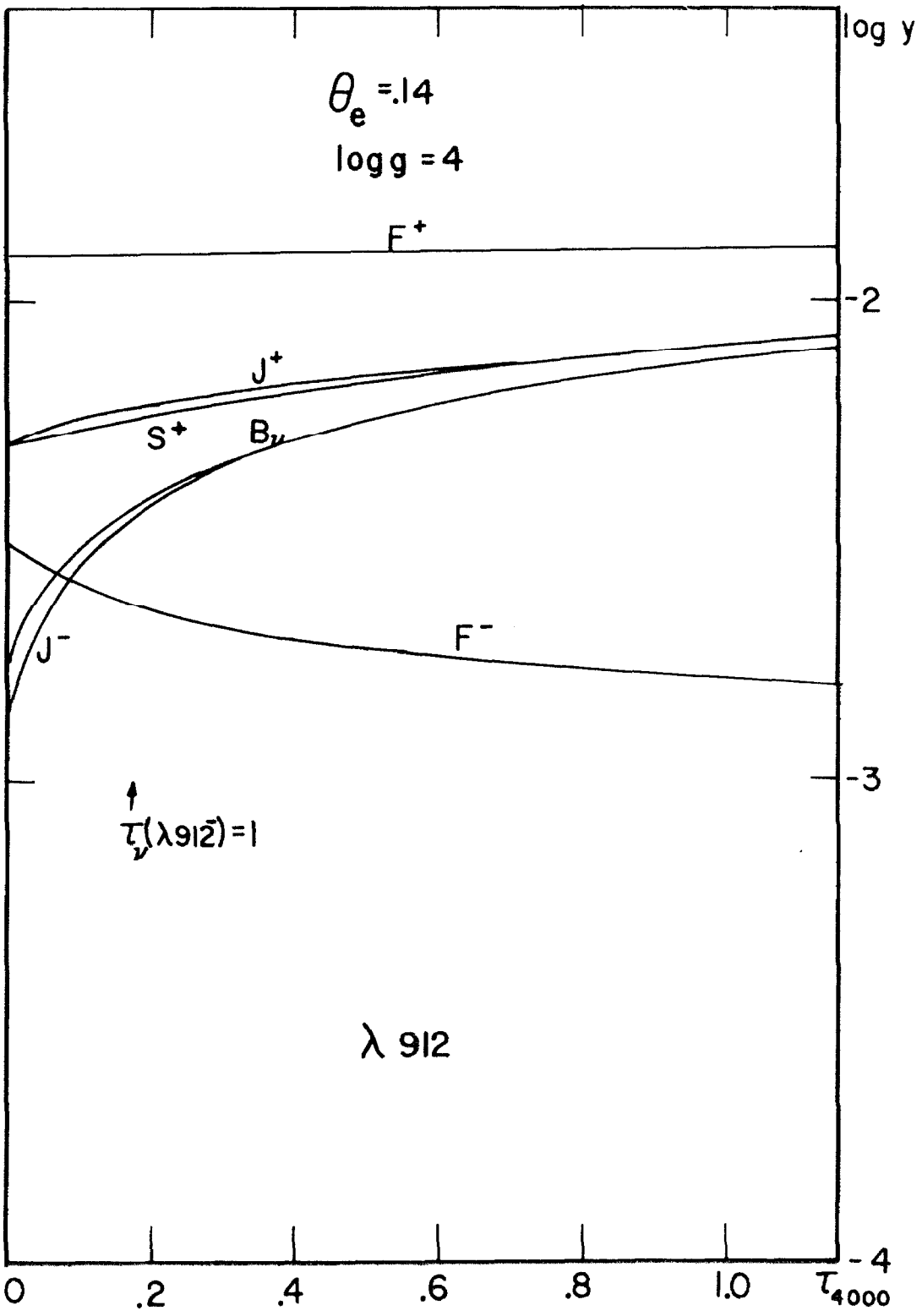
log y
θ_e =.14
log g = 4
F^+
-2
J^+
S^+
B_ν
J^-
F^-
-3
$\tau_\nu(\lambda 912\text{Å}) = 1$
λ 912
-4
0
.2
.4
.6
.8
1.0
τ_{4000}

Fig. 6

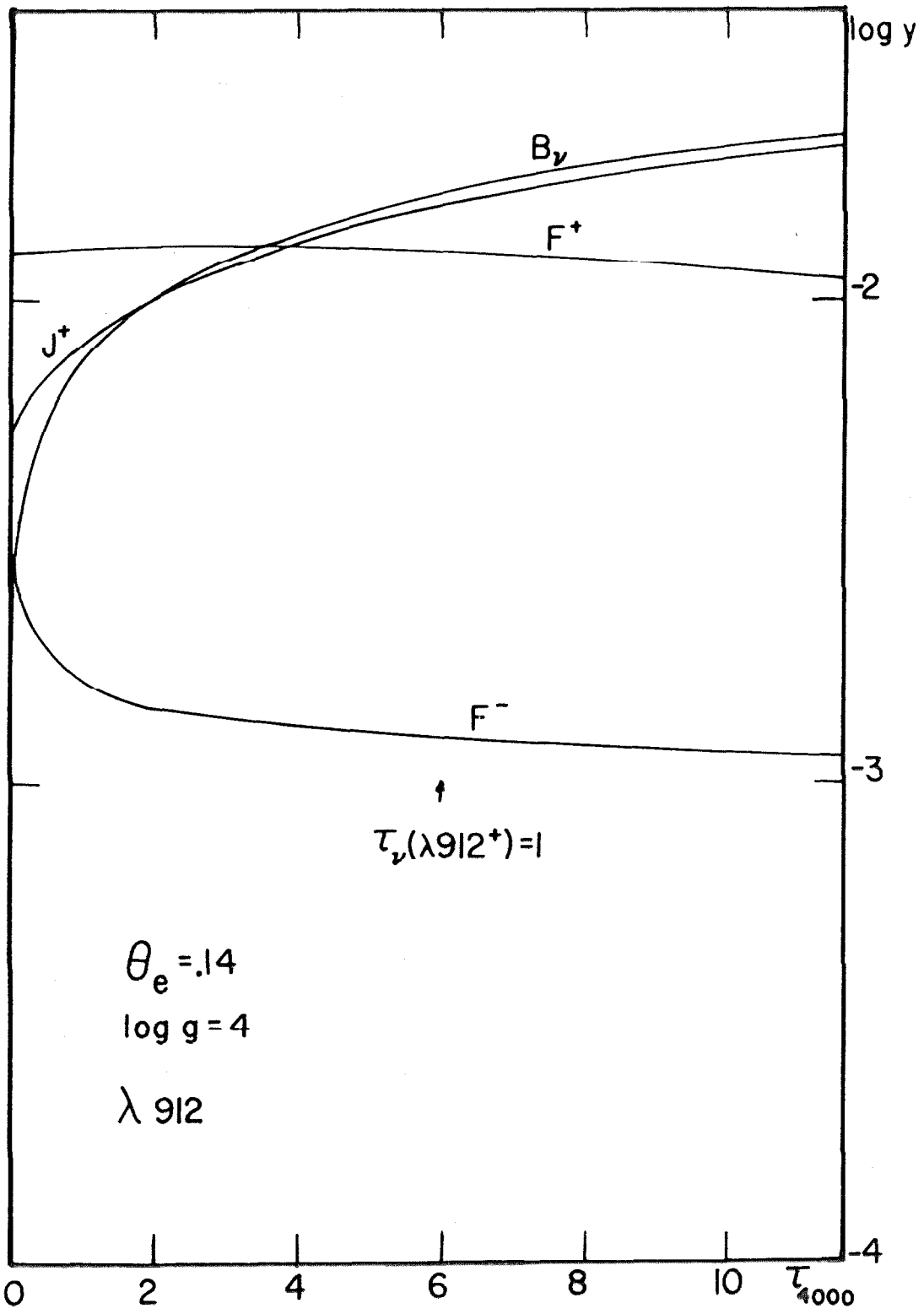
log y
B_ν
F^+
J^+
F^-
-2
-3
-4
$\tau_\nu(\lambda 912^+)=1$
$\theta_e = .14$
log g = 4
λ 912
0
2
4
6
8
10
τ_{4000}

Fig. 7

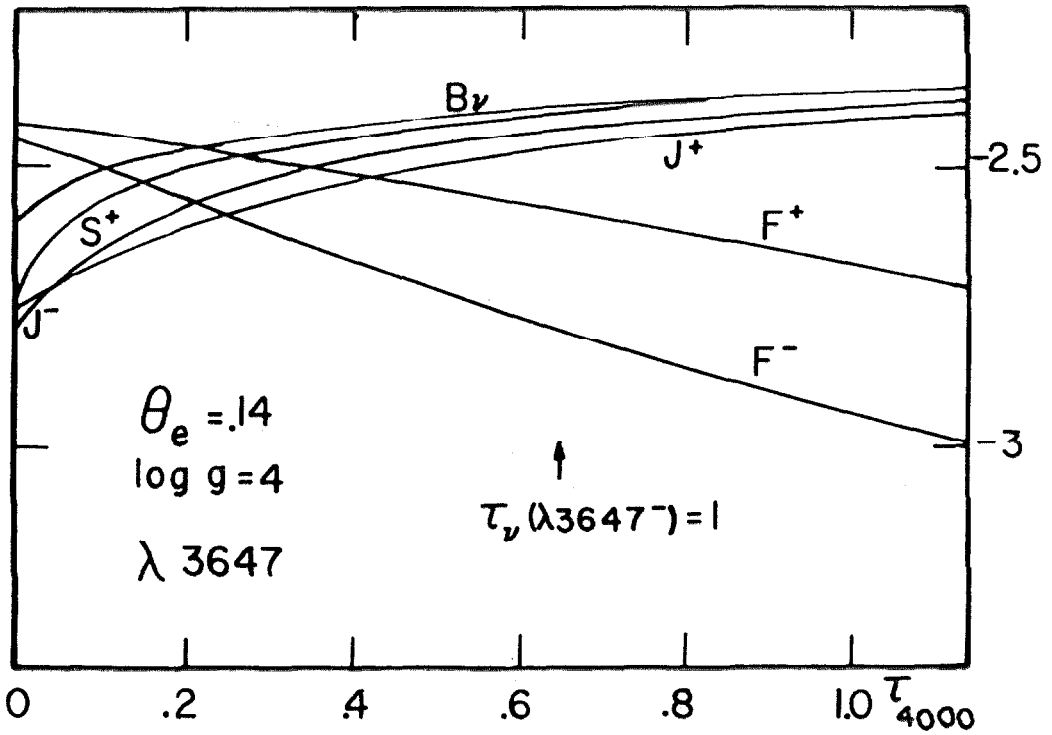
Bν
J+
F+
S+
J−
F−
θe =.14
log g =4
λ 3647
τν(λ3647−)=1
-2.5
-3
0
.2
.4
.6
.8
1.0
τ4000

Fig. 8

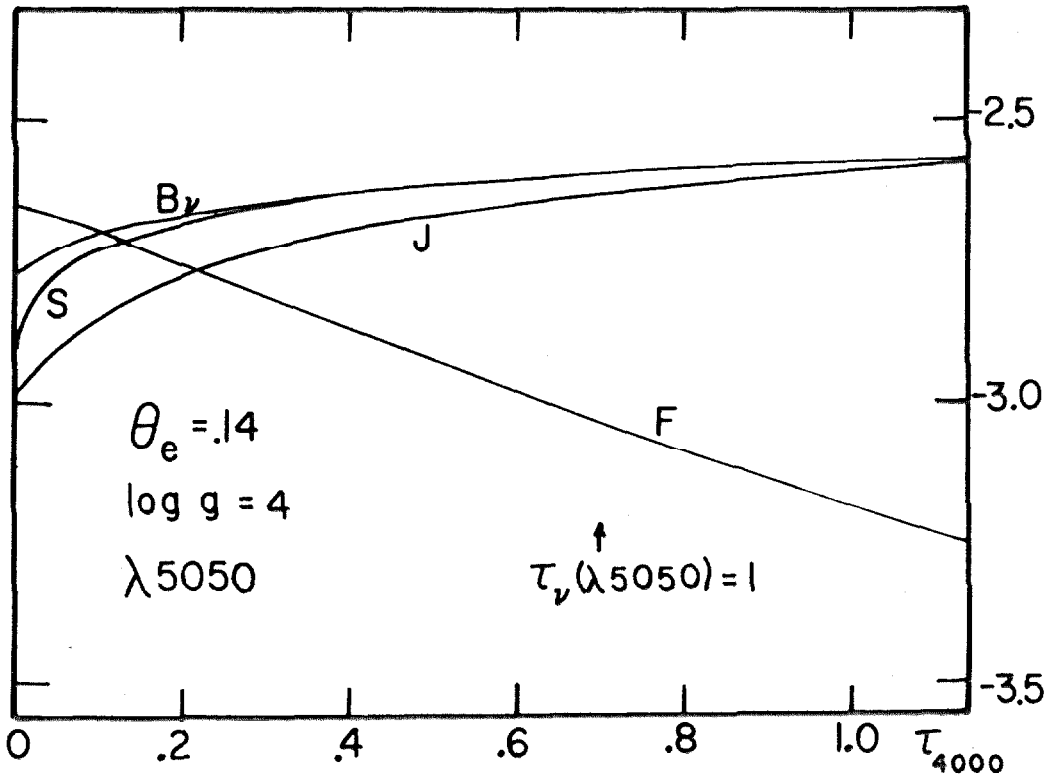
Bν
J
S
F
θe =.14
log g = 4
λ5050
τν(λ5050)=1
-2.5
-3.0
-3.5
0
.2
.4
.6
.8
1.0
τ4000

Fig. 9

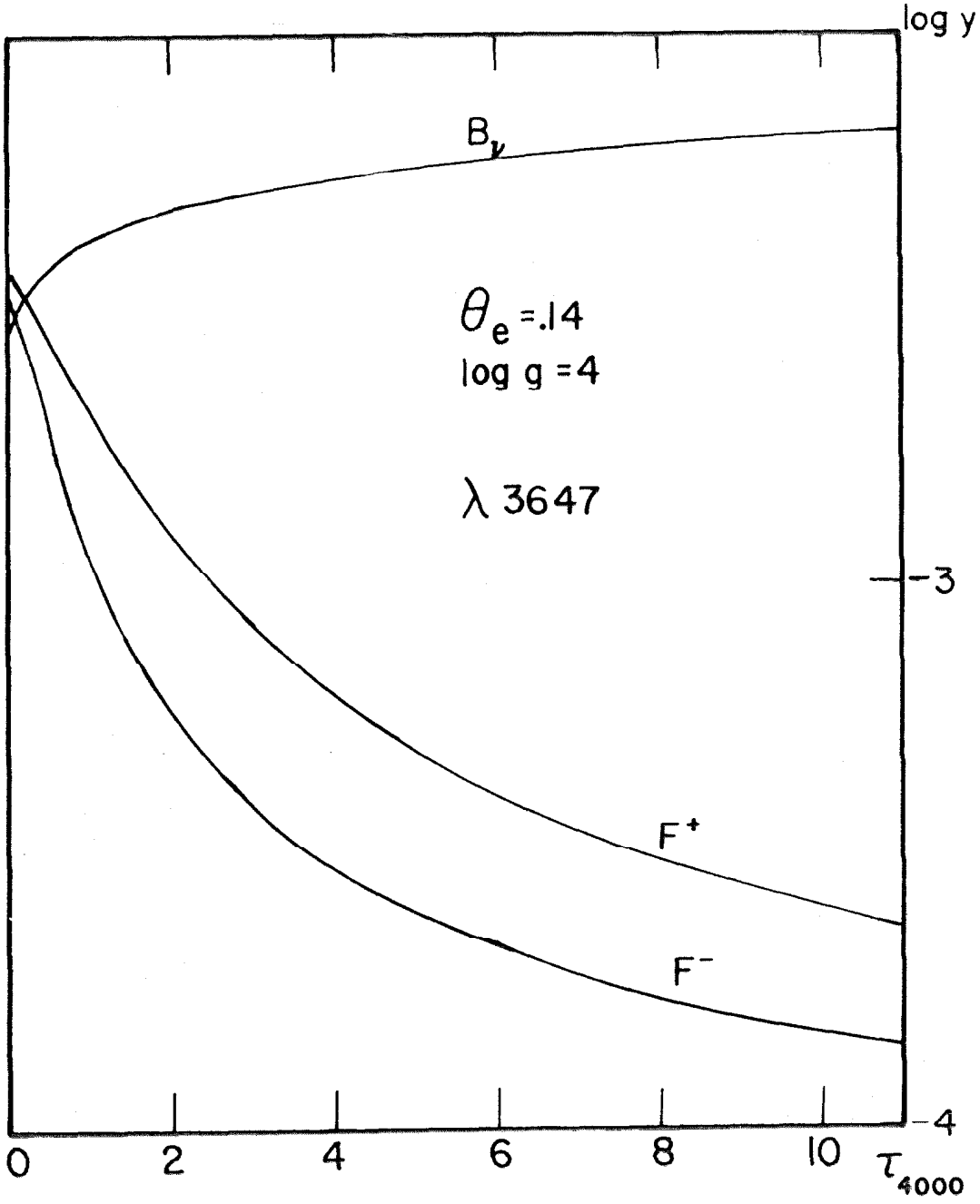

Fig. 10

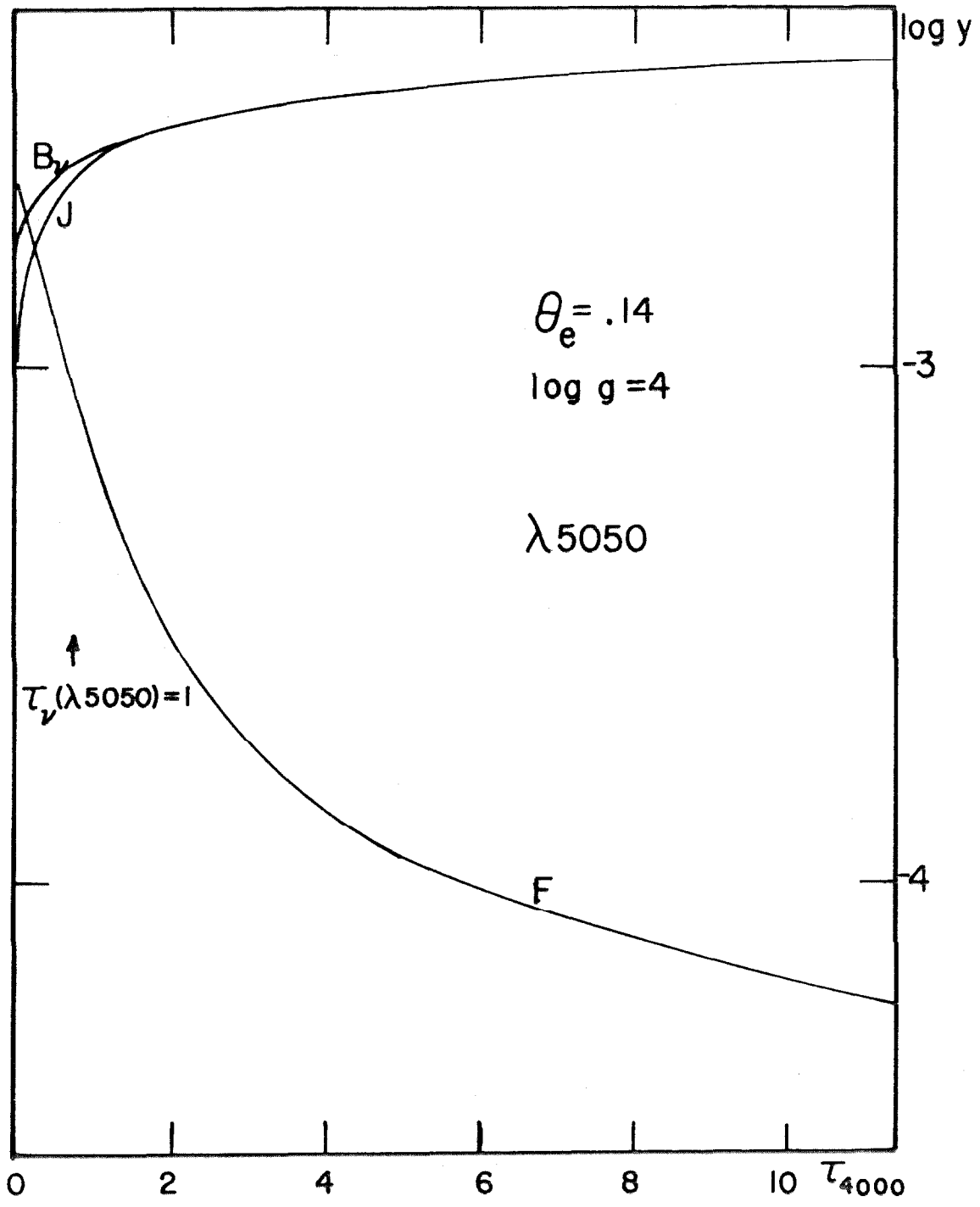
log y
B_ν
J
$\theta_e = .14$
log g =4
λ5050
$\tau_\nu(\lambda 5050)=1$
F
-3
-4
0
2
4
6
8
10
τ_{4000}

Fig. 11

for frequencies, and may show order of magnitude differences from B_ν as well as sharp reversals as shown before in figure 4. These order of magnitude differences occur only when scattering is important and the frequency under consideration is relatively far in the ultraviolet, so that Wien's approximation holds for B_ν. Then even a shallow temperature gradient causes a very rapid variation of B_ν, while J_ν shows only the relatively slow variation of a quasi-grey solution.

Having the monochromatic intensities and fluxes we now may form $\int_o^{\nu_o} F_\nu d\nu$ and $\int_o^{\nu_o} J_\nu d\nu$ where ν_o is the highest frequency considered; this is done by direct numerical quadrature using Newton-Cotes formulae over the frequency points. In all cases the highest frequency carried is adequate for the computation of the emergent fluxes, but it is possible that in the $\theta = 0.25$ model frequencies beyond the Lyman limit should have been considered at great depths in the model. It is unlikely, however, that serious errors were made since graphical inspection of all of the physical characteristics of this model show them to be perfectly well behaved compared to those of neighboring models. If ν_L represents the lowest frequency considered, the contribution $\int_o^{\nu_L}$ should not be neglected. The Rayleigh-Jeans approximation for B_ν must be valid for $\nu < \nu_L$, and we argue that aside from a normalization constant, a ν^2 law should be a good approximation for J_ν and F_ν as well. Thus we include terms of the form $F_\nu = F(\nu_L)(\nu/\nu_L)^2$ for $\nu < \nu_L$ so that $\int_o^{\nu_L} F_\nu d\nu = \frac{1}{3}\nu_L F(\nu_L)$, and similarly for $\int_o^{\nu_L} J_\nu d\nu$. This procedure should account for the infrared tails quite adequately.

It is of interest to form also the integrals $\int \kappa_\nu J_\nu d\nu$, $\int \kappa_\nu B_\nu d\nu$, $4\pi\int \frac{\sigma_\nu J_\nu d\nu}{h\nu}$, $4\pi\int \frac{\kappa_\nu J_\nu d\nu}{h\nu}$ and $4\pi\int \frac{\kappa_\nu B_\nu d\nu}{h\nu}$ which are also computed by direct numerical quadrature. The first two integrals are of value in enforcing the condition of radiative equilibrium; the third integral gives us a measure of the effects of scattering; the remaining three may be identified with the number of scattering, absorptions and emissions respectively. Figure 12 shows a plot of the first three integrals as a function of depth for the model previously illustrated; the curves for other models are extremely similar in shape, differing basically by a scale factor. We find from graphs of $\int J_\nu d\nu$ that the scale factor is <u>not</u> proportional to T_e^4 as is required by elementary theory. The relative size of $\int \sigma_\nu J_\nu d\nu$ to $\int \kappa_\nu J_\nu d\nu$ shows a striking increase with increasing temperature at the highest temperature considered; thus with $\theta_e = 0.18$, 0.157, 0.14, and 0.101, the ratio of $\int \kappa_\nu J_\nu d\nu$ to $\int \sigma_\nu J_\nu d\nu$ is about 16.6, 8.8, 6.0, and 1.48 respectively.

In strict thermodynamic equilibrium, the last two integrals above should be equal when collisional ionizations can be neglected (Böhm, 1960), which is the case for H and He under the conditions relevant here. In practice, after constructing a model atmosphere, we may check the consistency of the assumption of LTE by forming the ratio:

$$C = \frac{\int \frac{\kappa_\nu J_\nu d\nu}{h\nu}}{\int \frac{\kappa_\nu B_\nu d\nu}{h\nu}} \qquad (2.42)$$

When this ratio is 1, the model is self-consistent; appreciable deviations of this ratio from 1 may indicate substantial deviations from LTE. It

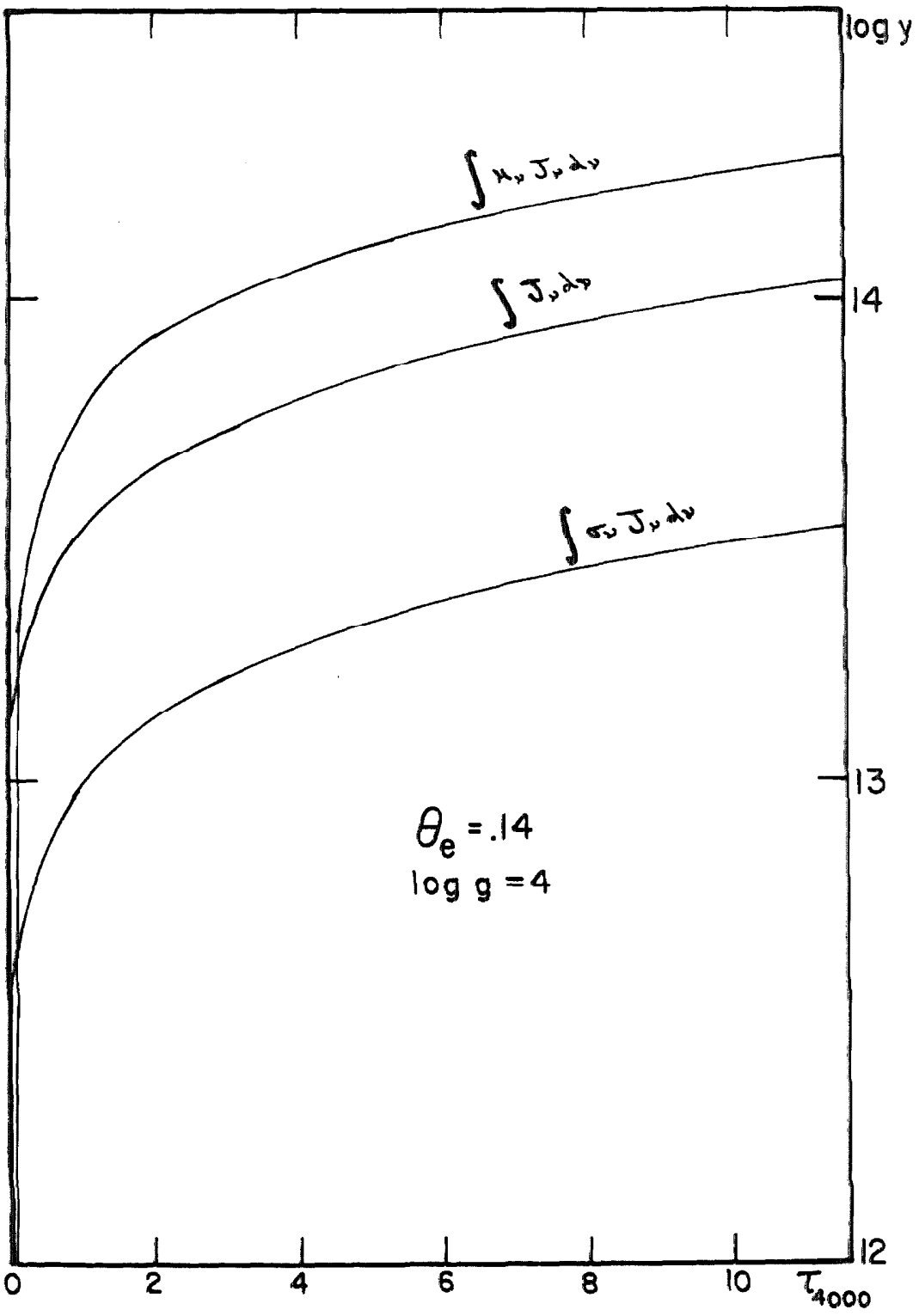
log y
$\int \kappa_\nu J_\nu d\nu$
$\int J_\nu d\nu$
$\int \sigma_\nu J_\nu d\nu$
14
13
12
$\theta_e = .14$
log g = 4
0
2
4
6
8
10
τ_{4000}

Fig. 12

comes as no particular surprise that such deviations are in fact found near the surface of the models as is shown for typical models in figure 13. C as a function of depth is given for each model in Appendix I.

It should be noted here that the upper limit of integration in practice is only ν_o, the highest frequency considered in the model; this will tend to emphasize the difference between the two integrals, particularly when ν_o corresponds to the Lyman edge. This is true because since κ_ν is generally huge when $\lambda < 912\,\text{Å}$, J_ν must be $\equiv B_\nu$ except for $\tau_\nu < 1$. Thus an appreciable contribution of the form $\int_o^\infty \frac{\kappa_\nu B_\nu d\nu}{h\nu}$ must be added to each integral. This clearly works in the direction of making the ratio more nearly unity. At the very surface, however, the opposite is true since $J_\nu \approx \frac{1}{2} B_\nu$ (J_ν includes a hemisphere of empty space), and this may work in the direction of further increasing the deviation of the ratio from unity. When no frequencies shortward of the Lyman limit are included in the computations, to aid in the estimation of such effects we make the simplified assumption that the opacity is due to hydrogen and may be written as

$$\kappa_\nu = \kappa(\nu_o)\left(\frac{\nu_o}{\nu}\right)^3 (1-e^{-h\nu/kT}) = \frac{C^*}{\nu^3}(1-e^{-h\nu/kT})$$

where

$$C^* = \frac{1.045 \times 10^{-14}}{\mu' m_H} (C^3 \cdot 10^{12}) f_1 \bar{g} \qquad (2.44)$$

Here f_1 is the fraction of H that is neutral, $\bar{g}$ is a mean gaunt factor, and μ' is defined in equation 2.19. We then find:

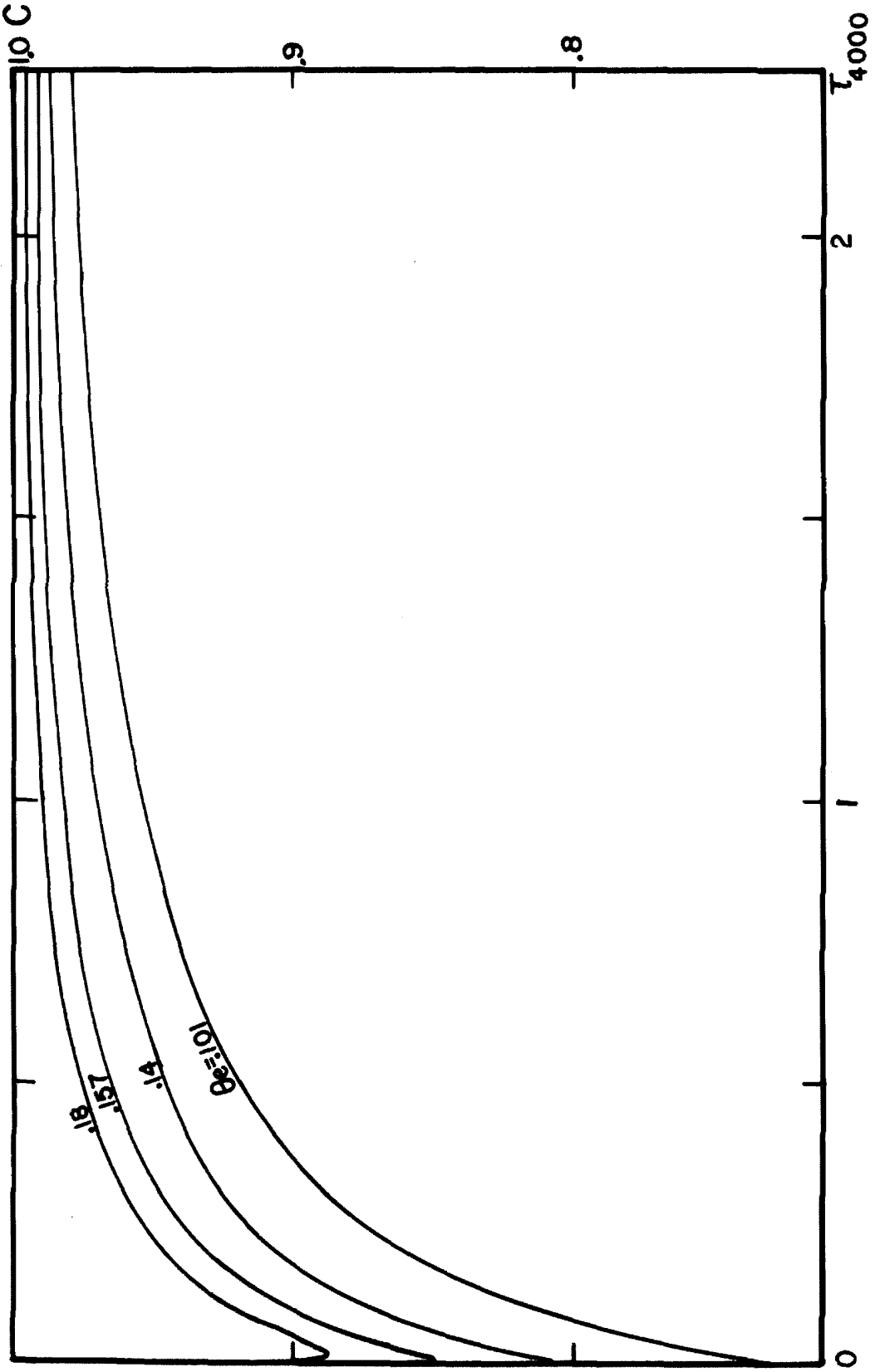

Fig. 13

$$\int_{\nu_o}^{\infty} \kappa_\nu B_\nu d\nu = \frac{2C^* kT}{C^2} e^{-k\nu_o/kT} = 2.26 \times 10^{20} \left(\frac{f_1}{\mu'}\right) e^{-13.6\theta} \qquad (2.45)$$

$$4\pi \int_{\nu_o}^{\infty} \frac{\kappa_\nu B_\nu d\nu}{h\nu} = \frac{8\pi C^*}{C^2} E_1\left(\frac{h\nu_o}{kT}\right) = 4 \times 10^{33} \left(\frac{f_1}{\mu'}\right) E_1(31.303\theta) \qquad (2.46)$$

$$\int_o^{\infty} \kappa_\nu \frac{\partial B_\nu}{\partial T} d\nu = \frac{2kC^*}{C^2} \sum_{m=1}^{\infty} \frac{1}{m^2} \left(m \frac{h\nu_o}{kT} + 1\right) e^{-mh\nu_o/kT}$$

$$\approx \frac{2kC^*}{C^2} \left(\frac{h\nu_o}{kT} + 1\right) e^{-k\nu_o/kT} = 4.48 \times 10^{16} \left(\frac{f_1}{\mu'}\right) (31.303\theta + 1) \cdot 10^{-13.6\theta} \qquad (2.47)$$

where we have set $\bar{g} = 0.9$ and made use of the fact, in equation 2.47 that usually $h\nu_o/kT >> 1$. The second integral is the one of interest in the present context, the others are useful in the temperature correction procedure. Computation of this integral usually shows it to be a quite substantial fraction of the total number of absorptions, so the surmise made above is correct. Nonetheless, we have (conservatively) not included this contribution in the values given for C in Appendix I, so the values given there represent the most pessimistic estimate of deviations from thermodynamic equilibrium. It is seen then that the deviations are really not too bad, for a study of continuum properties at least. At the same time we must realize that the integrals above conceal all detailed information about the distribution of the atoms in their individual states, so that the population of a given level may differ enormously from the LTE value even though the ratio studied here is about unity. Only a complete solution of the problem will answer all of the questions that may be raised concerning, for example,

the computation of line strengths.

Further numerical details

We should, for completeness, give the details of the numerical quadrature used in computing the flux and intensity integrals. This particular computation has proven one of the most difficult to deal with. This is due basically to two conflicting criteria: on the one hand the singular properties of the kernels $E_1(x)$ and $E_2(x)$ make it necessary to very carefully cover the interval of integration, and on the other hand the computations must be made as rapidly as possible because of the very large number of flux and intensity integrals necessary, which is compounded by the necessity of iterating to find the source function as described previously. Direct numerical integrations schemes fail in the latter respect, basically because the exponential integrals are rather time-consuming to compute even though elegant approximation formulae exist for them (Hastings, 1955). On the other hand, the use of quadrature formulae involving only two or three points (Chandrasekhar, 1950) is fast, but does not have the accuracy one would desire (Underhill, 1961) in view of the large number of intermediate steps required to construct a flux-constant atmosphere.

A compromise suggested by Cayrel (1961) has been adopted here. Basically the formulae are derived assuming the source function may be represented by a quadratic interpolating formula over some short interval, and the integrations against the exponential integrals may then be done explicitly. The result is a formula involving only the values of the ordinates and some weights for each of these ordinates. Thus the integrals may be done as quickly as the source functions may

be found; since the points are chosen on a τ_ν scale, while the source functions are tabulated at fixed points on a τ_{STD} scale (and thus at arbitrary points on a τ_ν scale) the source function is determined at the requisite points by interpolation in tables of $S(\tau)$. Thus the limit to the speed of the integration is determined by the speed of the interpolation; to this end special interpolators were written in machine language to allow interpolation forward and backward in a table starting from the last value interpolated at in the previous lookup. The time savings gained in the use of these special routines compared to the use of standard routines available on the library tape made the difference between doing the problem and finding the problem simply too expensive in terms of computing time. The Cayrel method has the advantage that the points in the integration may be chosen to be as close together as desired to insure accuracy. Cayrel has discussed the problem of doing the partial interval in $\int_0^{\tau_\nu}$, and this will not be re-discussed here. Tables 1 and 2 list the weights used in the present computations. The notation is the same as used by Cayrel and will not be redefined here. The formulae are exact for polynomials of order 2, and direct numerical tests against the Hopf function $q(\tau)$ have shown that they will give the correct fluxes and intensities to at least five places. Tests against $E_3(x)$, $E_4(x)$, $E_5(x)$ (which were interpolated from tables to simulate the interpolation of the source function) have shown no errors larger than 0.03% when compared with the values given by Kourganoff (1952). The formulae have been found to be roughly three times faster than direct numerical integration (which gave poorer accuracy) even before the special interpolators were devised.

TABLE 1

WEIGHTS FOR THE CALCULATION OF MEAN INTENSITY INTEGRALS

Interval		A	B	C	D
0.000 to	.002	-8.141 377(-5)	7.304 053(-3)	-5.842 500(-4)	1.000 000(-2)
.002	.004	3.498 020(-4)	4.668 703(-3)	2.355 927(-4)	5.639 391(-3)
.004	.006	-1.633 923(-3)	8.110 780(-3)	-1.724 014(-3)	4.948 241(-3)
.006	.008	7.040 058(-4)	3.033 577(-3)	6.574 573(-4)	4.544 771(-3)
.008	.010	-1.063 192(-3)	6.311 485(-3)	-1.103 938(-3)	4.259 082(-3)
.010	.015	1.224 223(-3)	7.278 768(-3)	1.057 052(-3)	1.009 482(-2)
.015	.020	1.550 182(-3)	5.740 567(-3)	1.432 222(-3)	9.093 583(-3)
.020	.025	1.093 399(-3)	6.008 440(-3)	1.001 822(-3)	8.386 769(-4)
.025	.030	1.039 875(-3)	5.607 608(-3)	9.651 558(-4)	7.841 271(-3)
.030	.040	2.508 441(-3)	9.280 321(-3)	2.277 802(-3)	1.479 559(-2)
.040	.050	2.078 163(-3)	8.874 467(-3)	1.899 548(-3)	1.340 632(-2)
.050	.060	2.031 475(-3)	7.975 232(-3)	1.887 529(-3)	1.233 949(-2)
.060	.070	1.838 989(-3)	7.548 133(-3)	1.718 372(-3)	1.147 653(-2)
.070	.080	1.797 889(-3)	6.944 865(-3)	1.694 325(-3)	1.075 419(-2)
.080	.100	3.366 012(-3)	1.281 565(-2)	3.026 343(-3)	2.026 941(-2)
.100	.125	3.794 569(-3)	1.431 385(-2)	3.379 752(-3)	2.278 655(-2)
.125	.150	3.370 736(-3)	1.285 444(-2)	3.039 791(-3)	2.029 282(-2)
.150	.175	3.036 461(-3)	1.166 221(-2)	2.763 420(-3)	1.830 577(-2)
.175	.200	2.779 067(-3)	1.062 937(-2)	2.548 518(-2)	1.666 732(-2)
.200	.225	2.530 776(-3)	9.810 552(-3)	2.332 311(-3)	1.528 313(-2)
.225	.250	2.350 029(-3)	9.034 620(-3)	2.176 966(-3)	1.409 238(-2)
.250	.275	2.169 493(-3)	8.400 065(-3)	2.016 593(-3)	1.305 353(-2)
.275	.300	2.020 598(-3)	7.816 405(-3)	1.884 462(-3)	1.213 701(-2)
.300	.350	3.768 690(-3)	1.412 793(-2)	3.304 635(-3)	2.264 192(-2)
.350	.400	3.308 779(-3)	1.243 716(-2)	2.926 472(-3)	1.985 538(-2)
.400	.450	2.925 331(-3)	1.103 967(-2)	2.604 490(-3)	1.755 950(-2)
.450	.500	2.602 697(-3)	9.860 377(-3)	2.329 494(-3)	1.563 328(-2)
.500	.600	4.651 701(-3)	1.680 320(-2)	3.775 070(-3)	2.798 868(-2)
.600	.700	3.777 631(-3)	1.373 393(-2)	3.106 799(-3)	2.271 898(-2)
.700	.800	3.108 708(-3)	1.135 613(-2)	2.582 907(-3)	1.868 844(-2)
.800	.900	2.583 396(-3)	9.476 672(-3)	2.163 695(-3)	1.552 983(-2)
.900	1.00	2.164 580(-3)	7.964 810(-3)	1.824 880(-3)	1.300 920(-2)
1.00	1.10	1.825 602(-3)	6.734 115(-3)	1.547 579(-3)	1.096 920(-2)
1.10	1.20	1.547 579(-3)	5.723 211(-3)	1.317 822(-3)	9.299 545(-3)
1.20	1.40	2.626 877(-3)	9.054 760(-3)	1.925 463(-3)	1.584 084(-2)
1.40	1.60	1.928 245(-3)	6.684 311(-3)	1.430 837(-3)	1.162 193(-2)
1.60	1.80	1.432 409(-3)	4.988 350(-3)	1.073 198(-3)	8.630 834(-3)
1.80	2.00	1.074 280(-3)	3.754 999(-3)	8.111 819(-4)	6.471 313(-3)
2.00	2.50	1.996 845(-3)	5.864 546(-3)	1.006 879(-3)	1.222 513(-2)
2.50	3.00	1.019 288(-3)	3.029 689(-3)	5.289 204(-4)	6.228 730(-3)
3.00	4.00	1.027 597(-3)	2.417 443(-3)	2.768 068(-4)	6.524 191(-3)
4.00	5.00	2.990 118(-4)	7.166 471(-4)	8.522 207(-5)	1.889 676(-3)
5.00	6.00	9.110 919(-5)	2.210 536(-4)	2.694 246(-5)	5.741 478(-4)
6.00	8.00	5.206 675(-5)	8.741 266(-5)	2.580 520(-6)	3.600 825(-4)
8.00	12.0	8.859 564(-6)	8.726 995(-6)	-7.391 918(-7)	7.533 125(-5)
12.0	20.0	1.558 821(-7)	7.933 380(-8)	-1.380 576(-8)	1.900 433(-6)

TABLE 2

WEIGHTS FOR THE CALCULATION OF FLUX INTEGRALS

Interval		A	B	C	D
0.000 to	.002	-1.959 220(-3)	7.907 550(-3)	-1.976 887(-3)	4.000 000(-3)
.002	.004	-2.730 598(-3)	9.395 957(-3)	-2.739 931(-3)	3.946 893(-3)
.004	.006	-8.767 892(-3)	2.143 351(-2)	-8.779 963(-3)	3.904 860(-3)
.006	.008	1.299 885(-4)	3.597 535(-3)	1.217 062(-4)	3.866 997(-3)
.008	.010	-1.033 753(-2)	2.450 386(-2)	-1.035 122(-2)	3.831 837(-3)
.010	.015	3.176 285(-4)	8.798 856(-3)	2.829 484(-4)	9.496 705(-3)
.015	.020	1.694 555(-3)	5.857 505(-3)	1.665 055(-3)	9.305 504(-3)
.020	.025	9.599 307(-4)	7.159 087(-3)	9.300 629(-4)	9.131 045(-3)
.025	.030	3.786 136(-4)	8.162 724(-3)	3.507 785(-4)	8.968 972(-3)
.030	.040	2.852 698(-3)	1.173 539(-2)	2.759 421(-3)	1.763 344(-2)
.040	.050	2.502 011(-3)	1.189 466(-2)	2.413 485(-3)	1.707 078(-2)
.050	.060	2.649 013(-3)	1.109 811(-2)	2.568 850(-3)	1.655 669(-2)
.060	.070	2.648 958(-3)	1.063 359(-2)	2.573 925(-3)	1.608 092(-2)
.070	.080	2.349 971(-3)	1.079 599(-2)	2.280 067(-3)	1.563 670(-2)
.080	.100	5.013 771(-3)	1.988 566(-2)	4.757 139(-3)	3.043 844(-2)
.100	.125	6.022 910(-3)	2.334 458(-2)	5.664 665(-3)	3.612 725(-2)
.125	.150	5.635 201(-3)	2.204 925(-2)	5.314 127(-3)	3.397 843(-2)
.150	.175	5.289 703(-3)	2.087 741(-2)	4.998 082(-3)	3.205 194(-2)
.175	.200	5.071 517(-3)	1.961 905(-2)	4.805 927(-3)	3.030 573(-2)
.200	.225	4.717 288(-3)	1.877 695(-2)	4.472 211(-3)	2.871 003(-2)
.225	.250	4.509 045(-3)	1.776 377(-2)	4.283 059(-3)	2.724 267(-2)
.250	.275	4.293 491(-3)	1.687 315(-3)	4.083 012(-3)	2.588 650(-2)
.275	.300	4.086 737(-3)	1.605 768(-2)	3.890 787(-3)	2.462 790(-2)
.300	.350	7.807 836(-3)	2.983 594(-2)	7.101 055(-3)	4.691 152(-2)
.350	.400	7.115 910(-3)	2.715 588(-2)	6.494 066(-3)	4.267 127(-2)
.400	.450	6.482 936(-3)	2.483 418(-2)	5.930 709(-3)	3.893 680(-2)
.450	.500	5.932 990(-3)	2.274 374(-2)	5.439 529(-3)	3.562 291(-2)
.500	.600	1.087 035(-2)	4.004 706(-2)	9.190 013(-3)	6.532 877(-2)
.600	.700	9.192 899(-3)	3.396 645(-2)	7.819 477(-3)	5.523 679(-2)
.700	.800	7.823 156(-3)	2.896 404(-2)	6.687 548(-3)	4.698 943(-2)
.800	.900	6.685 173(-3)	2.481 881(-2)	5.737 600(-3)	4.017 034(-2)
.900	1.00	5.740 998(-3)	2.133 660(-2)	4.944 345(-3)	3.448 082(-2)
1.00	1.10	4.944 206(-3)	1.840 713(-2)	4.270 813(-3)	2.969 910(-2)
1.10	1.20	4.270 487(-3)	1.592 413(-2)	3.698 050(-3)	2.565 622(-2)
1.20	1.40	7.377 425(-3)	2.577 454(-2)	5.566 352(-3)	4.444 164(-2)
1.40	1.60	5.571 637(-3)	1.953 337(-2)	4.234 677(-3)	3.355 597(-2)
1.60	1.80	4.238 263(-3)	1.490 116(-2)	3.240 630(-3)	2.522 128(-2)
1.80	2.00	3.243 051(-3)	1.142 947(-2)	2.492 033(-3)	1.952 610(-2)
2.00	2.50	6.144 434(-3)	1.831 940(-2)	3.212 147(-3)	3.753 427(-2)
2.50	3.00	3.244 899(-3)	9.754 509(-3)	1.730 055(-3)	1.979 770(-2)
3.00	4.00	3.364 056(-3)	8.027 911(-3)	9.466 074(-4)	2.128 385(-2)
4.00	5.00	1.014 367(-3)	2.455 033(-3)	2.977 178(-4)	6.396 460(-3)
5.00	6.00	3.167 167(-4)	7.740 129(-4)	9.566 080(-5)	1.992 939(-3)
6.00	8.00	1.846 060(-4)	3.124 592(-4)	9.780 400(-6)	1.273 030(-3)
8.00	12.0	3.223 516(-5)	3.196 989(-5)	-2.672 852(-6)	2.731 012(-4)
12.0	20.0	5.829 295(-7)	2.978 730(-7)	-5.174 127(-8)	7.086 628(-6)

One final numerical detail we must mention is that a r essary evil forced upon us is table extrapolation. This occurs in the llowing places:

1. Extension of tables of S_ν (or B_ν) to compute flux If $\tau_\nu(\tau = 60) - \tau_\nu$ (at the last depth at which S_ν is to be found) is 10, the upper limit in the flux quadrature, then the table is extrapolated by making a least squares fit of the form $S_\nu = a + b\tau + c\sqrt{\tau}$ to the last five points of the table. This fitting function is admittedly quite arbitrary, but it has the desirable property of not running away a large depth while still accounting for some curvature in S_ν. Tests have shown that the answers are reasonable, and since this region often contributes only negligibly to the final F_ν, the errors made here are not serious.

2. Extension of tables of ρ_ν and Δ_m in solving the Milne equation. Here only linear extrapolation could be used because other functions were unstable. ρ_ν may go negative, in which case it is set to zero.

3. Extrapolation of $dp_r/d\tau$ and $T(\tau)$. Since the monochromatic fluxes are available only to some fixed depth and the temperature corrections extend only to the same depth, the tables of these functions must be extrapolated. The same fitting function is used as in 1 above. In the case of T, the fit is made to $\frac{4}{3}(T/T_e)^4$ which in the grey case is linear at depth. Earlier models $dp_r/d\tau$ was extrapolated using a function of the form $a + b\tau + c\tau^2$ which often blew up in the interior and even caused negative pressure gradients at the last two points of the atmosphere in some cases. The present function does not have this undesirable property, but may tend to zero at depth. It is now evident

that the proper way to extrapolate $dp_r/d\tau$ is to recognize that at depth p_r approaches $\frac{1}{3}aT^4$ so that $dp_r/d\tau$ must go to $\frac{4}{d}T^3\frac{dT}{d\tau}$.

5. The temperature correction procedure

Having now computed all of the quantities describing the radiation field, we examine the atmosphere to see if the model satisfies the condition of radiative equilibrium. In particular we demand that

$$\int \kappa_\nu B_\nu d\nu = \int \kappa_\nu J_\nu d\nu \qquad (2.48)$$

and (logically equivalent) that

$$\int F_\nu d\nu = \text{constant} = \frac{\sigma T_e^4}{\pi} \qquad (2.49)$$

These two criteria are the same in principle, but are quite different in practice. Several authors have attacked the problem of satisfying these conditions with varying degrees of success (e.g. Osawa, 1956; Swihart, 1956a, 1956b, 1956c; Przybylski, 1955). Gingerich (1961) has discussed these earlier attempts in detail, and has given a good discussion of the practical differences in the two requirements, so no discussion will be given here. Recently, a fundamental advance in the problem has been offered by Krook (1963), and by Avrett and Krook (1963). Application of these new methods to the case where scattering is neglected has been made by Gingerich (1962). For logical completeness, we will review the Krook equations here and show how they have been extended in a very simple way to account for the effects of scattering. Some time after the present equations had been used with good success, an extension of the Krook-Averett procedure to the scattering

case by those authors became available (Avrett and Krook, 1962). Since the equations used here are so very much simpler than those suggested in the paper just cited, and since satisfactory convergence is obtained in practice, no attempt was made to use the extended procedure as suggested by Avrett and Krook.

The monochromatic equation of transfer is:

$$\mu \frac{\partial I_\nu}{\partial \tau_\nu} = I_\nu - B_\nu \qquad (2.50)$$

Now write $\eta_\nu = \kappa_\nu / \kappa$, where κ is the opacity at the standard frequency. Then:

$$\mu \frac{\partial I_\nu}{\partial \tau} = \eta_\nu [I_\nu - B_\nu] \qquad (2.51)$$

We now attempt to derive a correction to both the temperature and the depth distribution in such a way as to improve the constancy of the flux in the atmosphere. In particular, let the improved temperature T be given in terms of the present temperature T_o and a correction T_1, and the improved depth τ be given in terms of the present depth t and a correction τ_1, so that

$$T = T_o + \lambda T_1 + \ldots \qquad (2.52)$$

and

$$\tau = t + \lambda \tau_1 + \ldots \qquad (2.53)$$

Then expand all quantities relevant to the radiation field in terms of their present values and first order corrections depending upon the corrections in depth and temperature. Thus we write:

$$I_\nu = I_\nu^o + \lambda I_\nu^1 + \ldots \tag{2.54}$$

$$\eta_\nu(\tau) = \eta_\nu(t) + \lambda \tau_1 \eta_\nu'(t) \tag{2.55}$$

$$B_\nu = B_\nu(T_o) + \lambda T_1 \dot{B}_\nu(T_o) + \ldots \tag{2.56}$$

where $'$ denotes d/dt and $\cdot$ denotes $(\partial/\partial T)_o$. λ is a separation parameter. Then substituting into the equation of transfer we find:

$$\mu\left[\frac{\partial I_\nu^o}{\partial t} + \lambda \frac{\partial I_\nu^1}{\partial t} + \ldots\right]$$

$$= \left[1 + \lambda\tau_1' + \ldots\right]\left[\eta_\nu + \lambda\tau_1\eta_\nu' + \ldots\right]\left[I_\nu^o + \lambda I_\nu^1 + \ldots - B_\nu(T_o) - \lambda \dot{B}_\nu T_1 + \ldots\right] \tag{2.57}$$

Now collecting terms of equal order in λ, and setting $\lambda = 1$ we have:

Zero order equation:

$$\mu \frac{\partial I^o}{\partial t} = \eta_\nu\left[I_\nu^o - B_\nu(T_o)\right] \tag{2.58}$$

or

$$\frac{dH_\nu^o}{dt} = \eta_\nu\left[J_\nu^o - B_\nu(T_o)\right] \tag{2.59}$$

First order equation:

$$\mu \frac{\partial I_\nu^1}{\partial t} = \eta_\nu\left[I^1 - T_1 \dot{B}_\nu(T_o)\right] + \left[\tau_1'\eta_\nu + \eta_\nu'\tau_1\right]\left[I_\nu^o - B_\nu(T_o)\right] \tag{2.60}$$

Now define:

$$\mathcal{H} = \frac{T_e^4}{4\pi}\ , \quad H_\nu^o = \frac{1}{2}\int_{-1}^{+1} \mu I_\nu^o \, d\mu\ , \quad H^o = \int_o^\infty H_\nu^o d\nu$$

$$H_\nu^1 = \frac{1}{2}\int_{-1}^{+1} \mu I_\nu^1 \, d\mu\ , \qquad H^1 = \int H_\nu^1 d\nu$$

$$\mathcal{H} = H^o + H^1$$

We now assume that the Eddington approximation is valid for the perturbations in J_ν so that

$$J_\nu^1(0) = \sqrt{3}\, H_\nu^1(0) = \sqrt{3}\, H_\nu^o(0)\left[\frac{H^1}{H^o}\right] \tag{2.61}$$

and

$$K_\nu^1 = \frac{1}{2}\int_{-1}^{+1} \mu^2 I\, d\mu = \frac{1}{3} J_\nu^1 \tag{2.62}$$

Taking the first moment against μ of the first order equation we find:

$$\frac{\partial K_\nu^1}{\partial t} = \frac{1}{3}\frac{\partial J_\nu^1}{\partial t} = \eta_\nu H_\nu^1 + \left[\tau_1 \eta_\nu' + \tau_1' \eta_\nu\right] H_\nu^o \tag{2.63}$$

To solve this equation readily we demand:

$$\frac{\partial J_\nu^1}{\partial t} = 0 \tag{2.64}$$

(this is not a restrictive assumption in the sense that it merely lumps further terms into the specification of τ_1). Then:

$$\tau_1' = -\tau_1\left[\frac{\int_o^\infty H_\nu^o \frac{\eta_\nu'}{\eta_\nu}\, d\nu}{H^o}\right] + \left(1 - \frac{\mathcal{H}}{H^o}\right) \tag{2.65}$$

Equation 2.65 is to be solved subject to the boundary condition that $\tau_1(0) = 0$. An analytical solution may be written for this linear equation, but it is simpler to effect the solution by direct numerical integration, which in this case was done using a fourth order Runge-Kutta formula. Thus we have obtained the depth correction. To obtain a second equation, which will yield the temperature correction, we integrate equation 2.60 over angle and obtain

$$\frac{\partial H_\nu^1}{\partial t} = \eta_\nu\left[J_\nu^1 - T_1\dot{B}_\nu(T_o)\right] + \left[\tau_1\eta_\nu' + \tau_1'\eta_\nu\right]\left[J_\nu^o - B_\nu(T_o)\right] \qquad (2.66)$$

Making use of the relations

$$\frac{dH^1}{dt} = -\frac{dH^o}{dt} \qquad (2.67)$$

and

$$\int \eta_\nu J_\nu^1 d\nu = \sqrt{3}\left[\frac{H^1(0)}{H^o(0)}\right]\int \eta_\nu H_\nu^o(0)d\nu = \sqrt{3}\left[1 - \frac{\mathcal{K}}{H^o(0)}\right]\int \eta_\nu H_\eta^o(0)d\nu \qquad (2.68)$$

we find after integrating over frequency and grouping terms:

$$T_1 = \frac{1}{\int_o^\infty \eta_\nu \dot{B}_\nu(T_o)d\nu}\left\{(1+\tau_1')\frac{dH^o}{dt} - \sqrt{3}\left[1 - \frac{\mathcal{K}}{H^o(0)}\right]\int_o^\infty \eta_\nu H_\nu^o(0)d\nu + \tau_1\int_o^\infty (J_\nu - B_\nu)\eta_\nu d\nu\right\} \qquad (2.69)$$

Since we have already determined τ_1 and τ_1' from the solution of equation 2.65 we have all of the information required to determine the temperature correction T_1. In the solution of equations 2.65 and 2.69 η_ν' is obtained by direct numerical differentiation; $\frac{dH^o}{dt}$ is unstable if computed by numerical differentiation, so we substitute for it $\int \eta_\nu(J_\nu^o - B_\nu(T_o))d\nu$, obtained from equation 2.59.

Thus we have the distribution $T = T_o + T_1$ at the points $\tau = t + \tau_1$. By interpolation in this relation we find T at the standard values of τ adopted for the computation of the models. The model may then be recomputed using these corrected values for $T(\tau)$.

When scattering terms are present, the corrections to the temperature and depth distributions are, in principle much more difficult to obtain both because of the more complicated form of the source function and because of the decoupling of the radiation field from the local temperature distribution by the scattering terms. As mentioned above, an elaborate set of correction formulae has been given by Avrett and Krook (1962). A simplified approach is possible, however, by noting the analogy in the formalism between the pure absorption case and the scattering case with S_ν in the equation of transfer instead of B_ν:

$$\mu \frac{\partial I_\nu}{\partial \tau_\nu} = I_\nu - S_\nu = I_\nu - [(1-\rho_\nu)B_\nu + \rho_\nu J_\nu] \qquad (2.70)$$

Now let

$$\eta_\nu = \frac{\kappa_\nu + \sigma_\nu}{(\kappa_\nu + \sigma_\nu)_{STD}} \qquad (2.71)$$

so that in analogy to equation 2.51:

$$\mu \frac{\partial I_\nu}{\partial t} = \eta_\nu \cdot \frac{d}{dt} [I_\nu - ((1-\rho_\nu)B_\nu + \rho_\nu J_\nu)] \qquad (2.72$$

Expanding as in equations 2.52 through 2.56 with the additional equation:

$$\rho_\nu = \rho_\nu(t) + \tau_1 \rho'_\nu(t) + \ldots \qquad (2.73)$$

we find:

(zero order) $$\mu \frac{\partial I^o_\nu}{\partial t} = \eta_\nu [I^o_\nu - (\rho_\nu J_\nu + (1-\rho_\nu)B_\nu] \qquad (2.74)$$

and

$$\text{(first order)} \quad \mu \frac{\partial I_\nu^1}{\partial t} = (\tau_1' \eta_\nu + \tau_1 \eta_\nu')[I_\nu^o - (\rho_\nu J_\nu + (1-\rho_\nu) B_\nu)]$$

$$+ \eta_\nu [I_\nu^1 + \rho_\nu' \tau_1 (B_\nu - J_\nu^o) - (\rho_\nu J_\nu + (1-\rho_\nu) T_1 \dot{B}_\nu)] \qquad (2.75)$$

This treatment differs from that of Avrett and Krook for scattering in that explicit derivatives of ρ_ν, κ_ν and σ_ν with respect to the temperature are not taken, but are lumped implicitly in η_ν' and ρ_ν'.

Integrating the first order equation over angle as before and taking its first moment again assuming equations 2.61, 2.62 and 2.64, we find precisely the same equation as before for the depth correction while the temperature correction is given by:

$$T_1 = \frac{1}{\int_o^\infty \eta_\nu (1-\rho_\nu) \dot{B}_\nu d\nu} \left\{ (1+\tau_1') \int_o^\infty \eta_\nu (1-\rho_\nu)(J_\nu^o - B_\nu) d\nu \right.$$

$$\left. + \tau_1 \int_o^\infty [\eta_\nu' (1-\rho_\nu) - \eta_\nu \rho_\nu'] (J_\nu - B_\nu) d\nu + \sqrt{3} \left(\frac{\mathcal{H}}{H^o} - 1 \right) \int_o^\infty H_\nu^o (1-\rho_\nu) \eta_\nu d\nu \right\} \qquad (2.76)$$

which again may be computed directly once equation 2.65 has been integrated to give the depth correction.

Generally speaking this correction procedure has been found to be both stable and effective. If a grey distribution is assumed to construct the initial model, characteristically the flux predicted becomes much too large in the interior (perhaps by a few hundred per cent). The first few temperature corrections have their greatest effect

in bringing the flux in the interior to its proper value. Convegence generally becomes quite slow after several iterates, and it is important from the standpoint of economy to make as good a first guess at the temperature distribution as possible; in practice we have taken fairly large temperature jumps between successive models, and then interpolated the temperature distributions for intermediate models. Because of rather unexpected peculiarities of the shape of the temperature distributions along a temperature sequence, this sometimes trapped us into making very bad first guesses (see the results displayed in Chapter 3). When scattering is important the flux usually deviates several per cent too low at the boundary if the Milne-Eddington equation is not solved. This comes about since merely setting $S_\nu = B_\nu$ does not account for the efficient radiation leak provided efficiently in the ultraviolet by scattering, and the local B_ν at the surface simply cannot provide adequate flux.

Figures 14 and 15 show the deviations from flux constancy for a typical model. The curve with vertical hash marks is the result after two corrections, ignoring scattering, the curve marked with open circles is after three corrections, and the curve with horizontal hash marks is after four corrections. Note that after the third correction, the convergence in the interior is complete and there is an improvement only at the boundary. The effects of scattering were next accounted for and the Milne equations solved, resulting in the curve marked with filled circles. One iteration using equations 2.65 and 2.76 resulted in the plain curve. These results show clearly the important effect of the scattering terms near the surface. The general procedure of

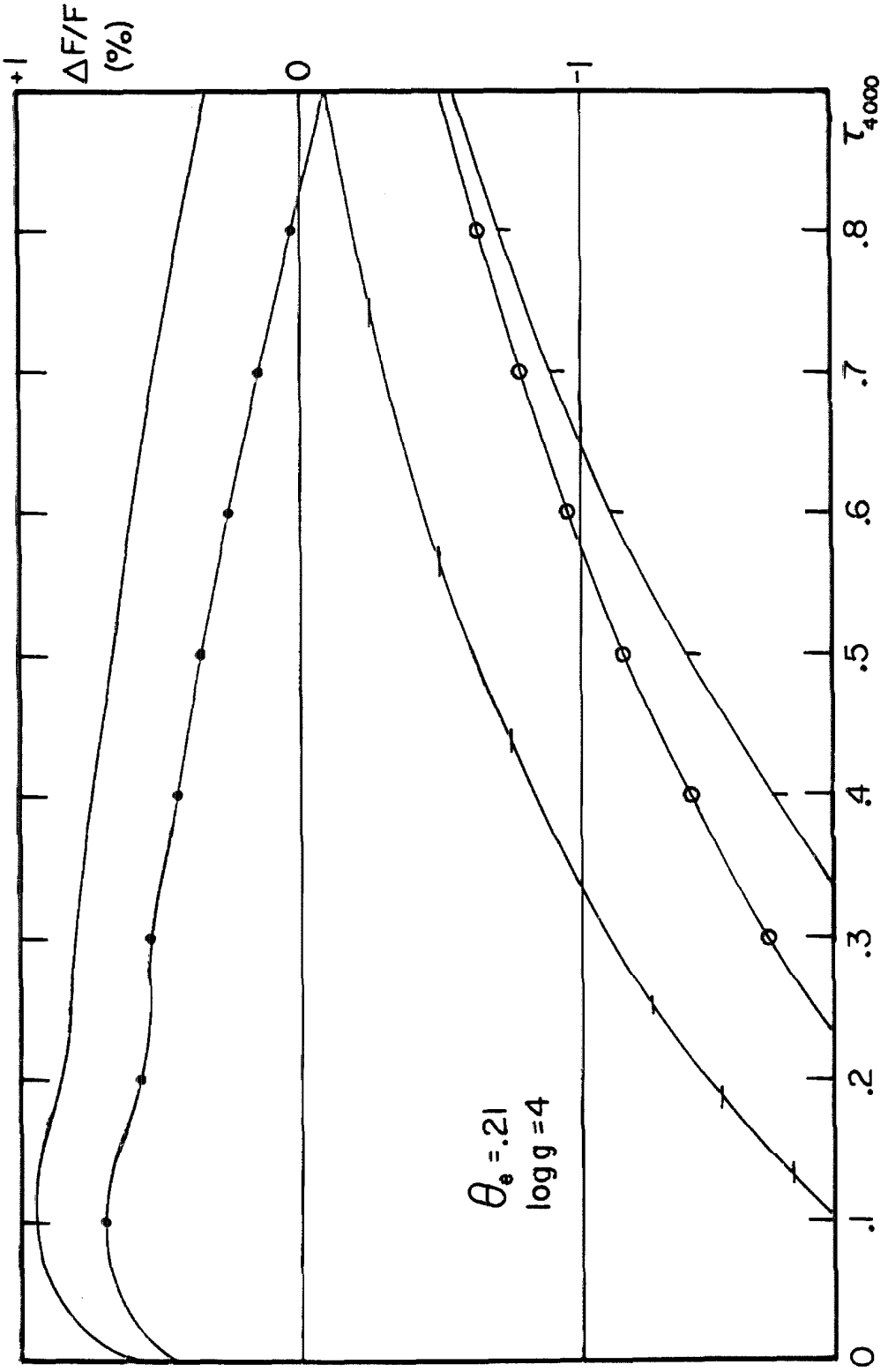

Fig. 14

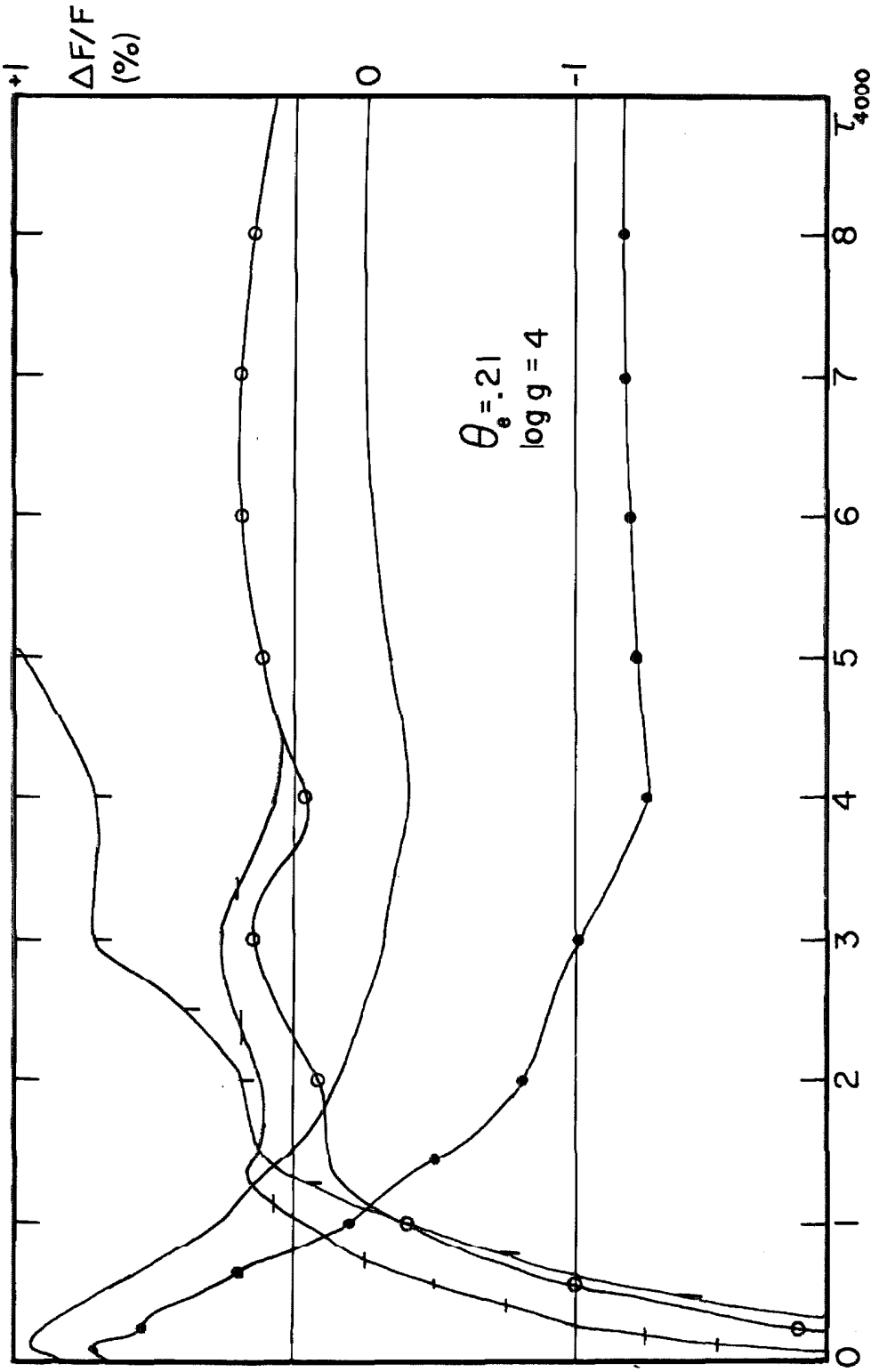

Fig. 15

constructing a sequence of models ignoring scattering at first, and then putting in the scattering only in the last iterate or two, is much more economical than solving the Milne equation each time since a full scattering model takes from three to four times as long to construct as a model in which we simply set $S_\nu = B_\nu$. Thus the most important deviations from flux constancy can be effectively removed by the ordinary Krook procedure ignoring scattering in the transfer equation, and the final touching-up of the solution made allowing for it. The results given in Appendix I have all been obtained in this way.

For the highest temperature models, the convergence was extremely slow due to the overwhelming dominance of scattering, and this shows that the present procedures should really be improved for the sake of economy. It was found, however, that in certain regions in the model the corrections predicted by equations 2.65 and 2.76 could be doubled and tripled to effectively speed up convergence to the correct solution. The actual recipe for doing this is based on experience and intuition, and this game is not recommended for the novice. Also, the instant at which we allow for scattering terms is dictated largely by experience. The only problem encountered by ignoring scattering in each iteration is that flux often falls so low at the surface that a spuriously large temperature correction is attempted here and a temperature inversion results. This can be remedied at least in part by not including the σ_ν terms in integrals of the form $\int \kappa_\nu B_\nu d\nu$ and $\int \kappa_\nu J_\nu d\nu$ even though this is logically inconsistent with ignoring the scattering terms and taking $S_\nu = B_\nu$. If this fails, the computer program used at present forces a non-inverted distribution at the surface

by smoothly hooking the preceeding non-inverted temperature distribution to the one just obtained from the correction procedure. Indeed, one reason we almost invariably have to do more than one scattering model after a sequence of models in which it is not allowed is to let the conditions at the surface relax into their proper values after being badly bludgeoned so as to avoid the temperature inversions.

One peculiarity of the Krook-Avrett procedure which should be noted here is the tendency for the integrated flux at the boundary to be too low even when scattering is quite negligible. This difficulty may stem from the approximations made in equations 2.61, 2.62 and 2.64; the deviations are rarely extreme, and considering the other approximations made, it does not seem worthwhile to devote a great deal of effort to attempting to correct the situation.

In summary we might offer the remarks that good models (at least within the framework of assumptions) can be constructed by the procedures described in this chapter, but the job is non-trivial because we are confronted with a highly nonlinear problem and can use only first order equations in its solution. Good models also require much persistence.

Chapter III

PROPERTIES OF THE MODELS

In this chapter we will summarize some of the results derived from the models.

1. The temperature-depth relationships

Since we have altered the temperature distribution in the models by successive iterations to obtain finally flux-constancy, the form of the temperature-depth relation now has some interest. To be sure, this relation is arbitrary in the sense that the depth scale is merely an intermediate parameter and the temperature-pressure relation is the relation of real physical interest; it is discussed later. Nonetheless, for a chosen τ_{STD}, $T(\tau_{STD})$ is somewhat meaningful if a group of models is intercompared.

One parameter of interest is T_o/T_e. The results derived from the models computed are shown in figure 16; the parameter of the curves is log g. This interesting graph shows that marked deviations occur from the grey body value for this ratio. Considering first the log g = 4 temperature sequence, we see that the most pronounced deviation occurs near $\theta_e = 0.18$; the ratio approaches the grey value again for the $\theta_e = 0.14$ model, and falls a bit lower for the $\theta_e = 0.101$ model. The curve is not well defined in the region between these last two models; it would be very desirable to have a $\theta_e = 0.127$ model to determine the behavior of T_o/T_e at this point. The log g = 3.5 models at $\theta_e = 0.14$ and $\theta_e = 0.18$ are shown by open circles; they lie much closer to the

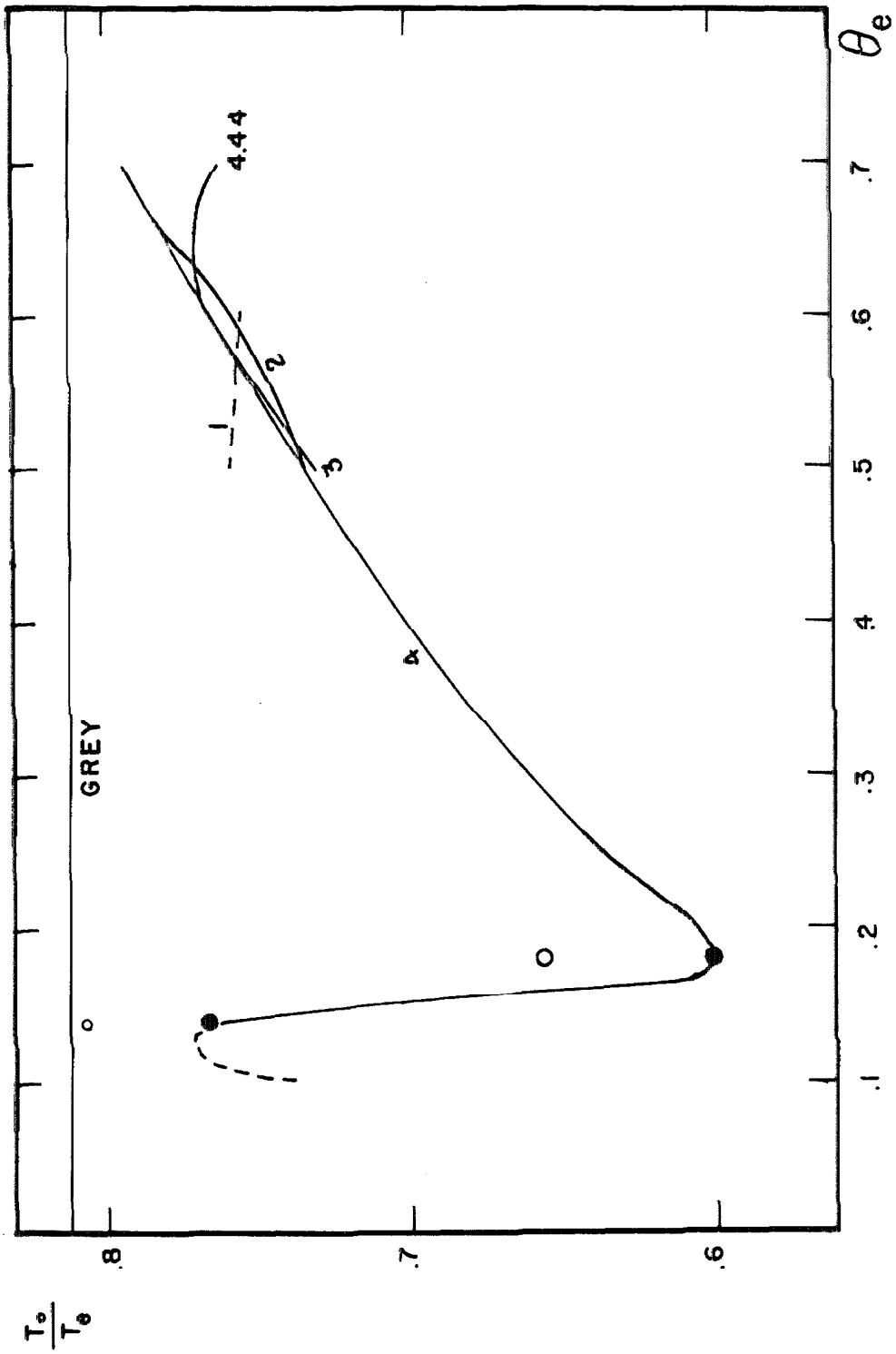

Fig. 16

grey body line, as would be expected since electron scattering constitutes a more important source of opacity for these lower gravity models. The gravity sensitivity of the boundary temperature is rather surprisingly large at these higher temperatures in view of the much smaller and more confused gravity sensitivity at lower temperatures. This may come about since the major effects of the relative increase in importance of electron scattering occurs near the Lyman absorption edge. In the cooler models, a much smaller part of the total flux is emergent here, and thus the net effects of increased scattering will be smaller here. In this light the greater gravity sensitivity at the higher temperatures appears quite reasonable. The two "low" helium-abundance models are plotted as filled circles; they show no significant deviation from the "normal" helium-abundance curve.

It should be remarked that the previously constructed models (see Münch, 1960, table 4; and Kolesov, 1962) showed a dip in the ratio of T_o/T_e near $\theta_e = 0.18$. The lack of homogeneity in the assumptions underlying the computations causes the results to scatter badly, however, and the lack of flux constancy in many of the models made them subject to some suspicion. Furthermore previous results showed no indication of a gradual progression of the ratio to a low at $\theta_e = 0.18$ as is shown here, but instead scattered around a value of 0.8 on the range $0.2 \leq \theta_e \leq 0.7$, some even lying above the grey value. The present computations are sufficiently homogeneous that we can assert the effect is real.

Figure 17 shows a related parameter, the depth at which $\theta(\tau_{STD}) = \theta_e$. The same general features show; the depths are generally

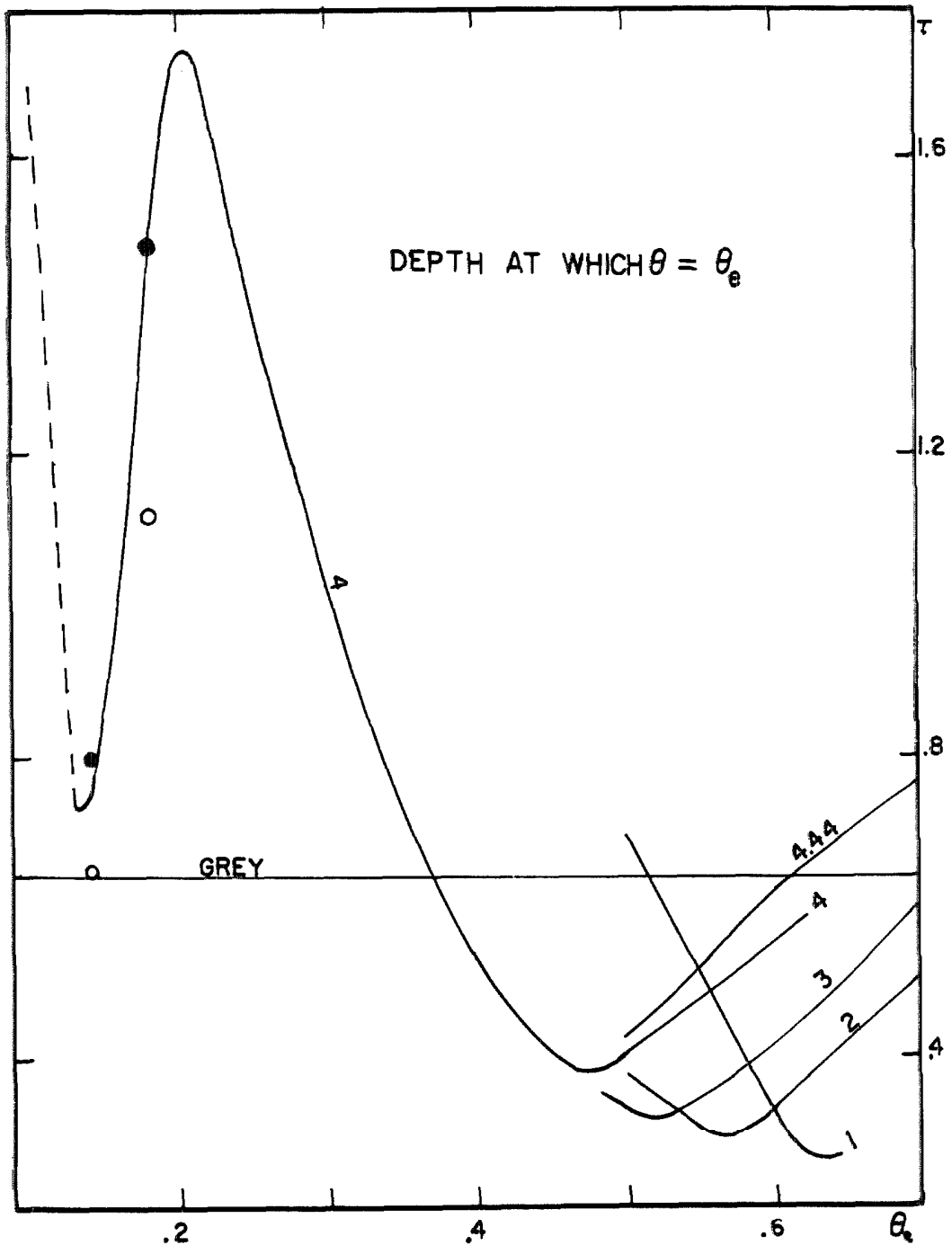

Fig. 17

larger than the depth if the model were grey. Thus the temperature distributions start at a lower boundary value and rise more slowly than the grey relation. In the curve shown in this figure the maximum deviation occurs at $\theta_e = 0.2$, instead of $\theta_e = 0.18$. Again the low gravity models lie much closer to the grey solution; as before, the "low" helium abundance models show no significiant deviations from the "normal" abundance models. The low gravity model at $\theta_e = 0.18$ happens to fall right on the grey value, but this is almost certainly only fortuitous agreement. The depth of θ_e for cooler models shows gravity sensitivity, and the value drops below the grey value. There are mitigating circumstances here, however; namely, these models have extensive zones which are unstable against convection. Thus by forcing a radiative solution, T increases too rapidly with respect to p_g. The relation between p_g and τ is not as sensitive, so in a rough way we would expect that allowing the proper convective gradient might decrease the gradient of T against τ and thus cause the depths of θ_e to become larger. No special emphasis should be placed upon the detailed shape of the curves at low gravities since only a few points are available here, and the curves are drawn largely by considerations of smoothness and similarity (if not by a good measure of imagination).

In an attempt to understand these variations, we followed the suggestion commonly made that such deviations should be in some sense correlated with the non-greyness of the radiation field. We formed an index of non-greyness by measuring, by planimetry, the fraction of the total flux that lies above the flux given by a black body curve at temperature T_e; obviously an equal fraction of the total flux will lie below

this same black body curve. The results are shown in figure 18. It is seen that while the curves do not match identically, a qualitative agreement holds for the most striking features in that the lowest temperatures have only a small fraction of "non-overlapping" flux, and going to higher temperatures the fraction becomes larger. At $\theta_e = 0.14$ there is abruptly good overlap again; this coincides nicely with the corresponding "greyness" of T_o/T_e and $\tau(\theta_e)$ shown in figures 16 and 17. At $\theta_e = 0.101$ there is again a small trend towards greater non-overlap of the fluxes, in agreement with the other properties mentioned. The measure fails to show the gradual deviation from "grey" properties culminating near $\theta_e = 0.2$ as is shown by the two preceeding figures, but we certainly cannot expect this conjecture to be correct in every detail, nor is the measure we have used necessarily the most relevant one. In any case the qualitative agreement is satisfying insofar as it goes.

To study the systematics of the shape of the $T(\tau)$ relation, in figures 19-25 we have plotted $Q(\tau) = \frac{4}{3}(T/T_e)^4$, which is analogous to the grey body $\tau + q(\tau)$. Inspection of these curves shows a progressively greater deviation from greyness as we go from $\theta_e = 0.4$ to $\theta_e = 0.21$. The curves go to progressively lower boundary values (although the sharp drop at the surface of the $\theta_e = 0.21$ model may be spurious--see the remarks preceeding Appendix I), and have progressively shallower slopes. At higher temperatures there is a sudden reversal of these trends, and the gradients become steeper until $\theta_e = 0.157$; then the $\theta_e = 0.14$ and 0.101 models reverse again and go towards

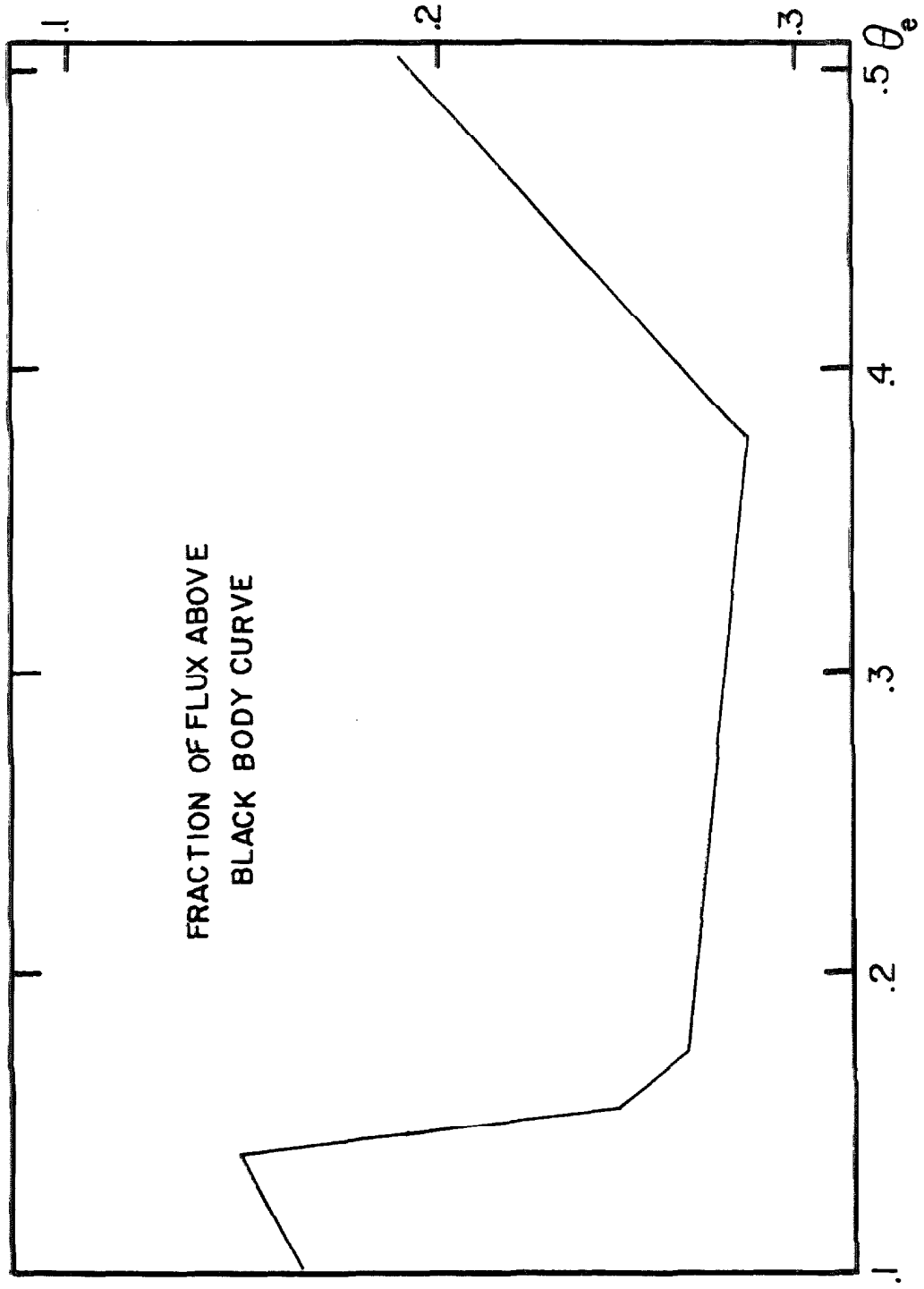

Fig. 18

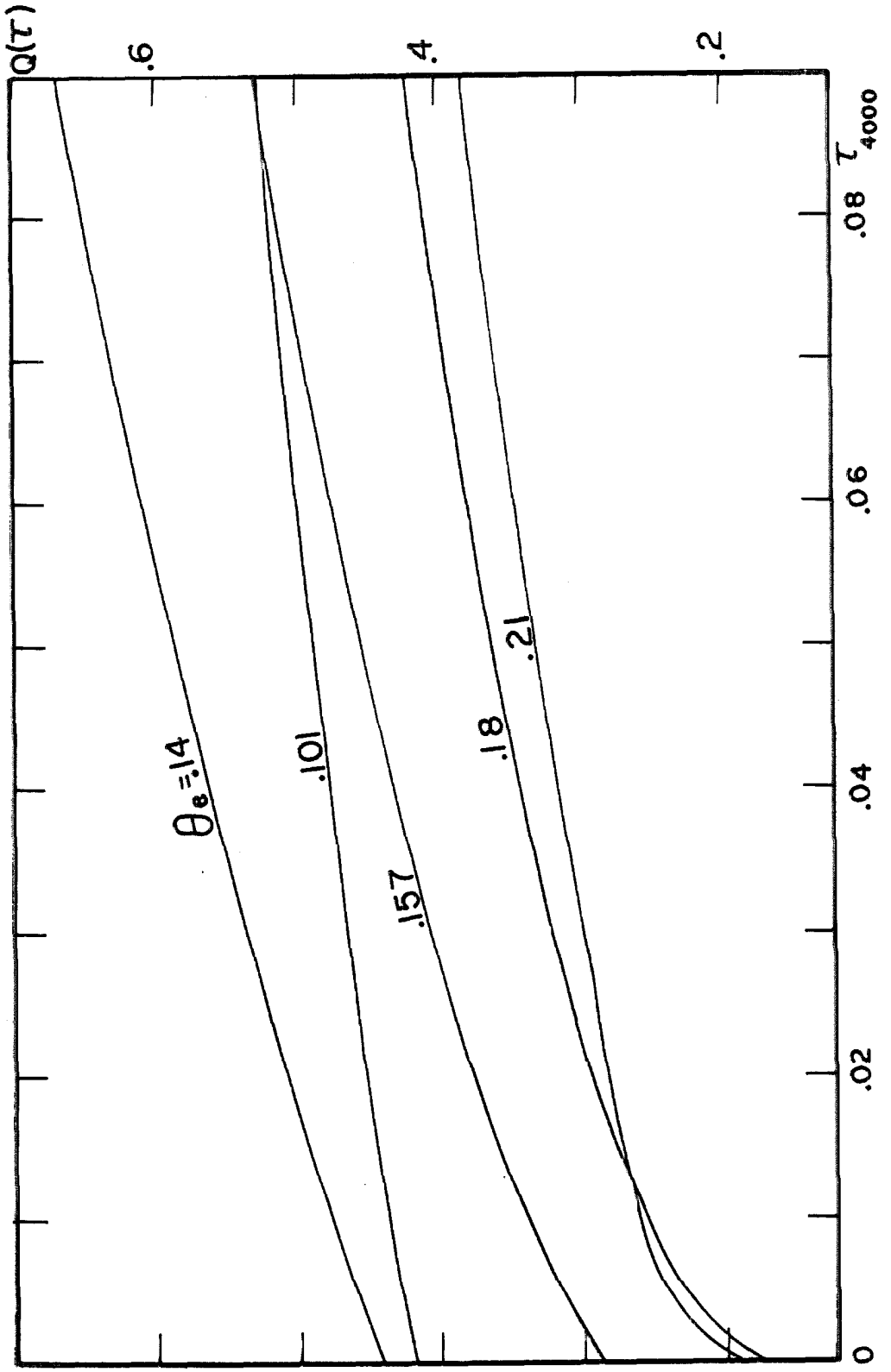

Fig. 19

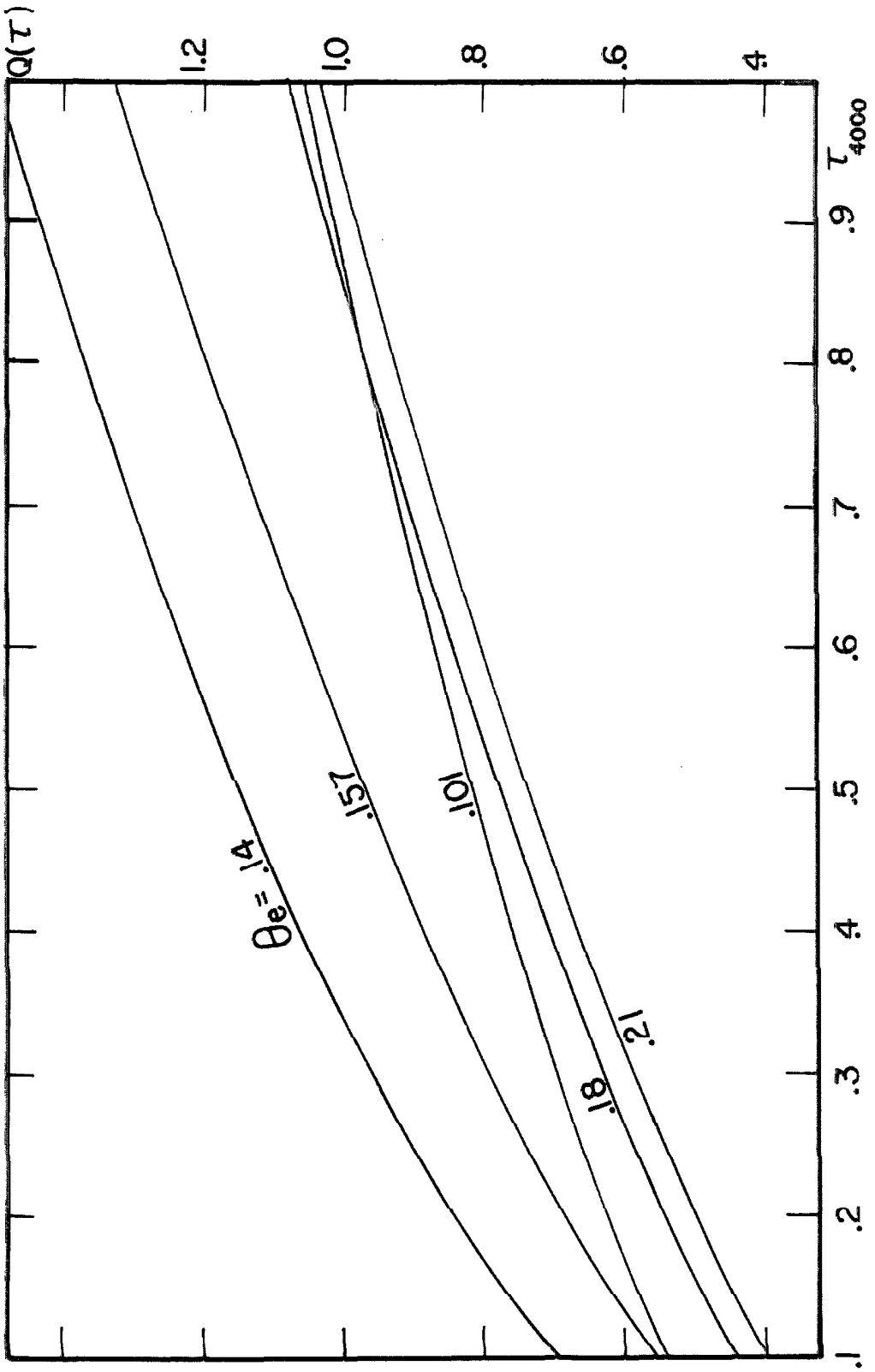

Fig. 20

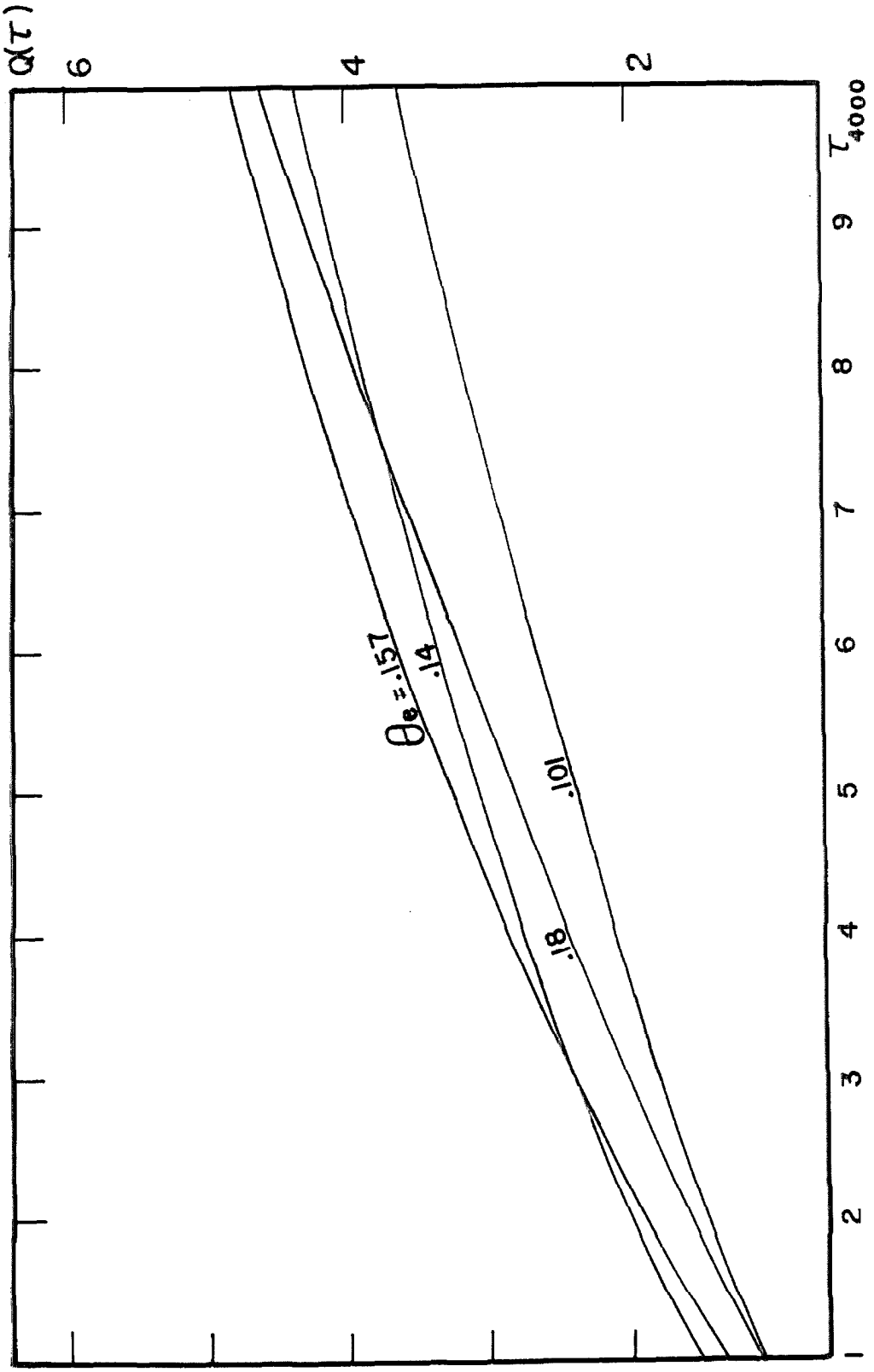

Fig. 21

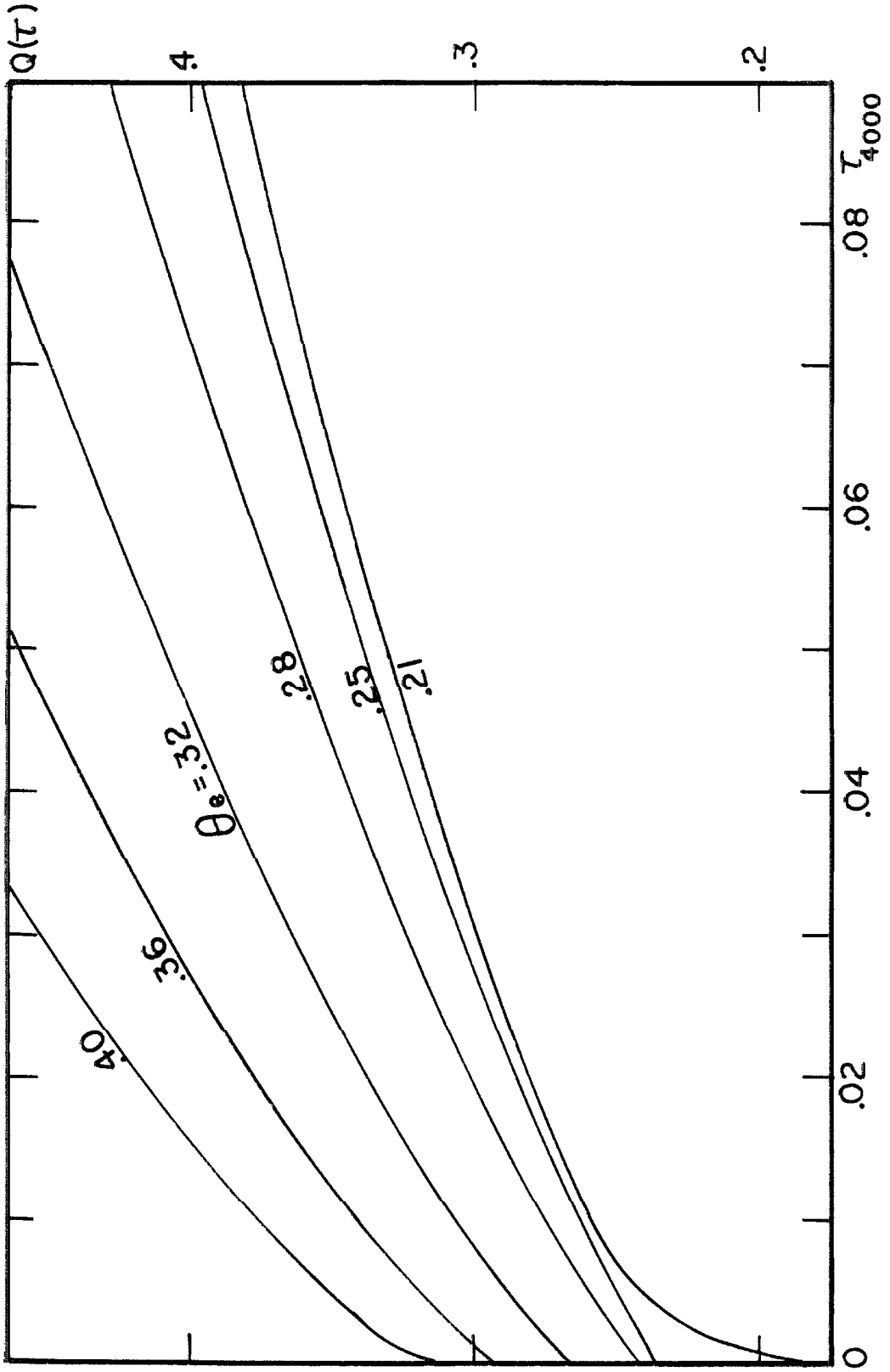

Fig. 22

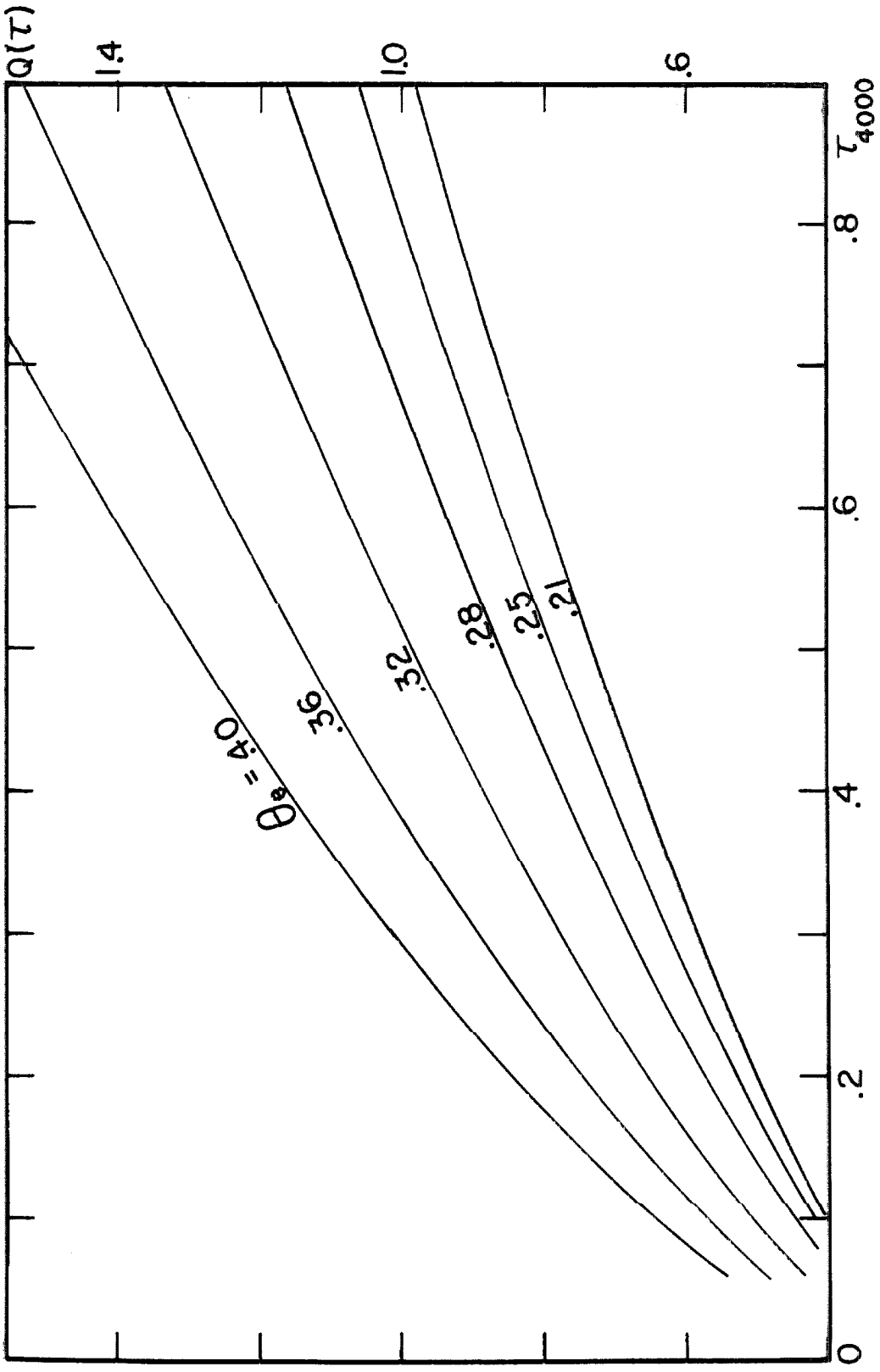

Fig. 23

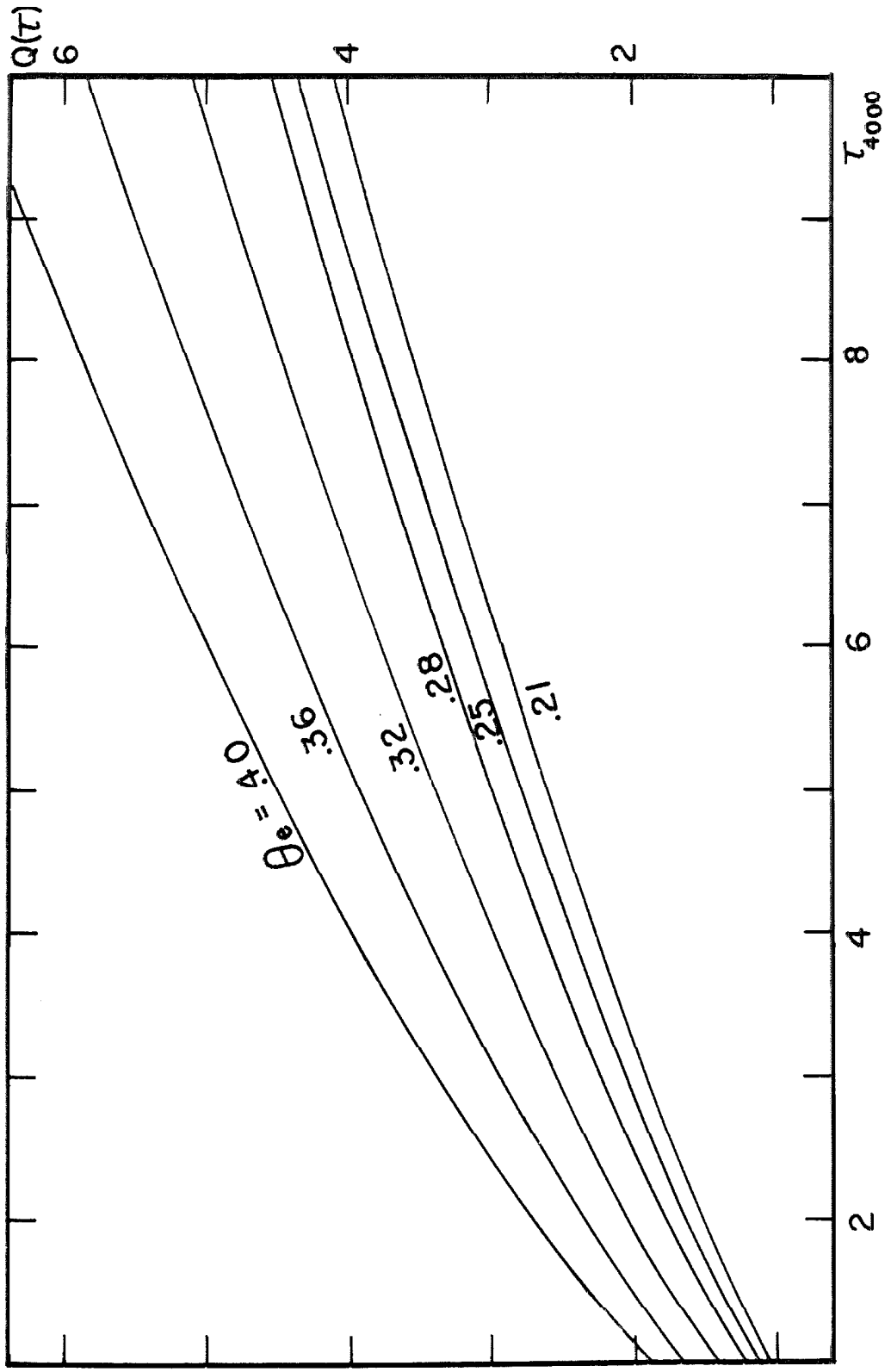

Fig. 24

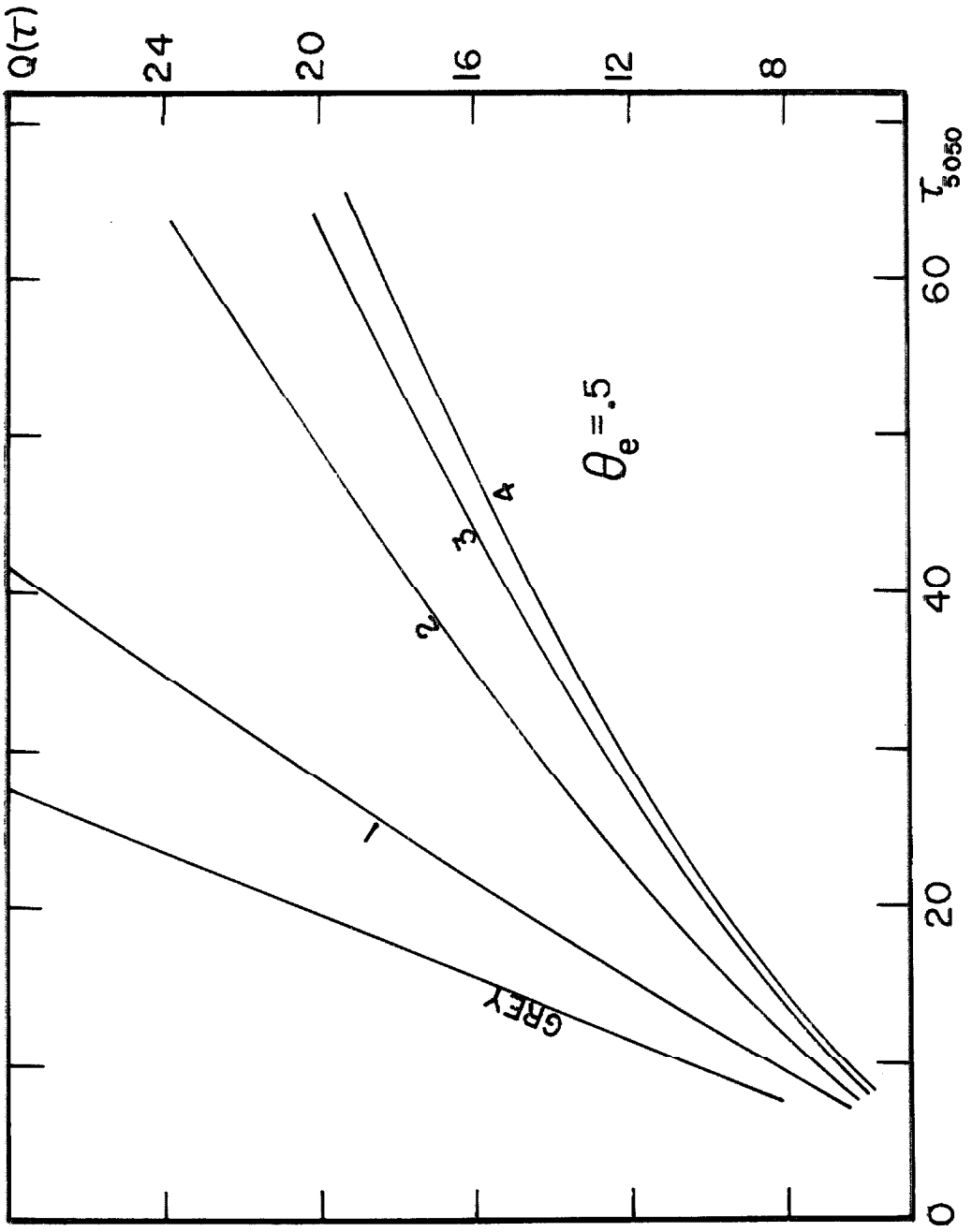

Fig. 25

progressively shallower gradients. These sudden and unexpected reversals in the nature of the temperature distribution made extrapolation from model to model completely unreliable, and we were led into (confidently) making bad guesses at the run of the temperatures for the initial model, and using a fair amount of computing time to get back to the correct solution. It might be interesting to construct a three-dimensional graph of these curves. Since our grid of models is not yet very closely spaced, we still will be able to make only relatively rough guesses at the shape of the temperature distribution for other intermediate models because of the complicated behavior the temperature-depth relations display.

The gravity sensitivity of the temperature-depth distribution is shown clearly in figure 25. A small caution here is that these values include the extrapolated tail of the temperature distribution, but in return we see that these extrapolated values appear perfectly reasonable. As we would expect from the increasing importance of electron scattering, the very low-gravity models lie much closer to the grey solution. This also holds for the low-gravity models at $\theta_e = 0.14$ and 0.18.

The change of helium abundance has only a very small effect upon the shape of the $T(\tau)$ relationships for the $\theta_e = 0.14$ and 0.18 models.

Finally, we might mention that an attempt was made to fit the temperature distribution analytically. It was found that a least-squares fit of the form: $Q(\tau) = a + b\tau + c\sqrt{\tau} + de^{-\tau} + fe^{-10\tau} + ge^{-50\tau} + he^{-300\tau}$ gives a fit good to about 3% or better for models with $\theta_e \geq 0.4$, no accurate fit could be made which did not "overshoot" near the surface.

This implies there are probably better fitting functions than the ones tried, and they could best be found by using a multiple non-linear regression technique. The main reason for attempting an analytical fit in the first place is to find if the coefficients are predictable at a chosen θ_e; then we would be able to make much better first guesses at the temperature distribution for the initial model. It turns out that this cannot be done easily with the fits made since the coefficients are rapidly oscillating functions of θ_e, probably because we have left too many degrees of freedom open in using a seven term fitting function. Use of a non-linear fitting technique might lead to a lower order fit which is as good or better, and in this case the coefficients might be smoother functions of θ_e. Such a search would not be a waste in view of the present expense of making a good model.

2. The temperature-pressure relationship

Since in the final analysis any optical depth we use in constructing a model is arbitrary, we must realize that the fundamental relationship is rather that between the temperature and pressure. Therefore we must confirm that the physical properties of our models do not in fact depend upon which specific optical depth (be it a monochromatic or mean depth) is used to construct them. This was verified for the present computations in that the $\theta_e = 0.4$ model was constructed twice, once choosing $\lambda 5050$ as a standard and once with $\lambda 4000$ as standard; the resulting temperature-pressure distributions are virtually identical. Perhaps another check would be useful, but this writer feels that we can

be fairly certain it would yield the same result.

Up to this point our approach has been "empirical" in the sense that we have just used numerical results at face value. It would be of value if we could now offer some synthesis in the form of reducing our results to a definite formulation. The possibility of doing this was suggested to me by Dr. L. Searle who pointed out that J. C. Stewart in his thesis (1956) had developed the idea of homology invariant atmospheres. In short, Stewart assumes an opacity law of the form $\kappa = \kappa(P_o, T_o) \cdot p t^{-11/2}$ (valid for the Planck mean of hydrogen) where $t = T/T_o$ and $p = p_e/P_o$; T_o is the boundary temperature and P_o is free at present. Further he assumes $p_g = P_g(P_o, T_o)p$ and writes $p_g(P_o, T_o) = C_1 P_o$ and $\kappa(P_o, T_o) = C_2 P_o T_o^{4/2}$. Finally assuming $t^4 = (T/T_o)^4 = [\tau + (2/3)]/(2/3)$, the hydrostatic equilibrium equation may be written as $t^3 dt = \mathcal{K} p t^{-11/2} dp$ which integrates to $t^{19/2} = p^2 +$ constant where P_o has now been chosen to cancel out all multiplicative factors in the equation. Applying the boundary condition that $t = 1$ when $p = 0$ we finally have $p^2 + 1 = t^{19/2}$. All of the constants are now known: $C_1 = 2[X + (Y/8)(1+y)]/[X + \frac{1}{4} yY]$, $C_2 = 1.75 \times 10^{21}(X + Yy)$, $Q \equiv X + \frac{1}{8} Y(1 + y)$, $y \equiv$ He II/total He, and $P_o^2 = \frac{16}{57} \frac{g}{7.61\, \theta_o^{11/2} Q}$ where X and Y are the mass fractions of H and He, defined as usual. Thus choosing a composition, θ_o, and g we may find P_o, and then the run of p_e vs. T by a simple formula. It should be noted that the asymptotic result $p \propto t^{19/4}$ was first given by Chandrasekhar (1931). To find if such a simple result might follow from the present computations we plotted $\log p_e$ vs. $\log T$ and found that on the range $0.25 \leq \theta_e \leq 0.4$ all the curves are of the same shape

and differ by only a zero point shift in each coordinate. The exact shape of the curve differed from Stewart's prediction (see figure 26) but has precisely the same asymptotic behavior at depth. This strongly suggested the possibility of reducing all the models on this temperature range to a single dimensionless relationship if we could find the scaling rule. As independent variable we also chose $t = T/T_o$; to scale p_e we must choose a fairly well-defined value. We have chosen a value, p_e^*, in analogy with Stewart's P_o; that is, we take p_e^* such that when $t^{19/2} = 2$, $p_e/p_e^* = 1$. Thus $\log p_e^*$ is simply the value of $\log p_e$ at $\log T^* = \log T_o + (2/19)\log 2 = \log T_o + 0.0317$. We then derived the mean relationship of $\log (p_e/p_e^*)$ vs. $\log (T/T_o)$ given in table 3 by simply plotting all the curves shifted by the $\log p_e^*$ determined above on the same graph and drawing a smooth curve through all the points. The average scatter is less than ± 0.02 in $\log p_e/p_e^*$, so that on this range of effective temperatures, use of the results in table 3 gives a model atmosphere to within about $\pm 5\%$ in p_e once the suitable p_e^* has been found. The final step is to derive a formula for p_e^*; we expect the functional relationship to be similar to that given by Stewart for $\log P_o$ so that we write $\log p_e^* = \underline{a} \log g + \underline{b} \log T_o + \underline{c} - \frac{1}{2} \log Q$. From the $\theta_e = 0.5$ models at $\log g = 4$ and 4.44 (even though these curves do not have precisely the correct shape) and by comparison of $\log p_e^*$ for the $\theta_e = 0.25$, $\log g = 3.8$ model with that expected from smooth extrapolation of the $\log g = 4$ results, we verified that p_e^* does scale as $g^{1/2}$ so that the constant $\underline{a}$ in our equation is 1/2. Over most of the relevant range, we find the slope of $\log p_e^*$ vs. $\log T$ is 2.12 as compared with 2.75 given by Stewart. Finally, since we have

Table 3

DIMENSIONLESS TEMPERATURE - PRESSURE RELATION

$\log(T/T_o)$	$\log (p_e/p_e^*)$	$\log (T/T_o)$	$\log (p_c/p_e^*)$
0.00	-1.10	0.25	1.35
0.01	-0.40	0.26	1.40
0.02	-0.18	0.27	1.45
0.03	-0.03	0.28	1.50
0.04	0.10	0.29	1.55
0.05	0.20	0.30	1.59
0.06	0.28	0.31	1.64
0.07	0.35	0.32	1.69
0.08	0.42	0.33	1.73
0.09	0.49	0.34	1.77
0.10	0.56	0.35	1.82
0.11	0.62	0.36	1.86
0.12	0.68	0.37	1.90
0.13	0.74	0.38	1.93
0.14	0.80	0.39	1.97
0.15	0.85	0.40	2.01
0.16	0.91	0.41	2.06
0.17	0.96	0.42	2.11
0.18	1.01	0.43	2.15
0.19	1.06	0.44	2.20
0.20	1.11		
0.21	1.17		
0.22	1.22		
0.23	1.27		
0.24	1.31		

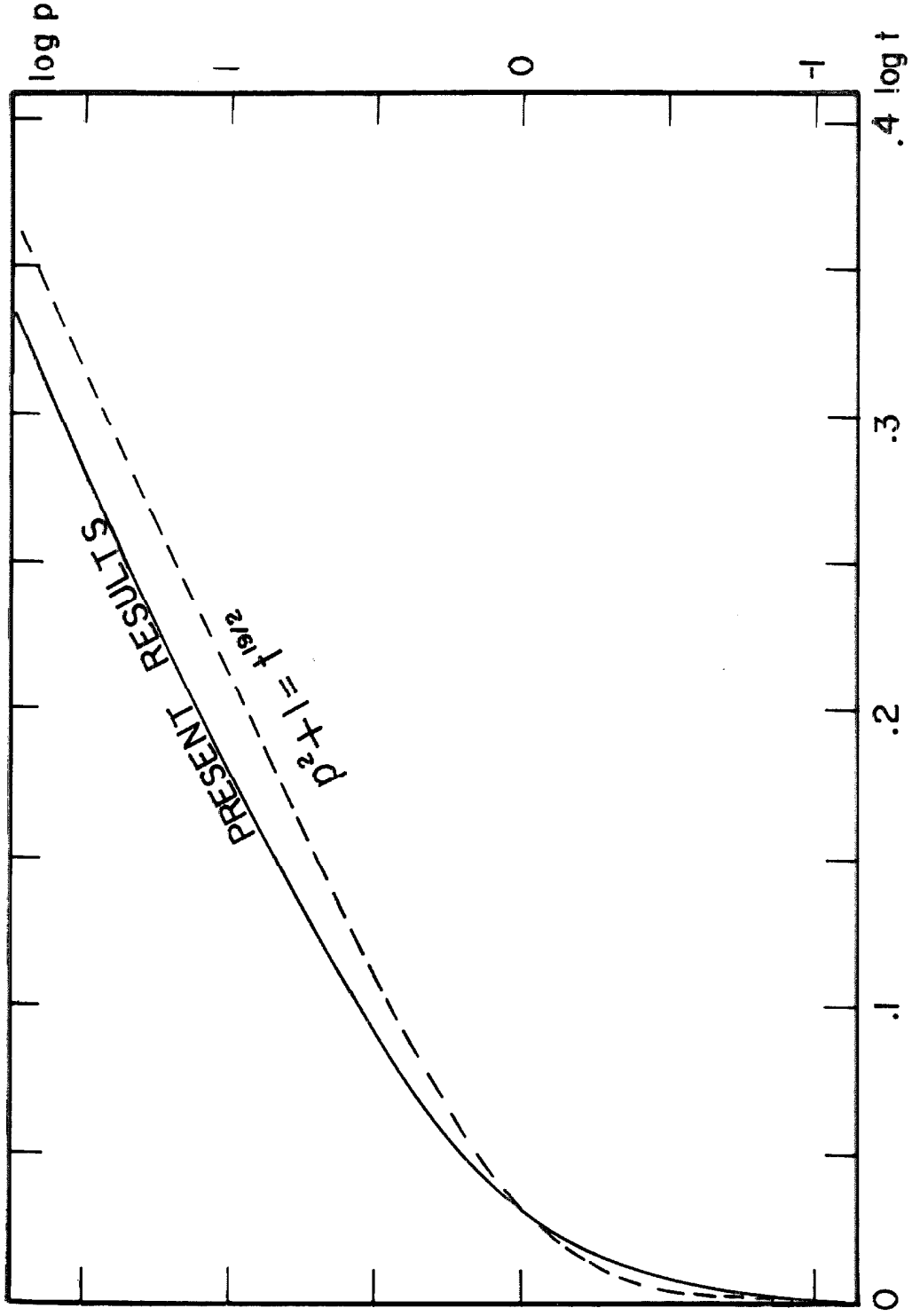

Fig. 26

used $N_{He}/N_H = 0.15$, $Y = 0.375$, and taking $y = 0$ (the correct value near T^*) we have $Q = 0.672$. Thus we evaluated the constant $\underline{c}$ and finally obtain

$$\log p_e^* = \frac{1}{2} \log g + 2.12 \log T_o - \frac{1}{2} \log Q - 8.577 \qquad (3.1)$$

The use of this equation and table 5 gives us a very quick and reasonable accurate estimate of the run of the electron pressure against temperature for the region of validity of the fits. This result should be of value in two contexts: 1. finding starting values for stellar interiors computations, and 2. interpolation among models obtained by actual integration.

The shape described by table 3 is no longer valid for models at lower temperatures as shown by figure 27 for the $\theta_e = 0.565$ model. The differences in shape may be attributed to a possible change in the opacity law as other opacity sources become important, and, more likely, to that fact that these models are unstable against convection so that the radiative gradient forced through them is very badly distorted from the gradient that would exist if convection were allowed in the computations. This is verified in part since the gravity sequence of models at $\theta_e = 0.5$ show the most distorted shapes in the $\log p_e$ - $\log T$ plane for the high gravities, while at the lower gravities, where the effects of convection become less important, the models look more like the standard curve; indeed, the model with $\theta_e = 0.5$ and $\log g = 1$ fits Stewart's original curve almost exactly. This might be attributed to the fact that the general level of ionization is much higher in the low gravity stars so that they tend to simulate stars of higher

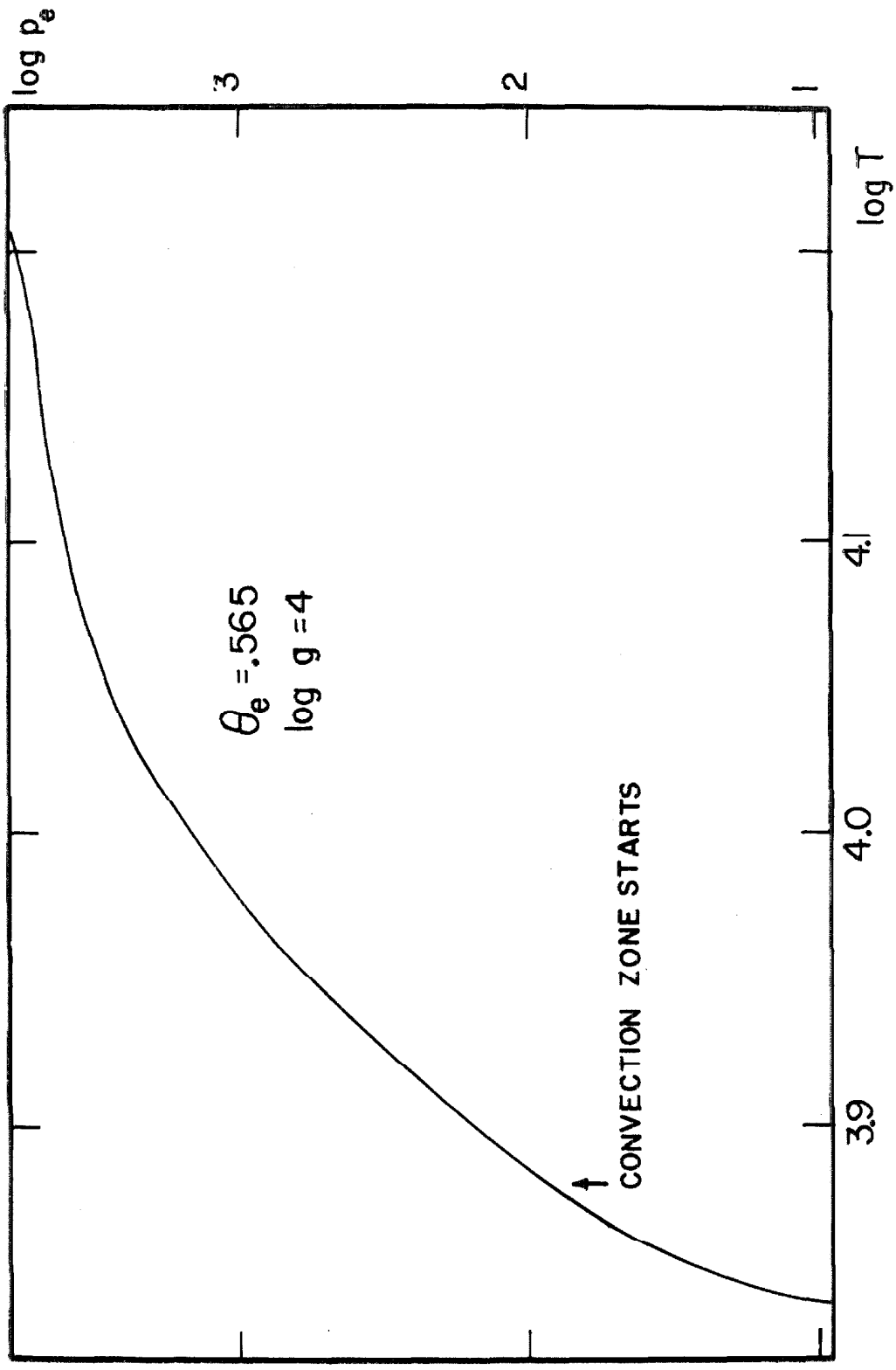
log p_e
3
2
1
log T
4.1
4.0
3.9
θ_e =.565
log g =4
CONVECTION ZONE STARTS

Fig. 27

temperature at higher gravities. At higher temperatures the picture is more confused, as might be expected from the large variations present in the $T(\tau)$ relation. The $\theta_e = 0.21$ and $\theta_e = 0.18$ models show a much too shallow slope near the very surface, whereas the $\theta_e = 0.157$ model goes the other direction and shows an extremely steep slope at the surface; this latter model is almost unique in that the temperature scale is very compressed relative to the pressure scale. At still higher temperatures the curves have qualitatively similar shapes but do not agree closely among themselves or with the standard relation. Therefore it seemed pointless to propose a multiplicity of approximate fits, but instead be satisfied that we found any connection among models at all.

One other important result is that changing the helium abundance in the $\theta_e = 0.14$ model and $\theta_e = 0.18$ model has little effect upon the run of $\log p_e$ vs. $\log T$. In particular, the 0.14 curves may be brought into good coincidence by shifting the high helium abundance curve by $+0.003$ in $\log T$ for constant $\log p_e$, and the shift for the 0.18 models is around 0.005 in $\log T$ for constant $\log p_e$. Thus to high accuracy, a change of a factor of three in the assumed helium abundance has no effect upon the relation between temperature and electron pressure. The gas pressures will of course be different, but we could derive a sequence of models with helium abundance as the parameter merely by using the same $T - p_e$ relation and revising the gas pressures; then we should integrate the $dp/d\tau$ equation, taking p_g as the independent variable and find the new depth distribution. This would certainly give models accurate enough to be used, for

example, in line computations where the helium abundance is to be regarded as free, and would be much more economical than actually recomputing the models for each helium abundance.

3. Stability of the models

We are concerned basically with two types of stability, namely, stability against convection, and stability against radiation effects.

(a) Convection

In many of the models computed the radiative gradient exceeds the adiabatic gradient in one or more places in the atmosphere, so that the model is unstable against convection. Table 4 summarizes the data on the convective zones encountered. If a model does not appear in the list it was stable against convection. We give the depths at which the radiative gradient is first larger than the adiabatic gradient, and the depth at which it is again exceeded by the adiabatic. Also listed is the ion currently undergoing ionization. In some cases an estimate was made of the ratio of the flux carried by the convection to the total flux using the Biermann mixing-length theory (see the summary by Demarque, 1960) with a ratio of the mixing length to pressure scale height of unity. Those models in the table in which the ion is indicated by H + He have hydrogen ionization zones which are overlapped at depth by helium ionization zones. The results are shown in figure 28. In this figure solid curves denote the onset of convection and dashed curves denote the depth at which convection ceases; no emphasis should be placed on the form of the curves for the gravity sequences having

Table 4

DEPTH OF CONVECTION ZONES (τ_{4000})

θ_e	log g	τ_{start}	τ_{stop}	Ion	F_e/F	τ_{start}	τ_{stop}	Ion	F_e/F
0.157	4	1.8	6	He^+	8.2×10^{-5}				
0.18	4	6	>60	He^+	4.1×10^{-4}				
0.18*	4	8	18	He^+	1.8×10^{-5}				
0.18	3.5	3	14	He^+	2.5×10^{-4}				
0.21	4	14	>60	He^+					
0.25	3.8	40	>60	He^+					
0.28	4	0.25	0.80	He					
0.32	4	0.6	2	He					
0.36	4	1.2	6	He					
0.40	4	0.025	0.4	H		2	10	He	
0.50	4.44	0.014	>33	H+He					
0.50	4	0.040	>33	H+He					
0.50	3	0.023	1.4	H		3.3	>34	He	
0.50	2	0.044	0.44	H		2.5	8.4	He	
0.50	1	2.5	5.0	He^+	3.1×10^{-4}				
0.55	3	0.056	>3	H+He	4.9×10^{-2}				
0.55	2	0.043	1.8	H	2.5×10^{-3}	3.5	15.2	He	3.9×10^{-5}
0.565	4	0.15	>33	H					
0.60	4.44	0.24	>33	H+He					
0.60	4	0.2	>33	H+He	8.3				
0.60	3	0.11	>33	H+He					
0.60	2	0.061	>34	H+He					
0.60	1	0.067	9.8	H+He	5×10^{-2}				
0.65	2	0.16	>34	H+He	4				
0.70	4.44	0.40	>34	H					
0.70	3	0.33	>33	H	46				
0.70	2	0.25	>34	H					

*N(He)/N(H) = 0.05

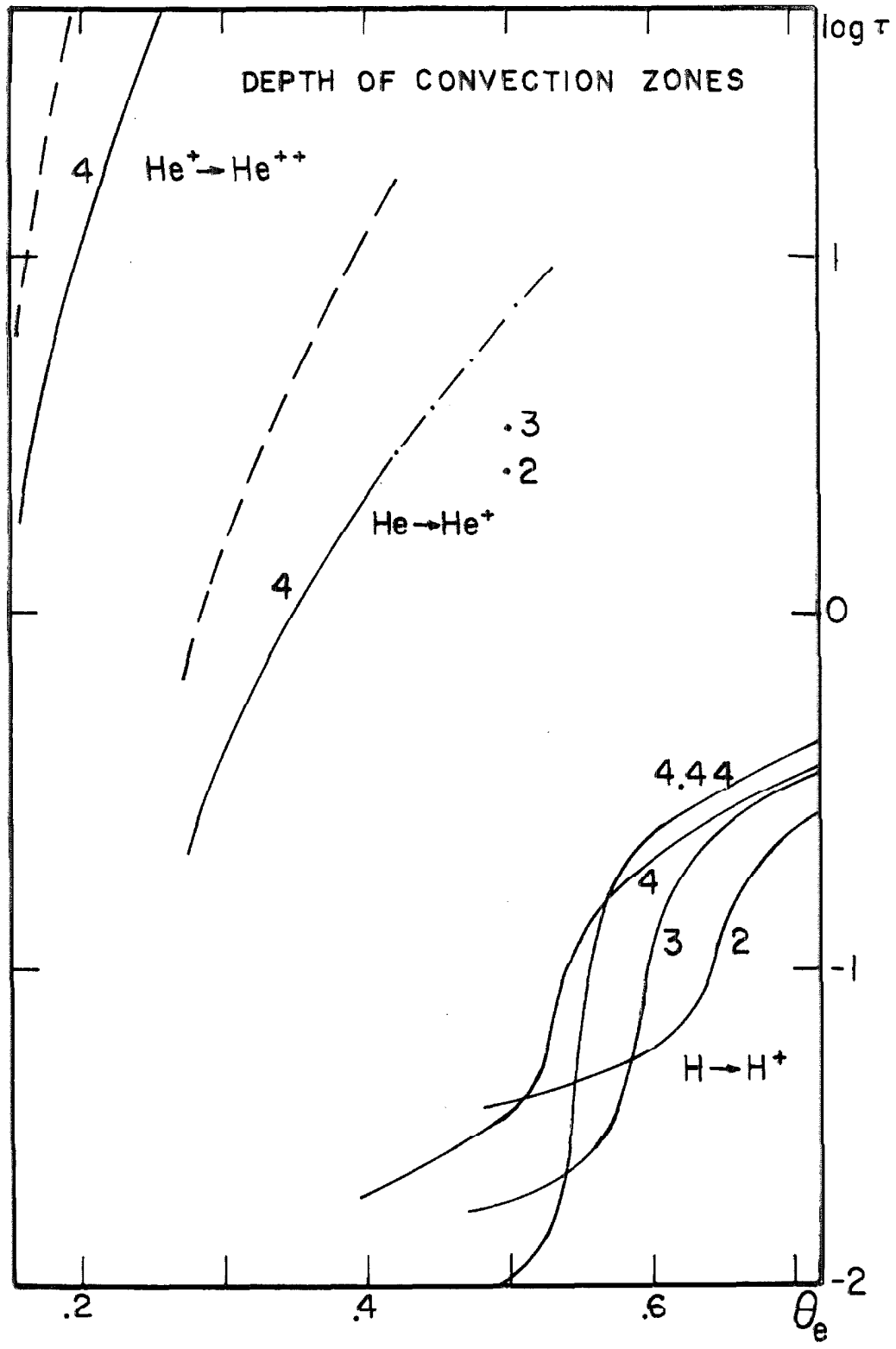
DEPTH OF CONVECTION ZONES
log τ
4
He⁺→He⁺⁺
1
.3
.2
He→He⁺
4
0
4.44
4
3
2
-1
H→H⁺
-2
.2
.4
.6
θe

Fig. 28

$0.5 \leq \theta_e \leq 0.7$ since too few points are available to determine them more than schematically.

The depths given here are the depths at which convection occurs assuming that convection does not occur (i.e. forcing the radiative gradient). The logical contradiction must be removed by considering models in which both processes are simultaneously allowed; this was attempted, but ultimately we met failure because we were unable to enforce the condition of constancy of the total flux at that time. What is needed is a temperature correction procedure which allows for the convective as well as the radiative terms. Such a procedure is given in Appendix II where we have rewritten the Krook-Avrett equations to include a convective term given by the simple mixing length theory; we hope to apply this technique in the near future.

Despite the contradiction just mentioned, the results given here still indicate places where the assumption of a radiative model is invalid. The worst region is for $\theta_e \geq 0.5$. Here the convection will carry a flux several times larger than the total flux through the atmosphere if the strict radiative gradient is enforced. The situation that occurs is illustrated in figure 29; as the hydrogen begins to ionize the opacity also increases rapidly, leading to an enormous radiative gradient, while at the same time the ionization lowers the adiabatic gradient. The result is a convective zone of great extent, and which transports considerable energy. Almost certainly the true temperature-pressure gradient must lie very near the adiabatic gradient in these cases. In this region, the effects of convection become less serious at lower gravities because of the rapid drop in the gas density for these models,

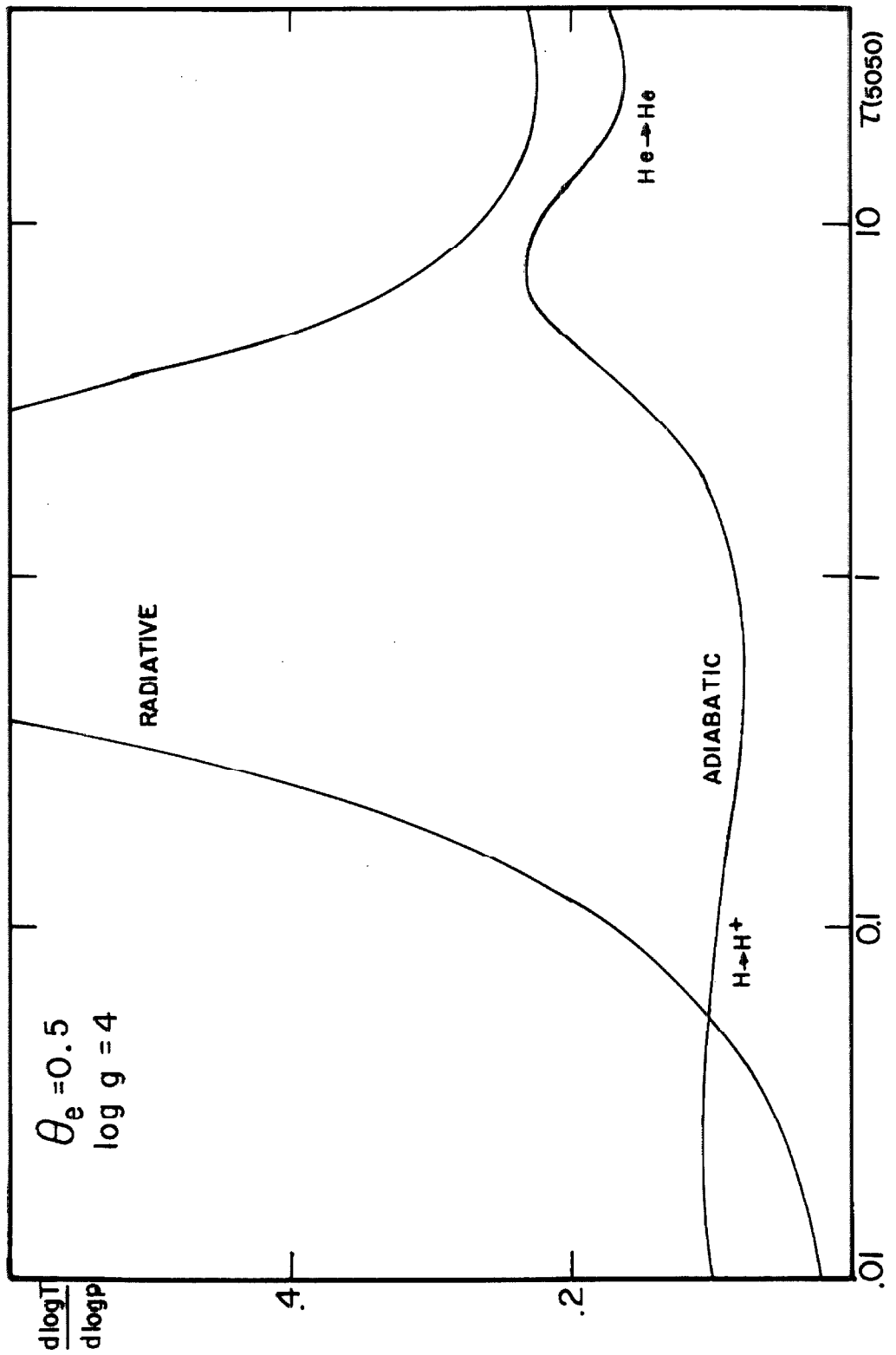
$\frac{d\log T}{d\log p}$
.4
.2
.01
.1
1
10
τ(5050)
RADIATIVE
ADIABATIC
H→H⁺
He→He
θ_e=0.5
log g =4

Fig. 29

as is shown by the fragmentary data on the ratio of the convective flux to total flux. In the cases where the convective flux is only a very small fraction of the total flux even assuming a strict radiative gradient, we may feel fairly safe that the departures of the true temperature gradient from the radiative gradient are quite small, and probably safely neglected. This holds true particularly for the hottest models which have zones of only limited extent and which carry essentially no flux convectively. Another consequence of the occurrence of convection in the models is that the density gradient usually becomes negative in the convective zone; this is clear considering that when we force a radiative gradient, T increases too rapidly with respect to P, so ρ must decrease.

It would seem that as a result of these computations we must be forced to admit that probably any line strength computations done in high gravity models on the critical range $0.5 \leq \theta_e \leq 0.7$ will be seriously influenced when convection is allowed. On the other hand, if this <u>is</u> the case, we gain in the sense that a set of such computations may tell us something about the convection.

(b) Radiation pressure

As pointed out some time ago by Miss Underhill (1949) there is a minimum gravity at which the radiative pressure gradient becomes larger than g/κ so that the net gas pressure gradient is negative; at such points the model may be dynamically unstable and large-scale mass motions may occur. This situation was encountered in the model having $\theta_e = 0.6$ and $\log g = 1$, on the range $\tau(5050) = 0.5$ to 0.8. This

is a slightly higher gravity than given by Miss Underhill's approximate arguments, but is certainly of the right order. Rather surprisingly, such a condition was not encountered for the $\theta_e = 0.5$, log g = 1 model. All of the other models constructed do not show this type of instability (excluding the spurious occurrences due to incorrect extrapolation of the radiative pressure gradient). Such effects have long been observed in low gravity stars in that turbulence is a well-established phenomenon for the supergiants.

4. Continuum properties

(a) Colors

We have computed the colors of the models using a program written by J. B. Oke. The sensitivity functions of the filters and photocell used in the computations contain arbitrary scaling factors, so that the computed colors differ from those of the Johnson-Morgan system (1953) by constants. These constants were evaluated by computing the colors of black bodies and forcing a fit to the values given by Matthews and Sandage (1963) in their table A3. It was found that a perfect fit could not be obtained between the results computed by Oke's program and either of the sets of data in the table cited. This may be due to errors in integration, differences in the sensitivity functions used, or differences in the method of taking the U magnitudes to zero extinction (although the B-V colors showed small discrepancies as well). The disagreements are not serious, and we will not attempt a critical analysis of this difficulty.

The colors normalized as well as possible to the Johnson-Morgan

system are given in table 5 and plotted in figure 30; the parameter of the curves is log g. Also plotted in the figure is the locus of unreddened main sequence stars. The black body curve is also shown with some temperatures (in units of 10^3 degrees) marked. The colors of the models agree qualitatively with those of the main sequence stars for $\theta_e \leq 0.6$. Better agreement is not expected since the effects of line absorption were not included in the models; these effects are most important on the range $0 < (B-V) < 0.4$ where the overlapping of the hydrogen lines causes the characteristic "S" shape of the observed main sequence color curve. For this reason, no direct comparison can be made between model and star by use of these colors. It would be dangerous to try to "unblanket" the observations to compare with the models since the hydrogen lines remove a substantial part of the flux in the ultraviolet and redistribute it elsewhere. The only satisfactory approach will be to put the hydrogen lines into the model. This may be done to first order by simply using one of the models given, computing the hydrogen line opacities, overlapping the lines near the Balmer jump and computing the emergent fluxes. These fluxes may be used to compute new colors, and the difference between the total flux of the unblanketed and blanketed models may be used to revise the effective temperature downward. This procedure is only approximate because the presence of the lines will alter the temperature distribution and change the model. The only completely satisfactory solution is to include the lines in the transfer problem at the outset; this can be done with existing computers. The first step indicated above would still be useful, however, because it would give a better estimate of the flux

Table 5

COMPUTED COLORS OF MODEL ATMOSPHERES TRANSFORMED TO JOHNSON AND MORGAN SYSTEM

θ_e	log g	V	U-B	B-V	B. C.
0.101	4	2.59	-1.30	-0.29	-4.27
0.14	4	2.95	-1.24	-0.29	-3.21
0.14*	4	2.95	-1.24	-0.28	-3.21
0.14	3.5	2.95	-1.26	-0.26	-3.21
0.157	4	3.20	-1.19	-0.28	-2.96
0.18	4	3.54	-1.10	-0.27	-2.71
0.18*	4	3.54	-1.09	-0.27	-2.71
0.18	3.5	3.47	-1.13	-0.26	-2.64
0.21	4	3.86	-0.99	-0.23	-2.40
0.25	3.8	4.21	-0.86	-0.22	-1.96
0.28	4	4.42	-0.75	-0.20	-1.67
0.32	4	4.66	-0.63	-0.18	-1.32
0.36	4	4.88	-0.52	-0.16	-1.04
0.40	4	5.08	-0.41	-0.14	-0.78
0.50	4.44	5.59	-0.21	-0.07	-0.32
0.504	4	5.60	-0.19	-0.08	-0.30
0.50	3	5.54	-0.17	-0.09	-0.28
0.50	2	5.54	-0.20	-0.07	-0.27
0.50	1	5.68	-0.42	0.06	-0.41
0.565	4	5.95	-0.14	0.00	-0.14
0.60	4.44	6.22	-0.21	0.10	-0.16
0.60	4	6.18	-0.15	0.01	-0.12
0.60	3	6.10	0.04	0.01	-0.04
0.60	2	6.05	0.00	-0.03	0.01
0.60	1	6.01	0.02	0.02	0.05
0.70	4.44	6.85	-0.30	0.27	-0.13
0.70	3	6.73	-0.10	0.20	0.00
0.70	2	6.66	0.02	0.14	0.07

*$N(He)/N(H) = 0.05$

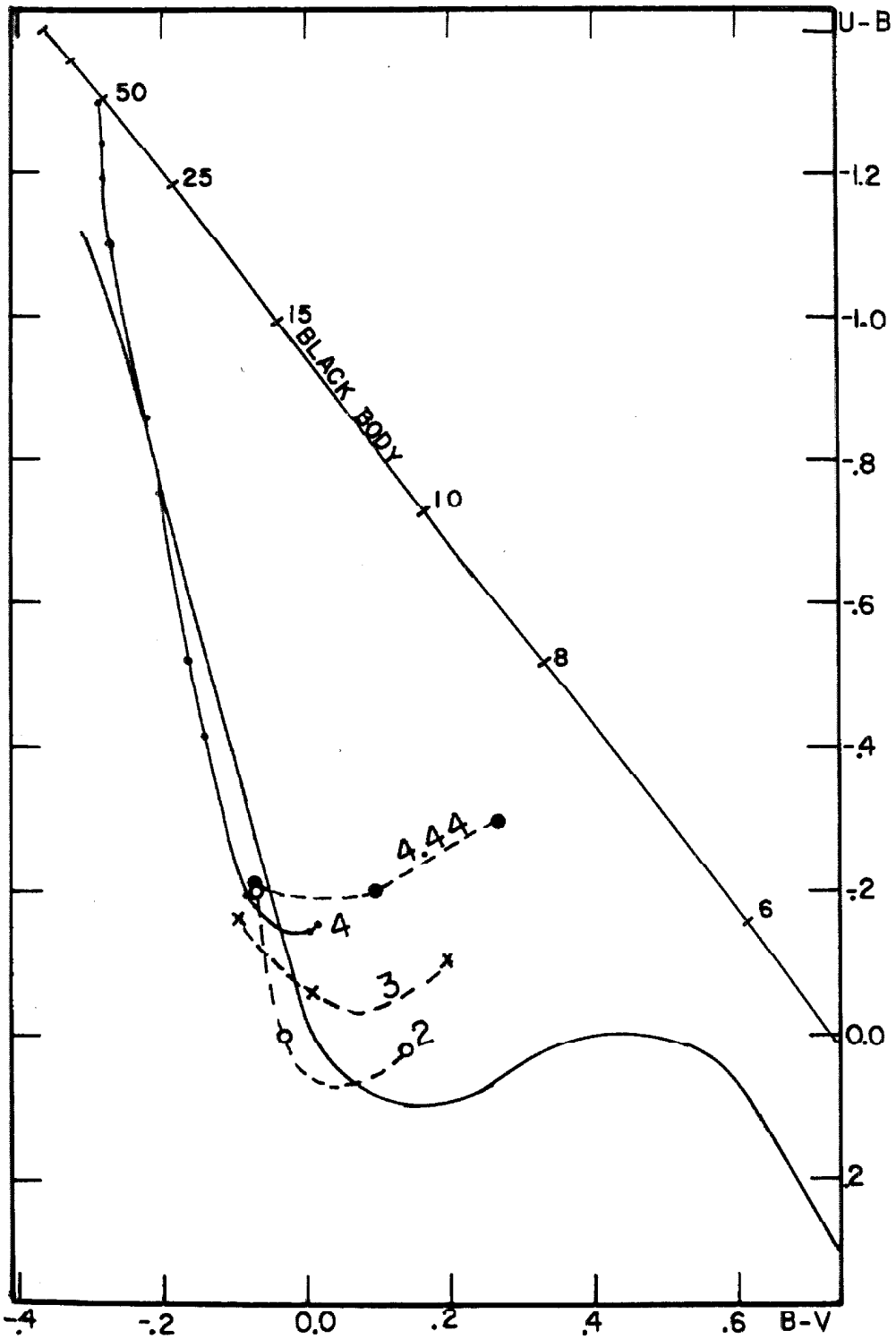

Fig. 30

toward which we should attempt to iterate the model when the lines are included.

Further, we cannot legitimately use the computed colors even differentially up and down a gravity sequence for, as is well known, the Stark broadened hydrogen line profiles are sensitive to pressure, and therefore gravity.

At the high temperature end the computed colors lie above the main sequence curve. This may indicate that the hottest main sequence stars observed have lower temperatures than the hottest models we have computed, but again we are confronted with the unknown blanketing effect of the overlapping hydrogen lines. This effect is more pronounced in the U, so the models essentially move down the curve they define. Better agreement would be obtained with higher gravities if the blanketing is negligible. It should be noted here that accounting for the overlap of the Lyman lines in the highest temperature models will tend to lower the effective temperature associated with a given computed color, but again we cannot yet reliably estimate how much.

(b) Bolometric corrections

In table 5 and in figure 31 we give the computed bolometric correction as a function of effective temperature normalized to the values given by Popper (1959). The values given here cannot be connected directly with observations because of the difficulties discussed above in making a connection between the colors and the effective temperature scale. A slight gravity dependence of the bolometric correction is evident at the lower temperatures considered. These values will have to be revised when models including the effects of lines are constructed

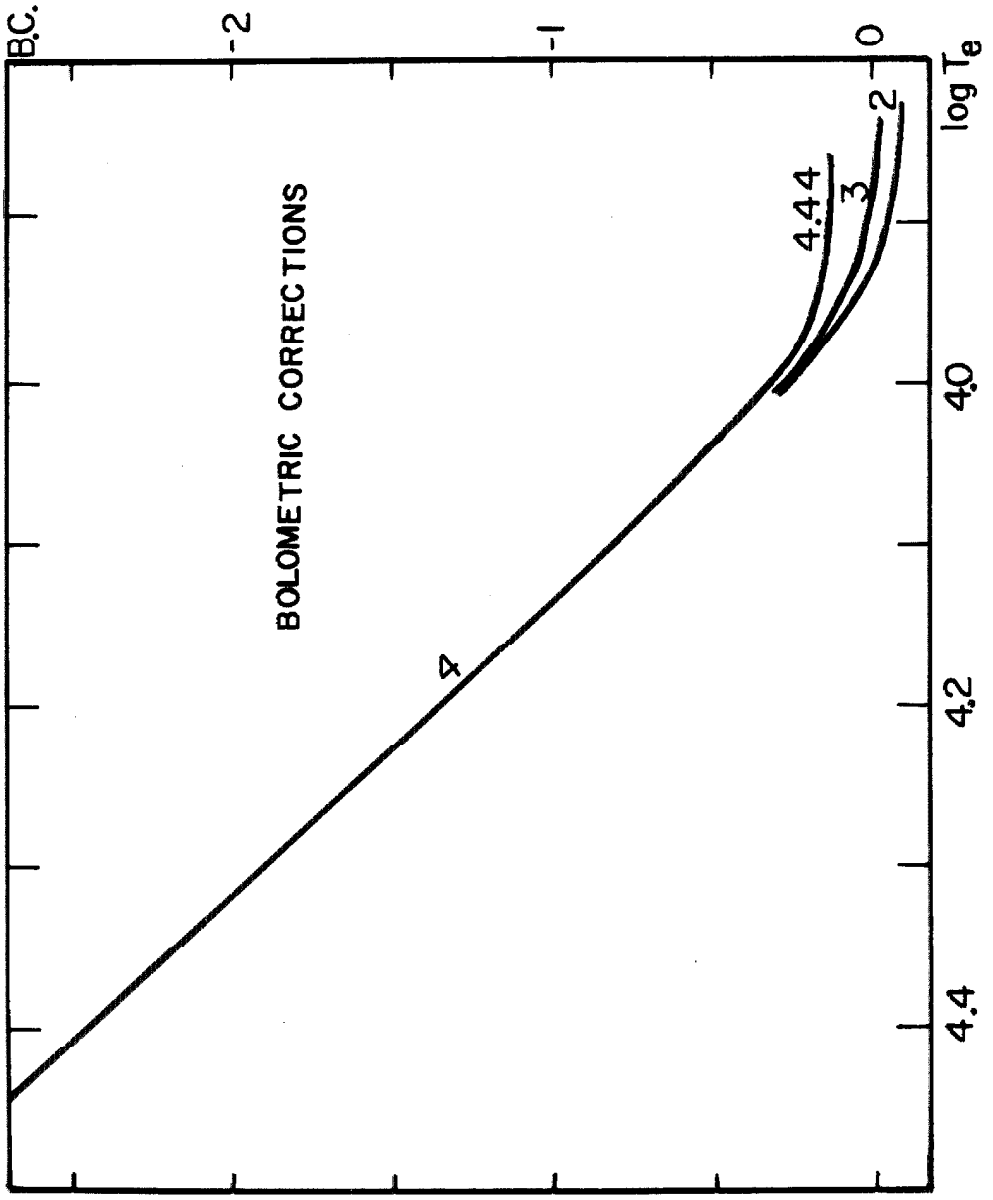

Fig. 31

insofar as the flux redistributed by the lines ultimately ends up in the visual pass-band. One would expect that accounting for this effect (as well as any additional ultraviolet opacity sources), the bolometric corrections at a given θ_e will become a bit smaller. On the other hand if the mechanism suggested by Meinel (see chapter II) is operative, the bolometric corrections may become substantially larger.

It is interesting to note that the values of the bolometric corrections increase as $5 \log T_e$ on the range $4.3 \leq \log T_e \leq 4.55$, whereas the difference between the B. C.'s of the $\theta_e = 0.101$ and $\theta_e = 0.14$ models is proportional to $7.5 \log T_e$. This latter slope is consistent with what would be obtained if the radiation in the visual pass-band had finally assumed the shape of a black body distribution since the Rayleigh-Jeans approximation will be valid and $F_{visual} \propto T$. Then F_{total}/F_{visual} would be proportional to $(\sigma T_e^4)/(cT_e) \propto T^3$, so that the B. C. would go as $7.5 \log T_e$.

(c) Continuum jumps

The continuum jumps due to the sudden onset of absorption beyond a series limit are quantities readily obtained theoretically and have been shown to be of great utility observationally (see, for example, Barbier and Chalonge, 1941; and Chalonge and Divan, 1952). The continuum jumps at the Balmer and Paschen edges are given in figures 32 and 33; the ordinates are $\Delta m = 2.5 \log I^+/I^-$ at $\lambda 3647$ and $\lambda 8204$ respectively, and the parameter of the curves is log g. As is known from basic considerations, these jumps peak at some definite temperature T^* and decrease with both higher and lower temperatures. The lower

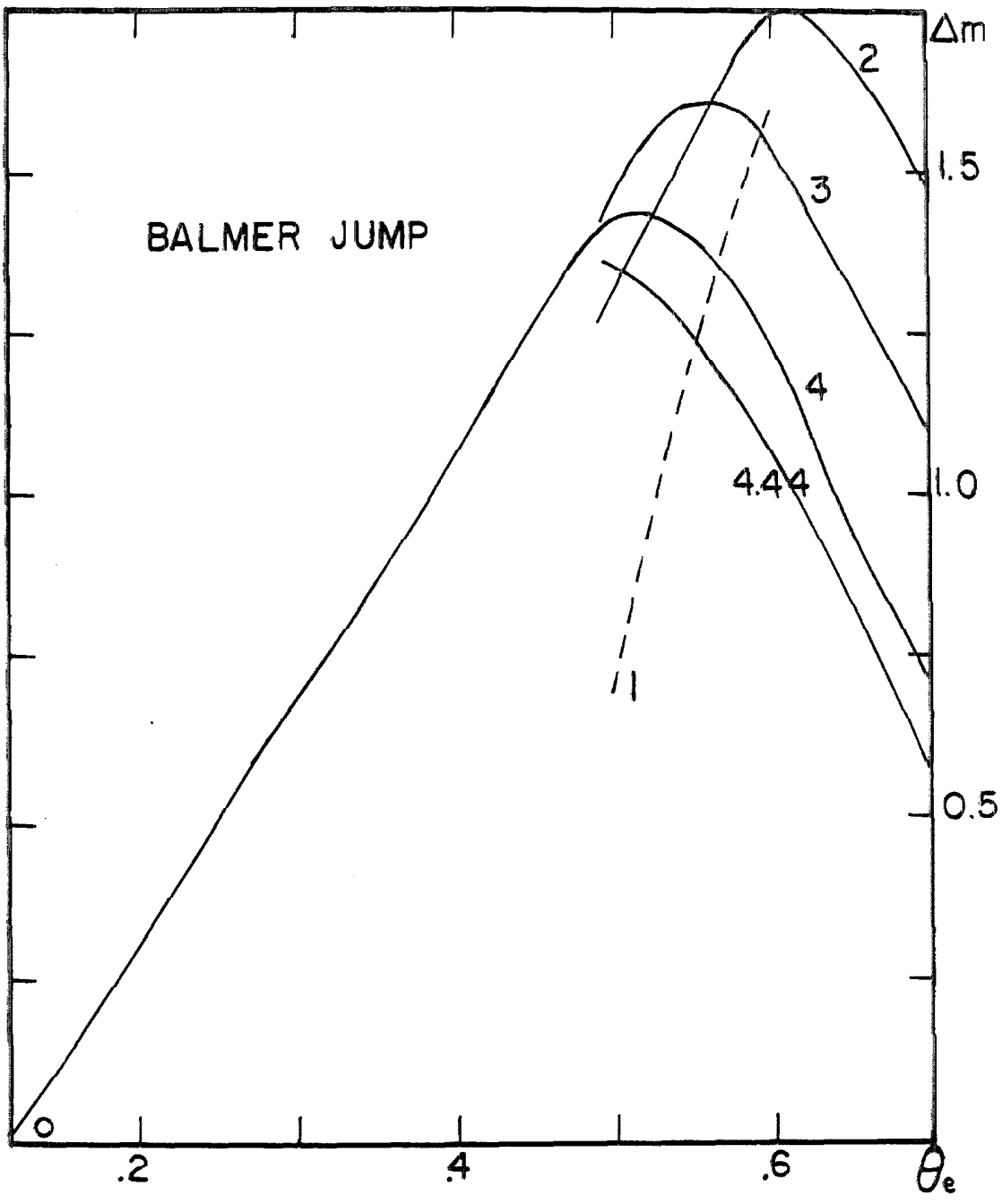

Fig. 32

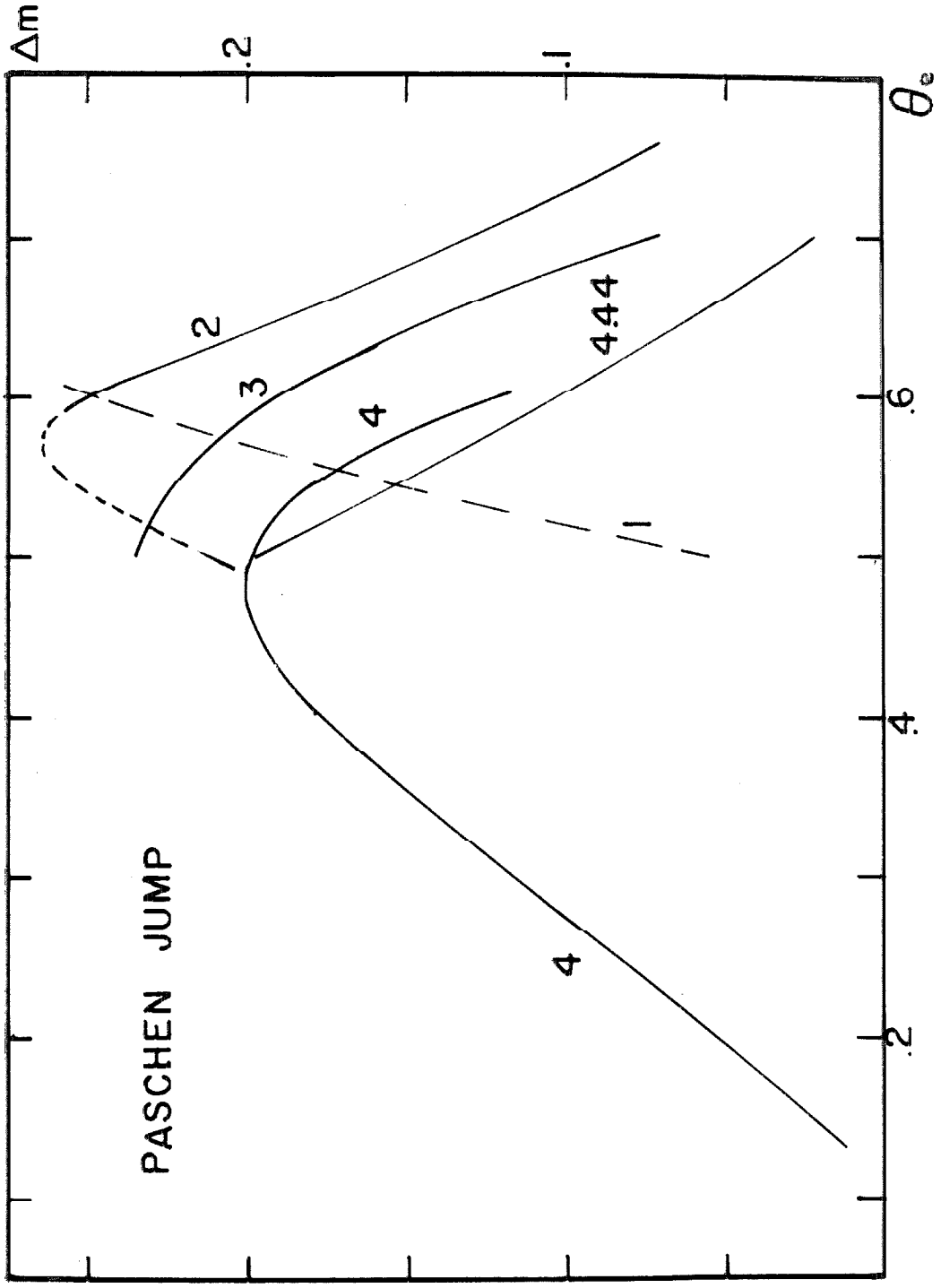

Fig. 33

the gravity, the lower is T^*. It should be noted that here again the details of shape of some of the curves as drawn may be incorrect because only a few points are available and they are drawn largely from considerations of similarity and symmetry.

Changing the helium abundance in the $\theta_e = 0.14$ and 0.18 models does not alter the Balmer or Paschen jumps perceptibly.

(d) Behavior of $\int \kappa_\nu J_\nu d\nu$

One curious result, discovered accidentally while plotting graphs of the various properties of the models, is that $\int \kappa_\nu J_\nu d\nu$ as a function of depths gives practically a unique curve for the models on the range $0.25 \leq \theta_e \leq 0.4$, which is precisely the range for which there is a unique shape to the $\log p_e(T)$ relationship, as discussed above. If we recall that since $\int \kappa_\nu B_\nu d\nu = \int \kappa_\nu J_\nu d\nu$ quite accurately for these models, we should have $\int \kappa_\nu J_\nu d\nu = \overline{\kappa}(\sigma T^4/\pi)$ where $\overline{\kappa}$ is the Planck mean. Following Stewart's analysis we find that this quantity should behave as $(\text{Const.})T_o^{-5/4}p/t^{3/2}$. The fact that the curves do <u>not</u> depend upon the value of T_o or T_e shows that we cannot use this simple theory to explain this result, though it is undoubtedly connected with the unique $p_e(T)$ relation.

Chapter IV

THE PROFILES OF THE HYDROGEN AND HELIUM LINES

Because of the complications of interstellar reddening and line blanketing, we may not easily compare our models to observations of the continuua of stars; furthermore, for the hottest models, the continuum is insensitive to changes in the physical parameters of interest (T_e, log g, N(He/H), so we look instead to the computation of line profiles, which are directly observable, to give us this correspondence between models and stars. In Section 1, we shall speak of hydrogen lines, but it is to be understood that we mean both hydrogen and ionized helium lines, the exception being that the effects of radiation damping for helium are ignored completely.

1. General considerations

The final absorption profile of a hydrogen line is most importantly influenced by the following three processes:

(a) Linear Stark effect caused by collisions of ions and electrons with the radiating atom

(b) Doppler broadening due to thermal or mass ("turbulent") motions

(c) Radiation damping or resonance damping.

Each of these processes may be described by some broadening function $b(\Delta\lambda)$ which for convenience we may assume is normalized to unity, i.e. $\int_{-\infty}^{\infty} b(\Delta\lambda)d\nu = 1$. If this $b(\Delta\lambda)$ represents the combined effects of the above three broadening mechanisms, then the line absorption

coefficient (per atom in the proper state) corrected for stimulated emission is

$$\ell^* = \frac{\pi e^2}{mc} f \cdot b(\Delta\lambda) \cdot (1 - e^{-h\nu/kT}) \qquad (4.1)$$

To find the net result of all the broadening mechanisms, we make the important assumption that the processes are statistically independent, so that the combined broadening function is merely the result of folding the individual broadening functions in the usual way. Let the Stark broadening function be $S(\Delta\lambda)$ normalized in ordinary frequency units. The doppler broadening function is simply $\frac{1}{\sqrt{\pi}\,\Delta\lambda_D} \exp\left(-\frac{\Delta\lambda}{\Delta\lambda_D}\right)^2$ where

$$\Delta\lambda_D = \frac{\lambda}{c}\left[\frac{2kT}{\mu m_H} + v^2_{TURB}\right]^{1/2} \qquad (4.2)$$

The damping terms give us a dispersion profile with half intensity width γ. Now assuming statistical independence of the broadening, it does not matter in what order we perform the folding procedure. We choose to fold together first the doppler and damping profiles; the result is the well-known Voigt function

$$H(a, v) = \frac{a}{\pi}\int_{-\infty}^{\infty} \frac{e^{-y^2}\,dy}{a^2+(v-Y)^2} \qquad (4.3)$$

where $a = (\gamma/4\pi\Delta\gamma_D)$ (γ being in wavelength units), and $v = \Delta\gamma/\Delta\gamma_D$. This function is normalized by multiplying by $1/\sqrt{\pi}$. The Voigt function has been studied quite carefully, and several convenient approximations for it exist (see e.g. Hunger, 1956; Harris, 1948), so that it may be treated as a known function. (I am indebted to Dr. B. Baschek

for an unpublished approximation for the function $H_1(v)$.) Performing now the folding against the Stark profile we obtain:

$$\ell_\nu^*(\Delta\lambda) = \frac{\sqrt{\pi}\, e^2}{mc} \int_{-\infty}^{\infty} s(\Delta\lambda + v \cdot \Delta\lambda_D) H(a, v)\, dv \qquad (4.4)$$

This formula was previously given by Miss Underhill (1951b).

Since ℓ_ν^* must be computed so often, it is important for economy's sake to perform the indicated integration as speedily as possible. If the damping parameter is small, $H(a, v) \rightarrow e^{-v^2}$, which suggests the use of the Gauss-Hermite quadrature. To estimate whether this is possible, we note that the damping effects are greatest for the first members of the series since the effects of Stark broadening are smallest here, and also the damping parameters are largest here (because of the rapidly decreasing f values for higher series members). Table 6 gives the damping parameters for some cases of astrophysical interest.

Table 6

T $\times 10^4$	θ	$\Delta\lambda_D$ at λ=1000 Å	L_α $\times 10^{-4}$	L_β^a $\times 10^{-5}$	H_α $\times 10^{-3}$	H_β $\times 10^{-4}$
4.2	0.12	0.147	1.9	8.2	1.2	7.7
3.2	0.16	0.127	1.7	6.2	1.2	7.6
1.8	0.28	0.096	1.8	4.7	1.2	8.2
1.0	0.50	0.072	2.2	4.8	1.5	9.7

It is clear that the damping terms are indeed small; we have not forsaken them entirely, however, since Miss Underhill has argued convincingly (1951b) that they are still important for the Lyman lines, and also Cayrel and Traving (1960) have shown that resonance damping (see e.g. Breen, 1961) is important for H_α at cooler temperatures. Thus to retain generality we have chosen to allow the possibility of damping. It should be noted in passing that we should always perform the folding in equation 4.4 rather than just add the additional damping terms to, say, the electron damping in the Stark profile, since otherwise improper normalization may result. Because of the smallness of a, we see that we may indeed use the Gauss-Hermite formula:

$$\int_{-\infty}^{\infty} e^{-x^2} f(x)\, dx \approx \sum_{i=1}^{N} w_i f(x_i)$$

where the points x_i and weights w_i are tabulated by Kopal (1955). Thus we write:

$$\ell_\nu^*(\Delta\lambda) = \frac{\sqrt{\pi} e^2 f}{mc} \int_{-\infty}^{\infty} \left[e^{v^2} H(a, v)\, s(\Delta\lambda + v \cdot \Delta\lambda_D) \right] e^{-v^2} \Delta v$$

$$\approx \frac{\sqrt{\pi}\, e^2 f}{mc} \sum_{i=1}^{N} w_i e^{v_i^2} H(a, v_i) s(\Delta\lambda + v_i \Delta\lambda_D) \qquad (4.5)$$

For convenience we may include the $e^{v_i^2}$ factor in the weights, so that writing

$$\omega_i = w_i e^{v_i^2} \qquad (4.6)$$

we have finally:

$$\ell_\nu^*(\Delta\lambda) \approx \frac{\sqrt{\pi}e^2}{mc} f \sum_{i=1}^{N} \omega_i H(a, v_i) s(\Delta\lambda + v_i \Delta\lambda_D) \qquad (4.7)$$

This expression has the advantages of high accuracy resulting from the use of an integration formula which is exact for polynomials of high order as well as the fact that the functions appearing in the kernel are easily accessible to numerical computation. The formula employed has $N = 19$, so that relatively few computations are necessary. As mentioned previously the damping terms are neglected for He II, so that we have taken simply

$$\ell_\nu^*(\Delta\lambda) = \frac{\sqrt{\pi}e^2}{mc} f \sum_{i=1}^{N} w_i s(\Delta\lambda + v_i \Delta\lambda_D) \qquad (4.8)$$

which is the folding of the Stark profile with the doppler profile.

2. The radiation damping constants

It is worthwhile to describe here the details of computation of the damping constants. Radiation depopulations of level n may occur by downward spontaneous and induced emissions or upward absorptions to another discrete level or to the continuum. Let us write the result of all bound-bound transitions as $(\Gamma_n)_{bound}$ and the results of absorptions to the continuum as $(\Gamma_n)_{free}$. Consideration of the bound-bound transitions gives (see Aller, 1953, p. 129)

$$(\Gamma_n)_{bound} = \frac{8\pi e^2}{mc} \sum_{n'<n} \frac{g_{n'}}{f_n} f_{n'n} \frac{(1-e^{-h\nu_{nn'}/kT})}{\lambda^2} + \sum_{n''>n} \frac{f_{nn''}}{\lambda^2} (e^{h\nu_{nn''}/kT} - 1)^{-1} \qquad (4.9)$$

For hydrogen, $g_k = 2k^2$, and the f values of the transitions may be computed from the formulae of Menzel and Pekeris (1935). If we write $a_n(\nu)(1-e^{h\nu/kT})$ as the continuum absorption coefficient from level n, corrected for stimulated emission, then the number of depopulations of level n into the continuum is

$$(\Gamma_n)_{free} = \int_{\nu_o}^{\infty} \frac{a_n(\nu)(1-e^{-h\nu/kT})}{h\nu} J_\nu \, d\nu \qquad (4.10)$$

This may be estimated by writing $a(\nu) = \frac{C^*}{\nu^3} g(\nu)$ and setting $J_\nu \equiv B_\nu$ (i.e. assuming T.E.), so that we find

$$(\Gamma_n)_{free} = \frac{2C^*}{c^3} \bar{g} E_1(u_o) \qquad (4.11)$$

where $u_o = h\nu \equiv kT$, and E_1 is the first exponential integral function. For hydrogen $C^* = (2.815 \times 10^{29})/n^5$ so that

$$(\Gamma_n)_{free} = \frac{6.26 \times 10^8}{n^5} \bar{g} E_1(u_o) \qquad (4.12)$$

The total damping widths of a line from level n to level m is

$$\Gamma_{mn} = \Gamma_m + \Gamma_n \qquad (4.13)$$

(see e.g. Wooley and Stibbs, 1953).

The actual computations were carried out for $n = 1, 2, 3, \ldots, 7$. In the computation of each Γ_n, 60 levels were considered for the bound-bound transitions. The f values were obtained using the rigorous formula of Menzel and Pekeris. In the case of the bound-free transitions we set $\bar{g} = 1 - \frac{0.1728}{n^{2/3}} - \frac{0.0496}{n^{4/3}}$, which is the value at the series

limit and thus slightly underestimates $\bar{g}$ which has been given more accurately by Baker and Menzel (1938). But in view of the generally small size of the damping terms, it is clear that no serious error is committed in this approximation. Tables of $\Delta\lambda_R$ (defined such that $a = \Delta\lambda_R/\Delta\lambda_D$, $\Delta\lambda_R$ in Å; i.e. $\Delta\lambda_R = 10^8\lambda^2\Gamma/4\pi c$ where Γ is the full intensity half-width) are given in appendix III for Lyman, Balmer, and Paschen lines up to $n_{upper} = 7$. A table of Γ_{rad} (the full intensity half-width in frequency units) is also given for $n = 1, 2, \ldots, 7$.

3. Stark broadening

The determination of the profiles of hydrogen lines broadened by Stark effect interactions during collisions with ions and electrons is a formidable theoretical problem. In the past the accuracy of the results was severely restricted by various simplifying assumptions, in particular the neglect of electron impacts (Odgers, 1952). Fortunately for astronomers, this problem has recently been the subject of intensive investigation by several physicists (Griem and others, 1959, 1960, 1961, 1962; Kolb and Griem, 1958). They have shown that while the assumptions made in the past (adiabaticity and statistical broadening) are valid for the relatively slowly moving ions, they break down for the fast-moving electrons. For the electrons, the assumption of adiabaticity must be removed, and the time-dependent quantum mechanical problem must be solved. This is done in the impact approximation, and results in a dispersion profile for the electrons which is combined with the Holtzmark profile for the ions. So far the new

results have been used in the computation of line profiles in the sun (Traving and Cayrel, 1960), F stars (Searle and Oke, 1962) and a limited range of B stars (Aller and Jugaku, 1959). These computations have shown good agreement between the profiles predicted by model atmospheres and those observed. Further, the laboratory investigations of Wiese, Paquette, and Solarski (1963) have shown excellent agreement with the Griem theory. We therefore may use the theory with great confidence.

The present results extend the previous ones to the very high temperature stars using the model atmospheres listed in appendix I, and give profiles of the ionized helium lines as well. We will now summarize the details of the computations.

The Stark broadened profile is given as $S(\alpha)$ where $\alpha = \Delta\lambda/F_o$, $\Delta\lambda$ being the distance in Å from the zero field position of the line and $F_o = 1.25 \times 10^{-9}(N_e)^{2/3}$ is the normal field strength in e. s. u. The usual normalization is $\int_{-\infty}^{\infty} S(\alpha)\, d\alpha = 1$. To normalize in ordinary frequency units as required in equation 4.4, we take

$$S(\Delta\lambda) = S(\alpha) \cdot \left(\frac{10^8 \lambda^2}{cF_o}\right) \qquad (4.14)$$

Detailed tables for the cores of the lines have been given (Griem, Kolb, and Shen 1962a and 1962b) for L_α, L_β, H_α, H_β, H_γ, and H_δ. We have used these tables to interpolate values of $S(\alpha)$ for the core of the line when the temperature and density fell within the table. When the tables do not apply for the temperature and density under consideration, the approximate theory given by Griem (1960) is used to fill in the line

core. Similarly the detailed tables are used for He II $\lambda 4686$ and $\lambda 3203$ when they are applicable, and the approximate theory is used elsewhere.

The wings of the lines may be computed using the asymptotic formulae given by Griem, Kolb, and Shen (1959). They write the absorption coefficient as

$$a(\Delta\lambda) = a_{ION}(\Delta\lambda)\left[1 + R(N_e, T)\Delta\lambda^{1/2}\right] \qquad (4.15)$$

where in the wings, the ion broadening on the α scale is simply $S(\alpha) = C/\alpha^{5/2}$. The constants C have been given for the 6 hydrogen lines and 2 ionized helium lines mentioned above. The function $R(N_e, T)$ expresses the ratio of the electron broadening to ion broadening and the multiplicative factor $\Delta\lambda^{1/2}$ gives a net $\Delta\lambda^{-2}$ dependence, which is characteristic of a dispersion profile. This function has been tabulated for the 8 lines mentioned. Considerable simplification in the computations resulted from avoiding the problem of interpolating in these tables by following the suggestion of J. B. Oke that the behavior of $R(N_e, T)$ can be reproduced to within $\sim 1\%$ by using Griem's approximate formula

$$R(N_e, T) = \frac{4.6Z^{3/2}}{T^{1/2}}\left[\log_{10}\left(\frac{4 \times 10^6 Z T}{b^2 N^{1/2}}\right) - 0.125\right]\frac{b^2+a^2}{a^2b^2(b^2-a^2)^{1/2}} \qquad (4.16)$$

scaled by some constant factor. a and b are respectively the principal quantum numbers of lower and upper levels of the transition. The need for such a factor is apparently due to the approximations

made for the values of the transition matrix elements entering the exact formula. Thus setting A = (exact result from tables of $r(N_e, T)$)/(approximate value of R obtained from equation 4.16) we obtain the results listed in table 7.

Table 7

Line	A
L_α	1.81
L_β	1.65
H_α	1.48
H_β	1.13
H_γ	1.06
H_δ	0.97
He II λ4686	0.816
He II λ3203	0.599

With these values of A we may reproduce the value of R with good accuracy, and we have a simple analytical expression that completely accounts for the variation with temperature and electron density.

In a later paper Griem (1962a) showed that the expression given above for the wing had to be modified to allow for strong collisions, and we have used his modified theory in the present computations.

Since detailed tables have not been given for higher series members, and for other cases of astrophysical interest, e.g. the Paschen and Pickering lines, we use the approximate theory for these lines, including the modifications given in the later paper. A comparison

by Griem of his approximate formulae with the exact results for the first few Balmer lines shows the errors made are sufficiently small that the approximate theory may be used with good confidence for the higher series members.

It should be noted here that we assume that the perturbers are singly ionized only. The effects of doubly charged perturbers has been discussed by Griem (1961) who points out that in the quasi-static approximation the broadening scales as $ZN_Z^{2/3}$ compared with $(ZN_Z)^{2/3}$ which, for a given electron density, is the mean field strength of an equivalent number of singly charged ions. Thus if all of the ions are doubly charged, the error is a factor of $2^{1/3}$, or 10%-15% (the order of accuracy of the theory itself). If we assume $N(He)/N(H) = 0.15$, and assume both H and He are completely ionized, the effect of doubly charged particles is only about 6%. Further, allowing for the fact that broadening by electrons is as important as the ion broadening, the effect drops to about 3%. Therefore no serious error is made here.

4. The transfer problem

The atomic absorption coefficient obtained above is converted to a mass absorption coefficient (per gram of stellar material) by multiplying by $F^*/\mu m_H$ where F^* is the number of neutral H atoms in the proper excitations state. Thus if f_1 is the fraction of all H atoms that are neutral,

$$F^* = f_1 \frac{2n^2}{B_o(T)} e^{-(\chi_{ION}/kT)(1-1/n^2)} \qquad (4.17)$$

where $B_o(T)$ is the partition function of neutral H. Now writing

$$\ell_\nu = \frac{\ell^*_\nu F^*}{\mu' m_H} \tag{4.18}$$

we find the total monochromatic optical depth at a distance $\Delta\lambda$ from the center of the line is

$$t_\nu = \int_o^\tau \frac{\kappa_\nu + \sigma_\nu + \ell_\nu(\Delta)}{(\kappa_\nu + \sigma_\nu)_{STD}} d\tau_{STD} \tag{4.19}$$

where κ_ν and σ_ν are respectively the mass absorption coefficient and mass scattering coefficient in the continuum at the center of the line, and $(\kappa_\nu + \sigma_\nu)_{STD}$ are the corresponding quantities at the standard wavelength used in the construction of the model. ℓ_ν here is the total line absorption coefficient; thus the problem of overlapping lines is treated by computing the absorption coefficient for each and summing all contributions. The emergent flux is then given by

$$F_\nu(\Delta\lambda) = 2\int_o^\infty S(t_\nu) E_2(t_\nu)\, dt_\nu \tag{4.20}$$

this integration being performed as described in Chapter III. The source function has been takes as $J_\nu \equiv B_\nu$ in most cases. In a few cases we have taken $S_\nu(\Delta\lambda) = (1-\rho_\nu)B_\nu + \rho_\nu J_\nu$ where now

$$\rho_\nu = \frac{\sigma_\nu}{\kappa_\nu + \sigma_\nu + \ell_\nu(\Delta\lambda)} \tag{4.21}$$

We again solve for the source function by the methods indicated in Chapter II. For the sake of economy we found it useful to take as the first estimate of the source function at a given $\Delta\lambda$, that found at the preceeding $\Delta\lambda$. We start from the point farthest in the line wing using

the continuum source function (found by solving the Milne-Eddington equation) and proceed towards the core of the line. Now since $\rho_\nu(J_\nu - B_\nu) = (S_\nu - B_\nu)$ we estimate J_ν at point i in terms of the source function at point i-1 as: $J_{\nu,i} = \frac{1}{\rho_{\nu,i-1}}(S_\nu - B_\nu)_{i-1} + B_\nu$. With this estimate of $J_{\nu,i}$ we estimate $(S_\nu - B_\nu)_i$. If $|S_{\nu,i} - S_{\nu,i-1}|/S_{\nu,i-1}$ is everywhere $< 5 \times 10^{-3}$, we do not solve the Milne equation but merely use the estimated value of $S_{\nu,i}$ in equation 4.20. For larger changes we again solve the Milne equation. At each point the newly computed flux is compared with the value obtained using $S_\nu \equiv B_\nu$; whenever the difference is less than 1/2 %, the black body solution is assumed to be valid throughout the remainder of the core of the line. If more than one line is present, we skip an equal distance beyond the core of the line we are currently approaching and test again; successive skips are made until we again reach a place where the Milne equation must be solved. Naturally it is found that important changes in the emergent flux occur only in the line wings; however, since the continuum flux also changes, the residual intensities $R(\Delta\lambda) = F_\nu(\Delta\lambda)/F_{cont.}$ change throughout the line.

To obtain the equivalent width of the line we have performed the integration $\int_{-\infty}^{\infty}(1-R_\nu)\,d\lambda$ using a three point Lagrangian integration formula for unequally spaced points.

5. Results for the hydrogen lines

The results given here assume the source function is simply the black body function and that in equation 4.2, $v_{turb} \equiv 0$. Detailed

profiles for H_β and H_γ are tabulated in appendix V. For models with $\theta_e \leq 0.157$, the blending with the overlapping Pickering series line is accounted for by direct addition of the absorption coefficients of each line. The vacuum wavelengths of the lines were determined from the ionization terms values given in Miss Moore's tables (1948).

One rather remarkable result of the computations is that the equivalent widths of H_β and H_γ are very nearly the same over the entire temperature and gravity range considered although the detailed profiles are, of course, appreciably different. A graph of log W for H_γ is given in figure 34. The profiles are nonetheless similar enough that the following qualitative remarks hold for both lines.

At $\theta_e = 0.7$, the gravity sensitivity of the line profile is small. Near the core ($\Delta\lambda < 10$ Å), the profile becomes broader with <u>decreasing</u> log g. This may be understood in terms of the increased degree of ionization which occurs for the low g models at these low temperatures; this increases the number of perturbing electrons available and gives a broader profile. In the wings, the situation changes in that the residual intensity is successively larger for the log g = 3, 4.44, and 2 models. The total equivalent widths reflect these features; the log g = 3 model has the greatest equivalent widths, followed by log g = 4.44 and log g = 2 successively. The total variation in equivalent width is only 10%.

At $\theta_e = 0.6$, we obtain already a monotone gravity dependence except near the very core ($\Delta\lambda < 5$ Å). The profiles for the log g = 4 and 4.44 models have virtually no gravity sensitivity, and they differ by about only 1 or 2 per cent. The log g = 3 profile falls onto the higher gravity profiles to within 1 or 2 per cent for $\Delta\lambda < 10$ Å (except

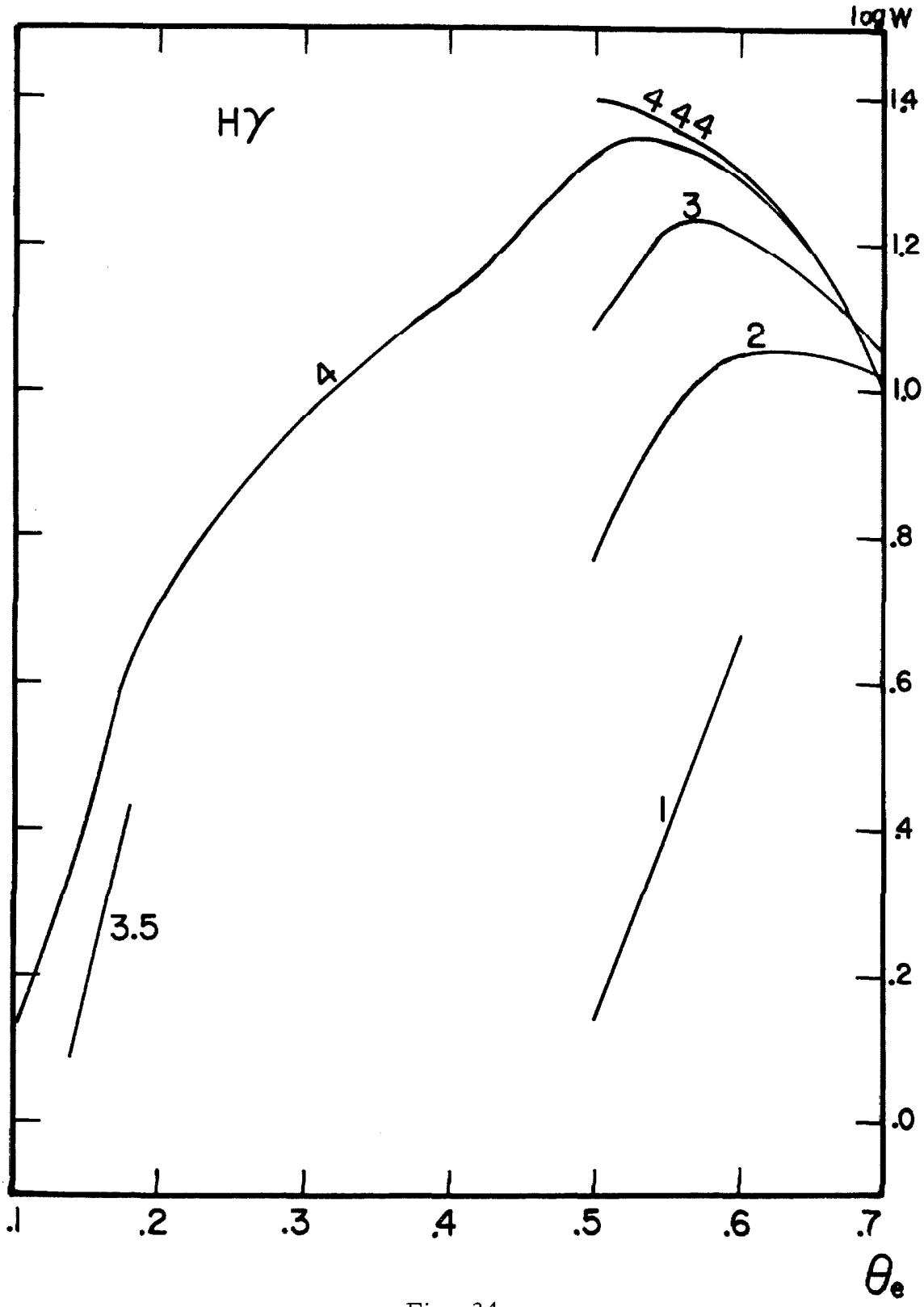

Fig. 34

at the center of the line), and at larger $\Delta\lambda$'s departs appreciably from these profiles. The log g = 2 and log g = 1 profiles stand quite distinct from the others.

At $\theta_e = 0.5$, the profiles are all distinct as a function of gravity. The broadest profile obtained in the present computations is the $\theta_e = 0.5$, log g = 4.44 case which still shows a depression of 5% into the continuum at $\Delta\lambda = 50$ Å.

For a given gravity, as is well known, the lines first increase in strength with increasing temperature, attain a maximum intensity, and then decrease in strength monotonically. The maximum equivalent widths appear to be reached at $\theta_e = 0.54$, 0.56, and 0.60 for log g = 4, 3, and 2 respectively.

The effects of the Pickering series lines is shown in figure 35; here it is seen that the helium lines add appreciably to the equivalent widths only for $\theta_e \leq 0.16$. The cross in figure 35 is the equivalent width of H_γ (including Pickering line) for the model with N(He)/N(H) = 0.05. The equivalent widths derived for H_β and H_γ ignoring the Pickering lines are given in table 8.

Table 8

θ_e	log g	$W(H_\beta)$	log W	$W(H_\gamma)$	log W
0.101	4			0.99	-0.003
0.14	4	2.02	0.304	2.01	0.303
0.14*	4			1.98	0.296
0.14	3.5	0.98	-0.011	0.94	-0.025
0.157	4	3.05	0.484	3.08	0.488

*N(Ne)/N(H) = 0.05; otherwise N(He)/N(H) = 0.15.

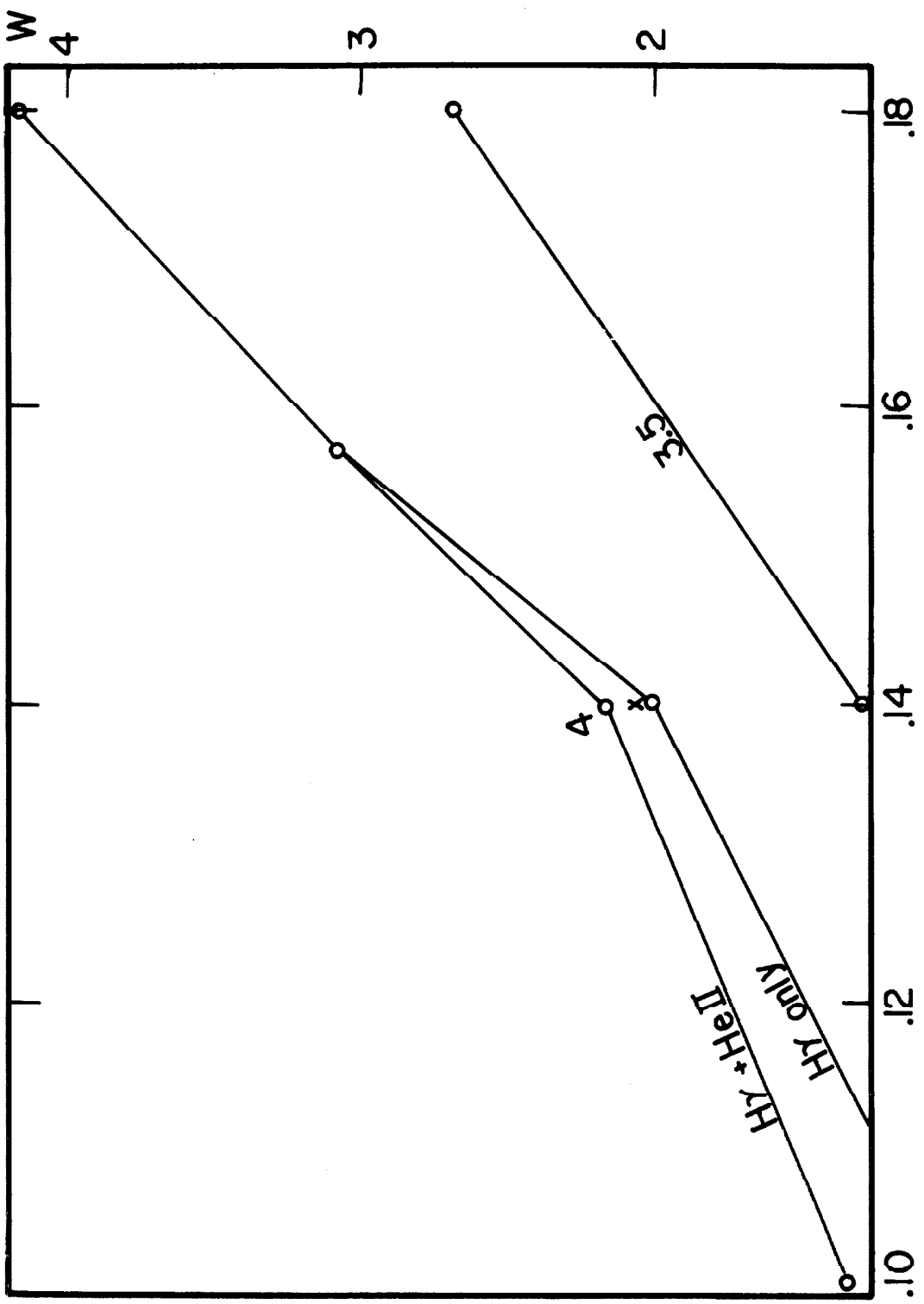

Fig. 35

It is important to note that at $\theta_e = 0.14$, changing the helium to hydrogen ratio by a factor of 3 produces only a quite unimportant change in equivalent widths of the line, as might be expected from the similarity of the $\log T - \log p_e$ relation as discussed in Chapter III. At $\theta_e = 0.18$, the change is again small, and in the opposite direction. Thus over this range the helium abundance gives rise to important changes in the observed equivalent widths of the hydrogen lines only because of the contribution of the Pickering series line to the blend. It should also be noted that at these temperatures the hydrogen lines are still sensitive to changes in the gravity.

To determine the true importance of the radiative damping terms discussed in section 2 we computed the cases where they were likely to have the largest effects, namely the $\theta_e = 0.101$ and the $\theta_e = 0.5$, $\log g = 1$ models, both allowing for radiative damping and not. It was found that there was no detectable change in the $\theta_e = 0.101$ case, while the $\theta_e = 0.5$ profiles were altered noticeably only in the steepest part of the profile, corresponding to a trivial increase in the half-widths of the core of the line. Therefore radiation damping can safely be neglected in all cases for the Balmer lines (as was done in these computations; the profiles tabulated for the $\theta_e = 0.5$, $\log g = 1$ model do, however, include the damping). The damping parameters tabulated in appendix III thus have no relevance to this work, but it is hoped they may be of value in other concepts.

Since the ultimate goal of this study is to compare theory with observation, we really need a fine network of models at various temperatures and gravities; such a network has not yet been constructed

at all the points desired, but will be done at the first opportunity. We therefore resorted to attempting to fit our results with a simple interpolating formula, and will use this formula below to fit the observations; this procedure may yet lack accuracy because insufficient data is at hand to devise an acceptable relation, but at present we have no alternative, and furthermore we may use the results of such a procedure to make a better guess for the atmospheric parameters to make a model for a specific star. We expect the strength of H_γ, say, to be the sum of a contribution from H and from He (due to the overlapping Pickering line), so we write $W(H_\gamma) = W_1(H) + W_2(He)$. For a given gravity we expect W_1 and W_2 to be functions of θ_e; elementary theory indicates that roughly W is proportional to $g^{1/3}$, so we write $W_1(H) = f(\theta_e)g^{p(\theta_e)}$, where the exponent of the gravity is assumed to be a function of θ_e (this was found to be necessary). Similarly we write $W_2(He) = (Y)^q(g)^r h(\theta_e)$, where $Y \equiv N(He)/N(H)$.

Now from the results at $\theta_e = 0.14$, log g = 4, we find $W(H) = 2.17$ for $Y = 0.15$, $W(H_\gamma) = 2.04$ for $Y = 0.05$, and $W(H_\gamma) = 1.98$ for $Y = 0$. Thus we find that the increase of the strength of the He component of H_γ is <u>linear</u> in Y, so we take $h(0.14) = 0.18$, $f(0.14) = 1.98$, and $q \equiv 1$. At $\theta_e = 0.14$, log g = 3.5 we have $W(H_\gamma) = 1.22$ for $Y = 0.15$, and we adopt $W(H_\gamma) = 0.91$ for $Y = 0$, so that $W_2(he) = 0.31$. In this way we find that the relative importance of the He component increases by a factor of $1.72 \approx \sqrt{3}$ so we have nearly a $g^{-1/2}$ dependence. Thus for lack of better information we adopt $W_2(He) = h(\theta_e)(Y/0.15)(g/10^4)^{-1/2}$. Similarly, by using the computed results at $\theta_e = 0.14$, $\theta_e = 0.18$, and interpolating graphically at $\theta_e = 0.25$ we find

that $W_1(H)$ is proportional to $g^{0.676}$, $g^{0.384}$, and $g^{0.238}$ respectively. The temperature dependence of the exponent was found, by trial and error, to be fitted well by $p(\theta_e) = 1.18 \times 10^{-2}(T_e/10^4)^3 + 0.126$. Finally, we wrote simply $f(\theta_e) = 1.98 + 63.5(\theta_e - 0.14)$ for $\theta_e \leq 0.157$, and $f(\theta_c) = 3.06 + 50.5(\theta_c - 0.157)$ for $\theta_c \geq 0.157$, and similarly $h(\theta_e) = 1.51 - 9.4\theta_e$. In this way we were led to adopt the interpolating formula:

$$W(H_\gamma) = \begin{Bmatrix} 1.98 + 63.5(\theta_e - 0.14) \\ 3.06 + 50.5(\theta_e - 0.157) \end{Bmatrix} \left(\frac{g}{10^4}\right)^{[1.18 \times 10^{-2}(T_e/10^4)^3 + 0.126]} + \left(\frac{\gamma}{0.15}\right)(1.51 - 9.4\theta_e)\left(\frac{10^4}{g}\right)^{1/2} \qquad (4.22)$$

with the understanding that if the second term goes negative it is set to zero. This formula should have decent accuracy at least on the range $3.5 \leq \log g \leq 4.5$ and $0.14 \leq \theta_e \leq 0.18$, although it will be important to check it carefully when further computations are available.

We may expect to use the strength of H_γ as an indicator primarily of the temperature and gravity. It will be important also to compare the theoretical profiles with the observed profiles since the equivalent width measured depends where the continuum is placed, although this can be done relatively unambiguously for the O stars. Further, if turbulent motions are present, and indications are that they are indeed present (Slettebak 1956), the equivalent width alone will lead to an incorrect value of the temperature and gravity. Since this study does not introduce new data on the profiles of the lines, a detailed comparison with other observers' data will be deferred until later.

6. Results for the ionized helium lines

The computed profile for the Pickering series lines λ4200, λ4542, and λ5412 as well as for λ4686 are given in appendix V, and their behavior is plotted in figure 36; we should emphasize that only a few points are actually available, so that the curves in figure 36 are only reasonable estimates of the detailed behavior of the line strengths. A model at $\theta_e = 0.12$ is badly needed to define clearly the maximum intensities of the lines. The earlier apparent discrepancy found by Miss Underhill (1951) that the helium lines were less intense in her "O5" model than in her "O9.5" model appears merely to be the result of the true maximum intensity of the lines occurring near $\theta_e = 0.125$ ($T_e = 40,000^\circ K$) (see also Traving, 1955); the indicators that allow us to distinguish clearly between the two sides of the maximum are the hydrogen and neutral helium lines, both of which are monotone decreasing on this range.

The resulting line profiles are very extended and shallow, emphasizing the observational difficulty of obtaining accurate measures of their intensities. Of the four lines computed, only λ4686 saturates heavily in the core, so the computed strengths should not be very sensitive to the boundary temperature of the model, which of course is the region of greatest uncertainty of the model. It is seen that λ4686 decreases in intensity at the highest temperatures more rapidly than the Pickering lines. This may mean that as the Boltzmann factor (which usually favors the $n = 3$ lower level of λ4686) approaches unity at even higher temperatures, the greater statistical weight and sensitivity to Stark broadening of the lower level ($n = 4$) of the

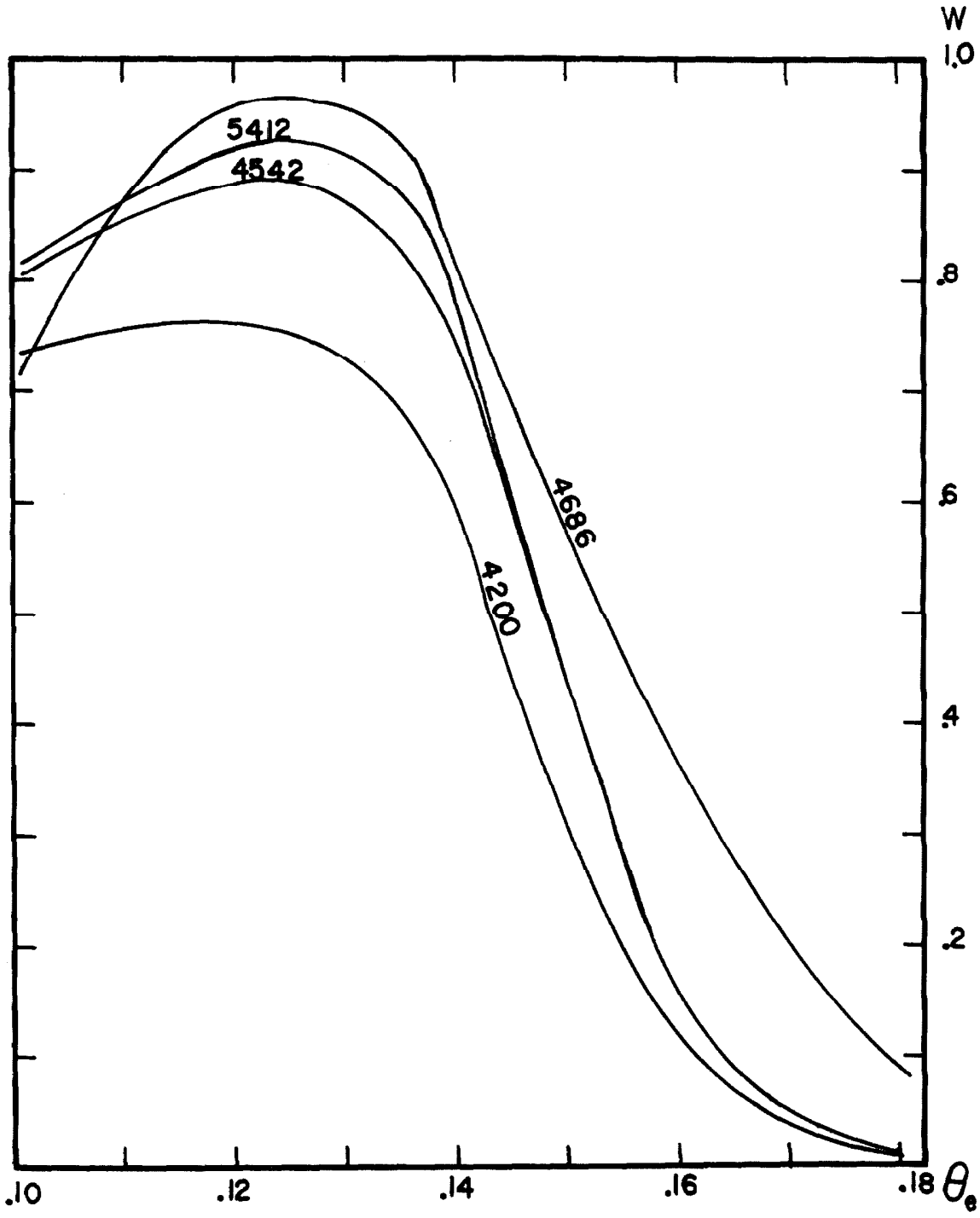

Fig. 36

Pickering series becomes dominant in determining the relative intensities of the lines.

As in the case of the hydrogen lines, we fitted analytical interpolation formulae to the computed points; the formulae are less elaborate than the hydrogen line formula because of the smaller number of data points available to make the fit, and may be correspondingly less reliable. They should be most reliable near $\theta_e = 0.14$. But again this is the best we can do at present; thus we write:

$$W(\lambda 4200) = f_1(\theta_e)(Y/0.15)^{0.621}(g/10^4)^{0.064} \qquad (4.23)$$

$$W(\lambda 4542) = f_2(\theta_e)(Y/0.15)^{0.504}(g/10^4)^{0.174} \qquad (4.24)$$

$$W(\lambda 5412) = f_3(\theta_e)(Y/0.15)^{0.416}(g/10^4)^{0.198} \qquad (4.25)$$

$$W(\lambda 4686) = f_4(\theta_e)(Y/0.15)^{0.375}(g/10^4)^{0.258} \qquad (4.26)$$

It is apparent that the ionized helium lines are relatively insensitive to gravity changes, but their strong temperature sensitivity makes them ideal for temperature determinations. The value of $f(\theta_e)$ is obtained either graphically or by interpolating in tables derived from the smooth curves shown in figure 36. The formulae derived here will be used to fit the observations below, and we wish to stress now that conclusions based upon them may need revision when more models become available. Probably at best we can only make a good estimate of the parameters for which we should construct the next model in order to fit the observations, and continue this process until either we obtain a good fit or conclusively fail.

7. The neutral helium lines

The neutral helium lines are broadened primarily by the quadratic Stark effect. The theoretical treatment of the problem has recently been completely revised by Griem, Baranger, Kolb, and Oertel (1962) to include the effects of non-adiabatic impacts with electrons; this theory has been shown to be in excellent agreement with laboratory measures. We have computed the profiles and equivalent widths of four neutral helium lines, λ4121, λ4438, λ4713, and λ5876; the results are listed in appendix V. The f values for λ5876 and λ4713 were taken from Trefftz, et al. (1957) and for λ4121 and λ4438 from Jugaku (1959).

The first three of these lines are members of the sharp singlet and triplet series, which are not as well observed in stellar spectra as are the diffuse series lines. However, since no theory exists for most of the diffuse series lines, we were able to use only λ5876. The computations show the lines are formed in the very outermost layers of the atmosphere for the O stars, and (except λ4438) are saturated so that their strengths depend strongly upon the boundary temperature of the model. Indeed, as will be shown below, our computed intensities are all too small for the O stars, although they may be correct and useful for lower temperature stars where the lines are formed deeper in the atmosphere. The discrepancy between observed and computed intensities is most probably due to too high a boundary temperature for our models; Traving (1956) showed that taking the Lyman lines into account in his model of 10 Lac lowered the boundary

temperature from about 27,000°K to 18,000°K. This will affect the computed equivalent widths of the neutral He lines since the residual intensities in the core of the lines (which contribute most to the equivalent widths) are given by the boundary $B_\nu(T)$, which has essentially the Rayleigh-Jeans value and therefore proportional to the temperature. Thus the residual intensity may decrease by a factor of 2/3 which, in the case of λ5876 for $\theta_e \approx 0.14$ roughly doubles the equivalent width of the line. As may be seen below, the discrepancy with observation is a factor of this order for λ5876 for 10 Lac. Thus we have another indication that at least the outer layers of our models will need revision; but to include the hydrogen lines is still a big job, and will take some time yet.

Chapter V

COMPARISON OF THEORY WITH OBSERVATION

1. Observational technique

Observations were made using the coudé scanner of the 100 inch telescope. This instrument is a slit instrument capable of high resolution; it has been described briefly by Oke and Greenstein (1961). The instrument makes use of the standard spectrograph collimator (f.l. = 192") and the conde 114" camera with the plateholder removed. Normally it is used with grating 46B which yields a dispersion of 2.8 Å/mm in the second order. The scanner makes use of two 1P21 photomultipliers, one of which (unrefrigerated) monitors two bands 50 Å on either side of the region scanned, and the second (refrigerated with dry ice) scans the intensity in a 55 Å band by means of a prism moved in the focal plane of the camera in the direction of the dispersion. The wavelength region to be studied is selected by rotating the grating using a pre-calibrated scale; fine scanning can be done at several rates by changing the gear train from a driving motor to the cam which moves the prism. The signal from each tube is fed to a preamplifier located in the spectrograph room via two short lengths of low capacitance coaxial cable, and thence to two General Radio Corp. amplifiers. Coarse gain changes (decade steps) are made at the preamplifier; fine gain changes in the scan signal are made using 1/2 magnitude steps in an auxiliary resistor network connected to the G. R. amplifier, and in the monitor signal using a continuously variable helipot. The output of the monitor amplifier is input to a Moseley

voltmeter as a reference signal; the output from the scan amplifier is input to the Moseley as the signal to be measured. The output of the Moseley is the ratio of the scan signal to the monitor signal, and is fed directly to a moving-chart recorder. Thus in principle the instrument removes the effects of extinction (which is constant over the wavelength region covered) and seeing and guiding errors, which cause large fluctuations in the total intensity of the light entering the slit. In practice, the compensation is not quite perfect, so that appreciably noisier scans result when seeing is poor. Apparently one reason for this imperfect compensation is the variation in sensitivity across the face of the phototubes, which do not match exactly. Another troublesome effect which occurs when observations are made at large zenith distances is that atmospheric dispersion of the image gives it a "hot" and "cold" side, so that the slope between the two monitor points depends upon the position of the image upon the slit, and guiding errors or seeing tremor cause this slope to fluctuate, introducing another source of noise into the tracing. Still another difficulty is that since we do not integrate as one could with a photographic plate, we must widen the slit to work on faint objects, with a consequent loss of resolution. In the present observations the stars studied were mostly of the 6th magnitude, and it was necessary to use an entrance-exit slit combination of 800-500 microns, although in some observations of 10 Lac the slits were narrowed to 500-300 microns. The former slit width implies, then, an infinitely narrow line from a source, filling the entrance slit, would be observed to have a triangular profile whose base is 2.8 Å. This relatively low resolution made it impossible to

observe accurate line profiles, and as a result we give here only equivalent widths, which of course are completely unaffected by the wide slit since the instrumental intensity response is linear. Further, the problem of blends is worsened, so with this slit width one should observe only stars of early type where most of the lines are well separated.

One of the strongest arguments for the scanner is that we now have an instrument whose response is absolutely linear, and requires no linearity calibration with all of its associated uncertainties. This freedom from all of the intermediate steps required by the usual photographic processes promises a much higher systematic accuracy and far outweighs the difficulties mentioned above.

The usual observing procedure was to scan through the wavelength region towards increasing λ followed immediately by a scan in the reverse direction; this procedure was often repeated, giving two or more pairs of observations, although in some cases only 3 or 2 scans were obtained. At wavelengths longer than 4650 Å a Wratten 2A filter was inserted in the beam to eliminate the overlapping third-order ultraviolet.

We attempted to survey the entire observable spectrum, and as a guide used the list of lines in 10 Lac published by Traving (1956); this unfortunately led this inexperienced observer to overlook the neutral helium lines at λ5015 and λ5047, which are readily accessible to our equipment. To allow the survey, the scan rate most often used in these observations was to move the prism 5 mm/min (with an

effective dispersion of about 2.3 Å/mm), although a limited number of scans were made at 3 mm/min and 1.6 mm/min. In my opinion the 1.6 mm/min scans are so superior to the scans at higher rates for these fairly faint (at the conde) stars, that the slower scans of fewer spectrum features are strongly recommended.

The observations were reduced by superposing pairs of scans and drawing in a visual average of the tracings. The continuum was drawn in as a straight line; if the continuum sloped (as it would when the tube sensitivity changed through the region considered), it was rectified to full scale by using a uniformly expanding ruler; this procedure proved to be both accurate and quick. The equivalent widths was then determined by direct planimetry. The exact dispersion of the instrument was calibrated directly by scanning an iron arc spectrum, and was found to be given accurately by the relation: Effective dispersion = $2.2815 + 2.75 \times 10^{-5} (4000-\lambda)$ Å/mm where λ is in Å.

2. Observational results

The program stars were selected from the lists of early type stars given by Slettebak (1949, 1956) on the basis of having the lowest observed rotational velocities; stars with known emission features were also avoided. The stars whose observations will be discussed here are listed in table 9.

Table 9

Star	Spectrum	m_v	$v_{rot} \sin i$, reference
HD34078	09ssk	$5.4 \leq m_v \leq 6.1$	0 km/sec (1)
HD34656	07	6.79	90 km/sec (1)
HD47839	07n	4.65	90 km/sec (1)
HD55879	09s	5.99	0 km/sec (1)
HD57682	09 V	6.44	20 km/sec (1)
HD214680	09 V	4.88	0 km/sec (1), 25 km/sec (2)

(1) Slettebak, 1949, 1956

(2) Abt and Hunter, 1962

In addition we will refer to the results for τ Sco published by Traving (1955) and Jugaku (1959). At this point I would like to acknowledge that some scans of λ4686 in 10 Lac and HD34078 were kindly obtained for me by Drs. L. Searle and J. B. Oke.

The measured equivalent widths are given in tables 10 and 11, and plots of the hydrogen line strengths are shown in figure 37, and of the ionized helium lines in figure 38. A blank in one of the tables does not necessarily mean that the line is not present in the spectrum, but merely that the region may not have been scanned. When possible, an estimated standard deviation of the mean is given; if only two scans were available, the reduction procedure treated them essentially as one observation and no error is estimated. In many cases three scans, say A, B, and C, were combined in pairs AB and BC and were treated as two observations. Obviously this gives double weight

Table 10

SUMMARY OF 100" PHOTOELECTRIC OBSERVATIONS OF 10 Lac (HD214680)

λ	Ion	W ± σ	m
5876	He	.90±.02	4
5412	HeII	.71±.02	9
4922	He	.48±.02	6
4861	Hβ+HeII	3.31±.10	6
4713	He	.19	2
4686	HeII	.81±.04	5
4654	SiIV	.13±.01	4
4650-51	OII CIII	.47±.02	4
4647	CIII	.24±.02	4
4642	NIII OII	.15±.02	4
4631	SiIV	.12±.01	4
4553	SiIII	.12±.02	3
4542	HeII	.71±.02	4
4535	NIII	.13±.01	4
4524	NIII	.04±.01	2
4518	NIII	.05±.01	4
4515	NIII	.15±.02	4
4511	NIII	.15±.04	2
4481	MgII	.14±.01	9.5
4471	He	.99±.03	11.5
4438	He	.08	2
4388	He	.46±.02	5
4379	NIII	.11±.02	5
4340	Hγ+HeII	3.15±.09	4
4212	SiIV	.05	1
4196	NIII	.09	1
4190	OIII	.04	1
4187	CIII	.09	1
4185	OII	.03	1
4169	HeI OII	.06±.01	2
4163	CIII	.12±.03	3
4156	OII CIII	.10±.01	3
4153	OII	.14±.02	3
4151	NeII ?	.06	2
4144	He	.41±.01	2
4133	OII	.11±.03	3
4129	OII	.07	1
4121	He	.24±.01	2
4119	OII	.05±.004	2
4116	SiIV	.24±.02	2
4102	Hδ+HeII	3.12±.07	2
4097	NIII OII	.23±.02	*2
4089	SiIV OIII	.36±.02	2
4076	OII	.06	1
4026	He	1.15±.07	4.5
4009	He	.29±.05	2.5
4004	NIII	.12±.03	4
3995	NII	.06±.01	3
3970	Hε+HeII	3.62±.18	2.5
3965	He	.17±.003	**2
3962	OIII	.08±.01	**2
3934	CaII(INT.)	.18±.02	3
3820	He	.69	2
3807	SiIII	.04	2
3806	He	.05	2
3760	OIII	.17	2
3757	OIII	.13	2
3754	OIII NIII	.21	2
3727	NeII OII	.09	2
3634	He	.26	2

*Area Under Profile of Hδ (Determined by Symmetry)

**Area Under Profile of Hε

Table 11

SUMMARY OF 100" PHOTOELECTRIC OBSERVATIONS OF SELECTED LINES IN FIVE O TYPE STARS

Table Gives Equivalent Width in Å; m is Number of Scans;
One Standard Deviation is Given When Possible

λ	Ion	HD34078		HD34656		HD47839		HD55879		HD57682		"MEAN 09V"
		W ± σ	m	W ± σ	m	W ± σ	m	W ± σ	m	W ± σ	m	
5876	He											.90*
5412	HeII	.61	2	1.12±.01	3	.87±.05	2	.18±.02	2	.73±.04	3	
4922	He	.74	2	.69	2	.29	2	.84	2	.75±.04	6	.78**
4862	Hβ+HeII	3.18±.18	4			2.89	2	3.02	2	2.38±.16	3	
4686	HeII	.80±.05				.88±.05	4	.56±.07	2			
4713	He					.17	2	.33±.03	2			
4552	SiIII	.09	1					.16±.001	3			
4542	HeII	.49	2	.86	2			.42±.03	3			
4481	MgII	.17±.02	8					.20±.003	3	.19±.01	3	
4471	He	1.16±.03	12	.76±.02	8	.87±.01	3	.96±.02	3	1.11±.07	3	1.05
4437	He							.10	2			.09
4388	He	.54	2	.35±.03	4	.50	2	.56	2	.45±.02	3	.50
4341	Hγ+HeII	3.36	2	2.38±.05	5	2.84	2	3.38	3	2.91±.10	6	
4212	SiIV	.07	2							.12	2	
4200	HeII	.55	2	.59±.02	4	.53	2	.65	2	.64±.04	4	
4143	He	.45	2					.36	2	.37±.04	3	.40
4120	He	.32	2			.10	2	.27	2	.23	2	.26
4116	SiIV	.24	2			.10±.01	3	.34	1	.14	2	
4101	Hδ+HeII	3.50	2	2.47	2	2.53±.01	3	3.17	2	2.38±.18	3	
4089	SiIV	.33	2	.32	2	.20±.06	3	.37	1	.32±.02	3	
4026	He	1.11	2					1.11±.01	3	.94±.03	3	1.08
4009	He	.40±.03	4					.40±.01	3	.28	2	.34
4004	NIII							.14±.01	3			
3970	Hε+HeII	3.02±.04	4					3.50	1	2.69±.07	3	
3964	He							.10†	1	.09±.01	3	
3934	CaII(INT.)	.19±.01	5	.30±.03	5					.18±.01	3	
3923	HeII			.75	2							
3868	He	.15	1					.65±.03	3	.63±.00	3	.65
3820	He	.63	2	.32	2							.05*
3806	He							.41	1			.33
3634	He											.02***
3587	He	.02	1									

* 10 LAC only

** 10 LAC excluded

***HD 34078 only

†Area below Hε

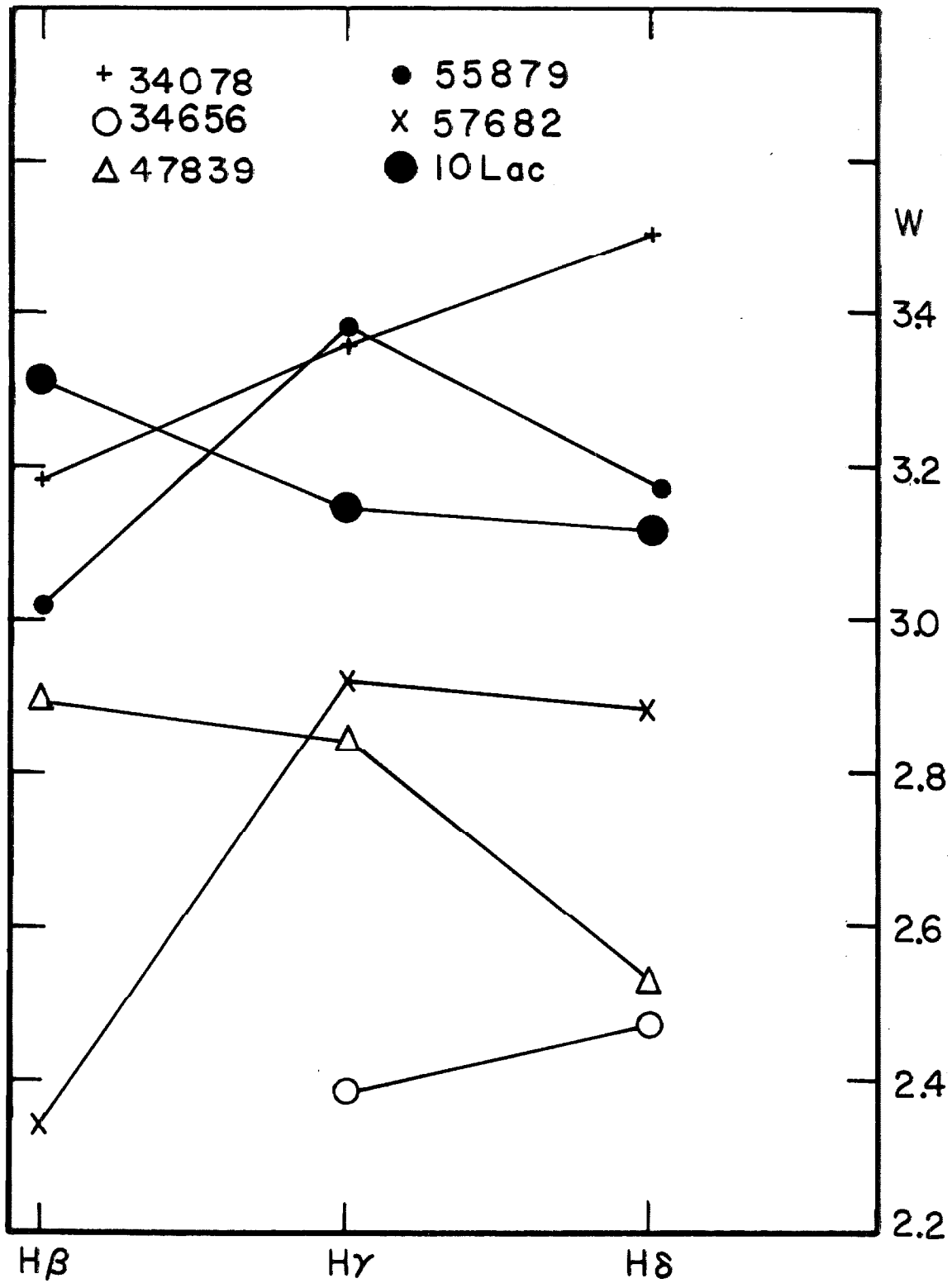
+ 34078
○ 34656
△ 47839
● 55879
x 57682
● 10 Lac
W
3.4
3.2
3.0
2.8
2.6
2.4
2.2
Hβ
Hγ
Hδ

Fig. 37

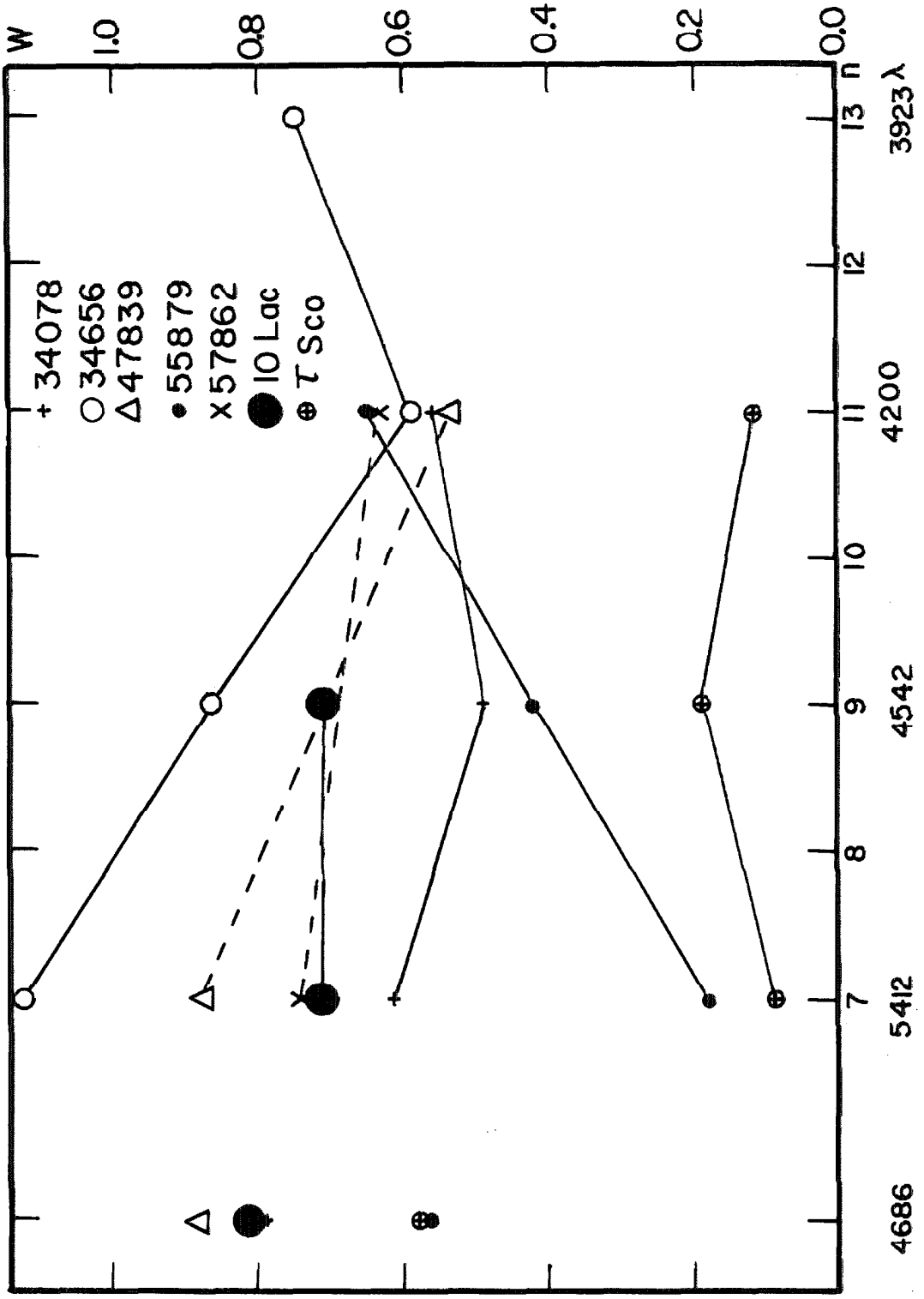
W
1.0
0.8
0.6
0.4
0.2
0.0
n
3923 λ
13
12
11
4200
10
9
4542
8
7
5412
4686
+ 34078
○ 34656
Δ 47839
• 55879
× 57862
10 Lac
⊕ τ Sco

Fig. 38

to one scan (usually taken to be the best of the three), so that the error quoted here does not have a rigorous meaning, but is basically just a useful guide to the internal consistency. We also give the number of individual scans employed in forming the mean; in the case of 10 Lac, some scans were assigned 1/2 weight, while no such distinction was made for the other stars. We note in passing that measures of λ4200 in 10 Lac unfortunately were not obtained because of equipment failure during the observations. Finally, in the last column of table 11 and in figure 39 we give mean values for the intensity of the diffuse singlet and triplet series in the four O9 stars (unless otherwise noted); these series show a very regular behavior with small scatter, which should be important to study theoretically. Unfortunately a definitive theory does not yet exist for the line broadening of the diffuse series, so we must leave the matter as an observational result only.

It is quite discouraging to inter-compare the published observed equivalent widths of lines in the O stars; there exist large systematic differences from observer to observer, and it will be of prime importance to obtain many more accurate observations of these objects with the highest photometric accuracy possible before we regard agreement or disagreement with theory as decisive. The most dramatic discrepancies occur for the hydrogen lines. For example, various measures of H_β and H_γ in HD47839 differ by a factor of about 1.5 to 2; this star is a variable, and while spectrum variations may be present, it is difficult to believe that the variation could be this large. Similarly, measures of H line strengths in 10 Lac show a range of almost a factor

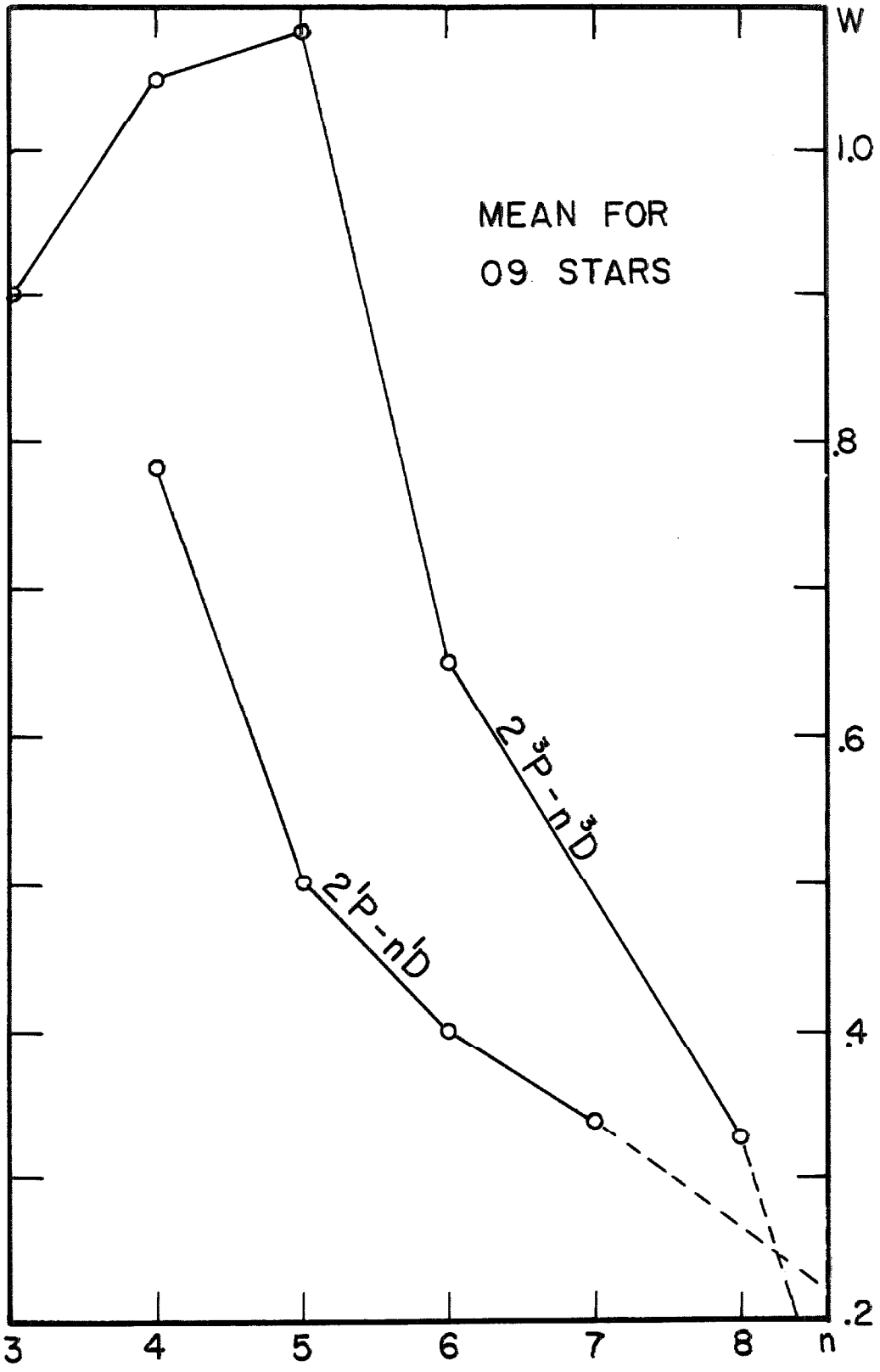

Fig. 39

of 2 and variability is certainly not the cause here. It appears that systematic errors have entered significantly into many of the observations of these objects. We therefore have correlated the present observations with those of previous observers. The correlation for 10 Lac of the present measures with those of Traving (1956) is shown in figures 40 and 41. It is gratifying to note there is no pronounced systematic difference between the two sets of observations; H_β and H_γ agree essentially exactly, although H_δ and H_ϵ disagree. Further observations will be required to resolve this discrepancy, but it may fairly be noted that the present measures of H_δ are from tracings of very high quality. Since H_γ falls in the most reliable photometric region, it alone will be adopted to characterize the strength of the hydrogen lines. We note here that the H_β measurement for HD55879 is quite uncertain, and needs badly to be remeasured.

The results of the correlations with other observers are given in table 12. The tabulated quantity is the slope of the line through the origin which best fits the scatter diagrams of the two sets of observations; in many cases, only a few points were common to both sets of observations, so the slopes given here are only approximate and should not be used for transformation purposes. As the table shows, the best agreement was obtained with Traving's and Williams's (1934, 1936) measures, and the worst with those of Rudnick (1936). We emphasize again the need for further observations of these stars in order to carry out more accurate analyses.

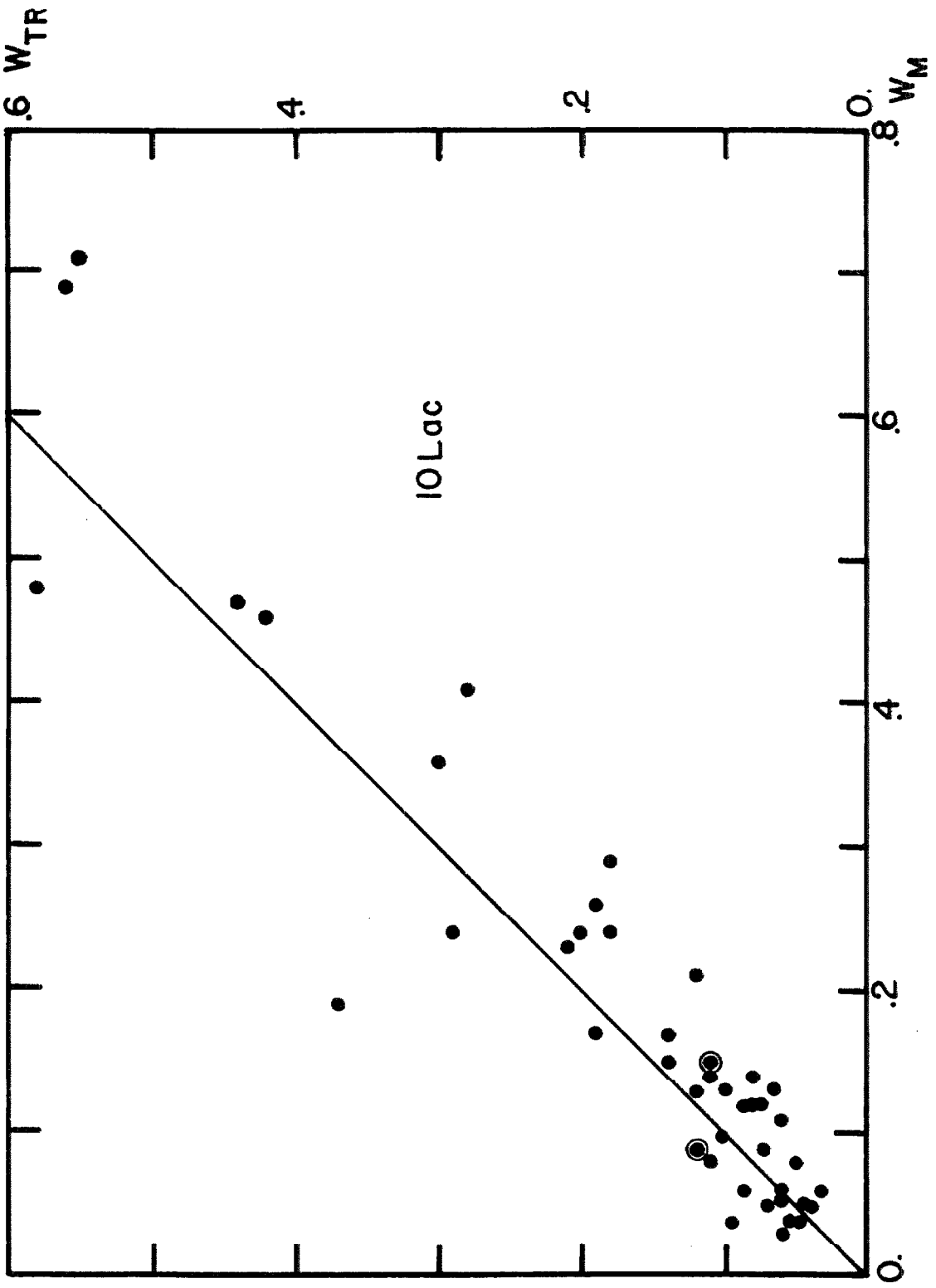

Fig. 40

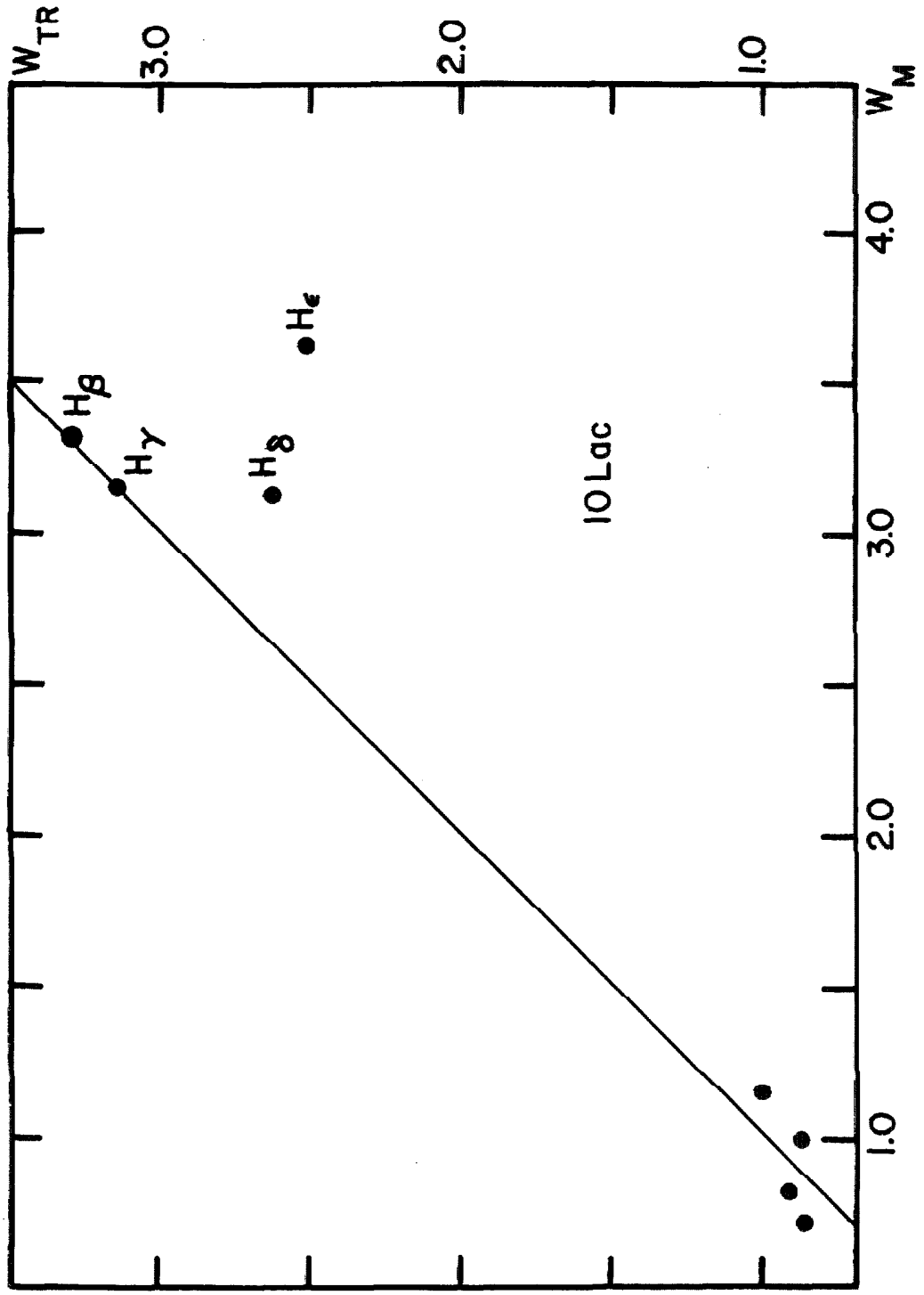

Fig. 41

Table 12

Table Gives $W_{Observer}/W_{Mihalas}$

Observer/ Star	Traving	Williams	Oke	Rudnick	Slettebak	Roach and Blitzer
34078					1.0:	
34656			0.96		0.76	
47839		0.86	0.78	0.54	0.78	
55879						
57862					0.82	
214680	1.00	1.00		0.55 for $W < 0.4$ W_m -0.17 for $W > 0.4$		0.83

3. The fitting procedure

From the observations we must untangle three unknowns: the temperature, the gravity, and the helium abundance. In our original attempt to find suitable fitting parameters, we adopted the ratios $[W(\lambda 4542) + W(\lambda 5412)]/[W(\lambda 4713) + W(\lambda 4121)]$ and $W(\lambda 4686)/W(\lambda 4713)$ as temperature indicators. They are ideal for the purpose as reference to equations 4.22-4.26 shows they should be quite insensitive to helium abundance and gravity changes; taking sums of line strengths has the advantage of decreasing the effects of observational errors. We then used the absolute strength of H_γ as the gravity indicator. With these values for θ_e and log g, we compared the strengths given by our interpolating formulae with the observed line strengths of all He lines except $\lambda 5876$ and derived a new estimate of the helium abundance. We then could repeat the cycle until we obtained a consistent set of

atmospheric parameters. When this procedure was actually carried through for 10 Lac it was found that self-consistent answers were obtained from H_γ and the ionized helium lines while the neutral helium lines gave helium abundance estimates that scattered by a factor of 4. The probable reason for this has already been discussed; we therefore abandoned the neutral helium lines as primary indicators. Instead, we make use of the fact that a given value for the equivalent width of a line defines a unique locus in the $\log g - \theta_e$ plane for an assumed value of N(He)/N(H). The intersection of the locus of H_γ with those of the four observable ionized He lines gives $\log g$ and T_e for the star. The intersection of all loci will be more or less at a point depending upon how closely the assumed helium abundance matches that in the star. By picking the value for which we obtain the best fit we can estimate the correct helium abundance. In practice, it turns out that the loci of the ionized helium lines determine the temperature while the locus of H_γ determines essentially the gravity. And as might be expected, it also turns out that the goodness of fit is not extremely sensitive to the helium abundance, so while one value is usually somewhat superior to the others, the derived abundances really are only estimates. This problem will be alleviated when correct predictions of the neutral helium line strengths can be made, since then we no longer need to force the ionized helium lines to do the double duty of indicating both temperature and He abundance. But at the same time this relative insensitivity to the He abundance implies that our estimates of θ_e and $\log g$ should be fairly reliable. The actual fits are shown in figures 42-47; in cases where estimates of the accuracy of

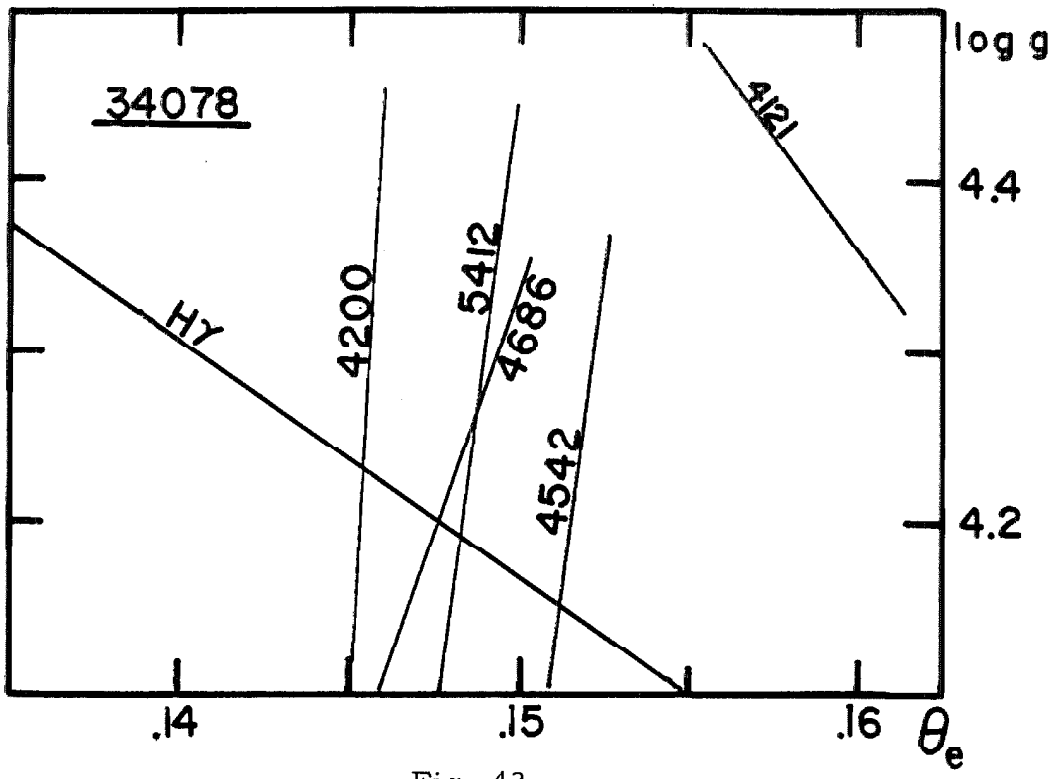
34078
log g
4.4
4.2
4121
5412
4686
4200
4542
HY
.14
.15
.16
θ_e

Fig. 42

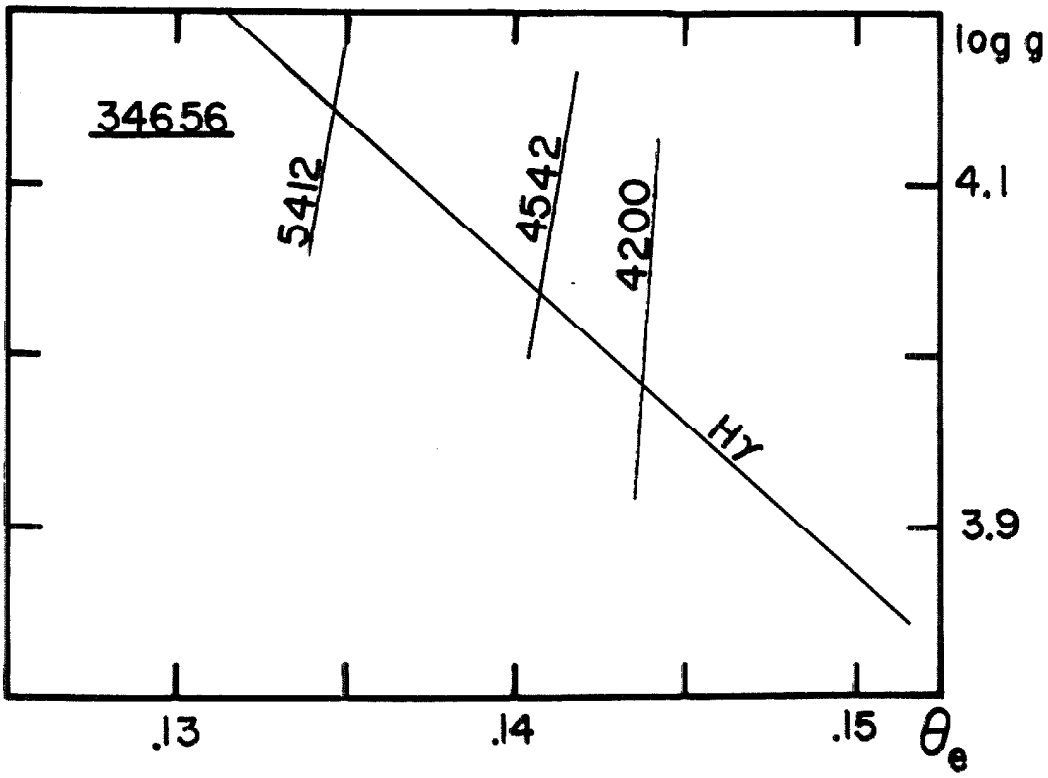
34656
log g
4.1
3.9
5412
4542
4200
HY
.13
.14
.15
θ_e

Fig. 43

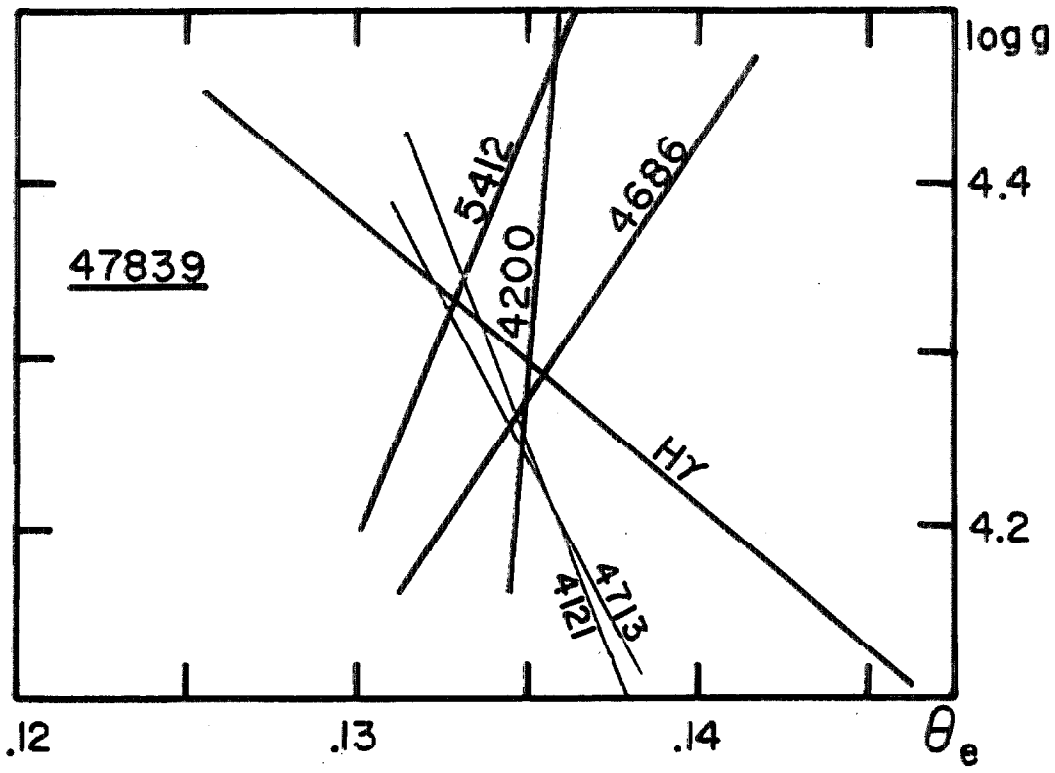
log g
4.4
4.2
47839
5412
4686
4200
Hγ
4713
4121
.12
.13
.14
θe

Fig. 44

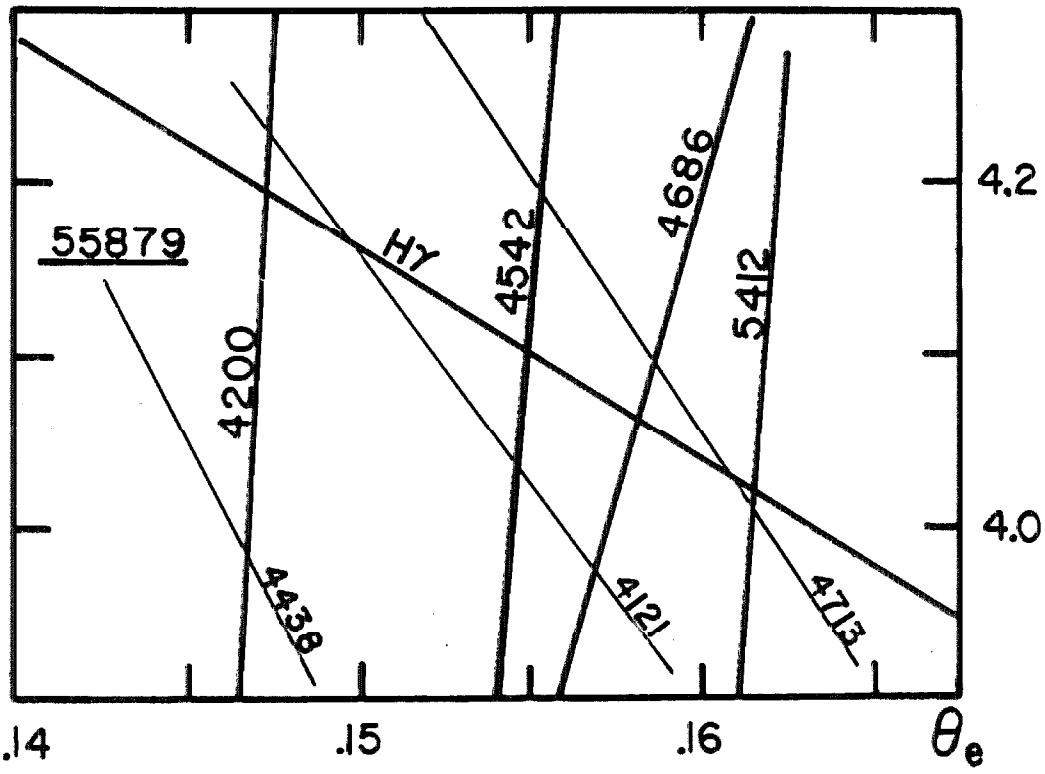
4.2
4.0
55879
Hγ
4542
4686
5412
4200
4438
4121
4713
.14
.15
.16
θe

Fig. 45

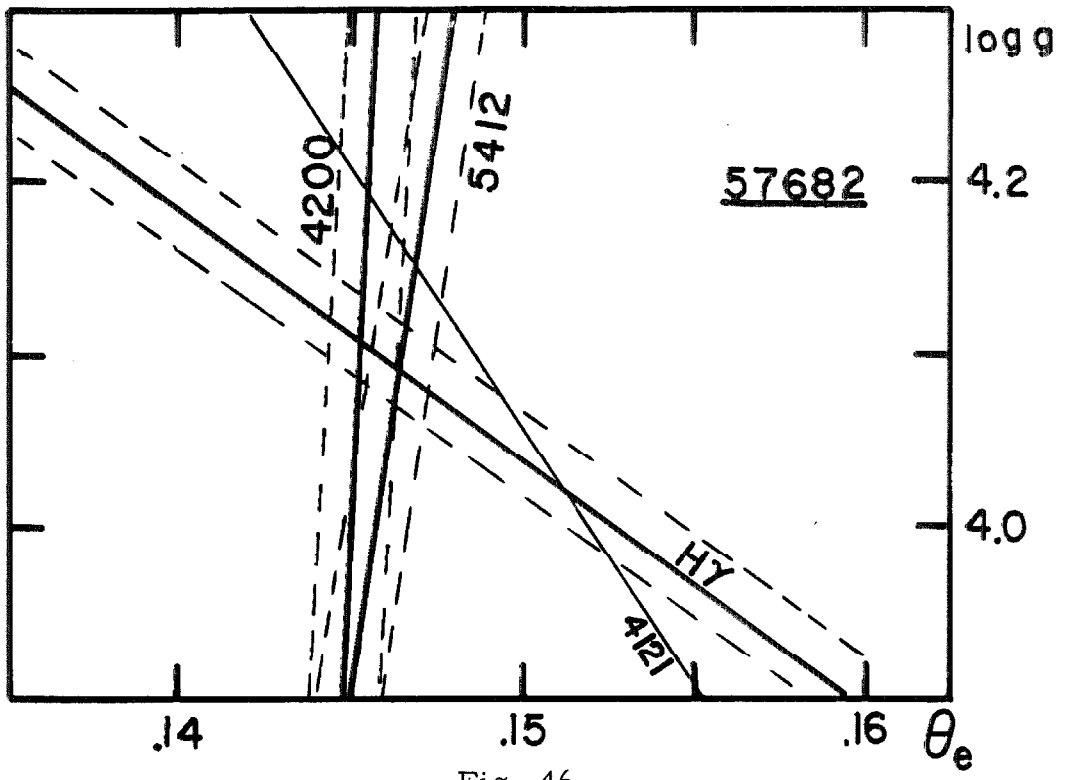
log g
4.2
4.0
57682
4200
5412
Hγ
4121
.14
.15
.16
θe

Fig. 46

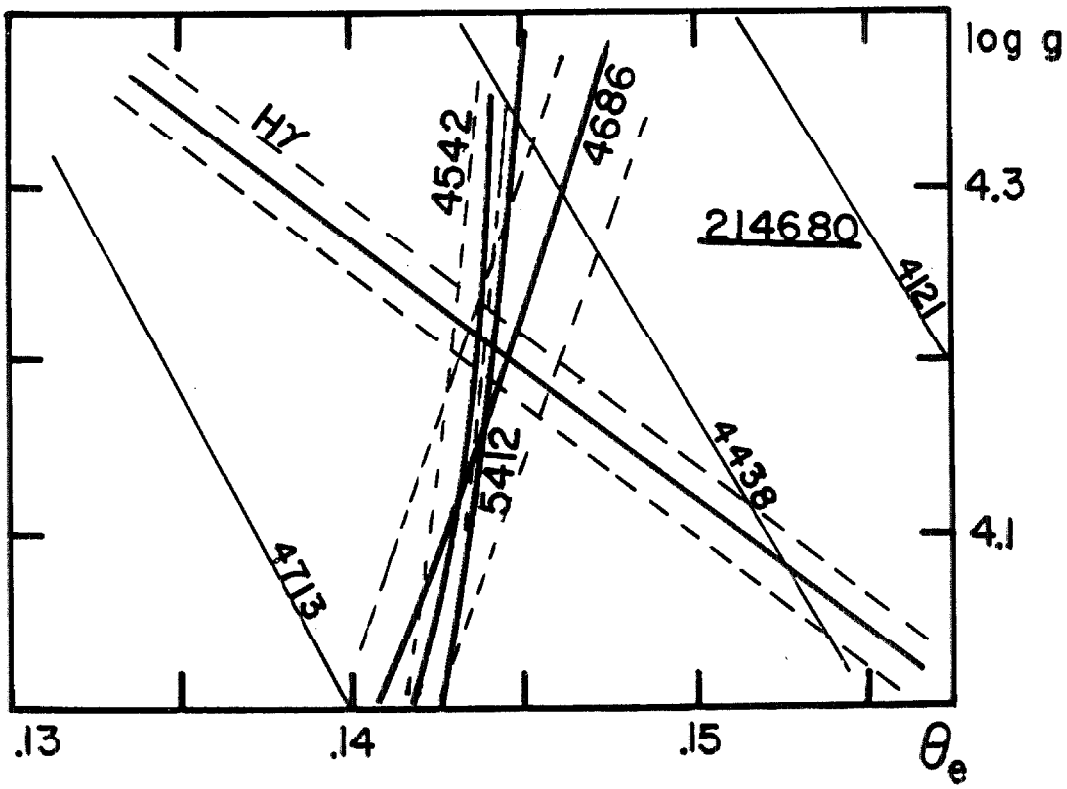
log g
4.3
4.1
214680
Hγ
4542
4686
4121
4438
5412
4713
.13
.14
.15
θe

Fig. 47

the observations are available, the dashed lines show the effects of changing the observed value by ± some error. In general the scatter due to observational error is smaller than the inconsistency of observation with theory so that the dispersion of the intersection of the loci should give a decent estimate of the errors possible in the derived values.

(a) HD34078 - This is a fairly good fit yielding $\theta_e = 0.148 \pm 0.003$, log g = 4.18 ± 0.04, and N(He)/N(H) ≈ 0.2. We may regard this star as a typical O9 star.

(b) HD34656 - This fit is relatively poor, but both increasing and decreasing the He abundance makes matters worse. Therefore we adopt $\theta_e = 0.139 \pm 0.0045$, log g = 4.06 ± 0.08, and N(He)/N(H) ≈ 0.2. The confidence that can be placed in this result will be increased when we obtain more observations of the lines already observed as well as an observation of λ4686.

(c) HD47839 - This star shows the lowest helium abundance of any in this study. We estimate $\theta_e = 0.134 \pm 0.0015$, log g = 4.31 ± 0.02, and N(He)/N(H) ≈ 0.1. The fit is good. Rather interestingly, the neutral helium line computations are consistent with observation for this object; this may be because the lines are not as fully saturated as at slightly lower temperatures. In any case we need a measure of λ4542 as well as more reliable computed line strengths at this temperature; otherwise the fit is good.

(d) HD55879 - This interesting object (see figure 38) is fitted best, although still poorly, by a very high helium abundance. Thus we estimate that N(He)/N(H) may be as high as 0.3 or more! Also we

find $\theta_e = 0.156 \pm 0.007$, and $\log g = 4.1 \pm 0.08$. Aside from the ever-present desire for better observations, we cannot regard this determination as definitive since we may have extrapolated our line strength estimation formulae beyond their range of validity, and obtained spurious results. This can be ascertained only with further computations. In any case this star certainly merits further study.

(e) HD57682 - Here we have too little data; we have only two observed He lines, so that we can force an exact fit for some He abundance, which obviously may be quite different from the true abundance. If we assume $N(He)/N(II) = 0.25$, we force a fit to within the observational error, and $\lambda 4121$ fits fairly well also. We estimate $\theta_e = 0.146 \pm 0.002$, and $\log g = 4.1 \pm 0.045$ which again we regard as typical of an O9 star, pending further observation; the helium abundance is undetermined.

(f) 10 Lac (HD214680) - This is the best fit of all, giving $\theta_e = 0.144 \pm 0.0015$, $\log g = 4.20 \pm 0.04$, and $N(He)/N(H) = 0.15$. As mentioned before, $\lambda 4200$ has not been observed here, but the other three lines are so consistent we can have good confidence in the result. The inconsistency of the neutral He lines is clearly shown in this fit, the closest agreement being given by $\lambda 4438$ which is the weakest of the three lines and the least saturated.

(g) τ_{Sco} - From the He line measures of Jugaku (1959) and the value given by Traving (1955) for H_γ we estimate $\theta_e = 0.160 \pm 0.006$, $\log g = 4.01 \pm 0.06$, and $N(He)/N(H) = 0.2$. The fit is inferior for both higher and lower He abundance. The temperature derived here is markedly lower than that proposed by Jugaku, and again it will be

important to check the validity of our line strength estimation formulae. Also it would be desirable to have observations on the same photometric system as the present set.

In summary we would estimate that a typical O9V star has $\theta_e = 0.146$ and $\log g = 4.2$, and that the best estimate for N(He)/N(H) is 0.15 to 0.20. The values for log g are lower than those derived previously, as to be expected from the broader hydrogen lines given by the new theory compared to the older Holtzmark theory. The difference is large considering we can reproduce the observed intensities of the hydrogen lines at $\log g = 4.2$ whereas Traving was unable to do so for 10 Lac assuming a log g of 4.45.

The value for the He abundance is in substantial agreement with the value published by the Kiel group (Traving 1955, 1956) and in disagreement with Miss Underhill's work (1948). This latter determination, however, rested upon a considerably less firm theoretical basis than either the present study or those by Traving and must be rejected. Further, the determination of the He abundance from stellar atmospheres is in disagreement with that from nebular studies (see e.g. Mathis, 1962). Whether the disagreement is due to errors of analysis or represents a real difference seems undecidable at present, and I would regret seeing the results given here used as evidence in any speculations.

Finally, making use of the empirical mass-luminosity relation in this range (taken from data summarized by Schwarzschild, 1958) in the form:

$$\log \frac{L}{L_\odot} = 2.45 \log \frac{\mathcal{M}}{\mathcal{M}_\odot} + 0.822 \qquad (5.1)$$

and making use of $L = 4\pi R^2 \sigma T_e^4$ and $g = G\mathcal{M}/R^2$ we may write:

$$\log \frac{\mathcal{M}}{\mathcal{M}_\odot} = -0.567 + 2.76 \log (T_e/T_{e\odot}) - 0.69 \log (g/g_\odot) \qquad (5.2)$$

$$\log \frac{R}{R} = \frac{1}{2} (\log \frac{\mathcal{M}}{\mathcal{M}_\odot} - \log \frac{g}{g_\odot}) \qquad (5.3)$$

and

$$\log \frac{L}{L_\odot} = 2 \log \frac{R}{R_\odot} + 4 \log \frac{T_e}{T_{e\odot}} \qquad (5.4)$$

In these equations we have assumed $M_{bol}(\odot) = 4.63$ and adopting $T_e(\odot) = 5760^\circ K$ and $\log g\ (\odot) = 4.44$ (Schwarzchild, 1958) we find the values given in table 13.

Table 13

Star	Spectrum	T_e	log g	$\log \frac{\mathcal{M}}{\mathcal{M}_\odot}$	$\log \frac{R}{R_\odot}$	$\log \frac{L}{L_\odot}$
HD34078	O9ssk	3.4×10^4	4.2	1.73	0.985	5.054
HD34656	O7	3.62×10^4	4.1	1.87	1.105	5.402
HD47839	O7n	3.76×10^4	4.3	1.78	0.960	5.176
HD55879	O9s	3.23×10^4	4.1	1.73	1.035	5.062
HD57682	O9V	3.45×10^4	4.1	1.81	1.075	5.258
HD214680	O9V	3.5×10^4	4.2	1.76	1.000	5.136

Thus we obtain for a typical O9V star: $\mathcal{M}/\mathcal{M}_\odot \sim 59$, $R/R_\odot \sim 10.5$, and $L/L_\odot \sim 1.4 \times 10^5$. These numbers are still very tentative in view of the rather large extrapolation made of the mass-luminosity relation. In particular, it is worth noting that the mass for HD34656 is above the

largest stable mass according to the calculations of Schwarzschild and Härm (1959). This may indicate that equation 5.1 is invalid or that we have derived incorrect values of θ_e and log g for this object; we consider the former to be more likely. All of the other stars in the list are near to, but below, the limit of pulsational instability.

It is to be hoped that both further observation and improved theory will soon improve our present estimates of the properties of these stars.

REFERENCES

Abt, H. and Hunter, J. H. 1962, Ap. J., 136, 381.

Aller, L. H. 1946, Ap. J., 104, 347.

_____. 1953, The Atmospheres of the Sun and the Stars, (New York: Ronald Press).

_____, and Jugaku, J. 1959, Ap. J., 130, 469.

_____, Elste, G., and Jugaku, J. 1957, Ap. J., Suppl., Vol. 3, No. 25.

Avrett, E. H. and Krook, M. 1962, Paper presented at Colloquium of I. A. U. Commission 36, Herstmonceux, England.

_____. 1963, Ap. J., 137, 874.

Baker, J. G. and Menzel, D. H. 1938, Ap. J., 88, 52.

Bates, D. R. 1952, M. N., 112, 40.

Berger, J. M. 1956, Ap. J., 124, 550.

Boggess, A. 1959, Ap. J., 129, 432.

Böhm, K.-H. 1960, Stellar Atmospheres, ed. J. L. Greenstein, Vol. 6 of Stars and Steelar Systems. (Chicago: University of Chicago Press), Chapter 2.

Breene, R. G. 1961, The Shift and Shape of Spectral Lines, (London: Pergamon Press).

Buckingham, R. A., Reid, S. and Spence, R. 1952, M. N., 112, 382.

Cayrel, R. 1961, Ann. d'Ap., 23, 245.

_____ and Traving, G. 1960, Z. f. Ap., 50, 239.

Chandrasekhar, S. 1931, M. N., 92, 186.

_____. 1950, Radiative Transfer, (London: Oxford University Press).

Claas, W. J. 1951, Pub. Astr. Obs. Utrecht, 12, Part I

de Jager, C. and Neven, L. 1960, B. A. N., 15, 55.

Demarque, P. 1960, Ap. J., 132, 366.

Erkovich, S. P. 1960, Opetha I. Spectr., 8, 307.

Gingerich, O. J. 1961, Thesis, Harvard University.

_____. 1962, Paper Presented at 110th Meeting of the American Astronomical Society.

Goldberg, L. 1939, Ap. J., 90, 414.

_____ Müller, E., and Aller, L. H. 1960, Ap. J., Suppl., Vol. 5, No. 45.

Griem, H. 1960, Ap. J., 132, 883.

_____. 1961, Proceedings of the Fifth International Conference on Ionization Phenomena in Gases, (Amsterdam: North Holland Publishing Co.), Vol. II, p. 1857.

_____. 1962a, Ap. J., 136, 422.

_____. 1962b, Phys. Rev., 128, 515.

_____ and Shen, K. Y. 1961, Phys. Rev., 122, 1490.

Griem, H., Kolb, A. C. and Shen, K. Y. 1959, Phys. Rev. 116, 4.

_____. 1962a, Ap. J., 135, 272.

_____. 1962b, N. R. L. Report No. 5805.

Griem, H., Baranger, M., Kolb, A. C., Oertel, G. 1962, Phys. Rev., 125, 177.

Harris, D. 1948, Ap. J., 108, 112.

Hastings, C. 1956, Approximations For Digital Computers (Princeton: Princeton University Press).

Huang, S. S. 1948, Ap. J., 108, 354.

Hunger, K. 1956, Z. f. Ap., 39, 36.

Iben, I. 1963, Submitted to Ap. J.

Johnson, H. L. and Morgan, W. W. 1953, Ap. J., 117, 313.

Jugaku, J. 1959, Pub. Astr. Soc. Japan, 11, 161.

Karzas, W. J. and Latter, R. 1961, Ap. J., Suppl., Vol. 6, No. 55.

Kolb, A. C. and Griem, H. 1958, Phys. Rev., 111, 514.

Kolesov, A. K. 1962, Soviet Astronomy A.J., 6, 24.

Kopal, Z. 1955, Numerical Analysis, (New York: John Wiley and Sons, Inc.).

Kourganoff, V. (with the collaboration of Ida Busbridge) 1952, Basic Methods in Transfer Problems, (London: Oxford University Press).

Krishna-Swamy, K. S. 1961, Ap. J., 134, 1017.

Krook, M. 1963, Ap. J., 137, 863.

Lecar, M. 1963, A.J., 68, 77.

Leftus, V. 1962, Bull. Astr. Inst. Czech., 13, 245.

Mathis, J. S. 1962, Ap. J., 136, 374.

Matthews, T. A. and Sandage, A. R. 1963, Ap. J., in press.

Meinel, A. B. 1963, Ap. J., 137, 321.

Menzel, D. H. and Pekeris, C. L. 1935, M.N., 96, 77.

Michard, R. 1949, Ann. d'Ap., 12, 291.

Moore, C. E. 1948, Atomic Energy Levels, Bureau of Standards Circular No. 467.

Münch, G. 1960, Stellar Atmospheres, ed. J. L. Greenstein, Vol. 6, of Stars and Stellar Systems, (Chicago: University of Chicago Press), Chapter 1.

Odgers, G. J. 1952, Ap. J., 116, 442.

Oke, J. B. 1954, Ap. J., 120, 22.

_____ and Greenstein, J. L. 1961, Ap. J., 133, 349.

Osawa, K. 1956, Ap. J., 123, 513.

Popper, D. M. 1959, Ap. J., 129, 647.

Przybylski, A. 1955, M.N., 115, 650.

Roach, F. E. and Blitzer, L. 1940, Ap. J., 92, 50.

Rudnick, P. 1936, Ap. J., 83, 439.

Saito, S. 1954, Cont. Inst. Ap. Univ. Kyoto, No. 48.

_____. 1956, Cont. Inst. Ap. Univ. Kyoto, No. 69.

_____. 1959, Pub. Astr. Soc. Japan, 11, 98.

_____ and Uesugi, A. 1959, Pub. Astr. Soc. Japan, 11, 90.

Schwarzschild, M. 1958, Structure and Evolution of the Stars, (Princeton; Princeton University Press).

_____ and Härm, R. 1959, Ap. J., 129, 637.

Searle, L. and Oke, J. B. 1962, Ap. J., 135, 790.

Slettebak, A. 1949, Ap. J., 110, 498.

_____. 1956, Ap. J., 124, 113.

Stecher, T. P. 1962, Ap. J., 136, 686.

_____ and Milligan, J. E. 1962, Ap. J., 136, 1.

Stewart, J. C. 1956, Thesis, California Institute of Technology.

Stock, J. 1956, Ap. J., 123, 253.

Swihart, T. L. 1956a, Ap. J., 123, 139.

_____. 1956b, Ap. J., 123, 143.

_____. 1956c, Ap. J., 123, 151.

_____ and Fischel, D. 1961, Ap. J., Supp., Vol. 5, No. 49.

Traving, G. 1955, Z. f. Ap., 36, 1.

_____. 1956, Z. f. Ap., 41, 215.

_____. 1960, Über die Theorie der Druckverbreiterung von Spektrallinien (Karlsruge: Verlag G. Braun).

Trefftz, E., Schlüter, A., Dettmar, K. H., and Jörgens, K. 1957, Z. f. Ap., 44, 1.

Ueno, S. 1954, Cont. Inst. Ap. Univ. Kyoto, No. 42.

_____, Saito, S. and Jugaku, J. 1954, Cont. Inst. Ap. Kyoto, No. 43.

Underhill, A. B. 1949, M.N., 109, 563.

_____. 1951a, Canadian Jour. Phys., 29, 147.

_____. 1951b, Pub. Dom. Ap. Obs. Victoria, 8, 357.

_____. 1951c, " " " " " , 8, 385.

_____. 1956, " " " " " , 10, 169.

_____. 1957, " " " " " , 10, 357.

_____. 1961, " " " " " , 12, 363.

_____ and Waddell, J. H. 1959, N.B.S. Circular No. 603.

Unsöld, A. 1948, Z. f. Ap., 24, 355.

_____. 1955, Physik der Sternatmosphären (2nd ed.; Berlin, Springer).

_____. 1958, M.N., 118, 3.

Vardya, M.S. 1960, Ap. J., Suppl., Vol. 4, No. 42.

_____. 1961, Ap. J., 133, 107.

Varsavsky, C. 1957, A.J., 62, 97.

Verweij, S. 1936, Pub. Astr. Inst. Amsterdam, No. 5.

Wiese, W. L., Paquette, D.R., and Solarski, J. E. 1963, Phys. Rev., 129, 1225.

Williams, E.G. 1934, P.A.S.P., 46, 292.

_____. 1936, Ap. J., 83, 279.

Woolley, R.v.d.R., and Stibbs, D.W.N. 1953, The Outer Layers of a Star (Oxford: At the University Press).

Zwaan, C. 1960, Ann. d'Ap., 23, 811.

_____. 1962, B.A.N., 16, 225.

Appendix I

TABLES OF MODEL ATMOSPHERES

In these tables are summarized the most important data concerning 28 flux-constant models constructed according to the methods described in chapter II. Each model represents the result of about three iterations neglecting scattering (sometimes more) followed by about two taking scattering into account in the solution of the transfer equation (again sometimes more for the hottest models). The data given are basically those quantities which are frequency-independent since a tabulation of frequency-dependent quantities would clearly be prohibitive. The exception to this rule is that the emergent monochromatic fluxes are given. The information given here will allow the reconstruction of any monochromatic quantities with the aid of modest computing facilities.

The first line of the tables gives the assumed effective theta, log g, helium abundance, and the total flux (this is the physical flux $\mathcal{F} = \pi F$). The first column gives τ_{STD}. The standard wavelength was chosen as $\lambda 5050$ for all models with $\theta_e > 0.4$, and as $\lambda 4000$ for all models with $\theta_e \leq 0.4$. Next follows $\theta(\tau)$, $\log p_g(T)$, and $\log p_e(\tau)$. Now follows the fraction of hydrogen that is neutral (except for some of the cooler models in which the fraction of hydrogen that is ionized is given), the fraction of helium that is neutral and that is singly ionized; the notation is exponential, i.e. 9.07-4 implies 9.07×10^{-4}. Then we give $(\kappa+\sigma)_{STD}$ in $cm^2 gm^{-1}$, $dp_r/d\tau$, and the logarithmic adiabatic gradient ∇_A. A single underscore is placed in this column at the depth

where the radiative gradient exceeds the adiabatic gradient, so that this region is unstable against convection; a double underscore denotes the depth at which the adiabatic gradient is again greater. No double underscore means the adiabatic gradient remains smaller throughout the remainder of the model. The last two columns give the chosen wavelengths in Å and the emergent fluxes F_ν (not including the factor of π) at these wavelengths; an asterisk before one of these entries denotes that the iterations for the source function did not converge, as described in chapter II, so these values may be badly in error and should be used with due caution. Immediately below this table of fluxes is given the extreme values of the error in the flux, these values are the extrema on at least the range $0 \leq \tau_{STD} \leq 14$. In most cases the low value represents the point right at the surface of the model. Since the errors are generally not symmetrical about zero, one may choose to make a small adjustment in the value of the flux given at the top of the page, as well as to θ_e, in order to force coincidence with the mean computed flux.

It is appropriate here to make some notes concerning individual models:

(a) The quality of flux constancy is poorest for the $\theta_e = 0.101$, $\log g = 4$ and $\theta_e = 0.5$, $\log g = 1$ models.

(b) As mentioned in chapter III, the model with $\theta_e = 0.6$, $\log g = 1$ shows a negative pressure gradient on the range $0.5 \leq \tau_{5050} \leq 0.8$ due to the predominance of $dp_r/d\tau$.

(c) The very steep temperature drop right at the surface of the $\theta_e = 0.21$ and the $\theta_e = 0.5$, $\log g = 2$ models is probably spurious;

this came about because a temperature inversion demanded by the correction procedure was not allowed. However, the computed inversion in this case was only a small overshoot which arose because the drop at the surface was so sharp. This shows that temperature inversions should be examined carefully when they occur since in a case such as this they may be smoothed graphically and another iteration will not give an inversion again.

(d) As discussed previously in chapter II, the extrapolation of $dp_r/d\tau$ by a quadratic proved unsatisfactory as is shown by it "blowing up" at depth in several models; the places where this has occurred are obvious from the tables following. In most cases this caused no trouble, but in the three $\log g = 2$ models, the gas pressure at the last two points shows a spurious negative gradient due to this divergence, and the last few entries of the table are probably unreliable.

APPENDIX I

Eff. θ = 0.101 | Log G = 4.00 | Flux = 3.52 + 14 | N(He)/N(H) = 0.15

τ	θ	Log PG	Log PE	H I	He I	He II	$(\kappa+\sigma)_{STD}$	$dp_r/d\tau$	∇_A	λ	Flux
0.000	.136	1.357	1.082	8.26-6	2.70-8	3.26-3	3.20-1	1.17+4	.250	*227	2.32-3
0.001	.135	1.511	1.235	9.83-6	4.48-8	4.54-3	3.24-1	1.17+4	.250	*264	3.04-3
0.002	.135	1.711	1.435	1.23-5	8.69-8	7.02-3	3.31-1	1.16+4	.250	*313	4.36-3
0.003	.135	1.843	1.567	1.43-5	1.34-7	9.30-3	3.38-1	1.16+4	.250	386	6.50-3
0.004	.135	1.942	1.666	1.59-5	1.84-7	1.14-2	3.44-1	1.15+4	.250	504	9.87-3
0.006	.135	2.086	1.809	1.87-5	2.88-7	1.52-2	3.56-1	1.14+4	.250	504	1.00-2
0.008	.135	2.189	1.912	2.09-5	3.93-7	1.84-2	3.68-1	1.13+4	.250	567	1.12-2
0.010	.134	2.269	1.992	2.28-5	4.97-7	2.13-2	3.79-1	1.12+4	.250	649	1.22-2
0.015	.134	2.412	2.135	2.66-5	7.38-7	2.71-2	4.04-1	1.09+4	.250	758	1.30-2
0.020	.133	2.511	2.234	2.96-5	9.47-7	3.12-2	4.27-1	1.08+4	.250	912	1.34-2
0.025	.133	2.586	2.309	3.20-5	1.12-6	3.43-2	4.47-1	1.06+4	.249	912	2.25-2
0.030	.132	2.646	2.369	3.40-5	1.28-6	3.67-2	4.65-1	1.05+4	.249	990	2.19-2
0.035	.132	2.695	2.418	3.57-5	1.41-6	3.84-2	4.82-1	1.03+4	.249	1083	2.10-2
0.040	.131	2.737	2.461	3.72-5	1.51-6	3.96-2	4.98-1	1.02+4	.249	1196	1.98-2
0.060	.130	2.861	2.584	4.18-5	1.80-6	4.19-2	5.52-1	9.85+3	.249	1335	1.83-2
0.080	.128	2.945	2.668	4.50-5	1.94-6	4.20-2	5.96-1	9.55+3	.250	1511	1.64-2
0.100	.127	3.008	2.731	4.75-5	2.00-6	4.10-2	6.32-1	9.31+3	.250	1740	1.42-2
0.125	.126	3.069	2.792	4.97-5	1.99-6	3.91-2	6.72-1	9.03+3	.250	2051	1.17-2
0.150	.125	3.118	2.841	5.16-5	1.95-6	3.69-2	7.05-1	8.78+3	.251	2051	1.19-2
0.200	.123	3.194	2.917	5.45-5	1.86-6	3.33-2	7.62-1	8.40+3	.252	2303	1.02-2
0.250	.121	3.253	2.976	5.67-5	1.73-6	2.99-2	8.10-1	8.07+3	.252	2625	8.55-3
0.300	.119	3.300	3.024	5.83-5	1.59-6	2.67-2	8.50-1	7.79+3	.253	3053	6.85-3
0.350	.118	3.340	3.064	5.97-5	1.47-6	2.42-2	8.85-1	7.55+3	.253	3647	5.19-3
0.400	.117	3.375	3.099	6.08-5	1.35-6	2.18-2	9.17-1	7.34+3	.254	3647	5.31-3
0.500	.115	3.433	3.157	6.26-5	1.17-6	1.83-2	9.72-1	7.00+3	.255	4235	4.16-3
0.600	.113	3.482	3.205	6.40-5	1.01-6	1.55-2	1.019	6.71+3	.255	5049	3.09-3
0.700	.111	3.523	3.247	6.52-5	8.89-7	1.35-2	1.061	6.48+3	.256	6252	2.13-3
0.800	.110	3.559	3.283	6.61-5	7.88-7	1.18-2	1.099	6.26+3	.256	8205	1.30-3
1.00	.107	3.620	3.344	6.76-5	6.40-7	9.44-3	1.167	5.90+3	.257	8205	1.31-3
1.20	.105	3.672	3.396	6.89-5	5.33-7	7.76-3	1.226	5.61+3	.257	14588	4.43-4
1.40	.103	3.715	3.439	7.00-5	4.60-7	6.59-3	1.280	5.38+3	.257		
1.60	.102	3.754	3.478	7.09-5	4.01-7	5.70-3	1.328	5.17+3	.258	$\Delta F/F$	
1.80	.100	3.788	3.512	7.18-5	3.56-7	5.03-3	1.373	4.99+3	.258	-2.49, -0.52	
2.00	.099	3.819	3.543	7.25-5	3.18-7	4.47-3	1.415	4.82+3	.258		
2.50	.096	3.885	3.609	7.41-5	2.53-7	3.52-3	1.510	4.52+3	.259	τ	C
3.00	.094	3.939	3.666	7.54-5	2.07-7	1.01-3	1.599	4.26+3	.259	.000	.724
3.50	.092	3.986	3.712	7.64-5	1.75-7	1.17-3	1.671	4.04+3	.259	.004	.730
4.00	.090	4.027	3.752	7.72-5	1.50-7	1.68-3	1.732	3.87+3	.259	.010	.736
5.00	.088	4.094	3.815	7.81-5	1.15-7	5.77-3	1.823	3.85+3	.260	.040	.768
6.00	.085	4.146	3.863	7.81-5	8.62-8	2.72-2	1.867	3.76+3	.260	.080	.800
8.00	.081	4.288	3.995	8.29-5	2.01-8	7.10-1	1.975	3.35+3	.261	.200	.861
10.0	.079	4.379	4.090	8.69-5	3.26-8	4.61-1	2.103	2.83+3	.262	.400	.907
14.0	.075	4.477	4.196	8.94-5	4.26-8	4.82-2	2.740	2.34+3	.263	.800	.944
18.0	.072	4.546	4.269	9.02-5	3.43-8	3.69-3	2.981	2.04+3	.263	1.40	.967
22.0	.070	4.609	4.333	9.20-5	2.97-8	6.61-4	3.206	1.67+3	.263	2.00	.977
26.0	.069	4.670	4.394	9.02-5	2.52-8	4.29-4	3.454	1.32+3	.264	4.00	.991
30.0	.068	4.727	4.451	8.82-5	2.19-8	3.87-4	3.725	9.84+2	.264	8.00	.993
40.0	.065	4.858	4.582	8.62-5	1.79-8	3.31-4	4.507	1.99+2	.266	14.0	.998
50.0	.063	4.963	4.687	8.55-5	1.59-8	3.00-4	5.282	-	.268	18.0	.998
60.0	.062	5.041	4.765	8.43-5	1.41-8	2.75-4	5.916	-	.270		

Eff. θ = 0.140 Log G = 4.00 Flux = 9.52 + 13 N(HE)/N(H) = 0.15

τ	θ	Log PG	Log PE	H I	HE I	HE II	$(\kappa+\sigma)_{STD}$	$dp_r/d\tau$	∇_A	λ	Flux
0.000	.184	1.606	1.309	1.98-5	2.00-5	8.39-1	3.07-1	3.40+3	.238	*227	2.60-5
0.001	.184	1.738	1.440	2.30-5	2.47-5	8.72-1	3.13-1	3.54+3	.240	*264	3.01-5
0.002	.184	1.916	1.616	2.81-5	3.27-5	9.08-1	3.27-1	3.66+3	.242	313	2.67-5
0.003	.183	2.036	1.736	3.21-5	3.92-5	9.26-1	3.41-1	3.79+3	.243	386	3.68-5
0.004	.183	2.126	1.825	3.55-5	4.46-5	9.36-1	3.54-1	3.90+3	.244	504	1.66-4
0.006	.182	2.255	1.955	4.09-5	5.36-5	9.47-1	3.79-1	4.06+3	.246	504	1.22-4
0.008	.182	2.348	2.048	4.52-5	6.07-5	9.53-1	4.01-1	4.17+3	.246	567	1.50-3
0.010	.181	2.420	2.120	4.88-5	6.66-5	9.60-1	4.22-1	4.23+3	.247	649	1.87-4
0.015	.180	2.549	2.249	5.56-5	7.75-5	9.60-1	4.68-1	4.30+3	.248	758	2.39-3
0.020	.178	2.639	2.338	6.06-5	8.49-5	9.60-1	5.06-1	4.34+3	.248	912	3.08-3
0.025	.177	2.707	2.407	6.46-5	9.04-5	9.59-1	5.40-1	4.35+3	.248	912	1.24-2
0.030	.176	2.762	2.461	6.80-5	9.50-5	9.58-1	5.71-1	4.29+3	.248	990	1.23-2
0.035	.175	2.807	2.507	7.08-5	9.84-5	9.56-1	5.98-1	4.26+3	.248	1083	1.21-2
0.040	.174	2.846	2.547	7.32-5	1.01-4	9.54-1	6.24-1	4.23+3	.247	1196	1.16-2
0.060	.170	2.963	2.664	8.04-5	1.07-4	9.44-1	7.10-1	4.07+3	.246	1335	1.09-2
0.080	.168	3.044	2.744	8.53-5	1.10-4	9.32-1	7.77-1	3.94+3	.243	1511	9.92-3
0.100	.165	3.107	2.807	8.87-5	1.11-4	9.20-1	8.36-1	3.82+3	.241	1740	8.75-3
0.125	.163	3.168	2.869	9.22-5	1.11-4	9.02-1	9.00-1	3.68+3	.237	2051	7.37-3
0.150	.160	3.218	2.919	9.50-5	1.10-4	8.84-1	9.58-1	3.56+3	.234	2051	7.64-3
0.200	.157	3.295	2.998	9.97-5	1.08-4	8.52-1	1.060	3.38+3	.228	2303	6.64-3
0.250	.154	3.354	3.058	1.03-4	1.06-4	8.18-1	1.150	3.22+3	.223	2625	5.61-3
0.300	.152	3.402	3.107	1.06-4	1.02-4	7.85-1	1.213	3.10+3	.219	3053	4.54-3
0.350	.150	3.443	3.148	1.08-4	9.78-5	7.48-1	1.286	3.01+3	.215	3647	3.51-3
0.400	.148	3.477	3.186	1.10-4	9.39-5	7.14-1	1.359	2.93+3	.212	3647	3.77-3
0.500	.145	3.534	3.243	1.13-4	8.67-5	6.54-1	1.481	2.75+3	.209	4235	2.97-3
0.600	.143	3.580	3.291	1.15-4	7.93-5	5.95-1	1.589	2.60+3	.207	5049	2.22-3
0.700	.141	3.619	3.330	1.17-4	7.31-5	5.46-1	1.687	2.47+3	.207	6252	1.53-3
0.800	.139	3.653	3.364	1.19-4	6.76-5	5.02-1	1.778	2.36+3	.207	8205	9.42-4
1.00	.136	3.709	3.422	1.21-4	5.80-5	4.28-1	1.939	2.17+3	.209	8205	9.57-4
1.20	.133	3.756	3.469	1.23-4	5.00-5	3.66-1	2.081	2.02+3	.213	14588	3.24-4
1.40	.131	3.795	3.509	1.25-4	4.41-5	3.21-1	2.209	1.90+3	.216		
1.60	.130	3.829	3.546	1.27-4	3.93-5	2.84-1	2.335	1.80+3	.220	ΔF/F	
1.80	.128	3.860	3.577	1.28-4	3.52-5	3.53-1	2.441	1.72+3	.224	-1.13, 0.51	
2.00	.127	3.887	3.605	1.30-4	3.16-5	2.26-1	2.537	1.64+3	.227		
2.50	.124	3.945	3.664	1.32-4	2.52-5	1.78-1	2.750	1.51+3	.235	τ	C
3.00	.121	3.993	3.741	1.34-4	2.03-5	1.43-1	2.928	1.40+3	.241	.000	.801
3.50	.119	4.034	3.756	1.36-4	1.70-5	1.19-1	3.088	1.32+3	.246	.004	.806
4.00	.117	4.070	3.792	1.37-4	1.44-5	9.98-2	3.227	1.25+3	.251	.010	.811
5.00	.114	4.132	3.854	1.40-4	1.10-5	7.53-2	3.475	1.16+3	.257	.040	.837
6.00	.111	4.182	3.905	1.41-4	8.57-6	5.84-2	3.679	1.08+3	.262	.080	.863
8.00	.107	4.264	3.988	1.44-4	5.87-6	3.96-2	4.039	9.63+2	.268	.200	.905
10.0	.104	4.328	4.053	1.47-4	4.36-6	2.91-2	4.327	8.82+2	.271	.400	.939
14.0	.099	4.427	4.151	1.50-4	2.79-6	1.85-2	4.503	7.74+2	.275	.800	.963
18.0	.096	4.502	4.226	1.52-4	2.02-6	1.33-2	5.202	6.97+2	.278	1.40	.978
22.0	.093	4.563	4.287	1.54-4	1.58-6	6.49-3	5.566	6.17+2	.279	2.00	.985
26.0	.091	4.616	4.340	1.56-4	1.28-6	7.19-3	5.891	5.42+2	.280	4.00	.993
30.0	.089	4.661	4.385	1.58-4	1.08-6	7.86-3	6.183	4.71+2	.281	8.00	.997
40.0	.085	4.758	4.482	1.62-4	7.81-7	5.79-3	6.905	3.03+2	.283	14.0	.999
50.0	.083	4.838	4.562	1.66-4	6.20-7	3.96-3	7.595	1.45+2	.284	18.0	.999
60.0	.080	4.907	4.631	1.70-4	5.20-7	3.33-3	8.272	-	.286		

Eff. θ = 0.140 Log G = 3.50 Flux = 9.52 + 13 N(HE)/N(H) = 0.15

τ	θ	Log PG	Log PE	H I	HE I	HE II	$(\kappa+\sigma)_{STD}$	$dp_r/d\tau$	∇_A	λ	Flux
0.000	.174	1.017	0.735	9.13-6	2.31-6	2.40-1	3.10-1	3.18+3	.237	*227	4.89-5
0.001	.173	1.142	0.860	1.04-5	3.07-6	2.78-1	3.11-1	3.22+3	.235	*264	9.28-5
0.002	.172	1.317	1.034	1.27-5	4.71-6	3.47-1	3.13-1	3.27+3	.233	313	1.58-4
0.003	.172	1.440	1.155	1.45-5	6.25-6	3.99-1	3.15-1	3.32+3	.232	386	2.67-4
0.004	.172	1.534	1.248	1.60-5	7.68-6	4.40-1	3.17-1	3.36+3	.231	504	5.85-4
0.006	.171	1.674	1.386	1.87-5	1.03-5	5.03-1	3.22-1	3.45+3	.230	504	1.57-3
0.008	.171	1.776	1.487	2.08-5	1.26-5	5.46-1	3.27-1	3.53+3	.230	567	2.01-3
0.010	.170	1.856	1.566	2.27-5	1.46-5	5.77-1	3.31-1	3.60+3	.230	649	2.58-3
0.015	.169	2.001	1.709	2.65-5	1.88-5	6.26-1	3.43-1	3.74+3	.230	758	3.32-3
0.020	.169	2.102	1.810	2.94-5	2.19-5	6.53-1	3.54-1	3.86+3	.230	912	4.22-3
0.025	.168	2.179	1.886	3.18-5	2.44-5	6.69-1	3.65-1	3.95+3	.230	912	9.58-3
0.030	.167	2.240	1.947	3.38-5	2.65-5	6.80-1	3.75-1	3.98+3	.230	990	9.76-3
0.035	.167	2.291	1.998	3.56-5	2.82-5	6.85-1	3.85-1	4.03+3	.230	1083	9.81-3
0.040	.166	2.334	2.041	3.71-5	2.95-5	6.88-1	3.94-1	4.06+3	.229	1196	9.70-3
0.060	.164	2.460	2.166	4.17-5	3.30-5	6.83-1	4.25-1	4.10+3	.228	1335	9.39-3
0.080	.162	2.545	2.252	4.49-5	3.46-5	6.66-1	4.52-1	4.07+3	.227	1511	8.85-3
0.100	.160	2.609	2.317	4.74-5	3.52-5	6.46-1	4.75-1	4.02+3	.226	1740	8.05-3
0.125	.158	2.670	2.381	4.98-5	3.52-5	6.18-1	5.05-1	3.94+3	.225	2051	6.99-3
0.150	.157	2.719	2.430	5.15-5	3.45-5	5.89-1	5.27-1	3.86+3	.224	2051	7.12-3
0.200	.154	2.795	2.507	5.43-5	3.31-5	5.41-1	5.66-1	3.68+3	.224	2303	6.33-3
0.250	.152	2.855	2.567	5.64-5	3.12-5	4.94-1	5.95-1	3.55+3	.223	2625	5.46-3
0.300	.150	2.903	2.616	5.80-5	2.90-5	4.50-1	6.25-1	3.43+3	.224	3053	4.52-3
0.350	.148	2.944	2.657	5.94-5	2.72-5	4.14-1	6.53-1	3.31+3	.224	3647	3.54-3
0.400	.146	2.980	2.693	6.06-5	2.53-5	3.81-1	6.78-1	3.20+3	.225	3647	3.61-3
0.500	.144	3.040	2.754	6.23-5	2.22-5	3.27-1	7.23-1	3.02+3	.227	4235	2.90-3
0.600	.141	3.089	2.804	6.38-5	1.95-5	2.82-1	7.63-1	2.87+3	.230	5049	2.20-3
0.700	.139	3.130	2.848	6.52-5	1.73-5	2.47-1	8.04-1	2.74+3	.232	6252	1.55-3
0.800	.138	3.166	2.885	6.62-5	1.53-5	2.16-1	8.37-1	2.64+3	.234	8205	9.71-4
1.00	.135	3.227	2.947	6.79-5	1.23-5	1.70-1	8.94-1	2.46+3	.238	8205	9.76-4
1.20	.132	3.278	2.999	6.93-5	1.00-5	1.37-1	9.44-1	2.32+3	.241	14588	3.40-4
1.40	.130	3.322	3.043	7.05-5	8.42-6	1.14-1	9.89-1	2.22+3	.244		
1.60	.128	3.360	3.082	7.15-5	7.14-6	9.55-2	1.028	2.13+3	.246	ΔF/F	
1.80	.126	3.394	3.116	7.24-5	6.16-6	8.17-2	1.064	2.05+3	.248	-1.44, 0.43	
2.00	.124	3.425	3.147	7.31-5	5.34-6	7.02-2	1.096	1.99+3	.250		
2.50	.121	3.491	3.214	7.47-5	3.96-6	5.14-2	1.169	1.86+3	.252	τ	C
3.00	.118	3.546	3.268	7.57-5	3.00-6	3.86-2	1.227	1.75+3	.254	.000	.741
3.50	.116	3.593	3.316	7.68-5	2.42-6	3.08-2	1.284	1.67+3	.256	.004	.732
4.00	.114	3.635	3.358	7.75-5	1.97-6	2.49-2	1.334	1.60+3	.256	.010	.737
5.00	.110	3.704	3.428	7.90-5	1.44-6	1.79-2	1.425	1.49+3	.258	.040	.765
6.00	.107	3.761	3.485	8.00-5	1.08-6	1.34-2	1.501	1.40+3	.259	.080	.797
8.00	.103	3.854	3.578	8.19-5	7.13-7	8.69-3	1.636	1.27+3	.260	.200	.858
10.0	.100	3.926	3.650	8.33-5	5.18-7	6.29-3	1.748	1.17+3	.260	.400	.908
14.0	.095	4.037	3.761	8.59-5	3.30-7	1.23-3	1.945	1.04+3	.261	.800	.950
18.0	.091	4.120	3.844	8.75-5	2.35-7	1.75-3	2.104	9.44+2	.262	1.40	.973
22.0	.088	4.188	3.912	8.90-5	1.82-7	4.85-3	2.247	8.48+2	.262	2.00	.983
26.0	.086	4.247	3.971	9.05-5	1.48-7	1.61-2	2.380	7.57+2	.263	4.00	.993
30.0	.084	4.308	4.032	9.28-5	7.16-8	4.55-1	2.470	6.71+2	.263	8.00	.998
40.0	.080	4.444	4.168	9.92-5	7.05-8	3.37-1	2.719	4.68+2	.265	14.0	.999
50.0	.078	4.538	4.262	1.03-4	8.04-8	7.35-2	3.343	2.76+2	.266	18.0	.999
60.0	.075	4.618	4.343	1.06-4	7.40-8	1.08-2	3.775	9.35+1	.267		

Eff. θ = 0.140 Log G = 4.00 Flux = 9.52 + 13 N(HE)/N(H) = 0.05

τ	θ	Log PG	Log PE	H I	HE I	HE II	$(\kappa+\sigma)_{STD}$	$dp_r/d\tau$	∇_A	λ	Flux
0.000	.183	1.583	1.284	1.90-5	1.80-5	8.02-1	3.60-1	3.38+3	.245	*227	5.74-5
0.001	.183	1.702	1.402	2.17-5	2.18-5	8.36-1	3.68-1	3.48+3	.246	*264	8.68-5
0.002	.182	1.866	1.566	2.61-5	2.84-5	8.78-1	3.82-1	3.58+3	.247	313	1.14-4
0.003	.182	1.980	1.679	2.96-5	3.40-5	9.00-1	3.96-1	3.68+3	.248	386	1.49-4
0.004	.182	2.067	1.766	3.26-5	3.85-5	9.13-1	4.09-1	3.78+3	.248	504	3.24-4
0.006	.181	2.194	1.893	3.75-5	4.63-5	9.29-1	4.34-1	3.92+3	.249	504	1.09-3
0.008	.181	2.286	1.985	4.15-5	5.26-5	9.37-1	4.57-1	4.04+3	.250	567	1.36-3
0.010	.180	2.358	2.057	4.48-5	5.79-5	9.42-1	4.78-1	4.11+3	.250	649	1.75-3
0.015	.179	2.487	2.186	5.12-5	6.81-5	9.49-1	5.25-1	4.22+3	.251	758	2.29-3
0.020	.178	2.57	2.275	5.60-5	7.52-5	9.51-1	5.65-1	4.29+3	.252	912	3.01-3
0.025	.177	2.645	2.344	5.98-5	8.06-5	9.51-1	6.00-1	4.33+3	.252	912	1.21-2
0.030	.175	2.700	2.399	6.30-5	8.48-5	9.50-1	6.32-1	4.28+3	.253	990	1.21-2
0.035	.175	2.746	2.445	6.57-5	8.83-5	9.48-1	6.60-1	4.27+3	.253	1083	1.18-2
0.040	.174	2.785	2.484	6.80-5	9.09-5	9.46-1	6.86-1	4.25+3	.253	1196	1.14-2
0.060	.170	2.903	2.602	7.49-5	9.75-5	9.37-1	7.75-1	4.11+3	.253	1335	1.07-2
0.080	.168	2.985	2.684	7.97-5	1.00-4	9.25-1	8.45-1	3.97+3	.253	1511	9.85-3
0.100	.165	3.048	2.747	8.33-5	1.02-4	9.12-1	9.06-1	3.84+3	.253	1740	8.71-3
0.125	.163	3.110	2.809	8.64-5	1.02-4	8.95-1	9.70-1	3.69+3	.252	2051	7.35-3
0.150	.161	3.160	2.860	8.92-5	1.01-4	8.76-1	1.028	3.56+3	.251	2051	7.47-3
0.200	.158	3.240	2.940	9.39-5	1.01-4	8.45-1	1.130	3.33+3	.249	2303	6.52-3
0.250	.155	3.302	3.002	9.74-5	9.84-5	8.15-1	1.218	3.16+3	.248	2625	5.52-3
0.300	.153	3.352	3.052	1.00-4	9.53-5	7.78-1	1.293	3.01+3	.246	3053	4.49-3
0.350	.151	3.395	3.096	1.02-4	9.22-5	7.45-1	1.343	2.92+3	.244	3647	3.46-3
0.400	.149	3.432	3.134	1.04-4	8.88-5	7.12-1	1.408	2.82+3	.243	3647	3.72-3
0.500	.146	3.493	3.195	1.08-4	8.25-5	6.53-1	1.521	2.64+3	.242	4235	2.94-3
0.600	.144	3.543	3.246	1.10-4	7.60-5	5.95-1	1.619	2.49+3	.241	5049	2.20-3
0.700	.141	3.585	3.288	1.12-4	7.04-5	5.47-1	1.710	2.37+3	.241	6252	1.52-3
0.800	.140	3.622	3.325	1.14-4	6.50-5	5.01-1	1.791	2.27+3	.241	8205	9.38-4
1.00	.136	3.683	3.387	1.17-4	5.59-5	4.27-1	1.938	2.10+3	.243	8205	9.52-4
1.20	.134	3.734	3.438	1.20-4	4.85-5	3.66-1	2.066	1.96+3	.245	14588	3.24-4
1.40	.132	3.777	3.481	1.22-4	4.28-5	3.20-1	2.183	1.86+3	.247		
1.60	.130	3.814	3.519	1.24-4	3.80-5	2.82-1	2.293	1.77+3	.249	ΔF/F	
1.80	.128	3.846	3.552	1.25-4	3.40-5	2.50-1	2.389	1.70+3	.252	-1.23, 0.75	
2.00	.127	3.875	3.581	1.26-4	3.04-5	2.23-1	2.476	1.63+3	.253		
2.50	.124	3.938	3.644	1.30-4	2.46-5	1.77-1	2.678	1.52+3	.258	τ	C
3.00	.121	3.988	3.695	1.32-4	2.01-5	1.43-1	2.847	1.42+3	.261	.000	.782
3.50	.119	4.032	3.739	1.34-4	1.67-5	1.18-1	2.995	1.35+3	.264	.004	.786
4.00	.117	4.069	3.777	1.35-4	1.40-5	9.86-2	3.123	1.28+3	.266	.010	.793
5.00	.114	4.133	3.841	1.38-4	1.05-5	7.33-2	3.354	1.20+3	.269	.040	.826
6.00	.111	4.185	3.893	1.39-4	8.09-6	5.61-2	3.544	1.12+3	.272	.080	.856
8.00	.107	4.269	3.977	1.42-4	5.43-6	3.73-2	3.878	1.01+3	.274	.200	.903
10.0	.104	4.335	4.043	1.44-4	3.98-6	2.71-2	4.153	9.31+2	.276	.400	.937
14.0	.099	4.435	4.143	1.47-4	2.51-6	1.70-2	4.611	8.27+2	.278	.800	.964
18.0	.095	4.511	4.219	1.49-4	1.78-6	1.20-2	4.986	7.52+2	.280	1.40	.979
22.0	.093	4.572	4.280	1.51-4	1.38-6	6.07-3	5.319	6.75+2	.280	2.00	.985
26.0	.090	4.624	4.332	1.53-4	1.11-6	7.03-3	5.620	6.02+2	.281	4.00	.994
30.0	.088	4.670	4.378	1.54-4	9.23-7	7.86-3	5.897	5.34+2	.282	8.00	.998
40.0	.085	4.766	4.474	1.58-4	6.56-7	6.89-3	6.563	3.72+2	.283	14.0	.999
50.0	.082	4.844	4.553	1.61-4	5.13-7	3.43-3	7.191	2.21+2	.284	18.0	.999
60.0	.079	4.913	4.621	1.64-4	4.25-7	2.87-3	7.802	7.58+2	.285		

Eff. θ = 0.157 Log G = 4.00 Flux = 6.02 + 13 N(HE)/N(H) = 0.15

τ	θ	Log PG	Log PE	H I	HE I	HE II	$(\kappa+\sigma)_{STD}$	$dp_r/d\tau$	∇_A	λ	Flux
0.000	.230	1.544	1.243	2.96-5	1.14-4	1.00+0	3.13-1	2.33+3	.251	227	6.15-9
0.001	.229	1.694	1.392	3.47-5	1.42-4	1.00+0	3.28-1	2.43+3	.252	264	9.9-10
0.002	.228	1.882	1.581	4.28-5	1.94-4	1.00+0	3.54-1	2.52+3	.253	313	2.48-8
0.003	.226	2.004	1.703	4.90-5	2.34-4	1.00+0	3.79-1	2.59+3	.254	386	4.73-7
0.004	.225	2.094	1.792	5.38-5	2.66-4	1.00+0	4.00-1	2.63+3	.254	504	8.89-6
0.006	.223	2.221	1.919	6.15-5	3.12-4	1.00+0	4.39-1	2.67+3	.256	504	1.60-4
0.008	.222	2.312	2.010	6.75-5	3.44-4	9.99-1	4.73-1	2.68+3	.257	567	2.02-4
0.010	.220	2.381	2.079	7.23-5	3.68-4	9.99-1	5.03-1	2.67+3	.258	649	2.87-4
0.015	.218	2.506	2.204	8.14-5	4.04-4	9.99-1	5.67-1	2.63+3	.260	758	4.51-4
0.020	.215	2.593	2.291	8.79-5	4.18-4	9.99-1	6.20-1	2.58+3	.261	911	7.47-4
0.025	.213	2.660	2.358	9.29-5	4.22-4	9.99-1	6.64-1	2.54+3	.262	911	9.34-3
0.030	.211	2.714	2.412	9.73-5	4.30-4	9.99-1	7.06-1	2.48+3	.263	990	9.26-3
0.035	.209	2.759	2.457	1.01-4	4.28-4	9.99-1	7.42-1	2.42+3	.264	1083	9.04-3
0.040	.208	2.798	2.496	1.04-4	4.23-4	9.99-1	7.74-1	2.38+3	.265	1196	8.65-3
0.060	.203	2.916	2.614	1.12-4	4.07-4	9.99-1	8.85-1	2.23+3	.267	1335	8.09-3
0.080	.199	2.998	2.696	1.18-4	3.91-4	9.99-1	9.72-1	2.11+3	.269	1511	7.36-3
0.100	.196	3.061	2.760	1.23-4	3.77-4	9.98-1	1.047	2.02+3	.270	1740	6.47-3
0.125	.192	3.125	2.823	1.27-4	3.57-4	9.98-1	1.123	1.93+3	.271	2051	5.44-3
0.150	.189	3.176	2.874	1.30-4	3.42-4	9.97-1	1.190	1.84+3	.272	2051	5.53-3
0.200	.185	3.258	2.956	1.37-4	3.29-4	9.96-1	1.315	1.74+3	.273	2303	4.81-3
0.250	.182	3.321	3.019	1.42-4	3.14-4	9.94-1	1.416	1.67+3	.273	2625	4.07-3
0.300	.179	3.372	3.070	1.45-4	3.00-4	9.93-1	1.499	1.61+3	.273	3053	3.31-3
0.035	.176	3.415	3.114	1.48-4	2.90-4	9.91-1	1.574	1.57+3	.272	3647	2.60-3
0.400	.174	3.452	3.151	1.50-4	2.80-4	9.88-1	1.640	1.52+3	.271	3647	2.97-3
0.500	.170	3.515	3.214	1.54-4	2.66-4	9.83-1	1.757	1.45+3	.269	4235	2.34-3
0.600	.167	3.566	3.264	1.56-4	2.52-4	9.76-1	1.870	1.40+3	.265	5049	1.75-3
0.700	.164	3.609	3.308	1.58-4	2.43-4	9.68-1	1.965	1.35+3	.261	6252	1.21-3
0.800	.161	3.646	3.346	1.60-4	2.34-4	9.59-1	2.052	1.32+3	.256	8205	7.50-4
1.00	.157	3.708	3.409	1.63-4	2.19-4	9.37-1	2.209	1.26+3	.246	8205	7.70-4
1.20	.154	3.759	3.461	1.65-4	2.06-4	9.09-1	2.349	1.22+3	.236	14588	2.62-4
1.40	.151	3.802	3.504	1.67-4	1.95-4	8.80-1	2.442	1.19+3	.228		
1.60	.148	3.839	3.543	1.68-4	1.83-4	8.46-1	2.569	1.17+3	.219	ΔF/F	
1.80	.146	3.871	3.576	1.69-4	1.72-4	8.10-1	2.686	1.15+3	.213	-1.14, 0.76	
2.00	.144	3.899	3.605	1.70-4	1.61-4	7.71-4	2.798	1.13+3	.207		
2.50	.139	3.958	3.665	1.71-4	1.37-4	6.74-1	3.061	1.09+3	.200	τ	C
3.00	.135	4.005	3.714	1.71-4	1.13-4	5.74-1	3.296	1.05+3	.196	.000	.861
3.50	.132	4.044	3.754	1.71-4	9.54-5	4.91-1	3.510	1.01+3	.198	.004	.849
4.00	.130	4.078	3.792	1.71-4	8.02-5	4.18-1	3.722	9.69+2	.202	.010	.849
5.00	.126	4.134	3.850	1.72-4	5.93-5	3.15-1	4.046	9.00+2	.212	.040	.871
6.00	.122	4.180	3.898	1.71-4	4.43-5	2.38-1	4.303	8.37+2	.223	.080	.893
8.00	.117	4.255	3.975	1.72-4	2.82-5	1.54-1	4.722	4.34+2	.240	.200	.930
10.0	.114	4.316	4.037	1.73-4	1.98-5	1.08-1	5.061	6.64+2	.252	.400	.957
14.0	.108	4.410	4.133	1.76-4	1.17-5	6.43-2	5.619	5.76+2	.266	.800	.977
18.0	.104	4.482	4.206	1.78-4	8.01-6	4.38-2	6.063	5.10+2	.274	1.40	.988
22.0	.101	4.542	4.265	1.80-4	5.98-6	3.26-2	6.462	4.45+2	.278	2.00	.991
26.0	.099	4.593	4.317	1.81-4	4.74-6	2.58-2	6.833	3.84+2	.281	4.00	.994
30.0	.097	4.638	4.362	1.83-4	3.91-6	2.12-2	7.186	3.26+2	.284	8.00	.997
40.0	.093	4.733	4.458	1.88-4	2.73-6	1.32-2	8.019	1.92+2	.287	14.0	.999
50.0	.090	4.811	4.535	1.92-4	2.10-6	1.11-2	8.784	6.64+1	.290	18.0	.999
60.0	.088	4.877	4.601	1.96-4	1.72-6	9.01-3	9.519	-	.292		

Eff. θ = 0.180 Log G = 4.00 Flux = 3.48 + 13 N(HE)/N(E) = 0.15

τ	θ	Log PG	Log PE	H I	HE I	HE II	$(\kappa+\sigma)_{STD}$	$dp_r/d\tau$	∇_A	λ	Flux
0.000	.299	1.445	1.143	5.64-5	6.46-3	9.94-1	3.43-1	1.55+3	.252	227	3.2-15
0.001	.292	1.615	1.313	6.43-5	5.94-3	9.94-1	3.68-1	1.52+3	.254	264	2.8-13
0.002	.286	1.815	1.513	7.88-5	6.59-3	9.93-1	4.13-1	1.51+3	.255	313	2.4-11
0.003	.284	1.939	1.637	9.01-5	7.27-3	9.93-1	4.52-1	1.51+3	.257	386	1.96-9
0.004	.281	2.028	1.726	9.85-5	7.57-3	9.92-1	4.87-1	1.50+3	.258	504	1.43-7
0.006	.277	2.154	1.852	1.10-4	7.75-3	9.92-1	5.45-1	1.46+3	.260	504	2.72-6
0.008	.274	2.242	1.940	1.19-4	7.64-3	9.92-1	5.94-1	1.43+3	.261	567	5.62-6
0.010	.271	2.311	2.009	1.26-4	7.55-3	9.92-1	6.37-1	1.38+3	.263	649	1.34-5
0.015	.266	2.433	2.131	1.39-4	7.24-3	9.93-1	7.27-1	1.31+3	.266	758	3.42-5
0.020	.262	2.519	2.217	1.47-4	6.68-3	9.93-1	8.00-1	1.24+3	.268	911	8.96-5
0.025	.258	2.584	2.283	1.53-4	6.18-3	9.94-1	8.60-1	1.19+3	.270	911	5.87-3
0.030	.257	2.638	2.336	1.60-4	6.19-3	9.94-1	9.22-1	1.16+3	.271	990	5.72-3
0.035	.254	2.682	2.381	1.64-4	5.87-3	9.94-1	9.72-1	1.13+3	.273	1083	5.51-3
0.040	.252	2.721	2.419	1.68-4	5.58-3	9.94-1	1.018	1.10+3	.274	1196	5.21-3
0.060	.246	2.837	2.535	1.80-4	4.85-3	9.95-1	1.174	1.02+3	.278	1335	4.85-3
0.080	.241	2.919	2.617	1.88-4	4.32-3	9.96-1	1.299	9.79+2	.280	1511	4.40-3
0.100	.237	2.981	2.679	1.93-4	3.89-3	9.96-1	1.402	9.47+2	.282	1740	3.89-3
0.125	.233	3.044	2.742	1.98-4	3.42-3	9.97-1	1.510	9.11+2	.285	2051	3.30-3
0.150	.230	3.095	2.793	2.01-4	3.08-3	9.97-1	1.604	8.79+2	.286	2051	3.31-3
0.200	.225	3.175	2.873	2.08-4	2.69-3	9.97-1	1.775	8.30+2	.289	2303	2.93-3
0.250	.221	3.238	2.936	2.13-4	2.34-3	9.98-1	1.910	8.05+2	.291	2625	2.54-3
0.300	.217	3.288	2.987	2.16-4	2.06-3	9.98-1	2.021	7.82+2	.293	3053	2.12-3
0.350	.214	3.332	3.030	2.18-4	1.84-3	9.98-1	2.121	7.61+2	.294	3647	1.72-3
0.400	.211	3.369	3.067	2.20-4	1.67-3	9.98-1	2.207	7.42+2	.295	3647	2.12-3
0.500	.206	3.432	3.130	2.23-4	1.42-3	9.98-1	2.362	7.12+2	.297	4235	1.70-3
0.600	.201	3.484	3.182	2.24-4	1.22-3	9.98-1	2.488	6.86+2	.298	5049	1.28-3
0.700	.198	3.528	3.226	2.26-4	1.09-3	9.99-1	2.601	6.66+2	.299	6252	8.99-4
0.800	.195	2.566	3.264	2.28-4	9.77-4	9.98-1	2.700	6.48+2	.299	8205	5.68-4
1.00	.189	3.631	3.329	2.30-4	8.24-4	9.98-1	2.871	6.19+2	.300	8205	5.90-4
1.20	.185	3.684	3.382	2.31-4	7.16-4	9.98-1	3.017	5.93+2	.300	14588	2.05-4
1.40	.181	3.729	3.428	2.32-4	6.46-4	9.97-1	3.153	5.69+2	.299		
1.60	.178	3.769	3.467	2.33-4	5.92-4	9.96-1	3.271	5.54+2	.299	ΔF/F	
1.80	.175	3.804	3.502	2.34-4	5.50-4	9.95-1	3.380	5.43+2	.298	0.35, 1.93	
2.00	.172	3.835	3.534	2.35-4	5.14-4	9.93-1	3.475	5.32+2	.296		
2.50	.167	3.902	3.600	2.36-4	4.53-4	9.88-1	3.683	5.18+2	.290	τ	C
3.00	.162	3.956	3.655	2.37-4	4.07-4	9.81-1	3.851	5.05+2	.283	.000	.951
3.50	.158	4.003	3.702	2.38-4	3.77-4	9.71-1	4.011	4.92+2	.274	.004	.897
4.00	.155	4.043	3.743	2.37-4	3.51-4	9.58-1	4.234	4.82+2	.264	.010	.888
5.00	.149	4.109	3.810	2.38-4	3.12-4	9.26-1	4.456	4.82+2	.244	.040	.894
6.00	.145	4.163	3.865	2.38-4	2.77-4	8.78-1	4.728	4.81+2	.225	.080	.913
8.00	.137	4.245	3.950	2.35-4	2.16-4	7.52-1	5.266	4.76+2	.199	.200	.946
10.0	.132	4.307	4.015	2.31-4	1.65-4	6.09-1	5.787	4.59+2	.190	.400	.969
14.0	.124	4.396	4.111	2.27-4	9.68-5	3.82-1	6.673	4.38+2	.200	.800	.985
18.0	.118	4.461	4.180	2.21-4	5.54-5	2.31-1	7.217	4.09+2	.223	1.40	.993
22.0	.113	4.515	4.235	2.17-4	3.41-5	1.48-1	7.588	3.82+2	.244	2.00	.995
26.0	.110	4.562	4.282	2.15-4	2.38-5	1.05-1	7.927	3.54+2	.258	4.00	.998
30.0	.107	4.603	4.324	2.13-4	1.67-5	7.53-2	8.171	3.25+2	.268	8.00	.999
40.0	.100	4.690	4.413	2.09-4	8.29-6	3.87-2	8.704	2.54+2	.283	14.0	1.00
50.0	.096	4.763	4.487	2.07-4	4.93-6	2.36-2	9.192	1.82+2	.289	18.0	1.00
60.0	.092	4.827	4.552	2.06-4	3.29-6	1.59-2	9.665	1.10+2	.292		

Eff. θ = 0.180 Log G = 3.5 Flux = 3.48 + 13 N(HE)/N(H) = 0.15

τ	θ	Log PG	Log PE	H I	HE I	HE II	$(\kappa+\sigma)_{STD}$	$dp_r/d\tau$	∇_A	λ	Flux
0.000	.274	1.165	0.863	2.86-5	6.55-4	9.99-1	3.02-1	1.36+3	.251	227	1.3-13
0.001	.270	1.281	0.979	3.18-5	6.81-4	9.99-1	3.09-1	1.38+3	.251	264	6.6-12
0.002	.267	1.443	1.141	3.79-5	8.28-4	9.99-1	3.22-1	1.39+3	.252	313	3.3-10
0.003	.266	1.556	1.254	4.30-5	9.75-4	9.99-1	3.35-1	1.42+3	.253	386	1.58-8
0.004	.265	1.641	1.339	4.72-5	1.09-3	9.99-1	3.47-1	1.44+3	.253	504	6.86-7
0.006	.262	1.767	1.466	5.40-5	1.25-3	9.99-1	3.69-1	1.46+3	.254	504	1.01-5
0.008	.260	1.859	1.557	5.94-5	1.35-3	9.99-1	3.88-1	1.47+3	.254	567	1.79-5
0.010	.258	1.931	1.629	6.37-5	1.40-3	9.99-1	4.06-1	1.47+3	.255	649	3.70-5
0.015	.254	2.062	1.760	7.18-5	1.47-3	9.99-1	4.43-1	1.44+3	.256	758	8.30-5
0.020	.251	2.154	1.852	7.75-5	1.45-3	9.99-1	4.74-1	1.41+3	.258	911	1.90-4
0.025	.248	2.225	1.924	8.19-5	1.41-3	9.99-1	5.01-1	1.38+3	.258	911	4.96-4
0.030	.246	2.283	1.981	8.62-5	1.41-3	9.99-1	5.27-1	1.35+3	.259	990	5.06-3
0.035	.244	2.332	2.030	8.94-5	1.37-3	9.99-1	5.50-1	1.31+3	.260	1083	5.09-3
0.040	.242	2.374	2.072	9.21-5	1.33-3	9.99-1	5.70-1	1.29+3	.261	1196	5.02-3
0.060	.236	2.499	2.197	1.01-4	1.22-3	9.99-1	6.41-1	1.21+3	.263	1335	4.83-3
0.080	.232	2.587	2.286	1.07-4	1.14-3	9.99-1	7.00-1	1.15+3	.264	1511	4.54-3
0.100	.228	2.654	2.353	1.11-4	1.06-3	9.99-1	7.49-1	1.11+3	.266	1740	4.11-3
0.125	.225	2.721	2.419	1.16-4	9.75-4	9.99-1	8.01-1	1.06+3	.267	2051	3.57-3
0.150	.222	2.775	2.474	1.19-4	9.06-4	9.99-1	8.47-1	1.02+3	.268	2051	3.60-3
0.200	.217	2.860	2.558	1.25-4	8.34-4	9.99-1	9.30-1	9.68+2	.270	2303	3.20-3
0.250	.213	2.925	2.623	1.30-4	7.56-4	9.99-1	9.96-1	9.39+2	.271	2625	2.79-3
0.300	.210	2.977	2.675	1.32-4	6.88-4	9.99-1	1.051	9.14+2	.272	3053	2.33-3
0.350	.207	3.021	2.720	1.35-4	6.35-4	9.99-1	1.099	8.95+2	.273	3647	1.89-3
0.400	.204	3.060	2.758	1.36-4	5.87-4	9.99-1	1.140	8.78+2	.274	3647	2.21-3
0.500	.199	3.124	2.822	1.38-4	6.32-4	9.98-1	1.242	8.58+2	.274	4235	1.78-3
0.600	.195	3.170	2.869	1.39-4	9.44-4	9.97-1	1.406	8.38+2	.274	5049	1.35-3
0.700	.191	3.215	2.913	1.40-4	4.07-4	9.98-1	1.307	8.16+2	.275	6252	9.56-4
0.800	.188	3.255	2.953	1.41-4	3.73-4	9.97-1	1.351	7.98+2	.274	8205	6.06-4
1.00	.183	3.321	3.019	1.43-4	3.26-4	9.95-1	1.430	7.71+2	.274	8205	6.23-4
1.20	.178	3.376	3.074	1.44-4	2.92-4	9.92-1	1.496	7.47+2	.272	14588	2.19-4
1.40	.174	3.422	3.121	1.45-4	2.70-4	9.88-1	1.557	7.24+2	.270		
1.60	.171	3.462	3.161	1.46-4	2.52-4	9.83-1	1.608	7.13+2	.267	ΔF/F	
1.80	.168	3.497	3.195	1.46-4	2.38-4	9.77-1	1.668	7.00+2	.264	-1.05, 1.49	
2.00	.165	3.529	3.227	1.47-4	2.25-4	9.69-1	1.715	6.88+2	.260		
2.50	.160	3.594	3.294	1.48-4	2.03-4	9.44-1	1.828	6.71+2	.248	τ	C
3.00	.155	3.647	3.349	1.48-4	1.82-4	9.07-1	1.927	6.59+2	.236	.000	.862
3.50	.151	3.692	3.395	1.47-4	1.65-4	8.62-1	1.995	6.53+2	.224	.004	.840
4.00	.148	3.730	3.435	1.47-4	1.49-4	8.07-1	2.095	6.47+2	.215	.010	.844
5.00	.142	3.790	3.498	1.46-4	1.20-4	6.86-1	2.278	6.36+2	.203	.040	.862
6.00	.138	3.838	3.547	1.44-4	9.22-5	5.55-1	2.443	6.22+2	.201	.080	.886
8.00	.131	3.910	3.623	1.42-4	5.62-5	3.58-1	2.712	5.85+2	.210	.200	.931
10.0	.126	3.966	3.684	1.40-4	3.54-5	2.34-1	2.923	5.32+2	.225	.400	.961
14.0	.119	4.055	3.776	1.39-4	1.83-5	1.24-1	3.220	4.71+2	.246	.800	.982
18.0	.114	4.126	3.848	1.39-4	1.10-5	7.56-2	3.442	4.24+2	.257	1.40	.991
22.0	.110	4.186	3.909	1.40-4	7.55-6	5.22-2	3.646	3.71+2	.263	2.00	.994
26.0	.107	4.239	3.964	1.41-4	5.64-6	3.89-2	3.855	3.20+2	.267	4.00	.997
30.0	.105	4.287	4.011	1.42-4	4.44-6	3.05-2	4.049	2.69+2	.270	8.00	.998
40.0	.100	4.392	4.115	1.46-4	2.87-6	1.94-2	4.546	1.46+2	.274	14.0	.999
50.0	.097	4.483	4.206	1.51-4	2.16-6	1.43-2	5.084	2.58+1	.277	18.0	.999
60.0	.094	4.559	4.283	1.56-4	1.75-6	6.77-3	5.613	0.00	.279		

Eff. θ = 0.180 Log G = 4.00 Flux = 3.48 + 13 N(HE)/N(H) = 0.05

τ	θ	Log PG	Log PE	H I	HE I	HE II	$(\kappa+\sigma)_{STD}$	$dp_r/d\tau$	∇_A	λ	Flux
0.000	.300	1.405	1.103	5.39-5	6.20-3	9.94-1	4.02-1	1.48+3	.253	227	5.2-15
0.001	.294	1.565	1.264	6.22-5	6.23-3	9.94-1	4.28-1	1.49+3	.254	264	3.6-13
0.002	.290	1.759	1.457	7.66-5	7.23-3	9.93-1	4.75-1	1.49+3	.255	313	2.7-11
0.003	.287	1.881	1.579	8.71-5	7.84-3	9.92-1	5.16-1	1.49+3	.257	386	2.05-9
0.004	.284	1.970	1.668	9.49-5	8.04-3	9.92-1	5.51-1	1.48+3	.258	504	1.44-7
0.006	.280	2.096	1.794	1.06-4	8.08-3	9.92-1	6.12-1	1.44+3	.260	504	2.08-6
0.008	.276	2.186	1.884	1.14-4	7.88-3	9.92-1	6.63-1	1.39+3	.261	567	4.51-6
0.010	.273	2.255	1.953	1.21-4	7.74-3	9.92-1	7.09-1	1.34+3	.263	649	1.11-5
0.015	.268	2.379	2.077	1.33-4	7.36-3	9.92-1	8.06-1	1.27+3	.265	758	2.95-5
0.020	.264	2.466	2.164	1.41-4	6.74-3	9.93-1	8.83-1	1.21+3	.267	912	7.94-5
0.025	.260	2.532	2.230	1.46-4	6.20-3	9.94-1	9.49-1	1.16+3	.269	912	5.62-3
0.030	.259	2.586	2.284	1.53-4	6.24-3	9.94-1	1.016	1.13+3	.271	990	5.55-3
0.035	.256	2.631	2.330	1.58-4	5.92-3	9.94-1	1.071	1.10+3	.272	1083	5.40-3
0.040	.254	2.671	2.369	1.61-4	5.62-3	9.94-1	1.120	1.07+3	.273	1196	5.16-3
0.060	.248	2.788	2.486	1.72-4	4.84-3	9.95-1	1.289	1.00+3	.277	1335	4.82-3
0.080	.243	2.870	2.568	1.80-4	4.28-3	9.96-1	1.425	9.58+2	.279	1511	4.39-3
0.100	.239	2.933	2.631	1.84-4	3.81-3	9.96-1	1.536	9.29+2	.281	1740	3.88-3
0.125	.234	2.996	2.694	1.89-4	3.32-3	9.97-1	1.652	8.95+2	.283	2051	3.30-3
0.150	.231	3.048	2.746	1.92-4	2.96-3	9.97-1	1.754	8.64+2	.285	2051	3.30-3
0.200	.226	3.129	2.827	1.99-4	2.59-3	9.97-1	1.942	8.12+2	.287	2303	2.92-3
0.250	.222	3.191	2.889	2.03-4	2.25-3	9.98-1	2.089	7.89+2	.289	2625	2.52-3
0.300	.218	3.242	2.940	2.05-4	1.97-3	9.98-1	2.211	7.68+2	.291	3053	2.10-3
0.350	.214	3.285	2.984	2.08-4	1.76-3	9.98-1	2.319	7.50+2	.292	3647	1.68-3
0.400	.211	3.323	3.021	2.09-4	1.58-3	9.98-1	2.413	7.33+2	.293	3647	2.11-3
0.500	.206	3.386	3.084	2.12-4	1.33-3	9.98-1	2.580	7.04+2	.294	4235	1.68-3
0.600	.202	3.438	3.136	2.13-4	1.14-3	9.99-1	2.717	6.83+2	.295	5049	1.27-3
0.700	.198	3.481	3.180	2.14-4	1.64-3	9.98-1	2.918	6.75+2	.296	6252	8.93-4
0.800	.195	3.518	3.216	2.15-4	9.03-4	9.99-1	2.934	6.63+2	.297	8205	5.61-4
1.00	.189	3.583	3.281	2.17-4	7.63-4	9.98-1	3.124	6.27+2	.298	8205	5.85-4
1.20	.185	3.636	3.334	2.18-4	6.62-4	9.98-1	3.282	6.47+2	.298	14588	2.03-4
1.40	.181	3.680	3.378	2.19-4	5.97-4	9.97-1	3.421	7.25+2	.298		
1.60	.178	3.719	3.417	2.19-4	5.43-4	9.96-1	3.541	5.13+2	.298	ΔF/F	
1.80	.175	3.755	3.453	2.21-4	5.06-4	9.94-1	3.670	5.33+2	.298	-1.0, +0.62	
2.00	.172	3.786	3.485	2.21-4	4.74-4	9.93-1	3.778	5.48+2	.298		
2.50	.167	3.853	3.551	2.23-4	4.18-4	9.87-1	4.009	5.35+2	.296	τ	C
3.00	.162	3.907	3.606	2.23-4	3.76-4	9.79-1	4.194	5.22+2	.293	.000	.931
3.50	.158	3.954	3.652	2.24-4	3.48-4	9.68-1	4.397	5.04+2	.290	.004	.899
4.00	.155	3.994	3.693	2.23-4	3.24-4	9.54-1	4.552	4.90+2	.285	.010	.888
5.00	.150	4.061	3.761	2.24-4	2.88-4	9.18-1	4.750	4.90+2	.276	.040	.894
6.00	.145	4.117	3.816	2.24-4	2.56-4	8.67-1	4.989	4.87+2	.266	.080	.913
8.00	.138	4.203	3.904	2.23-4	2.00-4	7.39-1	5.423	4.74+2	.250	.200	.946
10.0	.132	4.269	3.971	2.21-4	1.55-4	6.00-1	5.807	4.53+2	.244	.400	.969
14.0	.124	4.368	4.073	2.19-4	9.46-5	3.87-1	6.478	4.29+2	.250	.800	.985
18.0	.119	4.441	4.147	2.17-4	5.93-5	2.51-1	6.960	4.07+2	.262	1.40	.993
22.0	.115	4.500	4.206	2.16-4	3.96-5	1.71-1	7.346	3.84+2	.272	2.00	.995
26.0	.111	4.550	4.256	2.15-4	2.79-5	1.23-1	7.671	3.62+2	.280	4.00	.998
30.0	.108	4.593	4.300	2.14-4	2.06-5	9.17-2	7.963	3.40+2	.285	8.00	.999
40.0	.103	4.682	4.390	2.13-4	1.13-5	5.11-2	8.590	2.85+2	.292	14.0	.999
50.0	.098	4.754	4.462	2.13-4	7.14-6	3.29-2	9.143	2.30+2	.296	18.0	.999
60.0	.095	4.816	4.524	2.13-4	4.98-6	2.32-2	9.655	1.77+2	.297		

Eff. θ = 0.210 Log G = 4.00 Flux = 1.88 + 13 N(HE)/N(H) = 0.15

τ	θ	Log PG	Log PE	H I	HE I	HE II	$(\kappa+\sigma)_{STD}$	$dp_r/d\tau$	∇_A	λ	Flux
0.000	.346	1.387	1.082	1.25-4	1.00-1	9.00-1	3.66-1	8.77+2	.241	227	5.3-18
0.001	.337	1.568	1.264	1.39-4	8.73-2	9.13-1	4.03-1	8.18+2	.243	264	1.3-15
0.002	.330	1.772	1.467	1.70-4	9.09-2	9.09-1	4.68-1	7.70+2	.242	313	2.9-13
0.003	.327	1.895	1.591	1.95-4	9.60-2	9.04-1	5.22-1	7.34+2	.241	386	5.8-11
0.004	.324	1.983	1.679	2.13-4	9.80-2	9.02-1	5.68-1	7.03+2	.241	504	9.82-9
0.006	.320	2.106	1.802	2.44-4	1.03-1	8.97-1	6.50-1	6.57+2	.240	504	4.36-8
0.008	.318	2.192	1.887	2.68-4	1.07-1	8.93-1	7.21-1	6.24+2	.238	567	1.93-7
0.010	.317	2.258	1.953	2.91-4	1.13-1	8.87-1	7.86-1	6.04+2	.237	649	8.51-7
0.015	.313	2.374	2.069	3.29-4	1.17-1	8.83-1	9.18-1	5.86+2	.235	758	3.67-6
0.020	.310	2.455	2.150	3.52-4	1.16-1	8.84-1	1.026	5.72+2	.235	911	1.51-5
0.025	.307	2.517	2.212	3.67-4	1.13-1	8.87-1	1.117	5.60+2	.236	911	2.86-3
0.030	.305	2.567	2.262	3.83-4	1.11-1	8.89-1	1.202	5.55+2	.237	990	2.82-3
0.035	.303	2.610	2.305	3.91-4	1.07-1	8.93-1	1.275	5.47+2	.238	1083	2.74-3
0.040	.301	2.646	2.341	3.97-4	1.03-1	8.97-1	1.340	5.40+2	.240	1196	2.64-3
0.060	.294	2.756	2.452	4.09-4	8.75-2	9.12-1	1.557	5.18+2	.247	1335	2.50-3
0.080	.289	2.833	2.529	4.13-4	7.58-2	9.24-1	1.727	5.03+2	.253	1511	2.32-3
0.100	.285	2.893	2.590	4.11-4	6.53-2	9.35-1	1.865	4.92+2	.260	1740	2.11-3
0.125	.280	2.954	2.651	4.05-4	5.44-2	9.46-1	2.006	4.78+2	.267	2051	1.86-3
0.150	.275	3.004	2.701	3.99-4	4.63-2	9.54-1	2.127	4.66+2	.273	2051	1.86-3
0.200	.269	3.083	2.780	3.93-4	3.66-2	9.64-1	2.338	4.42+2	.281	2303	1.69-3
0.250	.263	3.144	2.842	3.86-4	2.94-2	9.71-1	2.506	4.28+2	.287	2625	1.51-3
0.300	.258	3.195	2.893	3.79-4	2.40-2	9.76-1	2.643	4.14+2	.292	3053	1.30-3
0.350	.254	3.239	2.936	3.73-4	2.03-2	9.80-1	2.768	4.03+2	.296	3647	1.10-3
0.400	.250	3.276	2.974	3.67-4	1.74-2	9.83-1	2.874	3.92+2	.299	3647	1.49-3
0.500	.244	3.340	3.038	3.59-4	1.33-2	9.87-1	3.062	3.75+2	.304	4235	1.22-3
0.600	.238	3.393	3.091	3.52-4	1.05-2	9.90-1	3.216	3.60+2	.307	5049	9.36-4
0.700	.234	3.437	3.135	3.49-4	8.80-3	9.91-1	3.364	3.48+2	.310	6252	6.69-4
0.800	.230	3.476	3.174	3.46-4	7.46-3	9.93-1	3.490	3.38+2	.312	8205	4.34-4
1.00	.224	3.542	3.240	3.40-4	5.63-3	9.94-1	3.709	3.22+2	.314	8205	4.58-4
1.20	.218	3.596	3.294	3.36-4	4.47-3	9.96-1	3.892	3.08+2	.316	14588	1.64-4
1.40	.214	3.642	3.341	3.35-4	3.73-3	9.96-1	4.066	2.96+2	.318		
1.60	.210	3.683	3.381	3.32-4	3.17-3	9.97-1	4.213	2.84+2	.319	ΔF/F	
1.80	.207	3.718	3.416	3.32-4	2.80-3	9.97-1	4.362	2.76+2	.320	-0.42, 0.94	
2.00	.204	3.750	3.448	3.31-4	2.49-3	9.97-1	4.492	2.69+2	.320		
2.50	.197	3.818	3.516	3.30-4	1.96-3	9.98-1	4.783	2.57+2	.322	τ	C
3.00	.192	3.873	3.571	3.28-4	1.60-3	9.98-1	5.012	2.47+2	.322	.000	.819
3.50	.188	3.920	3.618	3.28-4	1.38-3	9.98-1	5.231	2.39+2	.323	.004	.881
4.00	.184	3.961	3.659	3.27-4	1.20-3	9.98-1	5.415	2.32+2	.322	.010	.889
5.00	.178	4.029	3.728	3.27-4	9.97-4	9.97-1	5.761	2.26+2	.322	.040	.911
6.00	.173	4.085	3.784	3.25-4	8.48-4	9.96-1	6.022	2.21+2	.319	.080	.931
8.00	.165	4.174	3.873	3.23-4	6.74-4	9.91-1	6.445	2.14+2	.311	.200	.959
10.0	.158	4.244	3.943	3.21-4	5.73-4	9.83-1	6.784	2.13+2	.299	.400	.977
14.0	.148	4.350	4.050	3.16-4	4.52-4	9.49-1	7.330	2.14+2	.264	.800	.989
18.0	.141	4.428	4.130	3.13-4	3.76-4	8.91-1	7.912	2.11+2	.230	1.40	.995
22.0	.136	4.489	4.193	3.08-4	3.14-4	8.07-1	8.514	2.10+2	.205	2.00	.997
26.0	.131	4.538	4.245	3.02-4	2.60-4	7.08-1	9.126	2.09+2	.192	4.00	.999
30.0	.127	4.579	4.290	2.98-4	2.12-4	6.04-1	9.757	2.09+2	.187	8.00	1.00
40.0	.119	4.658	4.373	2.88-4	1.21-4	3.77-1	10.93	2.09+2	.199	14.0	1.00
50.0	.114	4.718	4.435	2.79-4	7.01-5	2.31-1	11.68	2.09+2	.224	18.0	1.00
60.0	.109	4.767	4.487	2.72-4	4.27-5	1.47-1	12.17	2.10+2	.247		

Eff. θ = 0.250 Log G = 4.00 Flux = 9.37 + 12 N(HE)/N(H) = 0.15

τ	θ	Log PG	Log PE	H I	HE I	HE II	$(\kappa+\sigma)_{STD}$	$dp_r/d\tau$	∇_A	λ	Flux
0.000	.385	1.216	0.901	2.67-4	4.76-1	5.24-1	3.41-1	3.30+2	.215	911	1.10-3
0.001	.385	1.399	1.081	3.76-4	5.65-1	4.35-1	3.76-1	3.37+2	.209	994	1.16-3
0.002	.384	1.604	1.283	5.60-4	6.61-1	3.39-1	4.38-1	3.43+2	.204	1094	1.17-3
0.003	.383	1.728	1.405	7.02-4	7.08-1	2.92-1	4.91-1	3.47+2	.201	1215	1.17-3
0.004	.381	1.815	1.491	8.16-4	7.34-1	2.66-1	5.38-1	3.50+2	.199	1367	1.15-3
0.006	.379	1.937	1.612	9.86-4	7.62-1	2.38-1	6.19-1	3.52+2	.197	1563	1.10-3
0.008	.377	2.021	1.696	1.10-3	7.74-1	2.26-1	6.88-1	3.53+2	.195	1683	1.07-3
0.010	.376	2.086	1.761	1.20-3	7.79-1	2.21-1	7.49-1	3.52+2	.193	1823	1.04-3
0.015	.371	2.201	1.875	1.33-3	7.80-1	2.20-1	8.77-1	3.49+2	.189	1989	9.95-4
0.020	.368	2.281	1.956	1.40-3	7.71-1	2.29-1	9.82-1	3.56+2	.186	2188	9.46-4
0.025	.364	2.342	2.018	1.42-3	7.58-1	2.42-1	1.071	3.42+2	.182	2431	8.90-4
0.030	.362	2.392	2.068	1.44-3	7.48-1	2.52-1	1.153	3.37+2	.179	2735	8.29-4
0.035	.359	2.434	2.110	1.44-3	7.34-1	2.66-1	1.224	3.34+2	.177	3126	7.55-4
0.040	.356	2.470	2.146	1.43-3	7.18-1	2.82-1	1.289	3.30+2	.174	3647	6.78-4
0.060	.348	2.578	2.257	1.37-3	6.60-1	3.40-1	1.512	3.16+2	.168	3647	1.04-3
0.080	.341	2.654	2.335	1.30-3	6.02-1	3.98-1	1.686	3.05+2	.164	4019	9.36-4
0.100	.336	2.713	2.395	1.22-3	5.48-1	4.52-1	1.834	2.95+2	.163	4475	8.09-4
0.125	.329	2.773	2.457	1.13-3	4.82-1	5.18-1	1.994	2.84+2	.164	5049	6.82-4
0.150	.324	2.821	2.507	1.05-3	4.24-1	5.76-1	2.121	2.74+2	.168	5792	5.58-4
0.200	.316	2.897	2.585	9.53-4	3.41-1	6.59-1	2.349	2.60+2	.176	6790	4.39-4
0.250	.309	2.957	2.648	8.74-4	2.76-1	7.24-1	2.535	2.46+2	.186	8205	3.30-4
0.300	.303	3.007	2.699	8.07-4	2.24-1	7.76-1	2.683	2.35+2	.197	8205	3.56-4
0.350	.298	3.049	2.742	7.58-4	1.87-1	8.13-1	2.813	2.26+2	.208	10503	2.34-4
0.400	.293	3.085	2.779	7.16-4	1.56-1	8.44-1	2.924	2.18+2	.219	14588	1.34-4
0.500	.285	3.148	2.843	6.58-4	1.16-1	8.84-1	3.119	2.05+2	.237	14588	1.34-4
0.600	.279	3.199	2.895	6.11-4	8.85-2	9.12-1	3.275	1.94+2	.252	17790	9.32-5
0.700	.274	3.243	2.940	5.79-4	7.07-2	9.29-1	3.416	1.85+2	.264	22793	5.94-5
0.800	.269	3.282	2.979	5.53-4	5.74-2	9.43-1	3.534	1.77+2	.274	22793	5.94-5
1.00	.261	3.348	3.045	5.18-4	4.07-2	9.59-1	3.749	1.65+2	.288	30186	3.50-5
1.20	.255	3.402	3.100	4.91-4	3.05-2	9.70-1	3.930	1.54+2	.298	44675	1.66-5
1.40	.249	3.448	3.146	4.75-4	2.43-2	9.76-1	4.098	1.46+2	.304		
1.60	.245	3.489	3.187	4.62-4	1.98-2	9.80-1	4.246	1.39+2	.309	ΔF/F	
1.80	.241	3.525	3.222	4.52-4	1.67-2	9.83-1	4.386	1.33+2	.313	-0.84, -0.07	
2.00	.237	3.557	3.255	4.44-4	1.43-2	9.86-1	4.510	1.28+2	.316		
2.50	.230	3.625	3.323	4.32-4	1.04-2	9.90-1	4.803	1.19+2	.321	τ	C
3.00	.224	3.682	3.380	4.20-4	7.93-3	9.92-1	5.034	1.11+2	.324	.000	.720
3.50	.219	3.729	3.427	4.14-4	6.43-3	9.94-1	5.256	1.05+2	.326	.004	.750
4.00	.215	3.771	3.469	4.08-4	5.30-3	9.95-1	5.441	1.00+2	.328	.010	.786
5.00	.208	3.841	3.539	4.02-4	3.98-3	9.96-1	5.792	9.35+1	.330	.040	.872
6.00	.202	3.898	3.596	3.95-4	3.09-3	9.97-1	6.063	8.78+1	.331	.080	.916
8.00	.193	3.988	3.687	3.88-4	2.15-3	9.98-1	6.530	7.95+1	.332	.200	.958
10.0	.186	4.059	3.757	3.82-4	1.65-3	9.98-1	6.907	7.39+1	.333	.400	.979
14.0	.175	4.167	3.865	3.76-4	1.14-3	9.97-1	7.497	6.69+1	.330	.800	.991
18.0	.168	4.248	3.946	3.70-4	8.92-4	9.95-1	7.950	6.19+1	.325	1.40	.996
22.0	.162	4.313	4.011	3.68-4	7.52-4	9.90-1	8.335	6.22+1	.316	2.00	.997
26.0	.157	4.366	4.065	3.65-4	6.60-4	9.83-1	8.657	6.69+1	.305	4.00	.999
30.0	.152	4.412	4.112	3.62-4	5.94-4	9.74-1	8.926	7.59+1	.292	8.00	1.00
40.0	.144	4.503	4.203	3.58-4	4.85-4	9.34-1	9.596	1.18+2	.255	14.0	1.00
50.0	.138	4.565	4.267	3.49-4	4.04-4	8.71-1	10.16	1.87+2	.223	18.0	1.00
60.0	.133	4.607	4.312	3.38-4	3.34-4	7.84-1	10.62	2.83+2	.201		

Eff. θ = 0.280 Log G = 4.00 Flux = 5.95 + 12 N(HE)/N(H) = 0.15

τ	θ	Log PG	Log PE	H I	HE I	HE II	$(\kappa+\sigma)_{STD}$	$dp_r/d\tau$	∇_A	λ	Flux
0.000	.429	1.335	1.003	1.46-3	9.47-1	5.30-2	3.73-1	2.44+2	.241	911	6.36-4
0.001	.427	1.528	1.196	2.11-3	9.62-1	3.84-2	4.42-1	2.58+2	.244	994	6.59-4
0.002	.426	1.729	1.396	3.12-3	9.73-1	2.72-2	5.54-1	2.70+2	.249	1094	6.76-4
0.003	.424	1.845	1.512	3.83-3	9.77-1	2.30-2	6.44-1	2.75+2	.251	1215	6.87-4
0.004	.423	1.926	1.593	4.36-3	9.79-1	2.10-2	7.20-1	2.80+2	.253	1367	6.87-4
0.006	.420	2.039	1.705	5.09-3	9.81-1	1.93-2	8.46-1	2.83+2	.254	1563	6.77-4
0.008	.417	2.117	1.784	5.54-3	9.81-1	1.90-2	9.51-1	2.84+2	.255	1683	6.68-4
0.010	.415	2.177	1.844	5.85-3	9.81-1	1.90-2	1.041	2.84+2	.255	1823	6.54-4
0.015	.410	2.286	1.952	6.26-3	9.80-1	2.01-2	1.227	2.81+2	.255	1989	6.37-4
0.020	.406	2.362	2.028	6.32-3	9.78-1	2.21-2	1.373	2.78+2	.254	2188	6.16-4
0.025	.402	2.421	2.087	6.25-3	9.75-1	2.48-2	1.496	2.74+2	.252	2431	5.90-4
0.030	.399	2.469	2.136	6.24-3	9.73-1	2.68-2	1.608	2.70+2	.251	2735	5.61-4
0.035	.396	2.510	2.177	6.10-3	9.70-1	2.98-2	1.706	2.66+2	.249	3126	5.24-4
0.040	.393	2.545	2.212	5.92-3	9.67-1	3.30-2	1.791	2.63+2	.246	3647	4.80-4
0.060	.383	2.652	2.320	5.32-3	9.53-1	4.67-2	2.077	2.50+2	.236	3647	8.42-4
0.080	.375	2.728	2.397	4.77-3	9.37-1	6.30-2	2.299	2.39+2	.225	4019	7.56-4
0.100	.369	2.788	2.457	4.31-3	9.19-1	8.14-2	2.484	2.30+2	.214	4475	6.58-4
0.125	.361	2.848	2.519	3.81-3	8.91-1	1.09-1	2.681	2.20+2	.201	5049	5.60-4
0.150	.355	2.898	2.569	3.42-3	8.61-1	1.39-1	2.854	2.11+2	.189	5792	4.62-4
0.200	.346	2.976	2.649	2.94-3	8.05-1	1.95-1	3.167	1.98+2	.175	6790	3.66-4
0.250	.338	3.037	2.712	2.57-3	7.44-1	2.56-1	3.431	1.86+2	.165	8205	2.76-4
0.300	.331	3.086	2.764	2.28-3	6.79-1	3.21-1	3.662	1.77+2	.159	8205	3.04-4
0.350	.326	3.128	2.808	2.07-3	6.20-1	3.80-1	3.864	1.70+2	.156	10503	2.01-4
0.400	.320	3.165	2.846	1.90-3	5.62-1	4.38-1	4.052	1.63+2	.156	14588	1.14-4
0.500	.312	3.226	2.910	1.66-3	4.67-1	5.33-1	4.389	1.53+2	.159	14588	1.17-4
0.600	.305	3.276	2.963	1.47-3	3.85-1	6.15-1	4.674	1.44+2	.166	17790	8.19-5
0.700	.299	3.319	3.008	1.34-3	3.23-1	6.77-1	4.919	1.37+2	.174	22793	5.20-5
0.800	.294	3.356	3.046	1.24-3	2.72-1	7.28-1	5.128	1.31+2	.184	22793	5.24-5
1.00	.286	3.418	3.111	1.10-3	2.01-1	7.99-1	5.488	1.20+2	.203	30186	3.10-5
1.20	.279	3.470	3.164	1.00-3	1.53-1	8.47-1	5.779	1.12+2	.222	44675	1.47-5
1.40	.273	3.514	3.209	9.36-4	1.23-1	8.77-1	6.046	1.06+2	.238		
1.60	.269	3.553	3.248	8.84-4	1.00-1	9.00-1	6.272	1.00+2	.252	ΔF/F	
1.80	.264	3.587	3.283	8.49-4	8.40-2	9.16-1	6.484	9.59+1	.263	-0.91, 0.12	
2.00	.261	3.618	3.315	8.15-4	7.11-2	9.29-1	6.669	9.19+1	.274		
2.50	.253	3.684	3.381	7.60-4	5.11-2	9.49-1	7.103	8.47+1	.292	τ	C
3.00	.246	3.739	3.436	7.17-4	3.81-2	9.62-1	7.441	7.88+1	.306	.000	.730
3.50	.241	3.785	3.483	6.90-4	3.04-2	9.70-1	7.769	7.43+1	.315	.004	.765
4.00	.237	3.826	3.524	6.67-4	2.46-2	9.75-1	8.043	7.04+1	.322	.010	.803
5.00	.229	3.894	3.592	6.40-4	1.79-2	9.82-1	8.558	6.53+1	.331	.040	.887
6.00	.223	3.950	3.648	6.17-4	1.35-2	9.86-1	8.966	6.10+1	.337	.080	.928
8.00	.214	4.039	3.737	5.91-4	8.89-3	9.91-1	9.683	5.48+1	.344	.200	.965
10.0	.206	4.108	3.806	5.72-4	6.48-3	9.94-1	10.26	5.08+1	.347	.400	.982
14.0	.195	4.214	3.912	5.51-4	4.08-3	9.96-1	11.17	4.58+1	.350	.800	.992
18.0	.187	4.294	3.992	5.37-4	2.94-3	9.97-1	11.90	4.23+1	.352	1.40	.996
22.0	.181	4.357	4.005	5.29-4	2.30-3	9.97-1	12.50	4.28+1	.352	2.00	.998
26.0	.176	4.410	4.109	5.22-4	1.90-3	9.97-1	13.01	4.67+1	.351	4.00	.999
30.0	.171	4.456	4.154	5.15-4	1.62-3	9.97-1	13.45	5.38-1	.349	8.00	1.00
40.0	.163	4.545	4.243	5.04-4	1.22-3	9.94-1	14.28	8.60+1	.342	14.0	1.00
50.0	.156	4.611	4.309	4.94-4	9.98-4	9.89-1	14.84	1.39+2	.329	18.0	1.00
60.0	.151	4.661	4.360	4.82-4	8.53-4	9.81-1	14.86	2.12+2	.313		

Eff. θ = 0.320 Log G = 4.00 Flux = 3.49 + 12 N(HE)/N(H) = 0.15

τ	θ	Log PG	Log PE	H I	HE I	HE II	$(\kappa+\sigma)_{STD}$	$dp_r/d\tau$	∇_A	λ	Flux
0.000	.479	1.286	0.952	7.69-3	9.97-1	2.86-3	4.08-1	1.75+2	.252	911	3.05-4
0.001	.477	1.481	1.146	1.10-2	9.98-1	2.10-3	4.98-1	1.91+2	.249	994	3.25-4
0.002	.475	1.678	1.342	1.60-2	9.99-1	1.51-3	6.37-1	2.03+2	.242	1094	3.42-4
0.003	.473	1.792	1.455	1.93-2	9.99-1	1.31-3	7.46-1	2.08+2	.235	1215	3.57-4
0.004	.471	1.871	1.534	2.16-2	9.99-1	1.22-3	8.37-1	2.12+2	.230	1367	3.68-4
0.006	.468	1.982	1.643	2.46-2	9.99-1	1.16-3	9.87-1	2.16+2	.223	1563	3.73-4
0.008	.465	2.059	1.720	2.63-2	9.99-1	1.17-3	1.110	2.17+2	.219	1683	3.73-4
0.010	.462	2.118	1.779	2.73-2	9.99-1	1.21-3	1.215	2.16+2	.217	1823	3.72-4
0.015	.456	2.225	1.886	2.82-2	9.99-1	1.35-3	1.432	2.14+2	.214	1989	3.68-4
0.020	.451	2.301	1.961	2.78-2	9.98-1	1.57-3	1.604	2.11+2	.215	2188	3.64-4
0.025	.446	2.359	2.020	2.68-2	9.98-1	1.83-3	1.746	2.09+2	.218	2431	3.57-4
0.030	.443	2.407	2.068	2.62-2	9.98-1	2.04-3	1.876	2.05+2	.219	2735	3.50-4
0.035	.439	2.447	2.109	2.51-2	9.98-1	2.34-3	1.986	2.02+2	.222	3126	3.39-4
0.040	.436	2.482	2.144	2.40-2	9.97-1	2.68-3	2.084	1.99+2	.224	3647	3.24-4
0.060	.424	2.590	2.252	2.05-2	9.96-1	4.21-3	2.406	1.89+2	.235	3647	6.53-4
0.080	.415	2.666	2.330	1.76-2	9.94-1	6.16-3	2.657	1.80+2	.242	4019	5.89-4
0.100	.408	2.726	2.390	1.54-2	9.91-1	8.56-3	2.858	1.73+2	.248	4475	5.18-4
0.125	.400	2.787	2.452	1.31-2	9.88-1	1.24-2	3.064	1.64+2	.252	5049	4.45-4
0.150	.393	2.838	2.503	1.14-2	9.83-1	1.71-2	3.240	1.58+2	.252	5792	3.72-4
0.200	.382	2.918	2.584	9.34-3	9.73-1	2.72-2	3.557	1.46+2	.248	6790	2.99-4
0.250	.373	2.981	2.647	7.85-3	9.60-1	4.02-2	3.817	1.38+2	.239	8205	2.28-4
0.300	.366	3.032	2.700	6.70-3	9.43-1	5.68-2	4.030	1.31+2	.227	8205	2.56-4
0.350	.360	3.076	2.745	5.90-3	9.25-1	7.48-2	4.234	1.25+2	.216	10503	1.72-4
0.400	.354	3.114	2.784	5.26-3	9.04-1	9.58-2	4.416	1.19+2	.204	14588	9.83-5
0.500	.345	3.178	2.849	4.40-3	8.60-1	1.40-1	4.757	1.11+2	.189	14588	1.02-5
0.600	.337	3.231	2.904	3.75-3	8.08-1	1.92-1	5.057	1.04+2	.173	17790	7.14-5
0.700	.330	3.275	2.950	3.31-3	7.56-1	2.44-1	5.343	9.91+1	.165	22793	4.55-5
0.800	.325	3.313	2.990	2.97-3	7.02-1	2.98-1	5.584	9.44+1	.159	22793	4.60-5
1.00	.316	3.377	3.057	2.50-3	6.02-1	3.98-1	6.055	8.67+1	.155	30186	2.73-5
1.20	.308	3.429	3.112	2.17-3	5.11-1	4.89-1	6.472	8.05+1	.156	44675	1.31-5
1.40	.302	3.473	3.158	1.96-3	4.40-1	5.60-1	6.841	7.58+1	.160		
1.60	.296	3.510	3.197	1.79-3	3.78-1	6.22-1	7.161	7.17+1	.166	ΔF/F	
1.80	.292	3.544	3.232	1.67-3	3.29-1	6.71-1	7.449	6.85+1	.173	-0.40, 0.59	
2.00	.287	3.574	3.264	1.55-3	2.83-1	7.17-1	7.697	6.56+1	.182		
2.50	.279	3.638	3.330	1.37-3	2.08-1	7.92-1	8.251	6.03+1	.202	τ	C
3.00	.272	3.691	3.385	1.24-3	1.57-1	8.43-1	8.689	5.59+1	.223	.000	.740
3.50	.266	3.736	3.430	1.16-3	1.25-1	8.75-1	9.088	5.26+1	.240	.004	.775
4.00	.261	3.775	3.470	1.09-3	1.01-1	8.99-1	9.422	4.97+1	.255	.010	.811
5.00	.253	3.841	3.538	1.00-3	7.26-2	9.27-1	10.05	4.59+1	.278	.040	.893
6.00	.247	3.896	3.592	9.37-4	5.38-2	9.46-1	10.52	4.27+1	.297	.080	.932
8.00	.236	3.983	3.680	8.58-4	3.44-2	9.66-1	11.37	3.81+1	.319	.200	.969
10.0	.229	4.051	3.749	8.10-4	2.42-2	9.76-1	12.04	3.52+1	.332	.400	.985
14.0	.217	4.155	3.853	7.50-4	1.44-2	9.86-1	13.13	3.13+1	.346	.800	.993
18.0	.208	4.233	3.931	7.16-4	9.81-3	9.90-1	13.98	2.86+1	.352	1.40	.997
22.0	.202	4.296	3.994	6.94-1	7.30-3	9.93-1	14.70	2.89+1	.356	2.00	.998
26.0	.196	4.349	4.047	6.78-4	5.76-3	9.94-1	15.32	3.17+1	.358	4.00	.999
30.0	.192	4.394	4.092	6.64-4	4.72-3	9.95-1	15.86	3.68+1	.359	8.00	1.00
40.0	.182	4.483	4.181	6.41-4	3.22-3	9.96-1	16.90	6.03+1	.360	14.0	1.00
50.0	.175	4.549	4.247	6.23-4	2.43-3	9.97-1	17.62	9.90+1	.360	18.0	1.00
60.0	.169	4.599	4.297	6.05-4	1.95-3	9.96-1	18.05	1.53+2	.357		

Eff. θ = 0.360 Log G = 4.00 Flux = 2.18 + 12 N(HE)/N(H) = 0.15

τ	θ	Log PG	Log PE	H I	HE I	HE II	$(\kappa+\sigma)_{STD}$	$dp_r/d\tau$	∇_A	λ	Flux
0.000	.525	1.243	0.901	3.55-2	1.00+0	1.85-4	4.40-1	1.35+2	.214	911	1.53-4
0.001	.523	1.440	1.096	4.97-2	1.00+0	1.39-4	5.44-1	1.49+2	.192	994	1.67-4
0.002	.520	1.638	1.288	6.95-2	1.00+0	1.04-4	6.98-1	1.60+2	.164	1094	1.81-4
0.003	.518	1.752	1.399	8.18-2	1.00+0	9.18-5	8.16-1	1.64+2	.150	1215	1.93-4
0.004	.516	1.832	1.477	8.99-2	1.00+0	8.74-5	9.14-1	1.67+2	.141	1367	2.04-4
0.006	.512	1.943	1.585	9.95-2	1.00+0	8.60-5	1.077	1.70+2	.132	1563	2.12-4
0.008	.509	2.020	1.661	1.04-1	1.00+0	8.93-5	1.207	1.70+2	.128	1683	2.15-4
0.010	.506	2.080	1.720	1.06-1	1.00+0	9.41-5	1.324	1.70+2	.126	1823	2.17-4
0.015	.499	2.187	1.828	1.07-1	1.00+0	1.11-4	1.565	1.67+2	.124	1989	2.19-4
0.020	.493	2.263	1.905	1.03-1	1.00+0	1.34-4	1.764	1.65+2	.125	2188	2.20-4
0.025	.488	2.321	1.963	9.76-2	1.00+0	1.64-4	1.926	1.62+2	.128	2431	2.22-4
0.030	.483	2.369	2.012	9.46-2	1.00+0	1.87-4	2.078	1.60+2	.130	2735	2.24-4
0.035	.479	2.409	2.054	8.96-2	1.00+0	2.22-4	2.210	1.57+2	.133	3126	2.26-4
0.040	.475	2.443	2.090	8.48-2	1.00+0	2.60-4	2.328	1.54+2	.136	3647	2.25-4
0.060	.463	2.549	2.199	6.96-2	1.00+0	4.45-4	2.713	1.46+2	.148	3647	5.19-4
0.080	.452	2.624	2.277	5.83-2	9.99-1	6.95-4	3.011	1.39+2	.161	4019	4.71-4
0.100	.444	2.683	2.338	4.97-2	9.99-1	1.02-3	3.248	1.33+2	.173	4475	4.18-4
0.125	.435	2.742	2.400	4.12-2	9.98-1	1.57-3	3.490	1.27+2	.187	5049	3.63-4
0.150	.428	2.792	2.450	3.60-2	9.98-1	2.16-3	3.706	1.21+2	.198	5792	3.06-4
0.200	.415	2.870	2.531	2.77-2	9.96-1	3.87-3	4.042	1.13+2	.218	6790	2.49-4
0.250	.406	2.933	2.595	2.26-2	9.94-1	6.10-3	4.328	1.06+2	.231	8205	1.92-4
0.300	.397	2.984	2.647	1.87-2	9.91-1	9.14-3	4.557	1.00+2	.240	8205	2.21-4
0.350	.391	3.028	2.692	1.61-2	9.87-1	1.27-2	4.766	9.56+1	.246	10503	1.49-4
0.400	.384	3.066	2.730	1.40-2	9.83-1	1.71-2	4.943	9.16+1	.248	14588	8.66-5
0.500	.374	3.131	2.796	1.13-2	9.73-1	2.74-2	5.280	8.52+1	.245	14588	9.00-5
0.600	.366	3.184	2.850	9.32-3	9.59-1	4.12-2	5.544	7.98+1	.237	17790	6.35-5
0.700	.359	3.229	2.897	8.02-3	9.43-1	5.68-2	5.822	7.56+1	.226	22793	4.07-5
0.800	.352	3.269	2.937	7.02-3	9.25-1	7.53-2	6.061	7.19+1	.215	22793	4.13-5
1.00	.342	3.335	3.005	5.67-3	8.82-1	1.18-1	6.505	6.59+1	.194	30186	2.46-5
1.20	.334	3.389	3.060	4.76-3	8.33-1	1.67-1	6.909	6.10+1	.179	44675	1.18-5
1.40	.327	3.434	3.108	4.18-3	7.85-1	2.15-1	7.303	4.72+1	.169		
1.60	.322	3.473	3.149	3.73-3	7.34-1	2.66-1	7.634	5.42+1	.162	ΔF/F	
1.80	.317	3.508	3.185	3.40-3	6.86-1	3.14-1	7.974	5.17+1	.158	-0.36, 0.52	
2.00	.312	3.538	3.217	3.11-3	6.36-1	3.64-1	8.286	4.94+1	.156		
2.50	.303	3.603	3.285	2.66-3	5.32-1	4.68-1	9.015	4.54+1	.156	τ	C
3.00	.295	3.655	3.340	2.31-3	4.38-1	5.62-1	9.600	4.19+1	.161	.000	.750
3.50	.289	3.700	3.387	2.09-3	3.68-1	6.32-1	10.14	3.94+1	.168	.004	.784
4.00	.284	3.738	3.428	1.91-3	3.10-1	6.90-1	10.59	3.71+1	.178	.010	.818
5.00	.275	3.803	3.494	1.69-3	2.31-1	7.69-1	11.38	3.42+1	.197	.040	.896
6.00	.268	3.856	3.549	1.52-3	1.75-1	8.25-1	11.99	3.17+1	.217	.080	.934
8.00	.257	3.940	3.635	1.32-3	1.13-1	8.87-1	13.01	2.81+1	.251	.200	.970
10.0	.249	4.006	3.702	1.20-3	7.91-2	9.21-1	13.81	2.58+1	.277	.400	.986
14.0	.237	4.108	3.805	1.06-3	4.61-2	9.54-1	15.08	2.28+1	.311	.800	.994
18.0	.228	4.184	3.882	9.85-4	3.08-2	9.69-1	16.08	2.08+1	.330	1.40	.997
22.0	.221	4.246	3.944	9.38-4	2.27-2	9.77-1	16.96	2.10+1	.341	2.00	.998
26.0	.215	4.288	3.996	9.06-4	1.78-2	9.82-1	17.74	2.32+1	.348	4.00	.999
30.0	.210	4.342	4.040	8.72-4	1.39-2	9.86-1	18.26	2.73+1	.354	8.00	1.00
40.0	.200	4.430	4.128	8.25-4	9.01-3	9.91-1	19.53	4.58+1	.361	14.0	1.0
50.0	.192	4.496	4.194	7.79-4	6.17-3	9.94-1	20.20	7.62+1	.364		
60.0	.186	4.547	4.245	7.53-4	4.75-3	9.95-1	20.78	1.18+2	.365		

Eff. θ = 0.400 Log G = 4.00 Flux = 1.43 + 12 N(HE)/N(H) = 0.15

τ	θ	Log PG	Log PE	H I	HE I	HE II	$(\kappa+\sigma)_{STD}$	$dp_r/d\tau$	∇_A	λ	Flux
0.000	.571	1.271	0.898	1.57-1	1.00+0	1.15-5	4.57-1	1.12+2	.127	911	8.08-5
0.001	.568	1.456	1.068	1.98-1	1.00+0	9.36-6	5.44-1	1.22+2	.109	994	8.98-5
0.002	.565	1.652	1.247	2.52-1	1.00+0	7.38-6	6.69-1	1.29+2	.094	1094	9.89-5
0.003	.562	1.769	1.353	2.82-1	1.00+0	6.75-6	7.64-1	1.32+2	.088	1215	1.07-4
0.004	.560	1.851	1.428	3.01-1	1.00+0	6.55-6	8.44-1	1.34+2	.085	1367	1.15-4
0.006	.556	1.967	1.536	3.21-1	1.00+0	6.64-6	9.83-1	1.34+2	.082	1563	1.21-4
0.008	.552	2.048	1.614	3.30-1	1.00+0	7.04-6	1.104	1.35+2	.081	1683	1.24-4
0.010	.548	2.109	1.673	3.32-1	1.00+0	7.61-6	1.209	1.34+2	.080	1823	1.27-4
0.015	.541	2.219	1.784	3.30-1	1.00+0	9.30-6	1.451	1.32+2	.080	1989	1.30-4
0.020	.534	2.294	1.866	3.18-1	1.00+0	1.16-5	1.670	1.30+2	.081	2188	1.34-4
0.025	.528	2.351	1.927	3.02-1	1.00+0	1.46-5	1.861	1.25+2	.082	2431	1.38-4
0.030	.524	2.398	1.978	2.92-1	1.00+0	1.72-5	2.034	1.25+2	.083	2735	1.44-4
0.035	.519	2.436	2.022	2.78-1	1.00+0	2.08-5	2.202	1.23+2	.084	3126	1.50-4
0.040	.514	2.468	2.060	2.64-1	1.00+0	2.50-5	2.356	1.22+2	.086	3647	1.57-4
0.060	.500	2.566	2.173	2.18-1	1.00+0	4.61-5	2.871	1.15+2	.092	3647	4.19-4
0.080	.489	2.634	2.252	1.82-1	1.00+0	7.65-5	3.276	1.09+2	.098	4019	3.82-4
0.100	.480	2.687	2.314	1.54-1	1.00+0	1.18-4	3.611	1.05+2	.104	4475	3.42-4
0.125	.470	2.741	2.375	1.26-1	1.00+0	1.93-4	3.940	9.98+1	.114	5049	2.99-4
0.150	.461	2.785	2.425	1.06-1	1.00+0	2.94-4	4.210	9.54+1	.123	5792	2.55-4
0.200	.448	2.856	2.502	8.17-2	9.99-1	5.38-4	4.641	8.85+1	.139	6790	2.10-4
0.250	.438	2.912	2.564	6.49-2	9.99-1	9.02-4	4.980	8.33+1	.255	8205	1.64-4
0.300	.428	2.959	2.614	5.25-2	9.99-1	1.43-3	5.236	7.88+1	.170	8205	1.93-4
0.350	.421	3.000	2.657	4.42-2	9.98-1	2.08-3	5.467	7.53+1	.184	10503	1.32-4
0.400	.414	3.036	2.694	3.77-2	9.97-1	2.92-3	5.661	7.21+1	.196	14588	7.71-5
0.500	.403	3.097	2.758	2.93-2	9.95-1	5.02-3	6.012	6.71+1	.216	14588	8.06-5
0.600	.394	3.148	2.810	2.34-2	9.92-1	8.03-3	6.292	6.28+1	.230	17790	5.71-5
0.700	.386	3.192	2.855	1.96-2	9.88-1	1.17-3	6.549	5.94+1	.238	22793	3.68-5
0.800	.379	3.231	2.895	1.68-2	9.84-1	1.63-2	6.777	5.65+1	.243	22793	3.74-5
1.00	.368	3.296	2.961	1.30-2	9.72-1	2.78-2	7.192	5.17+1	.242	30186	2.23-5
1.20	.359	3.350	3.016	1.06-2	9.57-1	4.30-2	7.558	4.78+1	.234	44675	1.08-5
1.40	.352	3.396	3.063	9.04-3	9.40-1	6.00-2	7.912	4.48+1	.223		
1.60	.345	3.435	3.103	7.88-3	9.20-1	8.00-2	8.240	4.22+1	.212	ΔF/F	
1.80	.340	3.471	3.140	7.03-3	8.99-1	1.01-1	8.560	4.02+1	.201	-0.65, 0.35	
2.00	.335	3.502	3.172	6.32-3	8.74-1	1.26-1	8.854	3.84+1	.192		
2.50	.325	3.568	3.241	5.18-3	8.13-1	1.87-1	9.528	3.52+1	.174	τ	C
3.00	.317	3.623	3.298	4.35-3	7.40-1	2.60-1	10.14	3.26+1	.163	.000	.758
3.50	.310	3.668	3.345	3.84-3	6.75-1	3.25-1	10.74	3.05+1	.158	.004	.791
4.00	.304	3.707	3.387	3.43-3	6.10-1	3.90-1	11.28	2.87+1	.156	.010	.823
5.00	.295	3.772	3.455	2.93-3	5.04-1	4.96-1	12.25	2.63+1	.158	.040	.898
6.00	.288	3.825	3.511	2.56-3	4.13-1	5.87-1	13.06	2.43+1	.164	.080	.936
8.00	.276	3.908	3.598	2.13-3	2.90-1	7.10-1	14.38	2.15+1	.183	.200	.972
10.0	.267	3.973	3.665	1.87-3	2.11-1	7.89-1	15.38	1.97+1	.205	.400	.987
14.0	.255	4.072	3.766	1.57-3	1.27-1	8.73-1	16.93	1.72+1	.245	.800	.995
18.0	.245	4.146	3.842	1.40-3	8.48-2	9.15-1	18.10	1.57+1	.276	1.40	.998
22.0	.238	4.207	3.903	1.30-3	6.14-2	9.39-1	19.07	1.59+1	.298	2.00	.999
26.0	.232	4.257	3.955	1.22-3	4.68-2	9.53-1	19.90	1.76+1	.315	4.00	.999
30.0	.227	4.301	3.998	1.16-3	3.71-2	9.63-1	20.60	2.08+1	.326	8.00	1.00
40.0	.217	4.387	4.085	1.07-3	2.34-2	9.77-1	22.05	3.54+1	.345	14.0	1.00
50.0	.209	4.453	4.151	1.01-3	1.64-2	9.84-1	23.09	5.93+1	.355	18.0	1.00
60.0	.203	4.503	4.201	9.62-4	1.23-2	9.88-1	23.82	9.27+1	.360		

Eff. θ = 0.500 Log G = 4.44 Flux = 5.95 + 11 N(HE)/N(H) = 0.15

τ	θ	Log PG	Log PE	H I	HE I	HE II	$(\kappa+\sigma)_{STD}$	$dp_r/d\tau$	∇_A	λ	Flux
0.000	.682	2.045	0.913	9.09-1	1.00+0	1.28-8	1.91-1	3.91+1	.088	911	1.91-5
0.001	.680	2.250	1.041	9.24-1	1.00+0	1.11-8	2.16-1	3.73+1	.092	994	2.19-5
0.002	.678	2.471	1.175	9.39-1	1.00+0	9.31-9	2.49-1	3.58+1	.100	1094	2.45-5
0.003	.676	2.603	1.257	9.46-1	1.00+0	8.54-9	2.74-1	3.46+1	.105	1215	2.70-5
0.004	.674	2.697	1.317	9.50-1	1.00+0	8.17-9	2.97-1	3.36+1	.108	1367	2.94-5
0.006	.672	2.827	1.405	9.55-1	1.00+0	7.87-9	3.37-1	3.24+1	.113	1563	3.18-5
0.008	.669	2.917	1.471	9.58-1	1.00+0	7.86-9	3.74-1	3.15+1	.117	1683	3.31-5
0.010	.667	2.985	1.522	9.59-1	1.00+0	7.97-9	4.06-1	3.10+1	.119	1823	3.48-5
0.015	.662	3.107	1.621	9.62-1	1.00+0	8.52-9	4.80-1	3.01+1	.123	1989	3.72-5
0.020	.658	3.189	1.696	9.62-1	1.00+0	9.40-9	5.51-1	2.94+1	.125	2188	4.03-5
0.025	.654	3.251	1.759	9.62-1	1.00+0	1.05-8	6.20-1	6.89+1	.125	2431	4.46-5
0.030	.650	3.299	1.809	9.62-1	1.00+0	1.15-8	6.82-1	2.88+1	.126	2735	5.04-5
0.035	.647	3.339	1.856	9.61-1	1.00+0	1.27-8	7.49-1	2.86+1	.126	3126	5.80-5
0.040	.643	3.373	1.898	9.61-1	1.00+0	1.42-8	8.15-1	2.84+1	.125	3647	6.73-5
0.060	.632	3.469	2.034	9.56-1	1.00+0	2.10-8	1.081	2.81+1	.122	3647	2.34-4
0.080	.621	3.531	2.140	9.52-1	1.00+0	3.03-8	1.361	2.80+1	.118	4019	2.18-4
0.100	.613	3.575	2.228	9.46-1	1.00+0	4.25-8	1.662	2.79+1	.115	4475	2.01-4
0.125	.602	3.617	2.324	9.39-1	1.00+0	6.31-8	2.081	2.78+1	.110	5049	1.82-4
0.150	.593	3.647	2.405	9.30-1	1.00+0	9.08-8	2.536	2.77+1	.106	5792	1.62-4
0.200	.578	3.690	2.534	9.14-1	1.00+0	1.67-7	3.511	2.75+1	.100	6790	1.39-4
0.250	.566	3.719	2.641	8.96-1	1.00+0	2.84-7	4.644	2.71+1	.095	8205	1.13-4
0.300	.554	3.740	2.730	8.76-1	1.00+0	4.63-7	5.949	2.67+1	.092	8205	1.36-4
0.350	.545	3.756	2.806	8.55-1	1.00+0	7.04-7	7.356	2.62+1	.089	10503	9.80-5
0.400	.536	3.769	2.871	8.33-1	1.00+0	1.04-6	8.914	2.58+1	.087	14588	6.02-5
0.500	.521	3.788	2.977	7.90-1	1.00+0	2.01-6	12.21	2.48+1	.084	14588	6.37-5
0.600	.508	3.801	3.064	7.43-1	1.00+0	3.61-6	15.92	2.39+1	.082	17790	4.57-5
0.700	.498	3.812	3.130	6.97-1	1.00+0	5.90-6	19.63	2.31+1	.082	22793	2.97-5
0.800	.488	3.820	3.187	6.51-1	1.00+0	9.23-6	23.46	2.23+1	.081	22793	3.03-5
1.00	.473	3.833	3.271	5.65-1	1.00+0	1.96-5	30.64	2.09+1	.082	30186	1.82-5
1.20	.460	3.843	3.333	4.85-1	1.00+0	3.72-5	37.05	1.96+1	.084	44675	8.84-6
1.40	.451	3.851	3.377	4.20-1	1.00+0	6.22-5	42.14	1.86+1	.086		
1.60	.442	3.859	3.411	3.62-1	1.00+0	9.92-5	46.24	1.77+1	.090	ΔF/F	
1.80	.434	3.865	3.438	3.14-1	1.00+0	1.48-4	49.45	1.70+1	.093	-0.68, 0.62	
2.00	.427	3.872	3.459	2.71-1	1.00+0	2.17-4	51.79	1.63+1	.097		
2.50	.414	3.886	3.500	1.99-1	1.00+0	4.60-4	55.38	1.50+1	.108	τ	C
3.00	.402	3.899	3.528	1.47-1	9.99-1	8.87-4	56.69	1.39+1	.121	.000	.789
3.50	.394	3.912	3.550	1.15-1	9.99-1	1.48-3	57.15	1.31+1	.133	.004	.806
4.00	.386	3.924	3.568	9.14-2	9.98-1	2.34-3	56.89	1.23+1	.147	.010	.820
5.00	.374	3.948	3.600	6.46-2	9.95-1	4.64-3	56.51	1.12+1	.171	.040	.858
6.00	.363	3.971	3.627	4.77-2	9.92-1	8.28-3	55.73	1.04+1	.193	.080	.889
8.00	.349	4.014	3.674	3.10-2	9.81-1	1.88-2	55.15	8.97+0	.218	.200	.937
10.0	.338	4.053	3.717	2.28-2	9.66-1	3.40-2	55.33	8.07+0	.225	.400	.969
14.0	.322	4.122	3.788	1.51-2	9.24-1	7.58-2	56.61	6.97+0	.212	.800	.988
18.0	.310	4.180	3.849	1.15-2	8.71-1	1.29-1	58.96	6.28+0	.194	1.40	.995
22.0	.302	4.229	3.900	9.42-3	8.13-1	1.87-1	61.51	6.52+0	.180	2.00	.997
26.0	.295	4.271	3.945	8.08-3	7.53-1	2.47-1	64.12	7.53+0	.171	4.00	.999
30.0	.289	4.308	3.984	7.15-3	6.94-1	3.06-1	66.73	9.32+0	.166	8.00	1.00
40.0	.277	4.383	4.063	5.69-3	5.61-1	4.39-1	72.40	1.72+1	.163	14.0	1.00
50.0	.269	4.441	4.125	4.85-3	4.56-1	5.44-1	77.19	3.00+1	.169	18.0	1.00
60.0	.262	4.487	4.174	4.27-3	3.72-1	6.28-1	80.86	4.76+1	.178		

Eff. θ = 0.504 Log G = 4.00 Flux = 5.67 + 11 N(HE)/N(H) = 0.15

τ	θ	Log PG	Log PE	H I	HE I	HE II	$(\kappa+\sigma)_{STD}$	$dp_r/d\tau$	∇_A	λ	Flux
0.000	.688	1.706	0.688	8.79-1	1.00+0	1.53-8	1.57-1	3.88+1	.084	911	1.74-5
0.001	.685	1.907	0.818	8.99-1	1.00+0	1.34-8	1.73-1	3.79+1	.086	994	2.01-5
0.002	.683	2.131	0.956	9.18-1	1.00+0	1.12-8	1.94-1	3.70+1	.090	1094	2.27-5
0.003	.681	2.266	1.041	9.27-1	1.00+0	1.03-8	2.12-1	3.61+1	.093	1215	2.52-5
0.004	.679	2.361	1.105	9.33-1	1.00+0	9.91-9	2.29-1	3.54+1	.096	1367	2.74-5
0.006	.676	2.493	1.197	9.39-1	1.00+0	9.67-9	2.59-1	3.43+1	.100	1563	2.95-5
0.008	.673	2.585	1.266	9.42-1	1.00+0	9.77-9	2.86-1	3.35+1	.102	1683	3.07-5
0.010	.671	2.655	1.320	9.45-1	1.00+0	1.00-8	3.11-1	3.30+1	.104	1823	3.22-5
0.015	.666	2.777	1.424	9.47-1	1.00+0	1.09-8	3.70-1	3.21+1	.106	1989	3.44-5
0.020	.661	2.860	1.504	9.47-1	1.00+0	1.23-8	4.28-1	3.14+1	.107	2188	3.73-5
0.025	.656	2.921	1.569	9.47-1	1.00+0	1.40-8	4.84-1	3.09+1	.108	2431	4.13-5
0.030	.652	2.969	1.621	9.46-1	1.00+0	1.56-8	5.35-1	3.07+1	.108	2735	4.69-5
0.035	.648	3.009	1.671	9.45-1	1.00+0	1.75-8	5.91-1	3.05+1	.107	3126	5.45-5
0.040	.645	3.042	1.714	9.44-1	1.00+0	1.98-8	6.46-1	3.02+1	.107	3647	6.39-5
0.060	.632	3.135	1.853	9.37-1	1.00+0	3.06-8	8.73-1	2.98+1	.104	3647	2.36-4
0.080	.622	3.195	1.961	9.29-1	1.00+0	4.54-8	1.117	2.94+1	.100	4019	2.19-4
0.100	.612	3.237	2.049	9.20-1	1.00+0	6.50-8	1.379	2.92+1	.097	4475	2.01-4
0.125	.602	3.277	2.145	9.09-1	1.00+0	9.84-8	1.748	2.89+1	.094	5049	1.82-4
0.150	.593	3.305	2.224	8.96-1	1.00+0	1.44-7	2.147	2.86+1	.091	5792	1.60-4
0.200	.578	3.345	2.349	8.71-1	1.00+0	2.66-7	2.988	2.80+1	.087	6790	1.37-4
0.250	.565	3.372	2.449	8.45-1	1.00+0	4.55-7	3.954	2.74+1	.084	8205	1.12-4
0.300	.554	3.392	2.534	8.15-1	1.00+0	7.46-7	5.054	2.69+1	.082	8205	1.36-4
0.350	.544	3.407	2.603	7.86-1	1.00+0	1.14-6	6.211	2.63+1	.080	10503	9.72-5
0.400	.536	3.420	2.664	7.55-1	1.00+0	1.70-6	7.469	2.57+1	.079	14588	5.94-5
0.500	.521	3.438	2.759	6.95-1	1.00+0	3.30-6	10.02	2.47+1	.078	14588	6.30-5
0.600	.509	3.451	2.835	6.33-1	1.00+0	6.02-6	12.73	2.38+1	.078	17790	4.52-5
0.700	.498	3.462	2.893	5.75-1	1.00+0	9.96-6	15.27	2.29+1	.078	22793	2.94-5
0.800	.489	3.470	2.939	5.18-1	1.00+0	1.58-5	17.69	2.21+1	.079	22793	3.00-5
1.00	.474	3.484	3.009	4.21-1	1.00+0	3.44-5	21.75	2.07+1	.082	30186	1.80-5
1.20	.461	3.469	3.057	3.40-1	1.00+0	6.69-5	24.81	1.95+1	.087	44675	8.78-6
1.40	.451	3.506	3.092	2.79-1	1.00+0	1.14-4	26.90	1.85+1	.092		
1.60	.443	3.515	3.118	2.30-1	1.00+0	1.84-4	28.24	1.76+1	.097	ΔF/F	
1.80	.435	3.524	3.139	1.93-1	1.00+0	2.78-4	29.17	1.69+1	.104	-0.87, 0.57	
2.00	.428	3.532	3.156	1.61-1	1.00+0	4.10-4	29.68	1.62+1	.111		
2.50	.415	3.552	3.191	1.12-1	9.99-1	8.78-4	30.27	1.50+1	.128	τ	C
3.00	.403	3.571	3.218	8.08-2	9.98-1	1.69-3	30.14	1.39+1	.149	.000	.790
3.50	.395	3.589	3.241	6.25-2	9.97-1	2.81-3	29.99	1.30+1	.167	.004	.807
4.00	.387	3.607	3.262	4.94-2	9.96-1	4.41-3	29.69	1.22+1	.184	.010	.820
5.00	.375	3.640	3.300	3.49-2	9.91-1	8.61-3	29.57	1.12+1	.210	.040	.859
6.00	.364	3.672	3.333	2.60-2	9.85-1	1.51-2	29.41	1.03+1	.226	.080	.891
8.00	.350	3.729	3.393	1.73-2	9.67-1	3.32-2	29.75	8.92+0	.232	.200	.941
10.0	.339	3.778	3.445	1.30-2	9.42-1	5.82-2	30.46	8.04+0	.222	.400	.972
14.0	.323	3.860	3.530	8.86-3	8.77-1	1.23-1	32.16	6.93+1	.194	.800	.989
18.0	.311	3.926	3.599	6.84-3	7.99-1	2.01-1	34.18	6.24+0	.174	1.40	.995
22.0	.302	3.980	3.655	5.68-3	7.20-1	2.80-1	36.20	6.45+0	.164	2.00	.997
26.0	.295	4.025	3.703	4.92-3	6.44-1	3.56-1	38.08	7.44+0	.160	4.00	.999
30.0	.289	4.064	3.745	4.38-3	5.74-1	4.26-1	39.86	9.19+0	.159	8.00	1.00
40.0	.278	4.142	3.827	3.54-3	4.31-1	5.69-1	43.45	1.69+1	.166	14.0	1.00
50.0	.269	4.200	3.889	3.03-3	3.30-1	6.70-1	46.15	2.94+1	.178	18.0	1.00
60.0	.262	4.246	3.936	2.68-3	2.57-1	7.43-1	48.02	4.68+1	.196		

Eff. θ = 0.500 Log G = 3.00 Flux = 5.85 + 11 N(HE)/N(H) = 0.15

τ	θ	Log PG	Log PE	H I	HE I	HE II	$(\kappa+\sigma)_{STD}$	$dp_r/d\tau$	∇_A	λ	Flux
0.000	.683	0.620	0.048	5.80-1	1.00+0	9.12-8	1.79-1	3.32+1	.103	911	4.19-6
0.001	.681	0.841	0.208	6.51-1	1.00+0	7.10-8	1.79-1	3.59+1	.094	994	5.10-6
0.002	.679	1.096	0.384	7.23-1	1.00+0	5.33-8	1.82-1	3.78+1	.086	1094	6.08-6
0.003	.677	1.251	0.492	7.58-1	1.00+0	4.66-8	1.88-1	3.86+1	.082	1215	7.09-6
0.004	.675	1.362	0.570	7.79-1	1.00+0	4.35-8	1.96-1	3.92+1	.081	1367	8.10-6
0.006	.672	1.515	0.683	8.02-1	1.00+0	4.13-8	2.13-1	3.95+1	.079	1563	9.18-6
0.008	.669	1.620	0.765	8.14-1	1.00+0	4.13-8	2.31-1	3.96+1	.078	1683	9.83-6
0.010	.666	1.698	0.830	8.21-1	1.00+0	4.25-8	2.49-1	3.94+1	.078	1823	1.06-5
0.015	.659	1.834	0.950	8.28-1	1.00+0	4.77-8	2.93-1	3.90+1	.077	1989	1.18-5
0.020	.653	1.924	1.039	8.28-1	1.00+0	5.55-8	3.39-1	3.86+1	.076	2188	1.34-5
0.025	.648	1.989	1.113	8.24-1	1.00+0	6.50-8	3.87-1	3.82+1	.076	2431	1.56-5
0.030	.644	2.040	1.170	8.21-1	1.00+0	7.43-8	4.31-1	3.79+1	.075	2735	1.88-5
0.035	.639	2.081	1.222	8.15-1	1.00+0	8.66-8	4.80-1	3.75+1	.075	3126	2.31-5
0.040	.635	2.114	1.268	8.09-1	1.00+0	1.00-7	5.30-1	3.72+1	.075	3647	2.87-5
0.060	.621	2.207	1.411	7.81-1	1.00+0	1.70-7	7.35-1	3.63+1	.073	3647	9.95-5
0.080	.609	2.266	1.517	7.51-1	1.00+0	2.71-7	9.54-1	3.54+1	.072	4019	9.41-5
0.100	.599	2.306	1.599	7.19-1	1.00+0	4.10-7	1.183	3.47+1	.072	4475	8.78-5
0.125	.588	2.345	1.684	6.78-1	1.00+0	6.59-7	1.491	3.38+1	.071	5049	8.05-5
0.150	.578	2.372	1.752	6.37-1	1.00+0	1.01-6	1.804	3.30+1	.071	5792	7.22-5
0.200	.564	2.411	1.849	5.66-1	1.00+0	1.97-6	2.370	3.15+1	.072	6790	6.26-5
0.250	.551	2.440	1.923	4.98-1	1.00+0	3.54-6	2.918	3.04+1	.073	8205	5.19-5
0.300	.541	2.462	1.980	4.33-1	1.00+0	6.04-6	3.424	2.93+1	.075	8205	6.30-5
0.350	.531	2.480	2.025	3.79-1	1.00+0	9.53-6	3.855	2.84+1	.077	10503	4.54-5
0.400	.523	2.495	2.061	3.29-1	1.00+0	1.46-5	4.221	2.75+1	.080	14588	2.81-5
0.500	.510	2.522	2.115	2.54-1	1.00+0	2.97-5	4.758	2.61+1	.087	14588	2.96-5
0.600	.498	2.544	2.158	1.97-1	1.00+0	5.58-5	5.139	2.49+1	.095	17790	2.15-5
0.700	.488	2.564	2.190	1.56-1	1.00+0	9.40-5	5.371	2.39+1	.104	22793	1.41-5
0.800	.479	2.583	2.218	1.26-1	1.00+0	1.50-4	5.536	2.30+1	.113	22793	1.44-5
1.00	.465	2.617	2.262	8.70-2	1.00+1	3.27-4	5.710	2.14+1	.134	30186	8.78-6
1.20	.453	2.648	2.300	6.32-2	9.99-1	6.23-4	5.805	2.02+1	.155	44675	4.34-6
1.40	.444	2.676	2.331	4.90-2	9.99-1	1.04-3	5.872	1.91+1	.174		
1.60	.436	2.703	2.361	3.91-2	9.98-1	1.62-3	5.928	1.82+1	.191	ΔF/F	
1.80	.429	2.728	2.388	3.22-2	9.98-1	2.37-3	5.979	1.75+1	.206	-0.38, 1.17	
2.00	.422	2.752	2.413	2.70-2	9.97-1	3.37-3	6.025	1.68+1	.218		
2.50	.409	2.805	2.468	1.91-2	9.93-1	6.69-3	6.180	1.56+1	.239	τ	C
3.00	.398	2.852	2.516	1.42-2	9.88-1	1.20-2	6.308	1.45+1	.250	.000	.785
3.50	.389	2.893	2.558	1.14-2	9.81-1	1.87-2	6.464	1.36+1	.252	.004	.802
4.00	.381	2.931	2.597	9.34-3	9.72-1	2.77-2	6.610	1.28+1	.248	.010	.818
5.00	.370	2.995	2.662	7.04-3	9.51-1	4.93-2	6.944	1.18+1	.232	.040	.865
6.00	.360	3.048	2.717	5.54-3	9.20-1	7.95-2	7.247	1.09+1	.213	.080	.900
8.00	.345	3.134	2.806	4.00-3	8.48-1	1.52-1	7.876	9.48+0	.183	.200	.948
10.0	.334	3.201	2.875	3.17-3	7.63-1	2.37-1	8.475	8.58+0	.166	.400	.974
14.0	.318	3.301	2.981	2.31-3	5.98-1	4.02-1	9.512	7.42+0	.155	.800	.989
18.0	.306	3.375	3.060	1.87-3	4.59-1	5.41-1	10.41	6.71+0	.159	1.40	.995
22.0	.298	3.434	3.122	1.60-3	3.56-1	6.44-1	11.13	6.91+0	.169	2.00	.997
26.0	.291	3.483	3.173	1.42-3	2.81-1	7.19-1	11.71	7.88+0	.182	4.00	.999
30.0	.285	3.524	3.215	1.29-3	2.26-1	7.74-1	12.20	9.63+0	.196	8.00	1.00
40.0	.273	3.602	3.296	1.08-3	1.40-1	8.60-1	13.01	1.74+1	.230	14.0	1.00
50.0	.264	3.655	3.351	9.43-4	9.32-2	9.07-1	13.38	3.00+1	.258	18.0	1.00
60.0	.257	3.689	3.385	8.38-4	6.52-2	9.35-1	13.36	4.75+1	.280		

Eff. θ = 0.500 Log G = 2.00 Flux = 5.85 + 11 N(HE)/N(H) = 0.15

τ	θ	Log PG	Log PE	H I	HE I	HE II	$(\kappa+\sigma)_{STD}$	$dp_r/d\tau$	∇_A	λ	Flux
0.000	.710	-0.345	-0.786	3.42-1	1.00+0	1.22-7	1.78-1	2.47+1	.152	*911	9.06-6
0.001	.696	-0.153	-0.590	3.37-1	1.00+0	1.76-7	1.89-1	2.64+1	.148	994	1.23-5
0.002	.686	0.078	-0.373	3.68-1	1.00+0	2.00-7	1.95-1	2.78+1	.137	1094	1.64-5
0.003	.680	0.223	-0.237	3.90-1	1.00+0	2.14-7	2.02-1	2.92+1	.130	1215	2.12-5
0.004	.675	0.328	-0.138	4.02-1	1.00+0	2.30-7	2.10-1	3.03+1	.125	1367	2.64-5
0.006	.668	0.475	-0.003	4.25-1	1.00+0	2.45-7	2.22-1	3.19+1	.116	1563	3.18-5
0.008	.665	0.580	0.091	4.47-1	1.00+0	2.47-7	2.31-1	3.32+1	.110	1683	3.46-5
0.010	.664	0.662	0.158	4.74-1	1.00+0	2.28-7	2.35-1	3.42+1	.105	1823	3.73-5
0.015	.658	0.810	0.292	5.00-1	1.00+0	2.38-7	2.56-1	3.55+1	.098	1989	4.05-5
0.020	.652	0.911	0.388	5.08-1	1.00+0	2.65-7	2.80-1	3.66+1	.094	2188	4.41-5
0.025	.647	0.986	0.463	5.06-1	1.00+0	3.04-7	3.04-1	3.72+1	.091	2431	4.85-5
0.030	.643	1.044	0.524	5.01-1	1.00+0	3.48-7	3.29-1	3.71+1	.089	2735	5.43-5
0.035	.638	1.091	0.577	4.92-1	1.00+0	4.03-7	3.55-1	3.72+1	.088	3126	6.19-5
0.040	.634	1.131	0.624	4.82-1	1.00+0	4.68-7	3.82-1	3.73+1	.088	3647	7.11-5
0.060	.619	1.241	0.759	4.33-1	1.00+0	8.20-7	4.82-1	3.69+1	.087	3647	2.39-4
0.080	.608	1.312	0.853	3.84-1	1.00+0	1.36-6	5.74-1	3.63+1	.088	4019	2.28-4
0.100	.597	1.362	0.924	3.39-1	1.00+0	2.13-6	6.59-1	3.55+1	.090	4475	2.12-4
0.125	.586	1.410	0.992	2.87-1	1.00+0	3.61-6	7.50-1	3.47+1	.095	5049	1.93-4
0.150	.577	1.447	1.045	2.44-1	1.00+0	5.73-6	8.27-1	3.38+1	.100	5792	1.71-4
0.200	.562	1.505	1.122	1.86-1	1.00+0	1.17-5	9.38-1	3.23+1	.110	6790	1.45-4
0.250	.550	1.550	1.179	1.44-1	1.00+0	2.17-5	1.019	3.11+1	.122	8205	1.17-4
0.300	.539	1.588	1.227	1.13-1	1.00+0	3.79-5	1.080	3.00+1	.135	8205	1.42-4
0.350	.530	1.621	1.265	9.12-2	1.00+0	6.04-5	1.123	2.91+1	.147	10503	1.00-4
0.400	.522	1.650	1.299	7.45-2	1.00+0	9.30-5	1.159	2.83+1	.159	14588	6.05-5
0.500	.508	1.702	1.356	5.32-2	1.00+0	1.88-4	1.212	2.70+1	.180	14588	6.39-5
0.600	.496	1.747	1.405	3.93-2	1.00+0	3.48-4	1.251	2.59+1	.198	17790	4.59-5
0.700	.486	1.787	1.447	3.07-2	9.99-1	5.78-4	1.282	2.49+1	.213	22793	2.99-5
0.800	.478	1.823	1.484	2.45-2	9.99-1	9.09-4	1.309	2.41+1	.224	22793	3.05-5
1.00	.463	1.885	1.549	1.69-2	9.98-1	1.92-3	1.356	2.27+1	.240	30186	1.84-5
1.20	.451	1.939	1.604	1.24-2	9.96-1	3.56-3	1.396	2.14+1	.250	44675	8.95-6
1.40	.441	1.986	1.651	9.78-3	9.94-1	5.79-3	1.439	2.04+1	.255		
1.60	.433	2.028	1.693	7.91-3	9.91-1	8.91-3	1.476	1.96+1	.258	ΔF/F	
1.80	.426	2.065	1.731	6.60-3	9.87-1	1.29-2	1.510	1.89+1	.257	-1.10, 0.38	
2.00	.419	2.099	1.765	5.59-3	9.82-1	1.81-2	1.543	1.82+1	.255		
2.50	.405	2.171	1.839	4.05-3	9.65-1	3.50-2	1.624	1.70+1	.246	τ	C
3.00	.394	2.231	1.900	3.07-3	9.39-1	6.11-2	1.696	1.59+1	.231	.000	.937
3.50	.385	2.282	1.952	2.51-3	9.08-1	9.24-2	1.770	1.50+1	.216	.004	.803
4.00	.377	2.326	1.997	2.09-3	8.68-1	1.32-1	1.841	1.42+1	.202	.010	.800
5.00	.364	2.399	2.073	1.60-3	7.82-1	2.18-1	1.987	1.31+1	.183	.040	.848
6.00	.354	2.457	2.135	1.28-3	6.80-1	3.20-1	2.117	1.22+1	.172	.080	.887
8.00	.339	2.548	2.231	9.51-4	4.99-1	5.01-1	2.354	1.08+1	.170	.200	.941
10.0	.327	2.617	2.305	7.71-4	3.61-1	6.39-1	2.544	9.874	.179	.400	.970
14.0	.311	2.721	2.414	5.86-4	2.00-1	8.00-1	2.803	8.736	.207	.800	.987
18.0	.299	2.800	2.495	4.91-4	1.22-1	8.78-1	2.991	8.018	.233	1.40	.994
22.0	.289	2.863	2.559	4.35-4	8.08-2	9.19-1	3.132	8.250	.251	2.00	.996
26.0	.282	2.914	2.610	3.97-4	5.70-2	9.43-1	3.238	9.278	.264	4.00	.999
30.0	.275	2.955	2.652	3.69-4	4.21-2	9.58-1	3.312	1.11+1	.273	8.00	1.00
40.0	.263	3.022	2.720	3.18-4	2.22-2	9.78-1	3.347	1.92+1	.285	14.0	1.00
50.0	.254	3.044	2.742	2.75-4	1.27-2	9.87-1	3.157	3.22+1	.289	18.0	1.00
60.0	.246	3.016	2.714	2.32-4	7.31-3	9.93-1	2.735	5.02+1	.287		

Eff. θ = 0.500 Log G = 1.00 Flux = 5.85 + 11 N(HE)/N(H) = 0.15

τ	θ	Log PG	Log PE	H I	HE I	HE II	$(\kappa+\sigma)_{STD}$	$dp_r/d\tau$	∇_A	λ	Flux
0.000	.659	-1.60	-1.932	6.21-3	1.00+1	3.70-5	2.40-1	2.02+1	.247	*911	2.30-5
0.001	.658	-1.44	-1.780	8.52-3	1.00+0	2.75-5	2.40-1	2.04+1	.245	*994	2.65-5
0.002	.657	-1.24	-1.580	1.31-2	1.00+0	1.82-5	2.40-1	2.06+1	.243	*1094	2.86-5
0.003	.657	-1.11	-1.445	1.74-2	1.00+0	1.38-5	2.40-1	2.08+1	.241	*1215	2.77-5
0.004	.656	-1.01	-1.344	2.15-2	1.00+0	1.12-5	2.41-1	2.10+1	.239	*1367	1.73-5
0.006	.655	-0.857	-1.196	2.90-2	1.00+0	8.50-6	2.41-1	2.14+1	.235	*1563	2.60-5
0.008	.654	-0.748	-1.089	3.56-2	1.00+0	7.04-6	2.42-1	2.18+1	.231	*1683	3.14-5
0.010	.653	-0.663	-1.005	4.15-2	1.00+0	6.15-6	2.42-1	2.21+1	.228	1823	3.75-1
0.015	.651	-0.508	-0.853	5.33-2	1.00+0	5.03-6	2.44-1	2.29+1	.222	1989	4.44-5
0.020	.648	-0.400	-0.748	6.19-2	1.00+0	4.57-6	2.46-1	2.35+1	.218	2188	5.22-5
0.025	.646	-0.317	-0.667	6.80-2	1.00+0	4.39-6	2.48-1	2.41+1	.215	2431	6.06-5
0.030	.644	-0.251	-0.602	7.22-2	1.00+0	4.38-6	2.50-1	2.45+1	.212	2735	6.97-5
0.035	.641	-0.196	-0.548	7.50-2	1.00+0	4.47-6	2.53-1	2.49+1	.211	3126	7.93-5
0.040	.639	-0.150	-0.502	7.66-2	1.00+0	4.63-6	2.56-1	2.52+1	.210	3647	8.88-5
0.060	.630	-0.018	-0.369	7.60-2	1.00+0	5.84-6	2.65-1	2.60+1	.208	3647	1.68-4
0.080	.622	0.071	-0.279	7.04-2	1.00+0	7.82-6	2.74-1	2.64+1	.210	4019	1.70-4
0.100	.614	0.136	-0.212	6.32-2	1.00+0	1.06-5	2.82-1	2.66+1	.213	4475	1.69-4
0.125	.605	0.198	-0.148	5.43-2	1.00+0	1.56-5	2.89-1	2.66+1	.217	5049	1.63-4
0.150	.598	0.247	-0.097	4.68-2	1.00+0	2.22-5	2.96-1	2.65+1	.221	5792	1.53-4
0.200	.585	0.328	-0.014	3.63-2	1.00+0	4.01-5	3.06-1	2.56+1	.227	6790	1.37-4
0.250	.573	0.392	0.053	2.86-2	1.00+0	6.84-5	3.14-1	2.54+1	.232	8205	1.15-4
0.300	.563	0.443	0.105	2.25-2	1.00+0	1.23-4	3.20-1	2.53+1	.236	8205	1.21-4
0.350	.554	0.486	0.149	1.82-2	1.00+0	1.75-4	3.25-1	2.52+1	.240	10503	9.21-5
0.400	.546	0.523	0.186	1.49-2	1.00+0	2.66-4	3.28-1	2.51+1	.242	14588	5.90-5
0.500	.532	0.586	0.251	1.04-2	1.00+0	5.44-4	3.34-1	2.49+1	.246	14588	5.98-5
0.600	.520	0.639	0.305	7.56-3	9.99-1	1.04-3	3.38-1	2.46+1	.248	17790	4.43-5
0.700	.509	0.686	0.352	5.76-3	9.98-1	1.79-3	3.42-1	2.43+1	.250	22793	2.96-5
0.800	.499	0.729	0.395	4.49-3	9.97-1	2.94-3	3.45-1	2.40+1	.250	22793	2.98-5
1.00	.483	0.804	0.471	2.96-3	9.93-1	6.77-3	3.51-1	2.34+1	.251	30186	1.84-5
1.20	.469	0.869	0.536	2.09-3	9.86-1	1.37-2	3.56-1	2.29+1	.250	44675	9.07-6
1.40	.457	0.927	0.595	1.58-3	9.76-1	2.41-2	3.62-1	2.24+1	.248		
1.60	.447	0.978	0.646	1.24-3	9.60-1	3.98-2	3.68-1	2.19+1	.245	ΔF/F	
1.80	.438	1.023	0.692	1.00-3	9.39-1	6.06-2	3.74-1	2.15+1	.241	-1.71, 2.75	
2.00	.430	1.064	0.734	8.28-4	9.11-1	8.88-2	3.81-1	2.11+1	.236		
2.50	.414	1.148	0.821	5.69-4	8.18-1	1.82-1	3.97-1	2.04+1	.224	τ	C
3.00	.400	1.213	0.891	4.12-4	6.85-1	3.15-1	4.14-1	1.97+1	.216	.000	.728
3.50	.389	1.266	0.949	3.25-4	5.52-1	4.48-1	4.31-1	1.91+1	.213	.004	.730
4.00	.379	1.311	0.996	2.62-4	4.23-1	5.77-1	4.44-1	1.86+1	.215	.010	.737
5.00	.363	1.382	1.073	1.94-4	2.49-1	7.51-1	4.64-1	1.81+1	.225	.040	.767
6.00	.350	1.440	1.134	1.53-4	1.43-1	8.57-1	4.75-1	1.75+1	.236	.080	.799
8.00	.331	1.543	1.240	1.16-4	5.76-2	9.42-1	4.91-1	1.65+1	.247	.200	.867
10.0	.316	1.632	1.330	9.89-5	2.86-2	9.71-1	5.04-1	1.57+1	.252	.400	.925
14.0	.295	1.775	1.473	8.47-5	1.03-2	9.90-1	5.29-1	1.47+1	.255	.800	.966
18.0	.280	1.885	1.584	7.87-5	4.94-3	9.95-1	5.50-1	1.38+1	.256	1.40	.985
22.0	.268	1.977	1.675	7.60-5	2.85-3	9.97-1	5.70-1	1.29+1	.256	2.00	.992
26.0	.258	2.056	1.754	7.46-5	1.85-3	9.98-1	5.91-1	1.21+1	.257	4.00	.998
30.0	.250	2.126	1.824	7.42-5	1.31-3	9.99-1	6.11-1	1.13+1	.257	8.00	1.001
40.0	.235	2.273	1.972	7.47-5	6.90-4	9.99-1	6.62-1	9.354	.258	14.0	1.001
50.0	.224	2.396	2.094	7.62-5	4.52-4	9.99-1	7.16-1	7.504	.258	18.0	1.001
60.0	.215	2.501	2.200	7.82-5	3.36-4	9.99-1	7.72-1	5.706	.259		

Eff. θ = 0.565 Log G = 4.00 Flux = 3.59 + 11 N(HE)/N(H) = 0.15

τ	θ	Log PG	Log PE	H I	HE I	HE II	$(\kappa+\sigma)_{STD}$	$dp_r/d\tau$	∇_A	λ	Flux
0.000	.734	2.066	0.559	9.63-1	1.00+0		6.99-2	2.38+1	.118	911	7.64-6
0.001	.733	2.263	0.669	9.70-1	1.00+0		7.86-2	2.22+1	.128	994	8.80-6
0.002	.732	2.479	0.788	9.76-1	1.00+0		9.11-2	2.10+1	.142	1094	9.92-6
0.003	.731	2.608	0.860	9.79-1	1.00+0		1.01-1	2.01+1	.150	1215	1.11-5
0.004	.730	2.699	0.913	9.81-1	1.00+0		1.09-1	1.94+1	.157	1367	1.22-5
0.006	.728	2.828	0.990	9.83-1	1.00+0		1.24-1	1.85+1	.166	1563	1.35-5
0.008	.727	2.917	1.046	9.85-1	1.00+0		1.36-1	1.78+1	.172	1683	1.44-5
0.010	.726	2.986	1.091	9.86-1	1.00+0		1.47-1	1.74+1	.177	1823	1.55-5
0.015	.723	3.108	1.177	9.87-1	1.00+0		1.71-1	1.68+1	.184	1989	1.74-5
0.020	.719	3.192	1.242	9.87-1	1.00+0		1.93-1	1.63+1	.188	2188	2.00-5
0.025	.717	3.256	1.296	9.88-1	1.00+0		2.14-1	1.59+1	.191	2431	2.34-5
0.030	.714	3.307	1.341	9.88-1	1.00+0		2.32-1	1.58+1	.192	2735	2.82-5
0.035	.711	3.349	1.381	9.88-1	1.00+0		2.51-1	1.57+1	.193	3126	3.47-5
0.040	.709	3.385	1.418	9.88-1	1.00+0		2.70-1	1.55+1	.194	3647	4.32-5
0.060	.700	3.489	1.539	9.87-1	1.00+0		3.41-1	1.52+1	.193	3647	1.50-4
0.080	.692	3.558	1.635	9.86-1	1.00+0		4.12-1	1.52+1	.190	4019	1.44-4
0.100	.684	3.609	1.717	9.85-1	1.00+0		4.85-1	1.51+1	.186	4475	1.37-4
0.125	.675	3.656	1.807	9.84-1	1.00+0		5.82-1	1.51+1	.180	5049	1.29-4
0.150	.667	3.693	1.887	9.82-1	1.00+0		6.86-1	1.52+1	.174	5792	1.19-4
0.200	.653	3.746	2.022	9.78-1	1.00+0		9.10-1	1.54+1	.162	6790	1.06-4
0.250	.639	3.782	2.137	9.74-1	1.00+0	1.02-8	1.169	1.56+1	.152	8205	9.12-5
0.300	.628	3.808	2.240	9.68-1	1.00+0	1.67-8	1.472	1.58+1	.142	8205	1.06-4
0.350	.617	3.829	2.329	9.63-1	1.00+0	2.60-8	1.812	1.59+1	.134	10503	8.14-5
0.400	.607	3.844	2.412	9.56-1	1.00+0	3.95-8	2.206	1.60+1	.127	14588	5.60-5
0.500	.589	3.867	2.551	9.42-1	1.00+0	8.23-8	3.121	1.61+1	.116	14588	5.60-5
0.600	.574	3.883	2.669	9.25-1	1.00+0	1.59-7	4.270	1.61+1	.107	17790	4.08-5
0.700	.561	3.895	2.769	9.07-1	1.00+0	2.81-7	5.606	1.59+1	.101	22793	2.72-5
0.800	.549	3.903	2.856	8.87-1	1.00+0	4.70-7	7.181	1.57+1	.096	22793	2.72-5
1.00	.530	3.915	2.995	8.43-1	1.00+0	1.12-6	10.85	1.52+1	.089	30186	1.65-5
1.20	.514	3.923	3.103	7.95-1	1.00+0	2.35-6	15.20	1.46+1	.086	44675	8.05-6
1.40	.501	3.929	3.185	7.47-1	1.00+0	4.23-6	19.71	1.40+1	.084		
1.60	.490	3.933	3.252	6.97-1	1.00+0	7.19-6	24.50	1.34+1	.083	ΔF/F	
1.80	.481	3.937	3.305	6.50-1	1.00+0	1.13-5	29.15	1.29+1	.083	-0.42, +0.62	
2.00	.472	3.940	3.351	6.01-1	1.00+0	1.72-5	33.85	1.25+1	.083		
2.50	.455	3.946	3.430	4.96-1	1.00+0	4.05-5	43.75	1.16+1	.085	τ	C
3.00	.441	3.951	3.486	3.99-1	1.00+0	8.56-5	51.90	1.09+1	.089	.000	.762
3.50	.431	3.955	3.523	3.26-1	1.00+0	1.54-4	57.32	1.02+1	.093	.004	.787
4.00	.421	3.959	3.549	2.65-1	1.00+0	2.64-4	60.82	9.64+0	.099	.010	.804
5.00	.407	3.966	3.582	1.87-1	9.99-1	5.95-4	63.82	8.84+0	.111	.040	.843
6.00	.395	3.973	3.606	1.34-1	9.99-1	1.20-3	64.35	8.14+0	.126	.080	.871
8.00	.378	3.987	3.634	8.02-2	9.97-1	3.29-3	62.39	7.03+0	.157	.200	.919
10.0	.365	4.000	3.655	5.39-2	9.93-1	6.97-3	59.97	6.31+0	.185	.400	.957
14.0	.347	4.028	3.689	3.07-2	9.80-1	1.96-2	56.41	5.36+0	.219	.800	.984
18.0	.335	4.056	3.720	2.08-2	9.60-1	4.00-2	54.49	4.77+0	.225	1.40	.994
22.0	.325	4.083	3.749	1.56-2	9.32-1	6.76-2	53.29	4.91+0	.216	2.00	.997
26.0	.317	4.108	3.776	1.26-2	8.99-1	1.01-1	53.10	5.66+0	.203	4.00	.999
30.0	.311	4.132	3.802	1.05-2	8.62-1	1.38-1	53.31	7.03+0	.191	8.00	1.00
40.0	.298	4.185	3.859	7.60-3	7.58-1	2.42-1	54.64	1.31+1	.170	14.0	1.00
50.0	.289	4.229	3.907	6.07-3	6.55-1	3.45-1	56.42	2.31+1	.162	18.0	1.00
60.0	.281	4.265	3.945	5.10-3	5.60-1	4.40-1	57.92	3.69+1	.162		

Eff. θ = 0.600 Log G = 4.44 Flux = 2.82 + 11 N(HE)/N(H) = 0.15

τ	θ	Log PG	Log PE	H I	HE I	HE II	$(\kappa+\sigma)_{STD}$	$dp_r/d\tau$	∇_A	λ	Flux
0.000	.783	2.758	0.556	9.93-1	1.00+0		5.08-2	1.42+1	.223	911	4.92-6
0.001	.783	2.916	0.636	9.94-1	1.00+0		5.89-2	1.31+1	.237	994	5.67-6
0.002	.783	3.096	0.728	9.95-1	1.00+0		7.04-2	1.23+1	.254	1094	6.43-6
0.003	.782	3.209	0.787	9.96-1	1.00+0		7.90-2	1.18+1	.263	1215	7.33-6
0.004	.782	3.290	0.830	9.96-1	1.00+0		8.62-2	1.14+1	.270	1367	8.33-6
0.006	.781	3.406	0.895	9.97-1	1.00+0		9.85-2	1.10+1	.279	1563	9.68-6
0.008	.780	3.488	0.944	9.97-1	1.00+0		1.09-1	1.06+1	.284	1683	1.06-5
0.010	.779	3.552	0.985	9.97-1	1.00+0		1.18-1	1.04+1	.288	1823	1.18-5
0.015	.776	3.666	1.063	9.97-1	1.00+0		1.39-1	1.02+1	.294	1989	1.38-5
0.020	.774	3.746	1.124	9.97-1	1.00+0		1.57-1	9.92+1	.297	2188	1.63-5
0.025	.771	3.806	1.174	9.97-1	1.00+0		1.73-1	9.74+0	.299	2431	1.97-5
0.030	.768	3.855	1.218	9.98-1	1.00+0		1.89-1	9.71+0	.301	2735	2.42-5
0.035	.766	3.896	1.257	9.98-1	1.00+0		2.04-1	9.62+0	.301	3126	3.01-5
0.040	.763	3.931	1.293	9.98-1	1.00+0		2.19-1	9.55+0	.302	3647	3.76-5
0.060	.754	4.032	1.411	9.97-1	1.00+0		2.74-1	9.42+0	.301	3647	9.96-5
0.080	.746	4.100	1.505	9.97-1	1.00+0		3.29-1	9.38+0	.298	4019	9.93-5
0.100	.739	4.150	1.586	9.97-1	1.00+0		3.83-1	9.38+0	.295	4475	9.86-5
0.125	.730	4.198	1.676	9.97-1	1.00+0		4.53-1	9.39+0	.290	5049	9.73-5
0.150	.722	4.236	1.755	9.96-1	1.00+0		5.25-1	9.42+0	.286	5792	9.42-5
0.200	.708	4.291	1.888	9.96-1	1.00+0		6.72-1	9.51+0	.276	6790	8.84-5
0.250	.695	4.330	2.002	9.95-1	1.00+0		8.32-1	9.65+0	.266	8205	7.94-5
0.300	.683	4.360	2.104	9.94-1	1.00+0		1.008	9.80+0	.255	8205	8.63-5
0.350	.673	4.383	2.194	9.93-1	1.00+0		1.195	9.95+0	.245	10503	7.11-5
0.400	.663	4.401	2.278	9.92-1	1.00+0		1.403	1.01+1	.236	14588	5.03-5
0.500	.645	4.430	2.423	9.89-1	1.00+0		1.862	1.04+1	.218	14588	5.24-5
0.600	.630	4.450	2.553	9.86-1	1.00+0		2.414	1.06+1	.201	17790	3.90-5
0.700	.616	4.466	2.665	9.82-1	1.00+0	1.28-8	3.049	1.08+1	.186	22793	2.55-5
0.800	.603	4.478	2.768	9.77-1	1.00+0	2.2108	3.799	1.10+1	.173	22793	2.58-5
1.00	.581	4.494	2.943	9.67-1	1.00+0	5.72-8	5.638	1.12+1	.152	30186	1.56-5
1.20	.562	4.506	3.090	9.54-1	1.00+0	1.30-7	8.022	1.13+1	.135	44675	7.58-6
1.40	.546	4.514	3.210	9.40-1	1.00+0	2.56-7	10.87	1.12+1	.124		
1.60	.532	4.519	3.312	9.24-1	1.00+0	4.69-7	14.27	1.10+1	.115	ΔF/F	
1.80	.521	4.524	3.399	9.07-1	1.00+0	7.86-7	18.11	1.08+1	.109	-1.38, 0.48	
2.00	.510	4.527	3.477	8.88-1	1.00+0	1.26-6	22.59	1.06+1	.104		
2.50	.489	4.534	3.623	8.40-1	1.00+0	3.24-6	34.81	1.01+1	.097	τ	C
3.00	.472	4.538	3.737	7.83-1	1.00+0	7.27-6	49.78	9.58+0	.092	.000	.808
3.50	.459	4.541	3.820	7.30-1	1.00+0	1.35-5	64.65	9.06+0	.091	.004	.822
4.00	.447	4.543	3.887	6.74-1	1.00+0	2.38-5	80.49	8.59+0	.090	.010	.832
5.00	.430	4.547	3.976	5.77-1	1.00+0	5.51-5	107.4	7.93+0	.090	.040	.853
6.00	.416	4.549	4.040	4.84-1	1.00+0	1.14-4	131.7	7.33+0	.093	.080	.870
8.00	.397	4.554	4.113	3.47-1	1.00+0	3.32-4	162.1	6.32+0	.100	.200	.905
10.0	.382	4.557	4.152	2.54-1	9.99-1	7.45-4	176.4	5.66+0	.110	.400	.939
14.0	.363	4.564	4.192	1.52-1	9.98-1	2.34-3	182.2	4.81+0	.132	.800	.974
18.0	.349	4.571	4.213	1.01-1	9.95-1	5.31-3	177.9	4.22+0	.155	1.40	.991
22.0	.339	4.578	4.228	7.28-2	9.90-1	9.81-3	172.0	3.62+0	.176	2.00	.995
26.0	.331	4.586	4.240	5.59-2	9.84-1	1.60-2	166.3	3.06+0	.193	4.00	.998
30.0	.324	4.593	4.250	4.48-2	9.76-1	2.40-2	160.3	2.53+0	.204	8.00	1.00
40.0	.311	4.612	4.275	2.95-2	9.49-1	5.12-2	151.8	1.32+0	.214	14.0	1.00
50.0	.301	4.631	4.296	2.18-2	9.13-1	8.73-2	146.7	1.97-1	.207	18.0	1.00
60.0	.294	4.650	4.318	1.74-2	8.70-1	1.30-1	144.3	0.00	.196		

Eff. θ = 0.600 Log G = 4.00 Flux = 2.82 + 11 N(HE)/N(H) = 0.15

τ	θ	Log PG	Log PE	H I	HE I	HE II	$(\kappa+\sigma)_{STD}$	$dp_r/d\tau$	∇_A	λ	Flux
0.000	.782	2.407	0.383	9.89-1	1.00+1	1.1-10	3.82-2	1.60+1	.193	911	4.68-6
0.001	.781	2.575	0.474	9.91-1	1.00+0	9.4-11	4.42-2	1.47+1	.208	994	5.42-6
0.002	.780	2.765	0.575	9.93-1	1.00+0	7.8-11	5.27-2	1.38+1	.226	1094	6.16-6
0.003	.780	2.881	0.638	9.94-1	1.00+0	6.9-11	5.92-2	1.32+1	.237	1215	6.97-6
0.004	.779	2.965	0.685	9.94-1	1.00+0	6.4-11	6.46-2	1.27+1	.245	1367	7.84-6
0.006	.778	3.083	0.754	9.95-1	1.00+0	5.9-11	7.38-2	1.21+1	.255	1563	8.96-6
0.008	.777	3.167	0.806	9.95-1	1.00+0	5.7-11	8.17-2	1.18+1	.262	1683	9.75-6
0.010	.776	3.231	0.848	9.95-1	1.00+0	5.6-11	8.88-2	1.15+1	.266	1823	1.08-5
0.015	.772	3.346	0.930	9.96-1	1.00+0	5.5-11	1.04-1	1.12+1	.273	1989	1.26-5
0.020	.769	3.427	0.993	9.96-1	1.00+0	5.7-11	1.18-1	1.09+1	.277	2188	1.49-5
0.025	.767	3.487	1.044	9.96-1	1.00+0	6.0-11	1.30-1	1.06+1	.280	2431	1.80-5
0.030	.764	3.536	1.089	9.96-1	1.00+0	6.4-11	1.42-1	1.06+1	.281	2735	2.23-5
0.035	.765	3.577	1.129	9.96-1	1.00+0	6.8-11	1.54-1	1.05+1	.282	3126	2.80-5
0.040	.759	3.612	1.166	9.96-1	1.00+0	7.3-11	1.65-1	1.04+1	.282	3647	3.53-5
0.060	.749	3.713	1.286	9.96-1	1.00+0	9.8-11	2.09-1	1.03+1	.280	3647	1.09-4
0.080	.741	3.781	1.383	9.96-1	1.00+0	1.3-10	2.51-1	1.02+1	.276	4019	1.07-4
0.100	.733	3.831	1.466	9.95-1	1.00+0	1.7-10	2.94-1	1.02+1	.272	4475	1.05-4
0.125	.724	3.879	1.557	9.95-1	1.00+0	2.4-10	3.50-1	1.02+1	.266	5049	1.02-4
0.150	.716	3.915	1.638	9.94-1	1.00+0	3.3-10	4.08-1	1.03+1	.259	5792	9.73-5
0.200	.701	3.968	1.773	9.93-1	1.00+0	5.8-10	5.28-1	1.04+1	.246	6790	9.02-5
0.250	.688	4.006	1.890	9.91-1	1.00+0	9.7-10	6.62-1	1.06+1	.233	8205	8.01-5
0.300	.676	4.034	1.995	9.90-1	1.00+0	1.58-9	8.12-1	1.08+1	.220	8205	8.92-5
0.350	.665	4.056	2.087	9.88-1	1.00+0	2.46-9	9.77-1	1.10+1	.208	10503	7.22-5
0.400	.655	4.074	2.173	9.86-1	1.00+0	3.75-9	1.162	1.12+1	.198	14588	4.99-5
0.500	.637	4.100	2.321	9.81-1	1.00+0	7.94-9	1.586	1.15+1	.178	14588	5.24-5
0.600	.620	4.118	2.452	9.75-1	1.00+0	1.58-8	2.112	1.18+1	.162	17790	3.88-5
0.700	.606	4.132	2.566	9.68-1	1.00+0	2.88-8	2.735	1.19+1	.148	22793	2.54-5
0.800	.593	4.142	2.667	9.60-1	1.00+0	5.03-8	3.482	1.20+1	.137	22793	2.58-5
1.00	.571	4.156	2.838	9.42-1	1.00+0	1.31-7	5.348	1.21+1	.120	30186	1.56-5
1.20	.552	4.166	2.978	9.20-1	1.00+0	2.97-7	7.784	1.20+1	.109	44675	7.60-6
1.40	.573	4.172	3.089	8.97-1	1.00+0	5.80-7	10.64	1.17+1	.101		
1.60	.524	4.177	3.183	8.70-1	1.00+0	1.04-6	14.00	1.14+1	.096	ΔF/F	
1.80	.513	4.180	3.260	8.43-1	1.00+0	1.73-6	17.70	1.11+1	.092	-1.19, 0.60	
2.00	.503	4.183	3.329	8.13-1	1.00+0	2.76-6	21.90	1.08+1	.090		
2.50	.483	4.188	3.455	7.40-1	1.00+0	6.94-6	32.67	1.02+1	.087	τ	C
3.00	.467	4.192	3.550	6.60-1	1.00+0	1.55-5	44.73	9.64+0	.086	.000	.809
3.50	.454	4.194	3.617	5.87-1	1.00+0	2.92-5	55.64	9.00+0	.086	.004	.823
4.00	.443	4.197	3.668	5.15-1	1.00+0	5.17-5	65.91	8.44+0	.087	.010	.832
5.00	.427	4.200	3.730	4.08-1	1.00+0	1.18-4	79.82	7.76+0	.091	.040	.854
6.00	.414	4.203	3.774	3.19-1	1.00+0	2.42-4	89.73	7.18+0	.097	.080	.872
8.00	.395	4.208	3.821	2.01-1	9.99-1	7.41-4	97.80	6.29+0	.112	.200	.908
10.0	.381	4.214	3.845	1.38-1	9.98-1	1.65-3	98.24	5.64+0	.130	.400	.944
14.0	.361	4.224	3.873	7.50-2	9.95-1	5.39-3	93.49	4.79+0	.167	.800	.978
18.0	.348	4.235	3.890	4.90-2	9.88-1	1.18-2	88.46	4.14+0	.196	1.40	.993
22.0	.338	4.246	3.906	3.52-2	9.78-1	2.17-2	84.47	3.48+0	.214	2.00	.996
26.0	.330	4.257	3.919	2.70-2	9.65-1	3.48-2	81.45	2.85+0	.220	4.00	.998
30.0	.323	4.269	3.933	2.19-2	9.49-1	5.09-2	78.95	2.25+0	.219	8.00	1.00
40.0	.310	4.298	3.965	1.48-2	8.98-1	1.02-1	76.18	8.36-1	.203	14.0	1.00
50.0	.301	4.326	3.996	1.12-2	8.36-1	1.64-1	75.36	0.00	.186	18.0	1.00
60.0	.293	4.352	4.025	9.17-3	7.71-1	2.29-1	75.67	0.00	.174		

Eff. θ = 0.600 Log G = 3.00 Flux = 2.82 + 11 N(HE)/N(H) = 0.15

τ	θ	Log PG	Log PE	H I	HE I	HE II	$(\kappa+\sigma)_{STD}$	$dp_r/d\tau$	∇_A	λ	Flux
0.000	.786	1.586	-0.069	9.74-1	1.00+0		2.32-2	1.89+1	.139	911	3.90-6
0.001	.784	1.771	0.041	9.78-1	1.00+0		2.53-2	1.81+1	.146	994	4.66-6
0.002	.782	1.982	0.163	9.83-1	1.00+0		2.87-2	1.73+1	.157	1094	5.39-6
0.003	.781	2.111	0.239	9.85-1	1.00+0		3.16-2	1.67+1	.165	1215	6.09-6
0.004	.780	2.203	0.296	9.86-1	1.00+0		3.42-2	1.61+1	.170	1367	6.73-6
0.006	.777	2.331	0.378	9.87-1	1.00+0		3.88-2	1.54+1	.178	1563	7.47-6
0.008	.775	2.420	0.439	9.88-1	1.00+0		4.28-2	1.49+1	.183	1683	7.97-6
0.010	.773	2.489	0.488	9.89-1	1.00+0		4.65-2	1.46+1	.187	1823	8.66-6
0.015	.769	2.610	0.581	9.89-1	1.00+0		5.47-2	1.41+1	.193	1989	1.02-5
0.020	.765	2.692	0.653	9.90-1	1.00+0		6.23-2	1.37+1	.196	2188	1.21-5
0.025	.761	2.755	0.712	9.90-1	1.00+0		6.95-2	1.34+1	.197	2431	1.48-5
0.030	.758	2.804	0.760	9.90-1	1.00+0		7.60-2	1.33+1	.198	2735	1.85-5
0.035	.755	2.845	0.804	9.90-1	1.00+0		8.27-2	1.31+1	.198	3126	2.38-5
0.040	.752	2.880	0.844	9.90-1	1.00+0		8.93-2	1.30+1	.197	3647	3.10-5
0.060	.741	2.980	0.976	9.89-1	1.00+0		1.15-1	1.28+1	.194	3647	1.28-4
0.080	.731	3.046	1.082	9.88-1	1.00+0		1.42-1	1.28+1	.188	4019	1.23-4
0.100	.722	3.093	1.171	9.86-1	1.00+0		1.70-1	1.28+1	.182	4475	1.17-4
0.125	.712	3.137	1.270	9.84-1	1.00+0		2.08-1	1.29+1	.174	5049	1.11-4
0.150	.703	3.171	1.357	9.82-1	1.00+0		2.49-1	1.30+1	.167	5792	1.03-4
0.200	.686	3.219	1.503	9.78-1	1.00+0		3.40-1	1.32+1	.154	6790	9.30-5
0.250	.672	3.251	1.627	9.72-1	1.00+0		4.48-1	1.34+1	.142	8205	8.05-5
0.300	.658	3.274	1.737	9.66-1	1.00+0		5.78-1	1.36+1	.131	8205	9.57-5
0.350	.646	3.292	1.832	9.59-1	1.00+0	1.35-8	7.27-1	1.37+1	.122	10503	7.40-5
0.400	.636	3.305	1.918	9.51-1	1.00+0	2.15-8	9.02-1	1.38+1	.115	14588	4.89-5
0.500	.617	3.324	2.063	9.34-1	1.00+0	4.76-8	1.317	1.38+1	.104	14588	5.20-5
0.600	.600	3.337	2.188	9.12-1	1.00+0	9.73-8	1.855	1.38+1	.096	17790	3.81-5
0.700	.587	3.346	2.290	8.90-1	1.00+0	1.79-7	2.491	1.38+1	.090	22793	2.50-5
0.800	.574	3.352	2.379	8.63-1	1.00+0	3.15-7	3.259	1.37+1	.086	22793	2.55-5
1.00	.552	3.361	2.525	8.03-1	1.00+0	8.39-7	5.147	1.31+1	.081	30186	1.55-5
1.20	.535	3.367	2.632	7.40-1	1.00+0	1.85-6	7.293	1.25+1	.078	44675	7.57-6
1.40	.523	3.371	2.705	6.83-1	1.00+0	3.34-6	9.288	1.18+1	.077		
1.60	.511	3.374	2.769	6.20-1	1.00+0	5.92-6	11.49	1.15+1	.077	ΔF/F	
1.80	.501	3.376	2.818	5.60-1	1.00+0	9.82-6	13.59	1.12+1	.078	-1.05, 0.78	
2.00	.492	3.379	2.860	5.00-1	1.00+0	1.57-5	15.59	1.09+1	.079		
2.50	.474	3.383	2.928	3.79-1	1.00+0	4.06-5	19.28	1.02+1	.083	τ	C
3.00	.459	3.386	2.971	2.80-1	1.00+0	9.32-5	21.66	9.56+0	.090	.000	.811
3.50	.448	3.389	2.997	2.13-1	1.00+0	1.79-4	22.75	9.00+0	.098	.004	.825
4.00	.437	3.392	3.017	1.63-1	1.00+0	3.23-4	23.20	8.50+0	.108	.010	.834
5.00	.422	3.399	3.039	1.05-1	9.99-1	7.87-4	22.93	7.83+0	.130	.040	.857
6.00	.410	3.405	3.055	7.06-2	9.98-1	1.68-3	22.10	7.24+0	.155	.080	.878
8.00	.391	3.418	3.077	3.91-2	9.95-1	5.00-3	20.53	6.28+0	.200	.200	.918
10.0	.378	3.433	3.095	2.51-2	9.89-1	1.11-2	19.29	5.66+0	.227	.400	.957
14.0	.359	3.463	3.128	1.37-2	9.67-1	3.29-2	17.89	4.85+0	.238	.800	.986
18.0	.346	3.493	3.161	9.10-3	9.31-1	6.88-2	17.25	4.28+0	.218	1.40	.996
22.0	.336	3.523	3.193	6.79-3	8.84-1	1.16-1	17.08	3.70+0	.195	2.00	.997
26.0	.328	3.551	3.222	5.43-3	8.30-1	1.70-1	17.14	3.16+0	.178	4.00	.999
30.0	.321	3.577	3.251	4.56-3	7.70-1	2.30-1	17.27	2.66+0	.167	8.00	1.00
40.0	.308	3.636	3.315	3.33-3	6.25-1	3.75-1	18.07	1.48+0	.156	14.0	1.00
50.0	.298	3.686	3.369	2.68-3	5.00-1	5.00-1	18.93	3.99-1	.157	18.0	1.00
60.0	.290	3.730	3.416	2.30-3	4.02-1	5.98-1	19.75	0.00	.165		

Eff. θ = 0.600 Log G = 2.0 Flux = 2.82 + 11 N(HE)/N(H) = 0.15

τ	θ	Log PG	Log PE	H I	HE I	HE II	$(\kappa+\sigma)_{STD}$	$dp_r/d\tau$	∇_A	λ	Flux
0.000	.790	0.315	-0.767	8.97-1	1.00+0		3.27-2	1.45+1	.142	911	2.46-6
0.001	.789	0.572	-0.622	9.22-1	1.00+0		2.78-2	1.60+1	.136	994	3.27-6
0.002	.788	0.883	-0.448	9.44-1	1.00+0		2.41-2	1.70+1	.130	1094	4.16-6
0.003	.786	1.074	-0.336	9.54-1	1.00+0		2.33-2	1.75+1	.129	1215	5.07-6
0.004	.785	1.207	-0.255	9.59-1	1.00+0		2.34-2	1.78+1	.128	1367	5.87-6
0.006	.782	1.388	-0.138	9.65-1	1.00+0		2.45-2	1.79+1	.129	1563	6.58-6
0.008	.779	1.510	-0.055	9.68-1	1.00+0		2.61-2	1.78+1	.130	1683	6.99-6
0.010	.776	1.599	0.011	9.70-1	1.00+0		2.77-2	1.76+1	.131	1823	7.52-6
0.015	.770	1.751	0.131	9.72-1	1.00+0		3.20-2	1.73+1	.133	1989	8.83-6
0.020	.765	1.851	0.222	9.73-1	1.00+0		3.64-2	1.70+1	.133	2188	1.05-5
0.025	.760	1.924	0.295	9.73-1	1.00+0		4.09-2	1.67+1	.133	2431	1.28-5
0.030	.756	1.980	0.354	9.72-1	1.00+0		4.51-2	1.66+1	.132	2735	1.63-5
0.035	.752	2.025	0.408	9.72-1	1.00+0		4.96-2	1.65+1	.131	3126	2.14-5
0.040	.748	2.062	0.457	9.71-1	1.00+0		5.42-2	1.64+1	.130	3647	2.85-5
0.060	.734	2.167	0.612	9.67-1	1.00+0		7.34-2	1.62+1	.124	3647	1.43-4
0.080	.722	2.232	0.733	9.63-1	1.00+0		9.47-2	1.61+1	.118	4019	1.36-4
0.100	.711	2.277	0.834	9.57-1	1.00+0		1.18-1	1.61+1	.112	4475	1.28-4
0.125	.699	2.317	0.942	9.50-1	1.00+0		1.52-1	1.61+1	.106	5049	1.18-4
0.150	.688	2.346	1.036	9.41-1	1.00+0		1.91-1	1.60+1	.100	5792	1.08-4
0.200	.670	2.385	1.182	9.23-1	1.00+0	1.44-8	2.78-1	1.59+1	.092	6790	9.50-5
0.250	.655	2.410	1.302	9.03-1	1.00+0	2.75-8	3.86-1	1.58+1	.086	8205	8.05-5
0.300	.641	2.427	1.405	8.80-1	1.00+0	4.94-8	5.18-1	1.57+1	.082	8205	1.01-4
0.350	.630	2.439	1.491	8.55-1	1.00+0	8.23-8	6.67-1	1.56+1	.079	10503	7.52-5
0.400	.619	2.449	1.565	8.27-1	1.00+0	1.33-7	8.39-1	1.55+1	.076	14588	4.79-5
0.500	.601	2.461	1.684	7.70-1	1.00+0	2.99-7	1.223	1.51+1	.073	14588	5.13-5
0.600	.585	2.470	1.780	7.05-1	1.00+0	6.20-7	1.676	1.48+1	.072	17790	3.74-5
0.700	.572	2.475	1.852	6.40-1	1.00+0	1.16-6	2.139	1.45+1	.071	22793	2.46-5
0.800	.561	2.479	1.911	5.74-1	1.00+0	2.05-6	2.613	1.41+1	.072	22793	2.52-5
1.00	.542	2.485	1.994	4.51-1	1.00+0	5.46-6	3.454	1.35+1	.074	30186	1.53-5
1.20	.526	2.488	2.047	3.45-1	1.00+0	1.27-5	4.087	1.29+1	.079	44675	7.53-6
1.40	.513	2.491	2.082	2.67-1	1.00+0	2.52-5	4.479	1.24+1	.085		
1.60	.503	2.494	2.105	2.05-1	1.00+0	4.68-5	4.688	1.19+1	.093	ΔF/F	
1.80	.493	2.497	2.122	1.60-1	1.00+0	8.02-5	4.785	1.15+1	.103	-0.80, 0.89	
2.00	.485	2.499	2.134	1.26-1	1.00+0	1.33-4	4.786	1.12+1	.114		
2.50	.468	2.506	2.155	7.55-2	1.00+0	3.58-4	4.650	1.04+1	.143	τ	C
3.00	.453	2.514	2.170	4.78-2	9.99-1	8.37-4	4.437	9.80+0	.176	.000	.794
3.50	.442	2.523	2.183	3.33-2	9.98-1	1.62-3	4.244	9.26+0	.202	.004	.819
4.00	.433	2.533	2.195	2.41-2	9.97-1	2.90-3	4.072	8.78+0	.225	.010	.830
5.00	.418	2.544	2.218	1.49-2	9.93-1	6.90-3	3.852	8.14+0	.249	.040	.856
6.00	.405	2.576	2.241	9.99-3	9.86-1	1.42-3	3.690	7.58+0	.256	.080	.880
8.00	.387	2.621	2.288	5.75-3	9.61-1	3.90-2	3.557	6.69+0	.242	.200	.929
10.0	.374	2.664	2.333	3.92-3	9.21-1	7.93-2	3.546	6.10+0	.216	.400	.967
14.0	.354	2.740	2.414	2.38-3	8.06-1	1.94-1	3.686	5.30+0	.178	.800	.989
18.0	.341	2.803	2.481	1.73-3	6.70-1	3.30-1	3.898	4.81+0	.162	1.40	.995
22.0	.330	2.855	2.537	1.37-3	5.43-1	4.57-1	4.109	4.90+0	.160	2.00	.997
26.0	.322	2.898	2.584	1.15-3	4.34-1	5.66-1	4.277	5.48+0	.165	4.00	.999
30.0	.315	2.934	2.622	9.98-4	3.47-1	6.53-1	4.414	6.56+0	.174	8.00	1.00
40.0	.301	2.997	2.690	7.57-4	2.03-1	7.97-1	4.572	1.14+1	.203	14.0	1.00
50.0	.291	3.026	2.721	6.04-4	1.23-1	8.77-1	4.459	1.94+1	.233	18.0	1.00
60.0	.282	3.021	2.717	4.86-4	7.50-2	9.25-1	4.080	3.043+1	.257		

Eff. θ = 0.600 Log G = 1.00 Flux = 2.82 + 11 N(HE)/N(H) = 0.15

τ	θ	Log PG	Log PE	H I	HE I	HE II	$(\kappa+\sigma)_{STD}$	$dp_r/d\tau$	∇_A	λ	Flux
0.000	.794	-1.02	-1.600	5.93-1	1.00+0	5.22-9	1.01-1	1.02+1	.152	*911	8.55-7
0.001	.791	-0.844	-1.740	6.43-1	1.00+0	4.50-9	9.01-2	1.06+1	.152	*994	1.40-6
0.002	.789	-0.592	-1.293	7.15-1	1.00+0	3.44-9	7.39-2	1.11+1	.152	*1094	2.21-6
0.003	.787	-0.409	-1.166	7.57-1	1.00+0	2.91-9	6.46-2	1.16+1	.151	*1215	3.36-6
0.004	.785	-0.267	-1.068	7.85-1	1.00+0	2.62-9	5.86-2	1.20+1	.150	1367	4.86-6
0.006	.781	-0.054	-0.921	8.20-1	1.00+0	2.30-9	5.14-2	1.28+1	.146	1563	6.68-6
0.008	.778	0.101	-0.811	8.40-1	1.00+0	2.15-9	4.76-2	1.34+1	.141	1683	7.67-6
0.010	.776	0.222	-0.725	8.53-1	1.00+0	2.08-9	4.54-2	1.39+1	.137	1823	8.72-6
0.015	.771	0.438	-0.571	8.75-1	1.00+0	1.95-9	4.23-2	1.48+1	.130	1989	1.04-5
0.020	.766	0.586	-0.456	8.86-1	1.00+0	1.98-9	4.20-2	1.55+1	.124	2188	1.22-5
0.025	.761	0.695	-0.365	8.91-1	1.00+0	2.12-9	4.31-2	1.61+1	.119	2431	1.46-5
0.030	.757	0.779	-0.289	8.93-1	1.00+0	2.34-9	4.50-2	1.62+1	.115	2735	1.80-5
0.035	.752	0.846	-0.222	8.93-1	1.00+0	2.60-9	4.74-2	1.65+1	.112	3126	2.30-5
0.040	.748	0.901	-0.163	8.92-1	1.00+0	2.93-9	5.04-2	1.68+1	.109	3647	3.02-5
0.060	.733	1.046	0.022	8.80-1	1.00+0	4.88-9	6.50-2	1.73+1	.100	3647	1.31-4
0.080	.719	1.130	0.160	8.62-1	1.00+0	8.11-9	8.36-2	1.76+1	.094	4019	1.32-4
0.100	.707	1.184	0.269	8.41-1	1.00+0	1.30-8	1.05-1	1.77+1	.090	4475	1.29-4
0.125	.693	1.229	0.381	8.10-1	1.00+0	2.28-8	1.37-1	1.78+1	.086	5049	1.22-4
0.150	.681	1.258	0.471	7.75-1	1.00+0	3.81-8	1.74-1	1.78+1	.083	5792	1.12-4
0.200	.662	1.293	0.603	7.05-1	1.00+0	8.90-8	2.50-1	1.75+1	.080	6790	9.88-5
0.250	.646	1.311	0.698	6.29-1	1.00+0	1.88-7	3.34-1	1.72+1	.079	8205	8.26-5
0.300	.632	1.321	0.771	5.49-1	1.00+0	3.75-7	4.22-1	1.70+1	.080	8205	1.04-4
0.350	.620	1.326	0.822	4.75-1	1.00+0	6.82-7	5.00-1	1.67+1	.083	10503	7.61-5
0.400	.609	1.328	0.861	4.03-1	1.00+0	1.20-6	5.70-1	1.65+1	.086	14588	4.76-5
0.500	.592	1.328	0.911	2.89-1	1.00+0	3.11-6	6.70-1	1.59+1	.097	14588	5.08-5
0.600	.576	1.325	0.938	2.01-1	1.00+0	7.41-6	7.23-1	1.54+1	.113	17790	3.70-5
0.700	.564	1.322	0.952	1.42-1	1.00+0	1.54-5	7.41-1	1.49+1	.131	22793	2.44-5
0.800	.553	1.319	0.961	1.02-1	1.00+0	2.96-5	7.43-1	1.45+1	.151	22793	2.50-5
1.00	.535	1.317	0.971	5.73-2	1.00+0	8.81-5	7.20-1	1.38+1	.187	30186	1.53-5
1.20	.520	1.320	0.979	3.48-2	1.00+0	2.18-4	6.92-1	1.32+1	.214	44675	7.54-6
1.40	.508	1.328	0.989	2.34-2	1.00+0	4.45-4	6.69-1	1.27+1	.230		
1.60	.497	1.339	1.002	1.65-2	9.99-1	8.33-4	6.51-1	1.23+1	.240	ΔF/F	
1.80	.488	1.352	1.016	1.23-2	9.99-1	1.42-3	6.38-1	1.20+1	.246	-0.75, 1.33	
2.00	.479	1.367	1.032	9.42-3	9.98-1	2.30-3	6.28-1	1.17+1	.250		
2.50	.462	1.409	1.075	5.64-3	9.94-1	5.94-3	6.17-1	1.12+1	.254	τ	C
3.00	.448	1.452	1.118	3.69-3	9.87-1	1.31-2	6.14-1	1.07+1	.253	.000	.819
3.50	.436	1.494	1.161	2.69-3	9.76-1	2.41-2	6.18-1	1.03+1	.249	.004	.805
4.00	.426	1.533	1.201	2.04-3	9.59-1	4.09-2	6.24-1	9.964	.244	.010	.801
5.00	.410	1.605	1.275	1.37-3	9.11-1	8.86-2	6.46-1	9.399	.230	.040	.838
6.00	.397	1.666	1.338	9.92-4	8.37-1	1.63-1	6.70-1	8.915	.215	.080	.869
8.00	.378	1.762	1.441	6.47-4	6.60-1	3.40-1	7.25-1	8.191	.198	.200	.927
10.0	.363	1.835	1.520	4.71-4	4.75-1	5.25-1	7.80-1	7.689	.197	.400	.965
14.0	.342	1.946	1.637	3.22-4	2.43-1	7.57-1	8.56-1	6.819	.215	.800	.986
18.0	.327	2.031	1.725	2.54-4	1.32-1	8.68-1	9.04-1	6.323	.233	1.40	.994
22.0	.316	2.103	1.799	2.18-4	7.90-2	9.21-1	9.41-1	5.736	.245	2.00	.996
26.0	.307	2.166	1.863	1.96-4	5.16-2	9.48-1	9.77-1	5.178	.253	4.00	.998
30.0	.299	2.223	1.920	1.82-4	3.60-2	9.64-1	1.012	4.642	.257	8.00	1.00
40.0	.283	2.346	2.044	1.64-4	1.80-2	9.82-1	1.101	3.362	.263	14.0	1.00
50.0	.272	2.450	2.148	1.57-4	1.09-2	9.89-1	1.194	2.141	.266	18.0	1.00
60.0	.263	2.540	2.238	1.54-4	7.39-3	9.93-1	1.289	9.61-1	.268		

Eff. θ = 0.700 Log G = 4.44 Flux = 1.52 + 11 N(HE)/N(H) = 0.15

τ	θ	Log PG	Log PE	H I	HE I	HE II	$(\kappa+\sigma)_{STD}$	$dp_r/d\tau$	∇_A	λ	Flux
0.000	.916	3.184	-0.181	3.94-4	1.00+0		1.47-2	7.30	.361	911	1.60-6
0.001	.915	3.372	-0.074	3.18-4	1.00+0		1.85-2	6.63	.367	994	1.72-6
0.002	.914	3.563	0.041	2.56-4	1.00+0		2.36-2	6.13	.373	1049	1.86-6
0.003	.912	3.675	0.117	2.32-4	1.00+0		2.78-2	5.87	.375	1215	2.15-6
0.004	.910	3.753	0.175	2.18-4	1.00+0		3.13-2	5.67	.376	1367	2.56-6
0.006	.906	3.861	0.256	2.02-4	1.00+0		3.71-2	5.45	.378	1563	3.27-6
0.008	.904	3.938	0.361	1.92-4	1.00+0		4.19-2	5.29	.379	1683	3.79-6
0.010	.902	3.997	0.362	1.85-4	1.00+0		4.61-2	5.21	.380	1823	4.47-6
0.015	.899	4.103	0.440	1.71-4	1.00+0		5.43-2	5.08	.381	1989	5.90-6
0.020	.896	4.177	0.500	1.74-4	1.00+0		6.15-2	4.98	.382	2188	7.73-6
0.025	.893	4.235	0.551	1.71-4	1.00+0		6.81-2	4.89	.382	2431	1.02-5
0.030	.891	4.281	0.594	1.60-4	1.00+0		7.43-2	4.87	.383	2735	1.35-5
0.035	.888	4.320	0.634	1.60-4	1.00+0		8.03-2	4.82	.383	3126	1.81-5
0.040	.885	4.353	0.669	1.61-4	1.00+0		8.60-2	4.79	.383	3647	2.41-5
0.060	.876	4.451	0.785	1.71-4	1.00+0		1.08-1	4.69	.382	3647	4.08-5
0.080	.867	4.517	0.878	1.87-4	1.00+0		1.28-1	4.64	.381	4019	4.43-5
0.100	.859	4.567	0.957	2.05-4	1.00+0		1.48-1	4.62	.380	4475	4.80-5
0.125	.849	4.614	1.046	2.31-4	1.00+0		1.74-1	4.59	.378	5049	5.16-5
0.150	.841	4.652	1.124	2.60-4	1.00+0		2.01-1	4.57	.377	5792	5.45-5
0.200	.825	4.708	1.255	3.23-4	1.00+0		2.54-1	4.53	.373	6790	5.55-5
0.250	.812	4.748	1.368	3.96-4	1.00+0		3.10-1	4.52	.370	8205	5.44-5
0.300	.800	4.778	1.470	4.79-4	1.00+0		3.70-1	4.52	.366	8205	5.56-5
0.350	.788	4.802	1.561	5.69-4	1.00+0		4.34-1	4.52	.362	10503	5.10-5
0.400	.778	4.822	1.644	6.71-4	1.00+0		5.02-1	4.53	.358	14588	4.22-5
0.500	.760	4.853	1.789	8.96-4	1.00+0		6.46-1	4.57	.350	14588	4.31-5
0.600	.744	4.875	1.919	1.17-3	1.00+0		8.08-1	4.61	.342	17790	3.38-5
0.700	.730	4.893	2.032	1.48-3	1.00+0		9.83-1	4.64	.334	22793	2.22-5
0.800	.716	4.907	2.136	1.83-3	1.00+0		1.176	4.68	.326	22793	2.23-5
1.00	.694	4.928	2.316	2.69-3	1.00+0		1.610	4.76	.310	30186	1.35-5
1.20	.674	4.943	2.472	3.76-3	1.00+0		2.124	4.86	.294	44675	6.56-6
1.40	.656	4.954	2.606	5.03-3	1.00+0		2.701	4.95	.278		
1.60	.641	4.963	2.728	6.57-3	1.00+0		3.371	5.04	.262	ΔF/F	
1.80	.627	4.970	2.837	8.34-3	1.00+0		4.129	5.13	.247	-1.08, 1.33	
2.00	.614	4.975	2.937	1.04-2	1.00+0		5.004	5.22	.232		
2.50	.587	4.985	3.146	1.67-2	1.00+0	2.42-8	7.598	5.38	.202	τ	C
3.00	.564	4.992	3.326	2.51-2	1.00+0	6.60-8	11.13	5.47	.176	.000	.867
3.50	.545	4.997	3.470	3.49-2	1.00+0	1.50-7	15.43	5.44	.158	.004	.855
4.00	.528	5.000	3.597	4.69-2	1.00+0	3.09-7	20.91	5.39	.143	.010	.847
5.00	.504	5.005	3.780	7.26-2	1.00+0	9.16-7	33.50	5.27	.125	.040	.863
6.00	.483	5.007	3.930	1.05-1	1.00+0	2.30-6	50.61	5.10	.113	.080	.876
8.00	.454	5.011	4.131	1.75-1	1.00+0	8.65-6	91.77	4.57	.102	.200	.902
10.0	.434	5.013	4.261	2.47-1	1.00+0	2.23-5	137.2	4.13	.098	.400	.928
14.0	.408	5.015	4.413	3.84-1	1.00+0	8.28-5	223.8	3.56	.096	.800	.959
18.0	.389	5.017	4.501	5.08-1	1.00+0	2.20-4	296.7	3.15	.099	1.40	.981
22.0	.375	5.018	4.556	6.07-1	1.00+0	4.69-4	348.1	2.72	.104	2.00	.990
26.0	.364	5.020	4.591	6.86-1	9.99-1	8.81-4	379.7	2.30	.110	4.00	.998
30.0	.355	5.021	4.616	7.46-1	9.99-1	1.50-3	398.0	1.91	.118	8.00	1.00
40.0	.337	5.023	4.649	8.41-1	9.96-1	4.33-3	404.8	9.64-1	.139	14.0	1.00
50.0	.323	5.026	4.667	8.94-1	9.90-1	9.67-4	390.0	6.68-1	.162	18.0	1.00
60.0	.313	5.029	4.679	9.24-1	9.82-1	1.83-2	372.9	0.00	.183		

Eff. θ = 0.700 Log G = 3.00 Flux = 1.52 + 11 N(HE)/N(H) = 0.15

τ	θ	Log PG	Log PE	H I	HE I	HE II	$(\kappa+\sigma)_{STD}$	$dp_r/d\tau$	∇_A	λ	Flux
0.000	.881	2.041	-0.522	2.93-3	1.00+0		7.20-3	9.18+0	.278	911	9.23-7
0.001	.880	2.239	-0.417	2.34-3	1.00+0		8.52-3	8.38+0	.295	994	1.06-6
0.002	.880	2.445	-0.308	1.85-3	1.00+0		1.04-2	7.77+0	.311	1094	1.19-6
0.003	.879	2.567	-0.242	1.62-3	1.00+0		1.17-2	7.41+0	.320	1215	1.37-6
0.004	.878	2.654	-0.194	1.47-3	1.00+0		1.29-2	7.13+0	.325	1367	1.59-6
0.006	.878	2.775	-0.128	1.29-3	1.00+0		1.47-2	6.80+0	.333	1563	1.95-6
0.008	.877	2.860	-0.076	1.19-3	1.00+0		1.63-2	6.57+0	.338	1683	2.23-6
0.010	.876	2.925	-0.036	1.12-3	1.00+0		1.77-2	6.44+0	341	1823	2.62-6
0.015	.874	3.043	0.039	1.01-3	1.00+0		2.06-2	6.23+0	.346	1989	3.78-6
0.020	.872	3.125	0.096	9.46-4	1.00+0		2.30-2	6.05+0	.349	2188	5.28-6
0.025	.871	3.188	0.139	9.01-4	1.00+0		2.52-2	5.92+0	.351	2431	7.30-6
0.030	.869	3.238	0.176	8.71-4	1.00+0		2.71-2	5.88+0	.353	2735	1.01-5
0.035	.867	3.281	0.212	8.58-4	1.00+0		2.91-2	5.81+0	.354	3126	1.41-5
0.040	.865	3.317	0.245	8.51-4	1.00+0		3.11-2	5.74+0	.354	3647	1.95-5
0.060	.857	3.424	0.355	8.61-4	1.00+0		3.84-2	5.60+0	.355	3647	5.29-5
0.080	.849	3.495	0.454	9.23-4	1.00+0		4.63-2	5.52+0	.353	4019	5.48-5
0.100	.841	3.547	0.538	1.00-3	1.00+0		5.41-2	5.49+0	.351	4475	5.69-5
0.125	.831	3.597	0.630	1.12-3	1.00+0		6.42-2	5.45+0	.347	5049	5.90-5
0.150	.823	3.634	0.712	1.25-3	1.00+0		7.46-2	5.42+0	.343	5792	6.03-5
0.200	.807	3.690	0.850	1.53-3	1.00+0		9.59-2	5.40+0	.335	6790	5.99-5
0.250	.794	3.730	0.969	1.86-3	1.00+0		1.19-1	5.43+0	.327	8205	5.72-5
0.300	.781	3.760	1.076	2.24-3	1.00+0		1.44-1	5.47+0	.318	8205	6.09-5
0.350	.770	3.783	1.170	2.65-3	1.00+0		1.71-1	5.52+0	.308	10503	5.40-5
0.400	.759	3.802	1.258	3.13-3	1.00+0		2.01-1	5.57+0	.299	14588	4.20-5
0.500	.741	3.831	1.410	4.20-3	1.00+0		2.65-1	5.71+0	.281	14588	4.36-5
0.600	.724	3.851	1.547	5.53-1	1.00+0		3.42-1	5.84+0	.262	17790	3.35-5
0.700	.709	3.867	1.667	7.08-3	1.00+0		4.30-1	5.97+0	.245	22793	2.21-5
0.800	.695	3.879	1.777	8.94-3	1.00+0		5.32-1	6.09+0	.228	22793	2.24-5
1.00	.670	3.897	1.971	1.35-2	1.00+0		7.85-1	6.32+0	.199	30186	1.36-5
1.20	.648	3.908	2.138	1.96-2	1.00+0		1.120	6.50+0	.174	44675	6.66-6
1.40	.629	3.916	2.282	2.70-2	1.00+0		1.545	6.63+0	.154		
1.60	.613	3.922	2.407	3.60-2	1.00+0		2.081	6.69+0	.138	ΔF/F	
1.80	.598	3.926	2.516	4.62-2	1.00+0		2.729	6.71+0	.126	-1.43, 0.76	
2.00	.585	3.929	2.615	5.82-2	1.00+0		3.531	6.70+0	.117		
2.50	.559	3.935	2.806	9.22-2	1.00+0		5.998	6.60+0	.101	τ	C
3.00	.537	3.938	2.962	1.36-1	1.00+0	7.98-7	9.515	6.45+0	.092	.000	.810
3.50	.520	3.940	3.075	1.82-1	1.00+0	1.73-6	13.55	6.21+0	.087	.004	.815
4.00	.505	3.941	3.170	2.34-1	1.00+0	3.46-6	18.38	5.99+0	.085	.010	.824
5.00	.484	3.943	3.294	3.32-1	1.00+0	9.68-6	27.76	5.63+0	.083	.040	.858
6.00	.466	3.945	3.383	4.36-1	1.00+0	2.35-5	37.52	5.28+0	.083	.080	.877
8.00	.441	3.946	3.482	6.03-1	1.00+0	8.63-5	51.60	4.62+0	.089	.200	.904
10.0	.424	3.948	3.533	7.22-1	1.00+0	2.31-4	59.00	4.15+0	.097	.400	.932
14.0	.400	3.950	3.578	8.49-1	9.99-1	9.10-4	62.09	3.51+0	.120	.800	.966
18.0	.384	3.953	3.597	9.08-1	9.98-1	2.42-3	59.83	3.07+0	.148	1.40	.988
22.0	.372	3.955	3.608	9.38-1	9.95-1	5.06-3	46.84	2.60+0	.175	2.00	.994
26.0	.362	3.958	3.615	9.55-1	9.91-1	9.14-3	53.85	2.16+0	.198	4.00	.998
30.0	.354	3.962	3.621	9.66-1	9.85-1	1.48-2	51.35	1.74+0	.214	8.00	1.00
40.0	.339	3.971	3.634	9.80-1	9.63-1	3.72-2	46.67	7.59-1	.227	14.0	1.00
50.0	.328	3.981	3.647	9.86-1	9.29-1	7.14-2	43.71	0.00+0	.215	18.0	1.00
60.0	.319	3.991	3.660	9.90-1	8.84-1	1.16-1	41.65	0.00+0	.197		

Eff. θ = 0.700 Log G = 2.00 Flux = 1.52 + 11 N(HE)/N(H) = 0.15

τ	θ	Log PG	Log PE	H I	HE I	HE II	$(\kappa+\sigma)_{STD}$	$dp_r/d\tau$	∇_A	λ	Flux
0.000	.882	1.140	-0.993	9.92-1	1.00+0		4.88-3	8.95+0	.208	*911	5.53-7
0.001	.882	1.379	-0.870	9.94-1	1.00+0		5.00-3	8.72+0	.220	*994	6.65-7
0.002	.882	1.634	-0.738	9.95-1	1.00+0		5.49-3	8.48+0	.237	*1094	7.69-7
0.003	.881	1.782	-0.659	9.96-1	1.00+0		5.97-3	8.20+0	.248	*1215	8.74-7
0.004	.881	1.884	-0.603	9.96-1	1.00+0		6.42-3	7.97+0	.255	1367	9.85-7
0.006	.879	2.025	-0.521	9.97-1	1.00+0		7.22-3	7.65+0	.265	1563	1.16-6
0.008	.878	2.121	-0.463	9.97-1	1.00+0		7.92-3	7.42+0	.272	1683	1.30-6
0.010	.877	2.195	-0.416	9.97-1	1.00+0		8.55-3	7.28+0	.276	1823	1.53-6
0.015	.874	2.323	-0.328	9.98-1	1.00+0		9.96-3	7.04+0	.283	1989	2.43-6
0.020	.870	2.411	-0.260	9.98-1	1.00+0		1.12+2	6.84+0	.287	2188	3.64-6
0.025	.867	2.477	-0.205	9.98-1	1.00+0		1.24-2	6.69+0	.289	2431	5.32-6
0.030	.865	2.529	-0.158	9.98-1	1.00+0		1.35-2	6.66+0	.291	2735	7.75-6
0.035	.862	2.573	-0.116	9.98-1	1.00+0		1.46-2	6.58+0	.291	3126	1.13-5
0.040	.859	2.610	-0.077	9.98-1	1.00+0		1.57-2	6.51+0	.292	3647	1.63-5
0.060	.849	2.716	0.050	9.98-1	1.00+0		1.98-2	6.36+0	.291	3647	6.26-5
0.080	.840	2.786	0.151	9.98-1	1.00+0		2.39-2	6.30+0	.287	4019	6.31-5
0.100	.832	2.838	0.237	9.97-1	1.00+0		2.81-2	6.27+0	.283	4475	6.36-5
0.125	.822	2.886	0.333	9.97-1	1.00+0		3.35-2	6.25+0	.278	5049	6.41-5
0.150	.813	2.924	0.418	9.97-1	1.00+0		3.92-2	6.25+0	.272	5792	6.38-5
0.200	.797	2.978	0.561	9.96-1	1.00+0		5.12-2	6.28+0	.259	6790	6.19-5
0.250	.783	3.016	0.685	9.95-1	1.00+0		6.47-2	6.36+0	.247	8205	5.78-5
0.300	.770	3.044	0.796	9.94-1	1.00+0		8.00-2	6.45+0	.234	8205	6.49-5
0.350	.758	3.066	0.895	9.92-1	1.00+0		9.69-2	6.55+0	.222	10503	5.55-5
0.400	.746	3.083	0.988	9.91-1	1.00+0		1.16-1	6.65+0	.210	14588	4.11-5
0.500	.726	3.108	1.149	9.88-1	1.00+0		1.61-1	6.87+0	.188	14588	4.33-5
0.600	.708	3.126	1.292	9.83-1	1.00+0		2.19-1	7.05+0	.169	17790	3.28-5
0.700	.692	3.138	1.418	9.78-1	1.00+0		2.89-1	7.20+0	.153	22793	2.18-5
0.800	.677	3.147	1.533	9.72-1	1.00+0		3.77-1	7.31+0	.139	22793	2.22-5
1.00	.651	3.160	1.728	9.56-1	1.00+0	1.29-8	6.11-1	7.47+0	.118	30186	1.36-5
1.20	.629	3.167	1.892	9.36-1	1.00+0	3.35-8	9.44-1	7.51+0	.104	44675	6.66-5
1.40	.611	3.172	2.023	9.12-1	1.00+0	7.48-8	1.370	7.44+0	.094		
1.60	.595	3.175	2.136	8.84-1	1.00+0	1.52-7	1.913	7.38+0	.087	ΔF/F	
1.80	.581	3.177	2.230	8.54-1	1.00+0	2.80-7	2.556	7.27+0	.083	-1.57, 0.74	
2.00	.569	3.179	2.312	8.20-1	1.00+0	4.95-7	3.325	7.16+0	.080		
2.50	.545	3.181	2.461	7.30-1	1.00+0	1.53-6	5.451	6.88+0	.076	τ	C
3.00	.525	3.182	2.571	6.27-1	1.00+0	4.11-6	7.961	6.60+0	.076	.000	.815
3.50	.509	3.183	2.643	5.33-1	1.00+0	8.90-6	10.20	6.29+0	.077	.004	.835
4.00	.496	3.183	2.697	4.42-1	1.00+0	1.80-5	12.23	6.01+0	.079	.010	.844
5.00	.476	3.184	2.758	3.09-1	1.00+0	5.26-5	14.69	5.62+0	.086	.040	.863
6.00	.460	3.184	2.793	2.10-1	1.00+0	1.34-4	15.83	5.25+0	.097	.080	.877
8.00	.437	3.185	2.825	1.09-1	1.00+0	5.22-4	15.79	4.61+0	.125	.200	.905
10.0	.420	3.186	2.838	6.37-2	9.99-1	1.44-3	14.84	4.16+0	.159	.400	.937
14.0	.397	3.190	2.850	2.92-2	9.94-1	5.82-3	13.05	3.56+0	.216	.800	.974
18.0	.381	3.195	2.859	1.68-2	9.85-1	1.54-2	11.76	3.20+0	.243	1.40	.992
22.0	.369	3.201	2.867	1.10-2	9.68-1	3.17-2	10.88	3.26+0	.242	2.00	.996
26.0	.360	3.208	2.875	7.96-3	9.44-1	5.58-2	10.26	3.68+0	.227	4.00	.999
30.0	.352	3.214	2.883	6.10-3	9.12-1	8.76-2	9.817	4.46+0	.208	8.00	1.00
40.0	.337	3.226	2.899	3.67-3	8.03-1	1.97-1	9.088	8.01+0	.172	14.0	1.00
50.0	.325	3.228	2.906	2.52-3	6.66-1	3.34-1	8.510	1.38+1	.157	18.0	1.00
60.0	.316	3.214	2.896	1.83-3	5.23-1	4.77-1	7.867	2.19+1	.156		

Appendix II

CONVECTIVE MODEL ATMOSPHERES IN THE MIXING LENGTH APPROXIMATION

In this appendix we shall consider how to extend the work reported above to allow for the presence of convection. The equations developed in section 4 have not yet been used in computation, but an attempt will be made to apply them in the near future.

1. The convection equations

According to the Schwarzschild criterion, the layers in a stellar atmosphere or interior become unstable against small perturbations whenever the actual logarithmic temperature gradient (with respect to pressure) exceeds the corresponding adiabatic gradient. That is, when

$$\frac{d \log T}{d \log p_g} > \frac{d \log T}{d \log p_g}_{\text{ADIABATIC}} \qquad \text{(A. II. 1)}$$

This gives rise to mass motions in the atmosphere which can transport considerable energy. This flux must be added to the radiative flux; the total (convective flux + radiative flux) must satisfy the flux constancy condition throughout the atmosphere. This in turn implies that the temperature distribution may be rather noticeably altered compared to that which would prevail if radiative equilibrium were strictly true.

A phenomenological approach to the convection problem was given by Biermann (summarized by Demarque, 1960) and will be used here. Let:

$$\nabla_A \equiv \left(\frac{d \log T}{d \log p_g} \right)_{ADIABATIC} \qquad (A.II.2)$$

$$\nabla_R = \left(\frac{d \log T}{d \log p_g} \right)_{RADIATIVE} \qquad (A.II.3)$$

and

$$\nabla \equiv \frac{d \log T}{d \log p_g} \qquad (A.II.4)$$

that is, ∇_R is the gradient which would prevail if convection were ignored; ∇ is the true temperature gradient which is intermediate between the adiabatic and the radiative gradients.

By equating the work done by the bouyancy forces to the mean kinetic energy of a rising element of gas one finds the root mean square convective velocity is given by:

$$\overline{V^2}^{1/2} = (gH)^{1/2} \left(\frac{\ell}{H}\right) (\nabla - \nabla_A)^{1/2} Q^{1/2} \cdot \frac{1}{2\sqrt{2}} \qquad (A.II.5)$$

where ℓ is the "mixing length"; this is the distance in which the rising element loses its identity and merges into the surrounding medium. The factor of $1/\sqrt{2}$ accounts roughly for viscous energy dissipation, and

$$Q = 1 - \left(\frac{\partial \log \mu}{\partial \log T} \right)_p \qquad (A.II.6)$$

allows for the change in effective mean molecular weight of the gas due to the presence of radiation pressure and due to ionization. An expression for Q will be given later on. H is taken here to be the local pressure scale height in the atmosphere,

$$H = \frac{p_g}{p\left[g - \kappa \frac{dp_r}{dT}\right]} \qquad \text{(A. II. 7)}$$

For the present calculations, the local scale height is computed at each point in the atmosphere, and the ratio ℓ/H is taken as a constant which is specified at the outset.

The expression for the convective flux is then:

$$\pi F_{CONV} = \frac{1}{2} \rho c_p T \overline{V} \left(\frac{\ell}{H}\right)(\nabla - \nabla_A) \qquad \text{(A. II. 8)}$$

where c_p is the specific heat of the gas at constant pressure.

Before proceeding further, we should justify this choice of convective theory; there are essentially two reasons for it. First, the equations written below will depend upon the convective theory chosen through some functional coefficients in the differential equations for the depth and temperature corrections; the same perturbation procedures may be applied to any convection theory for which the expression for the convective flux can be written down in terms of the local pressures, temperatures, etc. Since for the moment we are more concerned with establishing flux constancy in the presence of convection than with the details of the convective theory, the mixing length theory will suffice for illustrative purposes. Second, if we forget the physical interpretation of the "mixing length" and regard the ratio (ℓ/H) as merely an efficiency parameter for the transport of convective flux, we may, by suitable choice of (ℓ/H), interpolate smoothly between the pure radiative solution $[(\ell/H) = 0]$ and the adiabatic solution $[(\ell/H) \rightarrow \infty]$. By

forming a one-parameter family of models we can attempt to determine in a simple way what spectroscopic quantities may be sensitive to the presence of convection. If no such quantity can be found, then for the moment we may ignore convection; on the other hand, if some sensitive criterion is found, we will have an observational hold upon the problem, and may feel justified to attempt using a more sophisticated theory.

2. Thermodynamical quantities

To find the flux numerically, we must have expressions for ∇_A, c_p, $\partial\mu/\partial t$, etc. We assume that the gas under consideration consists of a set of n components each with a fractional abundance ν_i; we assume that each component may ionize once with the exception of helium, which is abundant enough to merit consideration of both its ionizations. This problem is treated by recognizing that since the second ionization potential lies some 30 volts above the first there is effectively no interlocking between more than two ionization states at a time, so that it may be considered as two atoms, each with abundance ν_{He}. Of course, it is counted only once in the sum over the nuclei. For such a gas we may write:

Gas pressure: $$PV = NkT \sum_i \nu_i(1 + x_i) + \frac{1}{3} aT^4 \qquad \text{(A. II. 9)}$$

Internal energy: $$U = \frac{3}{2} NkT \sum_i \nu_i(1 + x_i) + N \sum_i \nu_i x_i \chi_i + aT^4 V \qquad \text{(A. II. 10)}$$

Saha's equation: $$\frac{NkT}{V} \left(\sum \nu_i x_i\right) \frac{x_i}{1-x_i} = C_i T^{5/2} e^{-\chi_i/kT} \qquad (i = 1, \ldots, n)$$

(A. II. 11)

where in writing equation A. II. 11 we have ignored the temperature and pressure dependence of the partition functions. The expression for the adiabatic gradient derived by Krishna Swamy was given in chapter II, and will not be written again here. For the specific heats we have quite generally that:

$$c_v = \left(\frac{\partial U}{\partial \bar{T}}\right)_v \qquad \text{(A. II. 12)}$$

and

$$c_p = \left(\frac{\partial U}{\partial \bar{T}}\right)_p + p\left(\frac{\partial V}{\partial \bar{T}}\right)_p \qquad \text{(A. II. 13)}$$

A straightforward but lengthy calculation leads to:

$$c_v = \frac{k}{\mu m_H}\left\{\left(\frac{3}{2}+12\beta\right)(1+\bar{x}) + \frac{\frac{3}{2}\sum_i \nu_i x_i(1-x_i)\frac{\chi_i}{k\bar{T}}}{\bar{x}} + \frac{\sum_i \nu_i x_i(1-x_i)\left(\frac{\chi_i}{k\bar{T}}\right)^2}{\bar{x}} + \left(\frac{3}{2}\bar{x} - \sum \nu_i x_i(1-x_i)\frac{\chi_i}{k\bar{T}}\right)\frac{\frac{3}{2}(\bar{x}-\langle x^2\rangle)+\sum \nu_i x_i(1-x_i)\left(\frac{\chi_i}{k\bar{T}}\right)}{2\bar{x}-\langle x^2\rangle}\right\}$$

(A. II. 14)

and

$$c_p = \frac{k}{\mu m_{II}}\left\{\left(\frac{5}{2}+20\beta+16\beta^2\right)(1+\bar{x}) + \sum \nu_i x_i(1-x_i)\left(\frac{\chi_i}{k\bar{T}}\right)^2 + \left(\frac{5}{2}+4\beta\right)\sum \nu_i x_i(1-x_i)\frac{\chi_i}{k\bar{T}} + \left[\frac{5}{2}+4\beta+\frac{\sum \nu_i x_i(1-x_i)\frac{\chi_i}{k\bar{T}}}{\bar{x}-\langle x^2\rangle}\right] \times \left[\frac{\bar{x}-\langle x^2\rangle}{\bar{x}^2+2\bar{x}-\langle x^2\rangle}\right]\left[\bar{x}(1+\bar{x})\left(\frac{5}{2}+4\beta\right) - \sum \nu_i x_i(1-x_i)\frac{\chi_i}{k\bar{T}}\right]\right\}$$

(A. II. 15)

where $\bar{x} = \sum \nu_i x_i$, $\langle x^2 \rangle = \sum \nu_i x_i^2$, and $\mu = \sum \nu_i A_i / A_H$. Also $\beta = P_R/P_g$, $P = P_R + P_g$, and $P_R = \frac{1}{3} aT^4$. Further we find:

$$-\left(\frac{\partial \log \mu}{\partial \log T}\right)_p = 4\beta + \frac{\bar{x}(\bar{x} - \langle x^2 \rangle)}{\bar{x}^2 + 2x - \langle x^2 \rangle} \left\{ \frac{5}{2} + 4\beta + \frac{\sum \nu_i x_i (1-x_i) \frac{\chi_i}{kT}}{\bar{x} - \langle x^2 \rangle} \right\} \quad \text{(A. II. 16)}$$

3. The integrations

Starting with an assumed $T(\tau)$ relationship we integrate the equation of hydrostatic equilibrium in the usual way. At each point both the adiabatic and radiative gradients are computed and compared. The radiative gradient is computed as

$$\nabla_R = \frac{p}{T} \left(\frac{dT}{d\tau}\right) \cdot \left(\frac{d\tau}{dp}\right) \quad \text{(A. II. 17)}$$

where $dT/d\tau$ is determined by direct numerical differentiation. When the radiative gradient exceeds the adiabatic gradient, we must estimate the true superadiabatic gradient and proceed. Now in the deep interior, the flux transported by radiation is proportional to the temperature gradient. Thus in the interior we may write $F_{rad}/F_{total} = \nabla/\nabla_R$, or $F_{conv}/F_{total} = 1 - F_{rad}/F_{total} = 1 - \nabla/\nabla_R$. This relationship is no longer strictly valid in the atmosphere but holds only approximately, basically because the radiative flux "sees" the boundary. The situation is entirely analogous to the difference between writing the temperature gradient equation for the interior, and having to find the temperature distribution in the atmosphere by other means. Consequently we cannot estimate ∇ completely accurately, and in general, iterations will be required to enforce the condition of constancy of flux; it is, however,

a useful starting point. Within this framework we have

$$A^{*}(\nabla - \nabla_A)^{3/2} = 1 - \frac{\nabla}{\nabla_R}$$

or

$$A(\nabla - \nabla_A)^{3/2} = \nabla_R - \nabla \qquad \text{(A. II. 19)}$$

where

$$A = \frac{\nabla_R}{2\sqrt{2}}\left(\frac{1}{H}\right)^2 (gQH)^{1/2} \rho c_p T/\sigma T_e^4 \qquad \text{(A. II. 20)}$$

Rearranging terms we have $A(\nabla - \nabla_A)^{3/2} + (\nabla - \nabla_A) = \nabla_R - \nabla_A$, and finally, writing

$$x = (\nabla - \nabla_A)^{1/2} \qquad \text{(A. II. 21)}$$

we obtain

$$Ax^3 + x^2 + (\nabla_A - \nabla_R) = 0 \qquad \text{(A. II. 22)}$$

This cubis is solved for x by use of the regula falsi, starting with the two extreme estimates $x = 0$ and $x = \left[\frac{\nabla_A - \nabla_R}{A}\right]^{1/3}$. Successive iterates are made on x until $\left|Ax^3 + x^2 + (\nabla_A - \nabla_R)\right| \leq 10^{-6}$. We then have the true temperature gradient

$$\nabla = \frac{d \log T}{d \log p} \qquad \text{(A. II. 23)}$$

In addition we have the hydrostatic equilibrium equation

$$\frac{d\tau}{d \log p} = \frac{2.3025851\, p}{\left(\frac{g}{\kappa} - \frac{dp_r}{d\tau}\right)} \qquad \text{(A. II. 24)}$$

These last two equations are integrated simultaneously as a function of log p. At each point, the radiative gradient is evaluated using $dT/d\tau$ as the current value of T (since the τ scale is now floating, T and

p are the physically relevant parameters), and compared to the adiabatic gradient. The current value of T is used also to find the appropriate $dp_r/d\tau$ for the hydrostatic equilibrium equation. The integrations are now continued until either $\tau \geq 60$ (the last depth considered) or $\nabla_R \leq \nabla_A$, at which point the solution is continued using the radiative gradient in the usual manner.

It should be noted that the simultaneous integration of A. II. 23 and A. II. 24 amounts to a fundamental revision of the $T(\tau)$ relationship in the convective region. If the radiative solution is to be continued beyond this region, we proceed as follows: we backwards interpolate to find $\log p_g(\tau)$ at the standard τ's in the convective region; we then interpolate to find T at these values of $\log p_g$. Now we find the τ at which the last T in the convective region would have occurred using the old $T(\tau)$ relationship; a constant is added to this τ to make it equal to the last (new) τ found in the convective zone, and the whole old $T(\tau)$ relationship is shifted by this amount. The values of T at the remaining standard depths beyond the convective zone are found by interpolation in this shifted table. In this way we have hooked the old radiative solution onto the convective solution while assuring continuity of T at the boundary. Incidentally, from this new $T(\tau)$ relation we must form new tables of $dT/d\tau$ and $dp_r/d\tau$ before we can proceed; these are found by direct differentiation, and by interpolation against the old temperatures and $dp_r/d\tau$'s to find the values at the new standard temperatures. One difficulty never arises, namely, we never run off the end of the old temperature distribution; this is because while the $\tau(p)$ relationship changes only a small amount, the T(p) relationship

always gives a smaller T at a given p (since $\nabla \leq \nabla_R$).

Now when we actually evaluate the radiative and convective fluxes, we find, as anticipated because of the inexactness of A. II. 22 in the atmosphere, the total flux is not a constant, even though this is implicit in the method of solution. So we are forced to change the temperature distribution to attempt to obtain flux constancy; this is done by a modified Krook procedure. It should be noted that the method of integration just outlined starts from a model in radiative equilibrium. Thus it is assumed that a certain number of iterations using the ordinary Krook procedure will be necessary to attain at least fair flux constancy. Second, it should be realized that the above procedure is used only once because of the inexactness of the approximation $F_R/F = \nabla/\nabla_R$. After going through the above procedure once, the major revisions to the temperature-pressure scale will have been effected; further iterations are made by integrating the hydrostatic equation in the usual way with the currently assumed $T(\tau)$ relationship, and correcting this $T(\tau)$ distribution by the iteration procedure described in the next section, which allows for the convection terms.

4. The temperature correction procedure

The total flux is written $\mathcal{H} = \sigma T_e^4/4\pi$. We consider this to be divided into two parts, H, the radiative flux, and H_c, the convective flux. After calculating a model call the resultant radiative flux H^o and the resultant convective flux H_c^o. Now in general we find $H^o + H_c^o \neq \mathcal{H}$. Therefore we wish to revise the $T(\tau)$ relationship by calculating a

perturbation to the temperature scale (T_1) and to the depth scale (τ_1). These changes will change the radiative and convective fluxes; call these changes H^1 and H_c^1 respectively. We now demand

$$H^o + H^1 + H_c^o + H_c^1 = \mathcal{H} \qquad \text{(A. II. 25)}$$

In our previous attempt to allow for convection we essentially set the term H_c^1 to zero, and tried to iterate to a non-constant radiative flux $\mathcal{H} - H_c^o$. This failed and resulted in an oscillatory divergence of the error in the flux because, to first order, an increase in the radiative gradient increases the radiative flux and also the difference between the radiative gradient and the adiabatic gradients, hence also the convective flux. This positive feedback made the whole procedure unstable. For this reason it is essential to include the term H_c^1 explicitly.

We therefore write the Krook equations as

$$\tau_1'\left[\int_o^\infty H_\nu^o \, d\nu\right] + \tau_1\left[\int_o^\infty H_\nu^o \frac{\eta_\nu'}{\eta_\nu} \, d\nu\right] = H^o + H_c^o + H_c^1 - \mathcal{H} \qquad \text{(A. II. 26)}$$

and

$$\frac{d}{dt}\left[\mathcal{H} - H^o - H_c^o - H_c^1\right] = \sqrt{3}\,\frac{H^1(0)}{H^o(0)}\int_o^\infty \eta_\nu H_\nu(0)\, d\nu - T_1\int_o^\infty B_\nu(T_o)\eta_\nu \, d\nu$$

$$+ \tau_1\int_o^\infty \eta_\nu'(J_\nu^o - B_\nu)\, d\nu + \tau_1'\int_o^\infty \eta_\nu(J_\nu' - B_\nu)\, d\nu \qquad \text{(A. II. 27)}$$

The main change is to introduce expressions for H_c^1 in terms of τ_1 and T_1. Now

$$H_c = \frac{\rho(\ell/H)}{16\sqrt{2}}\,(gH)^{1/2}Q^{1/2}c_p T\,[\nabla - \nabla_A]^{3/2} = H_c^o + H_c^1 \qquad \text{(A. II. 28)}$$

Let us first determine the variations in $\left[\nabla-\nabla_A\right]^{3/2}$ due to changes τ_1 and T_1.

Let:

$$\begin{aligned} T &= T_o + T_1 \\ \tau &= t + \tau_1 \\ p_g &= p_g^o + \tau_1 p_g' \\ \kappa &= \kappa^o + \tau_1 \kappa' \\ \rho &= \rho_o + \tau_1 \rho' \\ g_* &= g_{\text{dynamical}} - \kappa \frac{dp_r}{d\tau} = g_*^o + g_*' \tau_1 \end{aligned} \qquad \text{(A. II. 29)}$$

where $'$ denotes d/dt, and $a \equiv \log_e 10$. We take λ as a separation parameter to be set to unity later after collecting terms of equal order in λ. By definition

$$\nabla \equiv \frac{d \log T}{d \log p_g} = \frac{d \log T}{d\tau} \cdot \frac{d\tau}{d \log p_g}$$

Consider first:

$$\begin{aligned} \frac{d \log T}{d\tau} &= \frac{1}{a} \frac{dT}{d\tau} \cdot \frac{1}{T} = \frac{1}{a} \cdot \frac{1}{(T_o + \lambda T_1)} \cdot \left(\frac{dT}{dt}\right) \cdot \left(\frac{dt}{d\tau}\right) \\ &= \frac{1}{a} \cdot \frac{1}{T_o} \cdot \frac{1}{\left(1 + \frac{\lambda T_1}{T_o}\right)} \left(\frac{dT_o}{dt} + \frac{\lambda dT_1}{dt}\right) \frac{1}{(1 + \lambda \tau_1')} \\ &= \frac{T_o'}{a T_o} \left(1 - \frac{\lambda T_1}{T_o} - \lambda \tau_1' + \frac{\lambda T_1'}{T_o'}\right) \end{aligned}$$

Therefore

$$\left(\frac{d \log T}{d\tau}\right) = \left(\frac{d \log T}{d\tau}\right)_o \left(1 - \frac{T_1}{T_o} - \tau_1' + \frac{T_1'}{T_o}\right) \qquad \text{(A. II. 30)}$$

Now consider

$$\frac{d \log p_g}{d\tau} = \frac{g_*}{a\kappa p_g}$$

$$= \frac{1}{a} \frac{g_*^o}{p_g^o \kappa^o} (1 + \lambda\tau_1 \frac{g_*'}{g_*^o}) \cdot \left(\frac{1}{1 + \lambda\tau_1 \frac{p_g'}{p_g}} \right) \cdot \left(\frac{1}{1 + \lambda\tau_1 \frac{\kappa'}{\kappa^o}} \right)$$

Therefore

$$\left(\frac{d \log p_g}{d\tau} \right) = \left(\frac{d \log p_g}{d\tau} \right)^o \left(1 + \lambda\tau_1 \frac{g_*'}{g_*} - \lambda\tau_1 \frac{p_g'}{p_g} - \lambda\tau_1 \frac{\kappa'}{\kappa^o}\right) \qquad \text{(A. II. 31)}$$

Combining A. II. 30 and A. II. 31 we have

$$\nabla = \nabla^o \quad 1 - \frac{T_1}{T_o} - \tau_1' + \frac{T_1'}{T_o'} + \tau_1 \left[\frac{\kappa'}{\kappa^o} + \frac{p_g'}{p_g^o} - \frac{g_*'}{g_*^o} \right] \qquad \text{(A. II. 32)}$$

Turning now to the adiabatic gradient:

$$\nabla_A = \nabla_A^o + \lambda T_1 \frac{\partial \nabla_A}{\partial T} + \lambda \tau_1 \nabla_A' \qquad \text{(A. II. 33)}$$

where the indicated derivatives may be computed numerically. Thus:

$$\nabla - \nabla_A = (\nabla - \nabla_A)^o + \nabla^o \left\{ \frac{T_1'}{T_o'} - \tau_1' - \frac{T_1}{T_o} + \tau_1 \left[\frac{\kappa'}{\kappa^o} + \frac{p_g'}{p_g^o} - \frac{g_*'}{g_*^o} \right] \right\}$$

$$- T_1 \left(\frac{\partial \nabla_A}{\partial T} \right) - \tau_1 \nabla_A'$$

and

$$(\nabla - \nabla_A)^{3/2} = (\nabla^o - \nabla_A^o)^{3/2}$$

$$\left\{ 1 + \frac{3}{2} \cdot \frac{\nabla_o \left[- \frac{T_1}{T_o} - \tau_1' + \frac{T_1'}{T_o'} + \tau_1 \left(\frac{\kappa'}{\kappa^o} + \frac{p_g'}{p_g^o} - \frac{g_*'}{g_*^o} \right) \right] - T_1 \left(\frac{\partial \nabla_A}{\partial T} \right) - \tau_1 \nabla_A'}{(\nabla - \nabla_A^o)} \right\}$$

(A. II. 34)

For brevity call the second term in the bracket ξ. We write now the additional expansion

$$c_p = c_p^o + \lambda \tau_1 c_p' + \lambda T_1 \frac{\partial c_p}{\partial T} = c_p^o + c_p^1$$

$$Q = Q_o + \lambda \tau_1 Q' + \lambda T_1 \frac{\partial Q}{\partial T} = Q_o + Q_1 \qquad \text{(A. II. 35)}$$

where again the indicated derivatives may be computed numerically. Now using A. II. 34 and A. II. 35 we find that

$$\frac{H_c}{H_c^o} = \frac{\rho' \tau_1}{\rho} + \frac{T_1}{T_o} + \frac{c_p^1}{c_p^o} + \frac{Q^1}{Q^o} + \xi \qquad \text{(A. II. 36)}$$

Finally, grouping terms to form the coefficients of the perturbations and multiplying by H_c^o/H^o we obtain:

$$\alpha(t) \equiv \frac{H_c^o}{H^o}$$

Coefficient of T_1:

$$\beta(t) = \frac{H_c^o}{H^o} \left\{ \frac{1}{T_o} + \frac{1}{c_p^o} \left(\frac{\partial c_p}{\partial T} \right) + \frac{1}{Q_o} \left(\frac{\partial Q}{\partial T} \right) + \frac{3}{2} \left[\frac{-\frac{\nabla_o}{T_o} - \frac{\partial \nabla_A}{\partial T}}{(\nabla^o - \nabla_A^o)} \right] \right\} \qquad \text{(A. II. 37)}$$

Coefficient of τ_1:

$$\gamma(t) = \frac{H_c^o}{H^o} \left\{ \frac{\rho'}{\rho^o} + \frac{c_p'}{c_p^o} + \frac{Q'}{Q_o} + \frac{3}{2} \cdot \frac{\nabla^o \left[\frac{\kappa'}{\kappa^o} + \frac{p_g'}{p_g^o} - \frac{g_*'}{g_*^o} \right] - \nabla_A'}{(\nabla^o - \nabla_A^o)} \right\} \qquad \text{(A. II. 38)}$$

Coefficient of T_1:

$$\delta(t) = \frac{H_c^o}{H^o}\left\{\frac{3}{2T_o'}\cdot\frac{\nabla^o}{\nabla^o - \nabla_A^o}\right\} \qquad \text{(A. II. 39)}$$

Coefficient of τ_1:

$$\epsilon(t) = \frac{H_c^o}{H^o}\left\{\frac{\nabla^o}{(\nabla^o - \nabla_A^o)}\right\} \qquad \text{(A. II. 40)}$$

Thus

$$\frac{H_c}{H^o} = \frac{H_c^o + H_c^1}{H^o} = \alpha(t) - \beta(t)T_1 + \gamma(t)\tau_1 + \delta(t)T_1' - \epsilon(t)\tau_1' \qquad \text{(A. II. 41)}$$

so that from equation A. II. 26 we obtain

$$(1+\epsilon(t))\tau_1' = \left[1 - \frac{\mathcal{H}}{H^o(t)} + \alpha(t)\right] + \beta(t)T_1 + \left[\gamma(t) - \int_o^\infty \frac{H_\nu^o}{H^o}\frac{\eta_\nu'}{\eta_\nu}\,d\nu\right]\tau_1 + \delta(t)T_1 \qquad \text{(A. II. 42)}$$

This is the first of our desired equations. To obtain a second equation we consider equation A. II. 27. Now in every case encountered so far we have $H_c^o(0) = 0$ and $H_c^1(0) = 0$, so that $H^1(0) = \mathcal{H} - H^o(0)$. Further, in order to obtain a solution, we are forced to make a bold approximation and set $dH_c^1/dt \equiv 0$. There is no <u>a priori</u> justification of this step, but if we do not allow this, the solution becomes extremely complicated. Thus tentatively we write:

$$\tau_1'\int_0^\infty \eta_\nu(J_\nu^o - B_\nu)d\nu + \tau_1\int_0^\infty \eta_\nu'(J_\nu^o - B_\nu)d\nu - T_1\int_0^\infty \dot{B}_\nu(T_o)\eta_\nu d\nu$$

$$= \sqrt{3}\left(1 - \frac{\mathcal{H}}{H^o(0)}\right)\int_0^\infty \eta_\nu H_\nu(0)d\nu - \frac{dH_c^o}{dt} - \int_0^\infty \eta_\nu(J_\nu - B_\nu)d\nu$$

(A. II. 43)

We have used in equation A. II. 43 the identity $\frac{dH^o}{dt} \equiv \int_0^\infty \eta_\nu(J_\nu^o - B_\nu)d\nu$ and it is understood that the derivative dH_c^o/dt is to be taken numerically.

To obtain the corrections τ_1 and T_1 we integrate the simultaneous equations A. II. 42 and A. II. 43, starting from the value of τ_1 and T_1 at the outer edge of the convective zone. It is not evident at present whether some of the terms in these equations might be negligible. In any case, there is no difficulty, in principle, of effecting the integration by standard numerical methods. At the inner edge of the convective zone, we return to the usual Krook equations, although there is no formal difference in the two sets of equations if we set $\alpha(t)$, $\beta(t)$, ..., $\eta(t)$, $dH_c^o/dt \equiv 0$ outside the convective zone. It may, however, be expedient computationally to consider the two zones separately. It may be noted that although we have set the source function $s_\nu \equiv B_\nu$, we may include the effects of scattering in the continuum simply by introducing terms in ρ_ν and ρ_ν' as was done in chapter II.

APPENDIX III

DAMPING CONSTANTS FOR LINES IN ANGSTROMS

θ	L_α	L_β	L_γ	L_δ	L_ϵ	L_y
0.04	1.301-4	6.996-5	5.502-5	4.881-5	4.559-5	4.368-5
0.05	9.824-5	5.075-5	3.916-5	3.437-5	3.189-5	3.043-5
0.06	7.783-5	3.849-5	2.906-5	2.520-5	2.321-5	2.204-5
0.07	6.395-5	3.017-5	2.224-5	1.902-5	1.737-5	1.640-5
0.08	5.409-5	2.428-5	1.744-5	1.469-5	1.328-5	1.245-5
0.09	4.687-5	1.998-5	1.395-5	1.155-5	1.033-5	9.614-6
0.10	4.146-5	1.677-5	1.136-5	9.233-6	8.154-6	7.523-6
0.11	3.733-5	1.433-5	9.406-6	7.490-6	6.523-6	5.961-6
0.12	3.413-5	1.244-5	7.906-6	6.160-6	5.285-6	4.777-6
0.13	3.162-5	1.096-5	6.742-6	5.136-6	4.335-6	3.872-6
0.14	2.962-5	9.793-6	5.828-6	4.338-6	3.599-6	3.173-6
0.15	2.801-5	8.854-6	5.105-6	3.711-6	3.024-6	2.629-6
0.16	2.671-5	8.096-6	4.527-6	3.215-6	2.572-6	2.204-6
0.17	2.565-5	7.477-6	4.062-6	2.819-6	2.214-6	1.868-6
0.18	2.477-5	6.967-6	3.683-6	2.501-6	1.928-6	1.603-6
0.19	2.404-5	6.543-6	3.373-6	2.243-6	1.699-6	1.391-6
0.20	2.343-5	6.188-6	3.117-6	2.033-6	1.514-6	1.221-6
0.22	2.248-5	5.631-6	2.724-6	1.717-6	1.240-6	9.728-7
0.24	2.177-5	5.219-6	2.442-6	1.497-6	1.054-6	8.068-7
0.26	2.124-5	4.905-6	2.232-6	1.338-6	9.229-7	6.925-7
0.28	2.083-5	4.657-6	2.071-6	1.219-6	8.274-7	6.112-7
0.30	2.049-5	4.457-6	1.943-6	1.127-6	7.554-7	5.514-7
0.32	2.023-5	4.292-6	1.839-6	1.053-6	6.992-7	5.058-7
0.34	2.000-5	4.152-6	1.752-6	9.935-7	6.540-7	4.698-7
0.36	1.981-5	4.032-6	1.678-6	9.428-7	6.165-7	4.405-7
0.38	1.965-5	3.928-6	1.614-6	8.992-7	5.847-7	4.160-7
0.40	1.952-5	3.837-6	1.557-6	8.612-7	5.573-7	3.950-7
0.42	1.940-5	3.756-6	1.507-6	8.276-7	5.331-7	3.767-7
0.44	1.929-5	3.684-6	1.462-6	7.975-7	5.116-7	3.604-7
0.46	1.920-5	3.619-6	1.421-6	7.704-7	4.922-7	3.459-7
0.48	1.912-5	3.561-6	1.385-6	7.457-7	4.746-7	3.327-7
0.50	1.905-5	3.508-6	1.351-6	7.232-7	4.586-7	3.207-7
0.52	1.899-5	3.460-6	1.320-6	7.025-7	4.439-7	3.097-7
0.54	1.893-5	3.416-6	1.292-6	6.835-7	4.303-7	2.996-7
0.56	1.888-5	3.376-6	1.266-6	6.658-7	4.177-7	2.902-7
0.58	1.884-5	3.339-6	1.241-6	6.495-7	4.061-7	2.815-7
0.60	1.879-5	3.305-6	1.219-6	6.342-7	3.952-7	2.734-7
0.65	1.871-5	3.232-6	1.169-6	6.004-7	3.710-7	2.553-7
0.70	1.865-5	3.171-6	1.127-6	5.716-7	3.504-7	2.399-7
0.75	1.860-5	3.121-6	1.091-6	5.467-7	3.325-7	2.266-7
0.80	1.856-5	3.079-6	1.060-6	5.251-7	3.170-7	2.149-7
0.85	1.853-5	3.043-6	1.033-6	5.062-7	3.033-7	2.046-7
0.90	1.851-5	3.013-6	1.009-6	4.894-7	2.912-7	1.955-7
0.95	1.849-5	2.987-6	9.883-7	4.745-7	2.803-7	1.874-7
1.00	1.847-5	2.964-6	9.696-7	4.612-7	2.706-7	1.801-7

θ	H_α	H_β	H_γ	H_δ	H_ϵ
0.04	2.673-3	1.270-3	9.362-4	7.976-4	7.249-4
0.05	2.203-3	1.047-3	7.729-4	6.592-4	6.996-4
0.06	1.893-3	9.006-4	6.654-4	5.682-4	5.172-4
0.07	1.675-3	7.971-4	5.898-4	5.041-1	4.593-4
0.08	1.513-3	7.208-4	5.340-4	4.569-4	4.167-4
0.09	1.390-3	6.624-4	4.914-4	4.209-4	3.841-4
0.10	1.293-3	6.165-4	4.580-4	3.927-4	3.587-4
0.11	1.215-3	5.798-4	4.312-4	3.702-4	3.383-4
0.12	1.151-3	5.497-4	4.094-4	3.518-4	3.218-4
0.13	1.098-3	5.248-4	3.913-4	3.366-4	3.081-4
0.14	1.053-3	5.038-4	3.761-4	3.238-4	2.966-4
0.15	1.016-3	4.861-4	3.633-4	3.130-4	2.869-4
0.16	9.834-4	4.708-4	3.523-4	3.038-4	2.786-4
0.17	9.552-4	4.576-4	3.428-4	2.958-4	2.715-4
0.18	9.306-4	4.461-4	3.345-4	2.889-4	2.653-4
0.19	9.089-4	4.360-4	3.272-4	2.828-4	2.598-4
0.20	8.897-4	4.270-4	3.208-4	2.775-4	2.550-4
0.22	8.573-4	4.119-4	3.100-4	2.685-4	2.470-4
0.24	8.311-4	3.997-4	3.013-4	2.613-4	2.405-4
0.26	8.094-4	3.897-4	2.941-4	2.553-4	2.353-4
0.28	7.914-4	3.813-4	2.882-4	2.504-4	2.309-4
0.30	7.761-4	3.742-4	2.832-4	2.463-4	2.272-4
0.32	7.631-4	3.682-4	2.789-4	2.428-4	2.241-4
0.34	7.518-4	3.630-4	2.752-4	2.397-4	2.214-4
0.36	7.420-4	3.585-4	2.720-4	2.371-4	2.191-4
0.38	7.335-4	3.545-4	2.692-4	2.348-4	2.171-4
0.40	7.260-4	3.510-4	2.668-4	2.328-4	2.153-4
0.42	7.193-4	3.479-4	2.646-4	2.311-4	2.138-4
0.44	7.134-4	3.452-4	2.627-4	2.295-4	2.124-4
0.46	7.082-4	3.427-4	2.610-4	2.281-4	2.112-4
0.48	7.035-4	3.406-4	2.595-4	2.269-4	2.101-4
0.50	6.992-4	3.386-4	2.581-4	2.258-4	2.091-4
0.52	6.954-4	3.368-4	2.569-4	2.248-4	2.082-4
0.54	6.920-4	3.352-4	2.557-4	2.239-4	2.075-4
0.56	6.889-4	3.337-4	2.547-4	2.231-4	2.068-4
0.58	6.861-4	3.324-4	2.538-4	2.223-4	2.061-4
0.60	6.835-4	3.312-4	2.530-4	2.217-4	2.055-4
0.65	6.781-4	3.287-4	2.512-4	2.202-4	2.043-4
0.70	6.738-4	3.266-4	2.498-4	2.191-4	2.034-4
0.75	6.703-4	3.249-4	2.487-4	2.182-4	2.026-4
0.80	6.674-4	3.235-4	2.477-4	2.175-4	2.020-4
0.85	6.651-4	3.223-4	2.469-4	2.169-4	2.015-4
0.90	6.632-4	3.214-4	2.463-4	2.164-4	2.011-4
0.95	6.616-4	3.205-4	2.457-4	2.160-4	2.007-4
1.00	6.602-4	3.198-4	2.453-4	2.156-4	2.004-4

θ	P_α	P_β	P_γ	P_δ
0.04	1.131-2	4.620-3	3.090-3	2.466-3
0.05	9.167-3	3.742-3	2.504-3	1.999-3
0.06	7.741-3	3.159-3	2.115-3	1.689-3
0.07	6.726-3	2.744-3	1.838-3	1.468-3
0.08	5.967-3	2.434-3	1.631-3	1.303-3
0.09	5.380-3	2.194-3	1.470-3	1.176-3
0.10	4.912-3	2.003-3	1.343-3	1.074-3
0.11	4.530-3	1.847-3	1.239-3	9.917-4
0.12	4.214-3	1.717-3	1.152-3	9.230-4
0.13	3.947-3	1.608-3	1.080-3	8.652-4
0.14	3.720-3	1.515-3	1.018-3	8.159-4
0.15	3.523-3	1.435-3	9.645-4	7.733-4
0.16	3.352-3	1.365-3	9.178-4	7.362-4
0.17	3.202-3	1.304-3	8.768-4	7.036-4
0.18	3.068-3	1.249-3	8.405-4	6.748-4
0.19	2.949-3	1.201-3	8.081-4	6.491-4
0.20	2.843-3	1.157-3	7.791-4	6.260-4
0.22	2.660-3	1.082-3	7.292-4	5.864-4
0.24	2.508-3	1.020-3	6.880-4	5.537-4
0.26	2.381-3	9.685-4	6.533-4	5.262-4
0.28	2.272-3	9.242-4	6.238-4	5.027-4
0.30	2.179-3	8.860-4	5.984-4	4.826-4
0.32	2.098-3	8.528-4	5.763-4	4.651-4
0.34	2.027-3	8.238-4	5.570-4	4.498-4
0.36	1.964-3	7.981-4	5.400-4	4.363-4
0.38	1.909-3	7.754-4	5.249-4	4.244-4
0.40	1.859-3	7.551-4	5.114-4	4.137-4
0.42	1.814-3	7.369-4	4.993-4	4.041-4
0.44	1.774-3	7.205-4	4.884-4	3.955-4
0.46	1.738-3	7.056-4	4.785-4	3.877-4
0.48	1.705-3	6.921-4	4.696-4	3.807-4
0.50	1.675-3	6.798-4	4.615-4	3.742-4
0.52	1.648-3	6.686-4	4.540-4	3.684-4
0.54	1.622-3	6.583-4	4.472-4	3.630-4
0.56	1.599-3	6.488-4	4.410-4	3.581-4
0.58	1.578-3	6.401-4	4.352-4	3.535-4
0.60	1.558-3	6.321-4	4.299-4	3.493-4
0.65	1.515-3	6.144-4	4.182-4	3.402-4
0.70	1.479-3	5.997-4	4.085-4	3.326-4
0.75	1.449-3	5.873-4	4.004-4	3.262-4
0.80	1.423-3	5.768-4	3.935-4	3.208-4
0.85	1.401-3	5.678-4	3.875-4	3.161-4
0.90	1.382-3	5.600-4	3.824-4	3.122-4
0.95	1.366-3	5.532-4	3.780-4	3.087-4
1.00	1.352-3	5.473-4	3.741-4	3.057-4

RADIATIVE DAMPING CONSTANTS FOR HYDROGEN

Table Gives Full Half-Width Gamma In Ordinary Frequency Units

θ	n = 1	2	3	4	5	6	7
0.04	1.742-9	1.575-9	7.625-8	4.490-8	2.962-8	2.101-8	1.569-8
0.05	1.197-9	1.306-9	6.196-8	3.621-8	2.380-8	1.686-8	1.257-8
0.06	8.535-8	1.130-9	5.248-8	3.042-8	1.993-8	1.409-8	1.050-8
0.07	6.230-8	1.007-9	4.573-8	2.629-8	1.716-8	1.211-8	9.018-7
0.08	4.626-8	9.163-8	4.070-8	2.320-8	1.505-8	1.063-8	7.906-7
0.09	3.476-8	8.473-8	3.680-8	2.080-8	1.348-8	9.481-7	7.043-7
0.10	2.636-8	7.934-8	3.370-8	1.889-8	1.219-8	8.560-7	6.352-7
0.11	2.013-8	7.504-8	3.118-8	1.733-8	1.114-8	7.807-7	5.787-7
0.12	1.546-8	7.155-8	2.910-8	1.603-8	1.027-8	7.180-7	5.316-7
0.13	1.192-8	6.868-8	2.734-8	1.493-8	9.529-7	6.649-7	4.918-7
0.14	9.222-7	6.628-8	2.584-8	1.399-8	8.895-7	6.195-7	4.576-7
0.15	7.154-7	6.426-8	2.455-8	1.318-8	8.346-7	5.801-7	4.281-7
0.16	5.562-7	6.254-8	2.342-8	1.247-8	7.867-7	5.457-7	4.002-7
0.17	4.332-7	6.106-8	2.244-8	1.184-8	7.444-7	5.153-7	3.794-7
0.18	3.379-7	5.978-8	2.156-8	1.129-8	7.068-7	4.883-7	3.592-7
0.19	2.639-7	5.866-8	2.079-8	1.079-8	6.732-7	4.642-7	3.410-7
0.20	2.063-7	5.768-8	2.009-8	1.035-8	6.430-7	4.425-7	3.247-7
0.22	1.264-7	5.604-8	1.890-8	9.587-7	5.909-7	4.050-7	2.965-7
0.24	7.773-6	5.474-8	1.791-7	8.951-7	5.476-7	3.738-7	2.731-7
0.26	4.788-6	5.368-8	1.708-8	8.414-7	5.109-7	3.474-7	2.532-7
0.28	2.954-6	5.280-8	1.638-8	7.955-7	4.796-7	3.248-7	2.362-7
0.30	1.826-6	5.207-8	1.578-8	7.559-7	4.525-7	3.053-7	2.215-7
0.32	1.130-6	5.145-8	1.525-8	7.214-7	4.288-7	2.882-7	2.086-7
0.34	6.999-5	5.092-8	1.479-8	6.910-7	4.079-7	2.731-7	1.973-7
0.36	4.340-5	5.047-8	1.439-8	6.641-7	3.894-7	2.597-7	1.872-7
0.38	2.693-5	5.008-8	1.404-8	6.402-7	3.729-7	2.478-7	1.782-7
0.40	1.672-5	4.974-8	1.372-8	6.187-7	3.580-7	2.370-7	1.701-7
0.42	1.039-5	4.944-8	1.344-8	5.993-7	3.446-7	2.273-7	1.627-7
0.44	6.462-4	4.918-8	1.318-8	5.818-7	3.324-7	2.185-7	1.561-7
0.46	4.020-4	4.895-8	1.295-8	5.659-7	3.213-7	2.104-7	1.500-7
0.48	2.502-4	4.875-8	1.275-8	5.514-7	3.112-7	2.030-7	1.444-7
0.50	1.558-4	4.857-8	1.256-8	5.381-7	3.019-7	1.963-7	1.393-7
0.52	9.705-3	4.841-8	1.239-8	5.259-7	2.933-7	1.900-7	1.346-7
0.54	6.048-3	4.826-8	1.223-8	5.146-7	2.854-7	1.842-7	1.302-7
0.56	3.769-3	4.813-8	1.209-8	5.042-7	2.780-7	1.789-7	1.262-7
0.58	2.350-3	4.802-8	1.195-8	4.945-7	2.712-7	1.739-7	1.224-7
0.60	1.466-3	4.792-8	1.183-8	4.856-7	2.648-7	1.692-7	1.189-7
0.65	4.507-2	4.771-8	1.157-8	4.658-7	2.507-7	1.589-7	1.110-7
0.70	1.387-2	4.754-8	1.135-8	4.490-7	2.387-7	1.501-7	1.043-7
0.75	4.275-1	4.742-8	1.117-8	4.346-7	2.283-7	1.424-7	9.854-6
0.80	1.318-1	4.732-8	1.102-8	4.222-7	2.193-7	1.358-7	9.347-6
0.85	4.066-0	4.724-8	1.089-8	4.114-7	2.114-7	1.299-7	8.900-6
0.90	1.255-0	4.718-8	1.079-8	4.020-7	2.044-7	1.247-7	8.504-6
0.95	3.874-1	4.714-8	1.069-8	3.936-7	1.982-7	1.201-7	8.150-6
1.00	1.196-1	4.710-8	1.061-8	3.862-7	1.926-7	1.159-7	7.832-6

Appendix IV

COMPUTATIONAL DETAILS

In this appendix we give the details of computation of the pressures and opacities.

(a) Gas pressure

Let

$a_i = N_i / N_H$, the abundance of element i relative to hydrogen

$f_{i,j}$ = the fraction of element i in ionization state j (j = 1 for single ionizations, etc.)

then:

$$\frac{N_a}{N_A} = \frac{\sum_i a_i \left(\sum_j j \cdot f_{i,j} \right)}{\sum_i a_i} \qquad \text{(A.IV.1)}$$

so that

$$\log p_g = \log p_e + \log \left\{ 1 + \frac{\sum_i a_i}{\sum_i a_i \sum_j j \cdot f_{i,j}} \right\} \qquad \text{(A.IV.2)}$$

We sum over H, He, and eleven other elements. Two ionization potentials are allowed for helium, and up to two for the other elements. Thus we have

$$f_{j,i} = \frac{\left(\frac{N_{j,i}}{N_{1,i}} \right)}{1 + \left(\frac{N_{2,i}}{N_{1,i}} \right) + \left(\frac{N_{3,i}}{N_{2,i}} \right) \cdot \left(\frac{N_{2,i}}{N_{1,i}} \right)} \qquad \text{(A.IV.3)}$$

Now from Saha's equation,

$$\log \frac{N_{j+1}}{N_j} = -\theta\chi_j - \log p_e - 2.5 \log \theta + \log \left(\frac{2B_{j+1}(\theta, p_e)}{B_j(\theta, p_e)}\right) + 8.778 \qquad \text{(A.IV.4)}$$

where

$\theta = 5040/T$

χ_j = ionization potential (in e.v.) of the element in ionization state j

$B_j(\theta, p_e)$ = the partition function of ionization state j

$$= \sum_{\ell} g_\ell e^{-\chi_\ell/kT} W_\ell(\theta, p_e) \qquad \text{(A.IV.5)}$$

where in turn

χ_ℓ = excitation of energy level ℓ of state j

g_ℓ = statistical weight of energy level ℓ

$W_\ell(\theta, p_e)$ = probability that an atom in energy state ℓ of state j is unperturbed.

In practice the partition functions of H and He are interpolated from tables stored in the memory of the computer. These tables were computed on the basis of the perturbation theory of de Jager and Neven (1960). This theory assumes the atoms are perturbed by the linear Stark effect, and while it is not a definitive theory (except possibly for hydrogen), it was felt that it might be more quantitative than the semi-classical arguments used in the past (Unsöld, 1948, 1955). A criticism of the theory has been advanced by Zwaan (1960). The newer and older theories give

quite different results at very high temperatures, but are not too terribly different at most temperatures (see also the remarks of Leftus, 1962). It should be noted, however, that for the hottest models to be presented, the ionization equilibrium for H and He differs substantially from the results of previous authors (e.g. Underhill, 1951a, 1957; Traving, 1956; Saito, 1954, 1959) who have not taken the partition functions into account.

de Jager and Neven give log W as a function of $v = \frac{2}{3} \log N_{perturber} + 4 \log n$, and W may be determined by direct interpolation for $v \leq 16.2$, while for $v \geq 16.2$, the asymptotic relation $\log W = 14.69 - v$ is valid. In the computations we assume the most important perturbations result from interactions with protons and electrons, so that $N_{perturber} = 2N_e = 2p_e/kT$. For hydrogen $g_n = 2n^2$, and $\chi_n = \chi_{ion} - \frac{Z^2 R}{n^2}$ so that the sum

$$\sum_{n=1}^{\infty} g_n W_n N e^{-\chi_n/kT} = 2e^{-\chi_{ion}/kT} \sum_{n=1}^{\infty} n^2 e^{-RZ^2/n^2 kT} W_n(N) \qquad \text{(A.IV.6)}$$

The sum was performed directly until $n/Z = 15$, at which point the term $\exp(-RZ^2/n^2kT)$ was set = 1, and the sum approximated simply by an integral. The computation of the integral was facilitated by fitting $\log W_n(N)$ by a series of straight line segments such that $\log W^* = a + bv$ for $v_1 \leq v \leq v_2$. This range of $[v_1, v_2]$ corresponds to some range $[n_1, n_2]$ such that $n_j = \text{antilog}\left(\frac{1}{4}\left(-\frac{2}{3}\log N + v_j\right)\right)$. Thus on the range $[n_1, n_2]$ we have a contribution to the partition

function of

$$2e^{-\chi_{ion}/kT} \int_{n_1}^{n_2} n^2 \, 10^{(a+\frac{2}{3}h \log N)} \, n^{4h} dn$$

$$= 2e^{-\chi_{ion}/kT} \cdot 10^{a} N^{2h/3} \left| \frac{n^{4h+3}}{4h+3} \right|_{n_1}^{n_2} \qquad \text{(A.IV.7)}$$

Thus the sum $\sum_{15Z}^{\infty} = \int_{15Z}^{\infty}$ is quite easily evaluated. For neutral helium, the sum over the lower non-hydrogenic terms was carried out directly using the term values given by Miss C. E. Moore (1948). Higher terms were added in by the hydrogenic approximation as described above. This procedure should be valid since the ℓ states of a given n level have the highest statistical weights for the nearly hydrogenic states. Some lower terms were estimated by finding the defect Δ in the formula $T_n = T_\infty - Z^2R/(n+\Delta)^2$ for low lying terms, and then extrapolating up a series.

The partition functions for the other eleven elements are taken from Aller's book (1953, p. 78). The abundances of the elements are taken from the work of Goldberg, Müller, and Aller (1960). Strictly speaking we should use accurate partition functions for the metals when computing the gas pressures, but in practice this is too laborious. Furthermore, the moment that hydrogen begins to ionize even slightly, its contribution to the electron pressure outweighs that of the metals. In any case the pressures are fairly insensitive to the assumed values of the partition functions. The assumed metallic partition functions and the relative abundances are collected in table A.IV.1. The metal abundances are usually set equal to the solar abundances (as is the case

Table A.IV.1

PARAMETERS FOR COMPUTATION OF GAS PRESSURES

Element	log N	a_i	I.P.	$\log \frac{2B_1}{B_o}$	A_i
H	12.00	1.00	13.595	-	1.008
He	-		24.580	-	4.003
C	8.72	5.3×10^{-4}	11.264	0.10	12.01
N	7.98	9.6×10^{-5}	14.54	0.62	14.008
O	8.96	9.1×10^{-4}	13.614	-0.05	16.000
Na	6.30	2.0×10^{-6}	5.138	-0.16	23.000
Mg	7.40	2.5×10^{-5}	7.644	0.52	24.32
Al	6.20	1.6×10^{-6}	5.984	-0.50	26.98
Si	7.50	3.2×10^{-5}	8.149	0.06	28.09
S	7.30	2.0×10^{-5}	10.357	0.01	32.07
Ca	6.15	1.4×10^{-6}	6.111	0.44	40.08
Fe	6.57	3.7×10^{-6}	7.90	0.40	55.85
Ni	5.91	8.1×10^{-7}	7.633	-0.12	58.71

The helium abundance is specified explicitly for each model.

$\sum a_i$ for metal = 0.001623.

for all of the results given later), but may be set to any chosen multiple of this value.

In certain pressure-temperature regions the presence of H_2 and H_2^+ molecules significantly affect the hydrogen ionization equilibrium. Such effects are included when important, following Vardya (1960, 1961). Fits to Vardya's tables are used to make a rough first estimate of the concentration of H_2 and H_2^+, and the final equilibrium is determined by a simple iteration process.

(b) The opacity

1. Neutral H

Let $x = 1/\lambda$ where λ is in microns. Then per neutral H atom:

$$a_\nu = \frac{2.08975 \times 10^{-14}}{x^3 B_o(\theta, p_e)} \left\{ \sum_{n=n_o}^{12} g_{bf}(x,n) \frac{e^{-31.30364 \cdot \theta \cdot (1-1/n^2)}}{n^3} + \frac{e^{-31.30364\theta}}{62.60729\theta} \left[e^{\frac{31.30364\theta}{n^{*2}}} + g_{ff}(x,\theta) - 1 \right] \right\} (1 - e^{-h_\nu/kT}) \qquad \text{(A. IV. 8)}$$

The summation in equation A. IV. 8 is the sum over all bound-free continua contributing at the frequency under consideration, that is, n_o is chosen to correspond to the first absorption edge lying redward of this frequency. The sum is always carried out over the first 12 levels. Following Unsöld (1955) the sum is replaced by an integral over all higher levels; to this is added the contribution from free-free absorptions. The result is the second term in equation A. IV. 8 in which we set

$n^* = 12.5$. The bound-free gaunt factors $g_{bf}(x, n)$ are interpolated from tables given by Karzas and Latter (1960) for $n \leq 7$. For $n \geq 8$, g_{bf} is simply set = 1. The free-free gaunt factor $g_{ff}(x, \theta)$ is interpolated from tables given by Berger (1956) for $0.0434 \leq \theta \leq 0.8686$; if θ lies outside this range it is assumed to have the closest tabular value (i.e. either 0.0434 or 0.8686). The wavelength range for Berger's tables is $500 \leq \lambda \leq 10,000$ A. If λ lies outside this range it is again set equal to the nearest tabular value. The errors made in this way are negligible.

2. Negative hydrogen ion

The very convenient interpolating function given by Gingerich (1961), corrected for typographical errors, is used. This formula includes the effects of stimulated emission; Gingerich estimates a numerical accuracy of $\pm \frac{1}{2}$ % for it. Since the partition function of hydrogren was not accounted for by Gingerich, the absorption coefficient is multiplies by $2/B_o(\theta, p_e)$ before adding it to the hydrogenic absorption coefficient.

3. Nuetral He

The absorption edges arising from the lowest terms are computed using the best opacity formulae available. We allow explicitly for the $1\,^1S - \kappa\,^1P$, $2\,^3S - \kappa\,^3P$, and $2\,^1S - \kappa\,^1P$ edges as computed by S. S. Huang (1948); the $2\,^1P - \kappa\,^1D$ and $2\,^3P - \kappa\,^3D$ edges as given graphically by L. Goldberg (1939); and the $2\,^3P - \kappa\,^3S$ and $2\,^1P - \kappa\,^1S$ edges as given approximately by Ueno (1954). The higher levels are

treated in the hydrogenic approximation as discussed by Münch (1960), Ueno (1954), and Ueno, Saito, and Jugaku (1954).

To speed the computation, approximate analytical fits to the results cited above were made. These fits are good so long as helium is not the most abundant constituent of the atmosphere. For a pure helium atmosphere, one might wish to take greater care in computing these cross sections. In the present models, the only neutral He edge of importance is from the ground state, which gives an edge at λ 504.

Again defining $x = 1/\lambda$ where λ is in microns, we obtain for the absorption coefficient per atom in the lower state specified:

$1\,^1S - \kappa\,^1P$:

$$a_\nu = 10^{-18}\left[0.06156 - \frac{26.3709}{x} + \frac{3984.53}{x^2}\right] \quad \text{for } x \geq 33.3333 \tag{A.IV.9}$$

$$a_\nu = 10^{-18}\left[-4.0566 + \frac{230.0538}{x}\right] \quad \text{for } 19.8305 \leq x \leq 33.3333 \tag{A.IV.10}$$

$2\,^3S - \kappa\,^3P$:

$$a_\nu = 10^{-18}\left[-1.5639099 + \frac{31.780372}{x} - \frac{59.73594}{x^2}\right]$$

$$\text{for } 3.845468 \leq 6.6666667 \tag{A.IV.11}$$

$$a_\nu = 10^{-18}\left[-0.563994 + \frac{16.272744}{x}\right] \quad \text{for } 6.6666667 \leq x \leq 13.426423 \tag{A.IV.12}$$

$$a_\nu = 10^{-18}\left[-0.03308745 + \frac{1.429452}{x} + \frac{96.022659}{x^2}\right]$$

$$\text{for } 13.426423 \leq x \tag{A.IV.13}$$

$2\,^1S - \kappa\,^1P$:

$$a_\nu = 10^{-18}\left[-4.21036 + \frac{46.855739}{x}\right] \quad \text{for } 3.20333 \leq x \leq 6.6666667 \tag{A.IV.14}$$

$$a_\nu = 10^{-18}\left[-0.494206 + \frac{9.9570129}{x} + \frac{80.829072}{x^2}\right] \quad \text{for } 6.6666667 \tag{A.IV.15}$$

Some of the formulae given above can go negative, but only when the absorption is infinitesimal anyway; a test is made for this and they are set to zero when it occurs (the total mass absorption coefficient will already be dominated by the contribution from some other atom or by scattering terms so this is of no importance in practice). Now letting $xx = \log_{10} x$ we have,

$2\,^1P - \kappa\,^1D$:

$$a_\nu = \exp\left[-2.3025851 \cdot (15.4351 + 3.4727 \cdot xx)\right] \tag{A.IV.16}$$

$2\,^3P - \kappa\,^3D$:

$$a_\nu = \exp\left[-2.3025851 \cdot (16.12903 + 0.67124 \cdot xx + 1.6735\, xx^2)\right] \tag{A.IV.17}$$

$2\,^3P - \kappa\,^3S$:

$$a_\nu = \exp\left[-2.3025851 \cdot (16.575272 + 3.3 \cdot xx)\right] \tag{A.IV.18}$$

$2\,^1P - \kappa\,^1S$:

$$a_\nu = \exp\left[-2.3025851 \cdot (16.6304 + 3.6 \cdot xx)\right] \tag{A.IV.19}$$

The term values and statistical weights necessary for the excitation equilibrium calculations are taken from the tables of atomic energy

levels by Miss C. E. Moore (1948). All levels with principal quantum number ≥ 3 are considered in the hydrogenic approximation with appropriate statistical weights. As in the case of H, all necessary partition functions are interpolated from tables stored in the memory of the computer.

4. Ionized He

The absorption coefficient for ionized helium is given by a hydrogenic formula; in the present computations the summation was carried out over all terms with $n \leq 15$, and the gaunt factors are set to unity.

5. H_2^+

The absorption coefficient of H_2^+ is most conveniently obtained from the emission coefficient, using the relationship $\kappa_\nu = \dot{j}\nu / B_\nu(T)$, valid in LTE. The emission coefficient may be found from the work of Bates (1952), Buckingham, Reid, and Spence (1952), and Boggess (1959). It is conveniently written in the form $\dot{j}\nu = 10^{(c'+d\cdot\theta)} N_H N_{H^+}$. Now

$$N_H N_{H^+} = f_1 f_2 N^2$$

where $N^2 = (\rho/\mu' m_H)^2$ and f_1 and f_2 are respectively the ionization fractions of H and H^+. μ' is defined in equation 2.19. Therefore,

$$\kappa_\nu \text{ (per gram of stellar material)} = \rho \cdot \frac{10^{(c+d\cdot\theta)}}{B_\nu(T)\cdot(\mu')^2} \qquad \text{(A.IV.20)}$$

The coefficients c and d are given in table A.IV.2; $B_\nu(T)$ is available from other computations, so this calculation is quite simple

Table A.IV.2

PARAMETERS FOR THE COMPUTATION OF THE H_2^+ ABSORPTION COEFFICIENT

x	C	D	x	C	D
0.05	1.821	-0.01917	1.0	4.817	-0.595
0.10	2.556	-0.04473	1.11111	4.915	-0.671
0.15	2.981	-0.07137	1.25	5.013	-0.766
0.20	3.275	-0.09884	1.42857	5.127	-0.893
0.25	3.499	-0.1268	1.66667	5.243	-1.067
0.30	3.684	-0.1544	2.0	5.395	-1.319
0.35	3.836	-0.1845	2.5	5.551	-1.716
0.40	3.967	-0.2138	3.33333	5.751	-2.424
0.50	4.182	-0.2738	4.0	5.863	-3.020
0.60	4.356	-0.3354	5.0	5.989	-3.976
0.70	4.499	-0.3985	6.66666	6.099	-5.708
0.80	4.611	-0.4626	10.0	6.289	-9.606
0.90	4.727	-0.5280	20.0	6.235	-26.70
1.0	4.817	-0.5946	32.916	-	$-\infty$

and quick. The stimulated emission is included.

The scattering coefficient is considered to be the sum of the following two contributions:

6. Thompson scattering from free electrons

The scattering coefficient from free electrons is independent of the frequency of the radiation scattered. The cross section per electron is $\sigma_T = 6.655 \times 10^{-25}$ cm^2, so that the mass absorption coefficient is given by $\sigma_e = \sigma_T N_e$ where N_e here is taken to be the number of free electrons per gram of stellar material. Writing

$$N_e = \frac{n_e(\text{electrons/cm}^3)}{N_{\text{atoms}}(\text{per cm}^3)} \times N_{\text{atoms}}(\text{per gm of stellar material})$$

we easily find the first term in the product is given by $p_e/(p_g - p_e)$ while the second term is simply $1/(\mu m_H)$ where μ was defined in equation 2.13. Thus

$$\sigma_e = \frac{6.655 \times 10^{-25}}{\mu m_H} \times \frac{1}{(p_g/p_e)-1} \qquad \text{(A. IV. 21)}$$

7. Rayleigh scattering from neutral hydrogen

When a photon interacts with an atom having a transition between energy levels whose characteristic frequency is much higher than that of the photon, the photon undergoes Rayleigh scattering. The calculation of the scattering cross section follows directly from the dispersion profile of a classical oscillator in the limit mentioned above. When more than one transition is possible we may sum over all such scattering cross sections weighting each by the appropriate f values of the

transitions. In the present calculations this sum was approximated by allowing a transition of f-value 0.42 at the position of L_α ($x = 8.23$) and a "synthetic" transition of f-value 0.58 at the Lyman continuum edge ($x = 10.97$). Using the results for the cross section of a classical oscillator (e.g. Aller, 1953, p. 113 ff.) we find:

$$\sigma_R(x) \text{ (per gram of stellar material)} = \frac{f_H \sigma_T}{\mu m_H} \left[\frac{0.42}{(1 - (\frac{8.23}{x})^2)^2} + \frac{0.58}{(1 - (\frac{10.97}{x})^2)^2} \right] \qquad \text{(A.IV.22)}$$

where f_H = fraction of H in ground state = (fraction of neutral H) x $(2/B_o, \theta, p_e))$. To avoid the obvious singularities of this function, we set $\sigma(x) = \sigma(5.84)$ for $x \geq 5.84$, and $\sigma(x) = 0$ beyond the Lyman limit ($x = 10.97$). The latter condition is clearly necessary from physical considerations. The former condition was chosen so that L_α was located half-way between the Lyman edge and the cut-off of the dispersion formula. Hence we have essentially taken care of the "far wings" of the Lyman lines; a more detailed treatment is needed for the actual region of formation of the Lyman lines.

APPENDIX V

Hβ PROFILES

Table Gives Residual Fluxes, Unit of Flux, and Equivalent Width

The Blending with the Overlapping Pickering Series Is Included

θ e / log ε	.101 4	.14 4	.14* 4	.14 3.5	.157 4
Δλ(Å)					
-15	0.996	0.991	0.992	0.997	0.985
-10	0.989	0.978	0.981	0.993	0.967
-8.0	0.982	0.967	0.970	0.988	0.951
-6.0	0.965	0.945	0.952	0.976	0.925
-4.0	0.920	0.902	0.915	0.941	0.880
-3.25	0.888	0.877	0.893	0.910	0.859
-3.00	0.873	0.863	0.881	0.890	0.846
-2.75	0.856	0.848	0.868	0.866	0.833
-2.30	0.827	0.818	0.846	0.808	0.824
-2.15	0.823	0.810	0.838	0.799	0.811
-2.00	0.826	0.811	0.835	0.806	0.799
-1.75	0.841	0.817	0.833	0.840	0.782
-1.50	0.857	0.816	0.827	0.864	0.768
-1.25	0.862	0.799	0.807	0.866	0.744
-1.00	0.858	0.785	0.793	0.856	0.726
-0.8	0.841	0.764	0.772	0.829	0.702
-0.6	0.824	0.743	0.754	0.800	0.671
-0.4	0.814	0.731	0.742	0.778	0.652
-0.3	0.818	0.728	0.739	0.784	0.639
-0.2	0.810	0.725	0.737	0.772	0.636
-0.1	0.816	0.728	0.740	0.783	0.639
0.0	0.809	0.724	0.737	0.770	0.624
0.1	0.816	0.728	0.740	0.783	0.639
0.2	0.810	0.725	0.737	0.772	0.636
0.3	0.818	0.728	0.739	0.784	0.639
0.4	0.814	0.731	0.742	0.778	0.652
0.6	0.824	0.743	0.754	0.800	0.671
0.8	0.842	0.764	0.772	0.830	0.702
1.0	0.861	0.786	0.793	0.858	0.726
1.5	0.896	0.824	0.830	0.899	0.768
2.0	0.919	0.852	0.857	0.924	0.800
3.0	0.946	0.892	0.900	0.953	0.847
4.0	0.963	0.921	0.923	0.970	0.881
6.0	0.980	0.954	0.955	0.985	0.926
8.0	0.988	0.972	0.972	0.992	0.952
10	0.993	0.981	0.982	0.995	0.967
15	0.997	0.992	0.992	0.998	0.985
20	0.998	0.996	0.996	0.999	0.992
25	0.999	0.997	0.998	0.999	0.995
30	0.999	0.998	0.998	1.000	0.997
35	1.000	0.999	0.999		0.998
40		0.999	0.999		0.998
Unit of Flux	3.53-3	2.45-3	2.44-3	2.56-3	1.91-3
W(Å)	1.38	2.21	2.07	1.28	3.06
log W	0.140	0.345	0.316	0.107	0.486

* N(He)/N(H) = 0.05, otherwise N(He)/N(H) = 0.15.

$H\beta$ PROFILES

Table Gives Residual Fluxes, Unit of Flux, and Equivalent Width

θ_e	.10	.10*	.10	.21	.25	.20	.32	.36	.40
$\log_{10} g$	4	4	3.5	4	3.5	4	4	4	4
$\Delta\lambda$(Å)									
0.0	0.527	0.525	0.588	0.526	0.553	0.511	0.472	0.436	0.401
0.1	0.529	0.527	0.590	0.526	0.553	0.511	0.472	0.436	0.401
0.2	0.536	0.533	0.593	0.533	0.553	0.512	0.472	0.436	0.401
0.3	0.536	0.532	0.595	0.533	0.554	0.512	0.473	0.436	0.402
0.4	0.559	0.547	0.612	0.557	0.555	0.515	0.475	0.439	0.404
0.6	0.602	0.593	0.649	0.603	0.573	0.530	0.488	0.453	0.416
0.8	0.648	0.642	0.705	0.634	0.598	0.542	0.502	0.464	0.426
1.0	0.675	0.669	0.736	0.650	0.602	0.553	0.512	0.474	0.436
1.5	0.720	0.715	0.783	0.683	0.631	0.579	0.536	0.497	0.458
2.0	0.754	0.749	0.817	0.711	0.660	0.604	0.561	0.522	0.482
3.0	0.804	0.800	0.864	0.758	0.711	0.651	0.608	0.568	0.526
4.0	0.843	0.839	0.898	0.798	0.758	0.695	0.652	0.612	0.570
6.0	0.896	0.894	0.941	0.860	0.829	0.770	0.730	0.691	0.648
8.0	0.929	0.928	0.964	0.901	0.879	0.827	0.791	0.756	0.716
10	0.951	0.950	0.976	0.929	0.913	0.869	0.838	0.803	0.771
15	0.977	0.977	0.990	0.966	0.958	0.932	0.912	0.891	0.865
20	0.988	0.987	0.995	0.981	0.977	0.961	0.948	0.934	0.917
25	0.992	0.992	0.997	0.988	0.986	0.976	0.967	0.958	0.947
30	0.995	0.995	0.998	0.992	0.991	0.984	0.978	0.972	0.964
35	0.996	0.996	0.999	0.995	0.994	0.989	0.985	0.980	0.974
40	0.998	0.997	0.999	0.996	0.995	0.992	0.989	0.986	0.981
50	0.998	0.998	0.999	0.998	0.997	0.995	0.994	0.992	0.989
60	0.999	0.999	1.000	0.998	0.998	0.997	0.996	0.995	0.993
80	1.000	1.000		0.999	0.999	0.998	0.998	0.998	0.997
Unit of Flux	1.38-3	1.38-3	1.49-3	1.00-3	7.26-4	5.92-4	4.69-4	3.81-4	3.13-4
W(Å)	4.12	4.19	2.69	5.19	6.09	8.21	9.77	11.35	13.21
log W	0.615	0.622	0.429	0.715	0.785	0.914	0.990	1.055	1.121

* N(He)/N(H) = 0.05, otherwise N(He)/N(H) = 0.15.

Hβ PROFILES

Table Gives Residual Fluxes, Unit of Flux, and Equivalent Width

θ_e / log g / $\Delta\lambda$(Å)	.5 4.44	.504 4.0	.5 3.0	.5 2.0	.5* 1.0	.565 4.0	.6 4.44	.6 4.0	.6 3.0	.6 2.0
0.0	0.340	0.330	0.320	0.270	0.414	0.359	0.360	0.345	0.306	0.279
0.1	0.340	0.330	0.320	0.270	0.414	0.359	0.360	0.345	0.306	0.279
0.2	0.341	0.330	0.320	0.270	0.415	0.359	0.360	0.345	0.306	0.279
0.3	0.341	0.330	0.320	0.271	0.415	0.360	0.360	0.345	0.306	0.279
0.4	0.344	0.334	0.324	0.278	0.417	0.363	0.362	0.348	0.309	0.279
0.6	0.352	0.346	0.351	0.383	0.472	0.372	0.377	0.366	0.342	0.331
0.8	0.359	0.354	0.363	0.418	0.538	0.380	0.392	0.381	0.360	0.356
1.0	0.366	0.363	0.377	0.444	0.563	0.389	0.408	0.397	0.377	0.378
1.5	0.384	0.385	0.410	0.506	0.866	0.413	0.446	0.434	0.417	0.426
2.0	0.403	0.407	0.442	0.564	0.919	0.437	0.480	0.468	0.453	0.469
3.0	0.438	0.447	0.501	0.667	0.964	0.482	0.536	0.524	0.512	0.540
4.0	0.471	0.485	0.556	0.750	0.981	0.522	0.582	0.570	0.562	0.600
6.0	0.531	0.551	0.652	0.857	0.992	0.590	0.650	0.640	0.640	0.696
8.0	0.582	0.608	0.731	0.914	0.996	0.644	0.701	0.693	0.701	0.769
10	0.627	0.657	0.794	0.945	0.998	0.689	0.740	0.734	0.749	0.825
15	0.718	0.755	0.892	0.977	0.999	0.774	0.810	0.808	0.834	0.910
20	0.786	0.825	0.938	0.988	1.000	0.831	0.856	0.857	0.887	0.949
25	0.837	0.875	0.962	0.993		0.873	0.888	0.891	0.922	0.969
30	0.875	0.909	0.975	0.996		0.903	0.912	0.916	0.944	0.980
35	0.903	0.932	0.983	0.997		0.925	0.929	0.934	0.959	0.986
40	0.924	0.949	0.987	0.998		0.941	0.943	0.948	0.970	0.990
50	0.952	0.969	0.993	0.999		0.963	0.962	0.966	0.982	0.994
60	0.968	0.980	0.995	0.999		0.975	0.973	0.977	0.988	0.996
80	0.984	0.990	0.998	1.000		0.988	0.986	0.988	0.994	0.998
Unit Flux	1.88-4	1.88-4	2.00-4	2.01-4	1.78-4	1.31-4	9.78-5	1.03-4	1.13-4	1.21-4
W (Å)	24.37	20.85	12.22	5.94	1.48	20.40	18.43	18.13	15.52	10.90
log W	1.387	1.319	1.087	0.774	0.171	1.309	1.265	1.258	1.191	1.038

* Radiation Damping Included

Hβ PROFILES

Table Gives Residual Fluxes, Unit of Flux, and Equivalent Width

θ_e / log g	.6 / 1.0	.7 / 4.44	.7 / 3.0	.7 / 2.0
Δλ(Å)				
0.0	0.263	0.317	0.338	0.307
0.1	0.263	0.317	0.338	0.307
0.2	0.263	0.317	0.338	0.307
0.3	0.264	0.324	0.338	0.307
0.4	0.266	0.381	0.343	0.307
0.6	0.363	0.466	0.426	0.403
0.8	0.411	0.510	0.465	0.441
1.0	0.445	0.545	0.497	0.473
1.5	0.518	0.609	0.559	0.534
2.0	0.588	0.656	0.605	0.582
3.0	0.710	0.719	0.671	0.651
4.0	0.803	0.763	0.718	0.702
6.0	0.904	0.820	0.783	0.774
8.0	0.948	0.856	0.826	0.823
10	0.968	0.882	0.857	0.859
15	0.988	0.921	0.906	0.916
20	0.994	0.944	0.935	0.947
25	0.996	0.958	0.954	0.965
30	0.998	0.968	0.966	0.976
35	0.998	0.975	0.974	0.983
40	0.999	0.980	0.980	0.987
50	0.999	0.987	0.988	0.993
60	1.000	0.991	0.992	0.995
80		0.995	0.996	0.998
Unit Flux	1.25-4	5.06-5	5.84-5	6.39-5
W(Å)	4.92	8.96	10.03	9.41
log W	0.692	0.952	1.001	0.974

Hγ PROFILES

Table Gives Residual Fluxes, Unit of Flux, and Equivalent Width

The Blending with the Overlapping Pickering Series Is Included

θ_e / log ε	.101 / 4	.14 / 4	.14* / 4	.14 / 3.5	.157 / 4
Δλ (Å)					
-15	0.997	0.992	0.993	0.998	0.987
-10	0.991	0.980	0.983	0.994	0.969
-8.0	0.984	0.969	0.973	0.990	0.954
-6.0	0.968	0.948	0.954	0.979	0.927
-4.0	0.928	0.908	0.918	0.947	0.879
-3.0	0.887	0.874	0.888	0.906	0.841
-2.75	0.874	0.862	0.875	0.889	0.826
-2.50	0.859	0.850	0.864	0.869	0.812
-2.32	0.850	0.854	0.871	0.853	0.824
-2.17	0.840	0.841	0.857	0.837	0.806
-2.00	0.833	0.828	0.843	0.821	0.789
-1.92	0.832	0.823	0.838	0.818	0.781
-1.67	0.839	0.820	0.834	0.834	0.774
-1.50	0.845	0.806	0.817	0.848	0.751
-1.25	0.850	0.786	0.795	0.856	0.723
-1.00	0.848	0.770	0.779	0.851	0.704
-0.8	0.836	0.751	0.760	0.830	0.680
-0.6	0.820	0.729	0.738	0.801	0.653
-0.4	0.805	0.712	0.723	0.779	0.626
-0.3	0.803	0.705	0.716	0.766	0.614
-0.2	0.797	0.701	0.713	0.760	0.611
-0.1	0.798	0.701	0.713	0.765	0.606
0.0	0.795	0.700	0.711	0.756	0.604
0.1	0.798	0.701	0.713	0.765	0.606
0.2	0.797	0.701	0.713	0.760	0.611
0.3	0.803	0.705	0.716	0.766	0.614
0.4	0.805	0.712	0.723	0.779	0.626
0.6	0.821	0.729	0.738	0.801	0.653
0.8	0.839	0.751	0.760	0.832	0.680
1.0	0.857	0.770	0.779	0.858	0.704
1.5	0.891	0.812	0.820	0.900	0.751
2.0	0.916	0.846	0.852	0.927	0.789
3.0	0.947	0.892	0.896	0.956	0.841
4.0	0.965	0.923	0.925	0.972	0.880
6.0	0.982	0.957	0.958	0.987	0.928
8.0	0.990	0.974	0.975	0.993	0.954
10	0.994	0.983	0.984	0.995	0.970
15	0.997	0.993	0.993	0.998	0.987
20	0.999	0.996	0.996	0.999	0.993
25	0.999	0.998	0.998	0.999	0.996
30	1.000	0.998	0.999	1.000	0.997
35		0.999	0.999		0.998
Unit of Flux	4.31-3	2.97-3	2.96-3	3.08-3	2.32-3
W(Å)	1.34	2.17	2.04	1.22	3.09
log W	0.127	0.336	0.309	0.085	0.489

* N(He)/N(H) = 0.05, otherwise N(He)/N(H) = 0.15.

Hγ PROFILES

Table Gives Residual Fluxes, Unit of Flux, and Equivalent Width

θ_e / log g	.18 / 4	.18* / 4	.18 / 3.5	.21 / 4	.25 / 3.8	.28 / 4	.32 / 4	.36 / 4	.40 / 4
Δλ(Å)									
0.0	0.497	0.491	0.560	0.484	0.492	0.447	0.404	0.366	0.330
0.1	0.500	0.494	0.562	0.487	0.493	0.447	0.405	0.366	0.330
0.2	0.509	0.501	0.575	0.496	0.494	0.448	0.405	0.367	0.330
0.3	0.524	0.516	0.578	0.512	0.496	0.451	0.407	0.369	0.332
0.4	0.539	0.530	0.602	0.533	0.502	0.456	0.413	0.374	0.338
0.6	0.587	0.580	0.650	0.570	0.520	0.471	0.427	0.388	0.350
0.8	0.619	0.614	0.687	0.591	0.538	0.486	0.440	0.400	0.362
1.0	0.646	0.641	0.716	0.609	0.554	0.500	0.454	0.413	0.373
1.5	0.697	0.694	0.769	0.646	0.591	0.532	0.485	0.443	0.401
2.0	0.736	0.733	0.808	0.682	0.627	0.564	0.516	0.472	0.429
3.0	0.793	0.790	0.860	0.740	0.690	0.621	0.573	0.529	0.483
4.0	0.837	0.834	0.898	0.788	0.745	0.675	0.627	0.583	0.535
6.0	0.896	0.894	0.943	0.857	0.828	0.762	0.719	0.677	0.630
8.0	0.931	0.930	0.966	0.903	0.882	0.827	0.789	0.751	0.708
10	0.953	0.952	0.978	0.932	0.918	0.873	0.841	0.809	0.772
15	0.979	0.979	0.991	0.968	0.962	0.937	0.918	0.898	0.873
20	0.989	0.989	0.996	0.983	0.980	0.965	0.953	0.941	0.926
25	0.993	0.993	0.997	0.990	0.988	0.979	0.971	0.963	0.954
30	0.996	0.996	0.998	0.993	0.992	0.986	0.981	0.976	0.969
35	0.997	0.997	0.999	0.996	0.995	0.990	0.987	0.983	0.979
40	0.998	0.998	0.999	0.997	0.996	0.993	0.991	0.988	0.985
50	0.999	0.999	1.000	0.998	0.998	0.996	0.995	0.993	0.991
60	0.999	0.999		0.999	0.999	0.998	0.997	0.996	0.995
80	1.000	1.000		0.999	0.999	0.999	0.999	0.998	0.997
Unit of Flux	1.66-3	1.65-3	1.78-3	1.19-3	8.51-4	6.89-4	5.40-4	4.34-4	3.54-4
W(Å)	4.17	4.22	2.68	5.29	6.20	8.31	9.91	11.48	13.28
log W	0.620	0.626	0.428	0.724	0.792	0.920	0.996	1.060	1.123

* N(He)/N(H) = 0.05, otherwise N(He)/N(H) = 0.15.

Hγ PROFILES

Table Gives Residual Fluxes, Unit of Flux, and Equivalent Width

θe / log g	.5 / 4.44	.504 / 4.0	.5 / 3.0	.5 / 2.0	.5* / 1.0	.565 / 4.0	.6 / 4.44	.6 / 4.0	.6 / 3.0	.6 / 2.0
Δλ(Å)										
0.0	0.269	0.258	0.250	0.211	0.362	0.283	0.288	0.272	0.234	0.209
0.1	0.269	0.258	0.250	0.211	0.362	0.283	0.288	0.272	0.234	0.209
0.2	0.269	0.258	0.250	0.212	0.362	0.284	0.288	0.272	0.234	0.209
0.3	0.271	0.261	0.258	0.222	0.364	0.286	0.289	0.276	0.236	0.209
0.4	0.274	0.266	0.263	0.263	0.376	0.290	0.295	0.283	0.251	0.223
0.6	0.283	0.278	0.285	0.338	0.562	0.300	0.312	0.301	0.278	0.272
0.8	0.292	0.288	0.301	0.370	0.669	0.311	0.332	0.320	0.298	0.297
1.0	0.300	0.298	0.317	0.401	0.788	0.322	0.351	0.338	0.317	0.320
1.5	0.321	0.323	0.355	0.475	0.892	0.350	0.393	0.379	0.359	0.371
2.0	0.342	0.348	0.392	0.546	0.938	0.378	0.430	0.416	0.397	0.416
3.0	0.383	0.394	0.460	0.668	0.974	0.428	0.491	0.476	0.461	0.495
4.0	0.421	0.436	0.525	0.760	0.986	0.473	0.539	0.524	0.515	0.562
6.0	0.488	0.511	0.640	0.872	0.995	0.548	0.613	0.600	0.601	0.675
8.0	0.546	0.576	0.734	0.926	0.997	0.608	0.668	0.658	0.669	0.762
10	0.598	0.634	0.804	0.954	0.998	0.659	0.711	0.704	0.724	0.827
15	0.703	0.749	0.904	0.982	0.999	0.755	0.789	0.788	0.823	0.918
20	0.782	0.820	0.948	0.991	1.000	0.822	0.841	0.844	0.885	0.956
25	0.840	0.884	0.969	0.995		0.869	0.879	0.884	0.924	0.974
30	0.882	0.919	0.980	0.997		0.903	0.906	0.913	0.948	0.984
35	0.912	0.942	0.986	0.998		0.928	0.926	0.933	0.963	0.989
40	0.934	0.957	0.990	0.998		0.945	0.942	0.949	0.975	0.992
50	0.960	0.976	0.995	0.999		0.967	0.963	0.968	0.985	0.996
60	0.974	0.984	0.997	1.000		0.978	0.974	0.979	0.990	0.997
80	0.987	0.992	0.998			0.989	0.987	0.989	0.995	0.999
Unit Flux	2.06-4	2.06-4	2.20-4	2.18-4	1.79-4	1.39-4	9.89-5	1.05-4	1.19-4	1.30-4
W(Å)	24.85	21.11	12.12	5.79	1.39	21.48	19.87	19.49	16.36	11.11
log W	1.395	1.325	1.084	0.762	0.142	1.332	1.298	1.290	1.214	1.046

* Radiation Damping Included

Hγ PROFILES

Table Gives Residual Fluxes, Unit of Flux, and Equivalent Width

θ_e	.6	.7	.7	.7
log g	1.0	4.44	3.0	2.0
$\Delta\lambda$ (Å)				
0.0	0.203	0.251	0.264	0.233
1.0	0.203	0.251	0.264	0.233
0.2	0.204	0.262	0.265	0.233
0.3	0.205	0.297	0.267	0.233
0.4	0.222	0.356	0.314	0.278
0.6	0.330	0.422	0.374	0.347
0.8	0.370	0.467	0.413	0.384
1.0	0.408	0.503	0.446	0.416
1.5	0.497	0.570	0.509	0.478
2.0	0.586	0.619	0.557	0.528
3.0	0.736	0.687	0.627	0.601
4.0	0.834	0.734	0.677	0.657
6.0	0.926	0.796	0.748	0.737
8.0	0.961	0.836	0.796	0.794
10	0.977	0.865	0.832	0.837
15	0.991	0.910	0.890	0.905
20	0.996	0.936	0.925	0.942
30	0.998	0.965	0.963	0.976
35	0.999	0.973	0.973	0.983
40	0.999	0.979	0.980	0.988
50	1.000	0.986	0.988	0.993
60		0.991	0.992	0.996
80		0.995	0.996	0.998
Unit Flux	1.30-4	4.69-5	5.63-5	6.32-5
W(Å)	4.61	9.96	11.32	10.48
log W	0.664	0.998	1.054	1.020

IONIZED HELIUM LINE PROFILES (λ4200)

Table Gives Residual Fluxes, Unit of Flux, and Equivalent Width

θ_e	.101	.14	.14*	.14	.157	.18	.18*	.18
log ε	4	4	4	3.5	4	4	4	3.5
Δλ(Å)								
0.0	0.854	0.916	0.952	0.843	0.985			
0.1	0.855	0.916	0.952	0.846	0.985			
0.2	0.859	0.918	0.953	0.853	0.985			
0.4	0.868	0.921	0.955	0.870	0.985			
0.6	0.878	0.925	0.957	0.885	0.985			
0.8	0.888	0.928	0.960	0.899	0.985			
1.0	0.897	0.932	0.962	0.912	0.986			
1.5	0.919	0.941	0.968	0.937	0.987			
2.0	0.936	0.950	0.973	0.955	0.988			
2.5	0.950	0.957	0.978	0.967	0.989			
3.0	0.961	0.964	0.982	0.976	0.990			
3.5	0.969	0.970	0.985	0.982	0.991			
4.0	0.976	0.975	0.988	0.986	0.992			
5.0	0.984	0.982	0.992	0.992	0.994			
6.0	0.989	0.987	0.994	0.994	0.995			
8.0	0.995	0.993	0.997	0.997	0.997			
10	0.997	0.996	0.998	0.998	0.998			
12	0.998	0.997	0.999	0.999	0.999			
15	0.999	0.998	0.999	0.999	0.999			
20	0.999	0.999	1.000	1.000	1.000			
25	1.000	1.000						
30								
Unit Flux	4.56-3	3.14-3	3.13-3	3.25-3	2.44-3	1.75-3	1.74-3	1.88-3
W(Å)	0.729	0.603	0.305	0.559	0.162	.010	.004	.036
log W	-0.137	-0.220	-0.516	-0.252	-0.789	-2.011	-2.396	-1.443

* N(He)/N(H) = 0.05, otherwise N(He)/N(H) = 0.15

IONIZED HELIUM LINE PROFILES (λ4542)

Table Gives Residual Fluxes, Unit of Flux, and Equivalent Width

θ_e / log g	.101 4	.14 4	.14* 4	.14 3.5	.157 4	.18 4	.18* 4	.18 3.5
$\Delta\lambda$ (Å)								
0.0	0.823	0.855	0.901	0.805	0.963			
0.1	0.825	0.857	0.902	0.809	0.969			
0.2	0.829	0.862	0.905	0.819	0.969			
0.4	0.842	0.873	0.914	0.846	0.970			
0.6	0.857	0.884	0.922	0.869	0.971			
0.8	0.870	0.894	0.930	0.889	0.972			
1.0	0.883	0.903	0.937	0.905	0.974			
1.5	0.910	0.923	0.952	0.935	0.978			
2.0	0.930	0.938	0.964	0.955	0.982			
2.5	0.947	0.951	0.972	0.968	0.985			
3.0	0.960	0.960	0.979	0.976	0.988			
3.5	0.969	0.968	0.984	0.982	0.990			
4.0	0.976	0.974	0.987	0.986	0.992			
5.0	0.984	0.982	0.992	0.992	0.994			
6.0	0.989	0.988	0.995	0.994	0.996			
8.0	0.994	0.993	0.997	0.997	0.998			
10	0.997	0.996	0.998	0.998	0.999			
12	0.998	0.997	0.999	0.999	0.999			
15	0.999	0.998	0.999	0.999	1.000			
20	0.999	0.999	1.000	1.000				
25	1.000	1.000						
30								
Unit Flux	3.98-3	2.76-3	2.74-3	2.86-3	2.15-3	1.54-3	1.54-3	1.66-3
W(Å)	0.306	0.743	0.427	0.608	0.213	.012	.005	.044
log W	-0.094	-0.129	-0.369	-0.216	-0.672	-1.904	-2.277	-1.355

* N(He)/N(H) = 0.05, otherwise N(He)/N(H) = 0.15.

IONIZED HELIUM LINE PROFILES (λ4686)

Table Gives Residual Fluxes, Unit of Flux, and Equivalent Width

θe / log g	.101 4	.14 4	.14* 4	.14 3.5	.157 4	.18 4	.18* 4	.18 3.5
Δλ (Å)								
0.0	0.798	0.713	0.726	0.756	0.724	0.910	0.936	0.842
0.1	0.798	0.714	0.727	0.756	0.738	0.915	0.941	0.852
0.2	0.798	0.715	0.730	0.757	0.774	0.931	0.953	0.885
0.4	0.808	0.781	0.813	0.776	0.868	0.963	0.976	0.949
0.6	0.854	0.846	0.878	0.872	0.910	0.979	0.987	0.972
0.8	0.880	0.876	0.908	0.898	0.934	0.986	0.993	0.983
1.0	0.896	0.896	0.927	0.915	0.951	0.991	0.995	0.989
1.5	0.925	0.926	0.954	0.944	0.971	0.996	0.998	0.994
2.0	0.946	0.946	0.969	0.962	0.981	0.998	0.999	0.996
2.5	0.960	0.958	0.978	0.973	0.986	0.999	1.000	0.998
3.0	0.970	0.968	0.984	0.980	0.989	0.999		0.998
3.5	0.977	0.974	0.988	0.985	0.992	0.999		0.999
4.0	0.982	0.979	0.990	0.988	0.993	1.000		0.999
5.0	0.989	0.986	0.994	0.993	0.996			0.999
6.0	0.992	0.990	0.996	0.995	0.997			1.000
8.0	0.996	0.994	0.998	0.997	0.998			
10	0.998	0.997	0.999	0.998	0.999			
12	0.998	0.998	0.999	0.999	0.999			
15	0.999	0.999	1.000	0.999	1.000			
20	1.000	0.999		1.000				
Unit Flux	3.77-3	2.61-3	2.60-3	2.72-3	2.04-3	1.47-3	1.46-3	1.58-3
W (Å)	0.715	0.824	0.566	0.613	0.425	0.092	0.057	0.144
log W	-0.146	-0.084	-0.247	-0.213	-0.371	-0.034	-0.243	-0.842

* N(He)/N(H) = 0.05, otherwise N(He)/N(H) = 0.15.

IONIZED HELIUM LINE PROFILES (λ 5412)

Table Gives Residual Fluxes, Unit of Flux, and Equivalent Width

θ_e / log g	.101 4	.14 4	.14* 4	.14 3.5	.157 4	.18 4	.18* 4	.18 3.5
Δλ (Å)								
0.0	0.834	0.805	0.844	0.806	0.945			0.985
0.1	0.835	0.809	0.847	0.808	0.946			0.986
0.2	0.838	0.818	0.856	0.816	0.947			0.986
0.4	0.849	0.842	0.878	0.844	0.952			0.988
0.6	0.864	0.863	0.897	0.871	0.957			0.990
0.8	0.877	0.880	0.912	0.892	0.962			0.992
1.0	0.889	0.895	0.925	0.909	0.967			0.993
1.5	0.913	0.921	0.948	0.937	0.976			0.996
2.0	0.933	0.940	0.963	0.955	0.982			0.997
2.5	0.948	0.954	0.973	0.967	0.987			0.998
3.0	0.959	0.964	0.980	0.975	0.990			0.999
3.5	0.968	0.971	0.985	0.981	0.992			0.999
4.0	0.974	0.977	0.988	0.985	0.994			0.999
5.0	0.982	0.984	0.993	0.990	0.996			1.000
6.0	0.988	0.989	0.995	0.993	0.997			
8.0	0.993	0.993	0.997	0.996	0.999			
10	0.996	0.996	0.998	0.998	0.999			
12	0.997	0.997	0.999	0.998	0.999			
15	0.998	0.998	0.999	0.999	1.000			
20	0.999	0.999	1.000	1.000				
25	1.000	1.000						
30								
35								
Unit Flux	2.91-3	2.04-3	2.03-3	2.13-3	1.59-3	1.16-3	1.15-3	1.25-3
W(Å)	0.817	0.785	0.496	0.625	0.221	.012	.005	.042
log W	-0.088	-0.105	-0.304	-0.204	-0.656	-1.929	-2.284	-1.395

* N(He)/N(H) = 0.05, otherwise N(He)/N(H) = 0.15.

NEUTRAL HELIUM LINE PROFILES (λ4121)

Table Gives Residual Fluxes, Unit of Flux, and Equivalent Width

θe / log g	.14 4	.14* 4	.14 3.5	.157 4	.18 4	.18* 4	.18 3.5	.21 4	.25 3.8
Δλ(Å)									
-1.2	0.998	1.000		0.995	0.991	0.997	0.996	0.987	0.987
-1.0	0.998	0.999		0.993	0.987	0.995	0.994	0.981	0.982
-0.9	0.997	0.999		0.991	0.984	0.994	0.993	0.978	0.978
-0.8	0.996	0.999		0.989	0.981	0.993	0.991	0.972	0.973
-0.7	0.995	0.998	1.000	0.986	0.976	0.991	0.988	0.966	0.966
-0.6	0.994	0.998	0.999	0.981	0.969	0.988	0.984	0.956	0.956
-0.5	0.991	0.997	0.999	0.974	0.958	0.983	0.978	0.941	0.942
-0.4	0.984	0.994	0.996	0.960	0.940	0.974	0.965	0.918	0.920
-0.3	0.956	0.982	0.976	0.920	0.892	0.948	0.907	0.869	0.876
-0.2	0.852	0.924	0.879	0.795	0.727	0.832	0.715	0.676	0.691
-0.1	0.768	0.854	0.823	0.657	0.551	0.630	0.579	0.513	0.503
0.0	0.747	0.827	0.803	0.639	0.529	0.592	0.566	0.494	0.484
0.1	0.764	0.848	0.823	0.656	0.550	0.626	0.579	0.512	0.502
0.2	0.839	0.912	0.878	0.777	0.708	0.802	0.712	0.658	0.673
0.3	0.936	0.973	0.975	0.885	0.855	0.918	0.891	0.828	0.842
0.4	0.975	0.990	0.996	0.939	0.913	0.958	0.954	0.888	0.897
0.5	0.987	0.995	0.999	0.962	0.942	0.974	0.973	0.922	0.926
0.6	0.992	0.997	0.999	0.974	0.958	0.983	0.981	0.942	0.946
0.7	0.994	0.998	0.999	0.981	0.968	0.988	0.986	0.956	0.958
0.8	0.996	0.998	1.000	0.986	0.976	0.991	0.990	0.965	0.967
0.9	0.997	0.999		0.989	0.980	0.993	0.992	0.972	0.974
1.0	0.997	0.999		0.991	0.984	0.994	0.993	0.977	0.978
1.2	0.998	0.999		0.994	0.989	0.996	0.996	0.984	0.985
1.4	0.999	1.000		0.996	0.992	0.997	0.997	0.988	0.989
1.6	0.999			0.997	0.994	0.998	0.998	0.991	0.991
1.8	0.999			0.997	0.995	0.998	0.998	0.993	0.993
2.0	0.999			0.998	0.996	0.999	0.998	0.994	0.994
3.0	1.000			0.999	0.998	0.999	0.999	0.998	0.998
Unit of Flux	3.24-3	3.23-3	3.35-3	2.52-3	1.80-3	1.79-3	1.93-3	1.29-3	9.14-4
W(Å)	0.129	0.073	0.088	0.210	0.291	0.192	0.240	0.348	0.341
log W	-0.889	-1.134	-1.057	-0.677	-0.536	-0.717	-0.620	-0.458	-0.467

* N(He)/N(H) = 0.05, otherwise N(He)/N(H) = 0.15.

NEUTRAL HELIUM LINES (λ4121)

Table Gives Residual Fluxes, Unit of Flux, and Equivalent Width

θ_e / log ε	.28 / 4	.32 / 4	.36 / 4	.40 / 4
Δλ(Å)				
-1.2	0.986	0.992	0.996	0.998
-1.0	0.982	0.988	0.994	0.997
-0.9	0.978	0.986	0.993	0.997
-0.8	0.973	0.983	0.992	0.996
-0.7	0.967	0.980	0.990	0.995
-0.6	0.958	0.974	0.987	0.994
-0.5	0.946	0.967	0.983	0.992
-0.4	0.928	0.956	0.977	0.989
-0.3	0.899	0.939	0.968	0.984
-0.2	0.816	0.899	0.948	0.974
-0.1	0.655	0.801	0.892	0.947
0.0	0.578	0.741	0.847	0.914
0.1	0.646	0.778	0.862	0.917
0.2	0.769	0.844	0.899	0.939
0.3	0.858	0.904	0.942	0.967
0.4	0.902	0.935	0.963	0.980
0.5	0.927	0.952	0.974	0.986
0.6	0.944	0.964	0.980	0.990
0.7	0.957	0.972	0.985	0.992
0.8	0.965	0.978	0.988	0.994
0.9	0.972	0.982	0.990	0.995
1.0	0.977	0.985	0.992	0.996
1.2	0.984	0.989	0.994	0.997
1.4	0.988	0.992	0.996	0.998
1.6	0.990	0.994	0.997	0.998
1.8	0.992	0.995	0.997	0.999
2.0	0.994	0.996	0.998	0.999
3.0	0.997	0.998	0.999	1.000
Unit of Flux	7.37-4	5.74-4	4.60-4	3.73-4
W(Å)	0.279	0.174	0.098	0.053
log W	-0.555	-0.760	-1.007	-1.277

NEUTRAL HELIUM LINE PROFILES (λ4438)

Table Gives Residual Fluxes, Unit of Flux, and Equivalent Width

θ_e / log g	.14 4	.14* 4	.14 3.5	.157 4	.18 4	.18* 4	.18 3.5	.21 4	.25 3.8
Δλ(Å)									
-1.2	1.000			0.998	0.997	0.999	0.999	0.996	0.996
-1.0	0.999			0.998	0.996	0.999	0.998	0.994	0.995
-0.9	0.999			0.997	0.995	0.998	0.998	0.993	0.994
-0.8	0.999			0.997	0.994	0.998	0.997	0.992	0.992
-0.7	0.998	1.000		0.996	0.993	0.997	0.996	0.989	0.990
-0.6	0.998	0.999		0.994	0.990	0.996	0.995	0.986	0.986
-0.5	0.997	0.999	1.000	0.992	0.986	0.995	0.993	0.981	0.981
-0.4	0.995	0.998	0.999	0.987	0.980	0.992	0.988	0.972	0.973
-0.3	0.987	0.995	0.992	0.974	0.962	0.985	0.971	0.951	0.954
-0.2	0.958	0.983	0.973	0.929	0.904	0.956	0.893	0.875	0.883
-0.1	0.921	0.965	0.945	0.848	0.768	0.869	0.750	0.710	0.713
0.0	0.898	0.953	0.930	0.817	0.728	0.833	0.721	0.665	0.664
0.1	0.910	0.959	0.944	0.831	0.751	0.850	0.747	0.693	0.697
0.2	0.942	0.976	0.972	0.897	0.856	0.924	0.877	0.816	0.828
0.3	0.975	0.991	0.992	0.947	0.926	0.966	0.954	0.907	0.917
0.4	0.990	0.996	0.998	0.974	0.960	0.984	0.982	0.947	0.953
0.5	0.995	0.998	1.000	0.985	0.976	0.991	0.990	0.967	0.971
0.6	0.997	0.999		0.990	0.984	0.994	0.993	0.978	0.980
0.7	0.998	0.999		0.993	0.988	0.996	0.995	0.984	0.985
0.8	0.998	1.000		0.995	0.991	0.997	0.997	0.988	0.989
0.9	0.999			0.996	0.993	0.998	0.997	0.990	0.991
1.0	0.999			0.997	0.995	0.998	0.998	0.992	0.993
1.2	0.999			0.998	0.996	0.999	0.999	0.995	0.995
1.4	1.000			0.999	0.997	0.999	0.999	0.996	0.997
1.6				0.999	0.998	0.999	0.999	0.997	0.997
1.8				0.999	0.998	1.000	0.999	0.998	0.998
2.0				0.999	0.999		1.000	0.998	0.998
3.0				1.000	1.000			0.999	0.999
Unit of Flux	2.87-3	2.86-3	2.97-3	2.23-3	1.60-3	1.60-3	1.72-3	1.15-3	8.26-4
W(Å)	0.046	0.020	0.026	0.090	0.135	0.070	0.118	0.173	0.166
log W	-1.334	-1.705	-1.587	-1.044	-0.871	-1.152	-0.926	-0.763	-0.780

* N(He)/N(H) = 0.05, otherwise N(He)/N(H) = 0.15.

NEUTRAL HELIUM LINES (λ4438)

Table Gives Residual Fluxes, Unit of Flux, and Equivalent Width

θ e / log g	.28 / 4	.32 / 4	.36 / 4	.40 / 4
$\Delta\lambda$(Å)				
-1.2	0.996	0.998	0.999	1.000
-1.0	0.995	0.997	0.999	0.999
-0.9	0.994	0.997	0.998	0.999
-0.8	0.993	0.996	0.998	0.999
-0.7	0.991	0.995	0.998	0.999
-0.6	0.988	0.993	0.997	0.999
-0.5	0.984	0.991	0.996	0.998
-0.4	0.977	0.988	0.994	0.998
-0.3	0.965	0.982	0.992	0.997
-0.2	0.935	0.968	0.986	0.995
-0.1	0.855	0.935	0.973	0.989
0.0	0.807	0.901	0.954	0.981
0.1	0.816	0.900	0.950	0.978
0.2	0.868	0.922	0.960	0.982
0.3	0.924	0.954	0.976	0.989
0.4	0.954	0.972	0.986	0.993
0.5	0.970	0.982	0.991	0.996
0.6	0.979	0.987	0.994	0.997
0.7	0.985	0.991	0.995	0.998
0.8	0.988	0.993	0.996	0.998
0.9	0.991	0.994	0.997	0.999
1.0	0.993	0.996	0.998	0.999
1.2	0.995	0.997	0.998	0.999
1.4	0.996	0.998	0.999	1.000
1.6	0.997	0.998	0.999	
1.8	0.998	0.999	0.999	
2.0	0.998	0.999	1.000	
3.0	0.999	1.000		
Unit of Flux	6.69-3	5.25-4	4.23-4	3.46-4
W(Å)	0.115	0.063	0.030	0.013
log W	-0.938	-1.200	-1.523	-1.880

NEUTRAL HELIUM LINE PROFILES (λ4713)

Tables Give Residual Fluxes, Unit of Flux, and Equivalent Widths

θ_e / log g	.14 / 4	.14* / 4	.14 / 3.5	.157 / 4	.18 / 4	.18* / 4	.18 / 3.5	.21 / 4	.25 / 3.8
Δλ(Å)									
-1.2	0.998	0.999		0.995	0.991	0.997	0.996	0.987	0.988
-1.0	0.997	0.999		0.992	0.987	0.995	0.994	0.982	0.983
-0.9	0.997	0.999		0.991	0.985	0.994	0.993	0.978	0.980
-0.8	0.996	0.999	1.000	0.988	0.981	0.993	0.991	0.973	0.975
-0.7	0.994	0.998	0.999	0.985	0.976	0.991	0.988	0.966	0.968
-0.6	0.992	0.997	0.999	0.980	0.968	0.987	0.984	0.956	0.959
-0.5	0.986	0.995	0.995	0.970	0.956	0.982	0.976	0.940	0.945
-0.4	0.950	0.978	0.962	0.934	0.924	0.965	0.936	0.909	0.919
-0.3	0.826	0.901	0.862	0.797	0.772	0.860	0.748	0.756	0.803
-0.2	0.749	0.805	0.800	0.656	0.587	0.647	0.616	0.569	0.572
-0.1	0.728	0.763	0.783	0.636	0.529	0.548	0.584	0.520	0.538
0.0	0.724	0.753	0.779	0.632	0.524	0.539	0.582	0.516	0.537
0.1	0.728	0.763	0.783	0.636	0.529	0.548	0.584	0.520	0.538
0.2	0.748	0.805	0.800	0.656	0.587	0.646	0.616	0.569	0.572
0.3	0.824	0.899	0.862	0.794	0.768	0.853	0.748	0.750	0.797
0.4	0.945	0.976	0.961	0.927	0.914	0.958	0.933	0.897	0.910
0.5	0.983	0.994	0.995	0.965	0.949	0.978	0.974	0.933	0.939
0.6	0.991	0.997	0.999	0.976	0.964	0.985	0.983	0.950	0.955
0.7	0.994	0.998	0.999	0.983	0.973	0.989	0.987	0.962	0.966
0.8	0.995	0.998	1.000	0.987	0.979	0.992	0.990	0.970	0.973
0.9	0.996	0.999		0.990	0.983	0.994	0.992	0.976	0.978
1.0	0.997	0.999		0.992	0.986	0.995	0.994	0.980	0.982
1.2	0.998	0.999		0.994	0.990	0.996	0.996	0.986	0.987
1.4	0.999	1.000		0.996	0.993	0.997	0.997	0.990	0.990
1.6	0.999			0.997	0.994	0.998	0.998	0.992	0.993
1.8	0.999			0.998	0.996	0.998	0.998	0.994	0.994
2.0	0.999			0.998	0.996	0.999	0.998	0.995	0.995
3.0	1.000			0.999	0.998	0.999	0.999	0.998	0.998
Unit of Flux	2.59-3	2.58-3	2.69-3	2.02-3	1.46-3	1.45-3	1.57-3	1.05-3	7.59-4
W(Å)	0.189	0.140	0.142	0.268	0.341	0.265	0.289	0.377	0.356
log W	-0.723	-0.854	-0.847	-0.573	-0.467	-0.576	-0.539	-0.424	-0.449

* N(He)/N(H) = 0.05, otherwise N(He)/N(H) = 0.15.

NEUTRAL HELIUM LINES (λ4713)

Table Gives Residual Fluxes, Unit of Flux, and Equivalent Width

θ_e / log g	.28 / 4	.32 / 4	.36 / 4	.40 / 4
$\Delta\lambda$(Å)				
-1.2	0.989	0.994	0.997	0.999
-1.0	0.985	0.992	0.996	0.998
-0.9	0.982	0.990	0.996	0.998
-0.8	0.978	0.988	0.995	0.998
-0.7	0.972	0.985	0.993	0.997
-0.6	0.965	0.981	0.991	0.996
-0.5	0.954	0.975	0.988	0.995
-0.4	0.936	0.965	0.984	0.993
-0.3	0.888	0.943	0.974	0.988
-0.2	0.712	0.853	0.929	0.969
-0.1	0.548	0.707	0.838	0.918
0.0	0.528	0.670	0.809	0.899
0.1	0.548	0.706	0.836	0.915
0.2	0.709	0.846	0.922	0.960
0.3	0.877	0.933	0.966	0.983
0.4	0.926	0.958	0.979	0.990
0.5	0.947	0.970	0.986	0.994
0.6	0.960	0.978	0.990	0.995
0.7	0.969	0.983	0.992	0.996
0.8	0.975	0.986	0.994	0.997
0.9	0.980	0.989	0.995	0.998
1.0	0.983	0.991	0.996	0.998
1.2	0.988	0.993	0.997	0.999
1.4	0.991	0.995	0.998	0.999
1.6	0.993	0.996	0.998	0.999
1.8	0.994	0.997	0.999	0.999
2.0	0.995	0.998	0.999	1.000
3.0	0.998	0.999	1.000	
Unit of Flux	6.18-4	4.88-4	3.95-4	3.24-4
W(Å)	0.298	0.176	0.092	0.046
log W	-0.526	-0.754	-1.038	-1.351

NEUTRAL HELIUM LINE PROFILES (λ 5876)

Tables Give Residual Fluxes, Unit of Flux, and Equivalent Widths

θ_e / log g	.14 4	.14* 4	.14 3.5	.157 4	.18 4	.18* 4	.18 3.5	.21 4	.25 3.8
$\Delta\lambda$(Å)									
0.0	0.767	0.778	0.796	0.689	0.590	0.591	0.646	0.602	0.646
0.1	0.767	0.778	0.796	0.689	0.590	0.591	0.646	0.602	0.646
0.2	0.767	0.778	0.797	0.689	0.590	0.591	0.646	0.602	0.646
0.3	0.767	0.779	0.798	0.689	0.591	0.592	0.646	0.603	0.646
0.4	0.768	0.781	0.802	0.691	0.601	0.611	0.649	0.615	0.651
0.5	0.773	0.796	0.811	0.715	0.679	0.724	0.682	0.733	0.786
0.6	0.815	0.860	0.832	0.844	0.841	0.897	0.836	0.841	0.860
0.7	0.920	0.962	0.954	0.909	0.888	0.934	0.927	0.863	0.878
0.8	0.954	0.981	0.989	0.926	0.903	0.945	0.940	0.878	0.892
0.9	0.963	0.985	0.994	0.936	0.914	0.954	0.949	0.891	0.903
1.0	0.969	0.988	0.995	0.944	0.924	0.961	0.956	0.902	0.913
1.2	0.977	0.992	0.997	0.956	0.938	0.971	0.966	0.919	0.929
1.4	0.983	0.994	0.998	0.965	0.950	0.977	0.973	0.933	0.942
1.6	0.986	0.995	0.998	0.972	0.958	0.982	0.978	0.944	0.951
1.8	0.989	0.996	0.999	0.977	0.965	0.985	0.982	0.952	0.959
2.0	0.991	0.997	0.999	0.980	0.970	0.988	0.985	0.959	0.965
2.5	0.994	0.998	0.999	0.987	0.980	0.992	0.990	0.971	0.975
3.0	0.996	0.999	1.000	0.990	0.985	0.994	0.993	0.979	0.982
3.5	0.997	0.999		0.993	0.989	0.996	0.995	0.984	0.986
4.0	0.998	0.999		0.994	0.991	0.997	0.996	0.987	0.989
5.0	0.998	1.000		0.996	0.994	0.998	0.997	0.992	0.993
6.0	0.999			0.998	0.996	0.998	0.998	0.994	0.995
8.0	0.999			0.999	0.998	0.999	0.999	0.997	0.997
Unit of Flux	1.76-3	1.76-3	1.86-3	1.38-3	1.01-3	1.01-3	1.09-3	1.09-3	5.51-4
W(Å)	0.392	0.306	0.277	0.552	0.731	0.560	0.556	0.806	0.709
log W	-0.407	-0.514	-0.557	-0.258	-0.136	-0.252	-0.255	-0.094	-0.149

* N(He)/N(H) = 0.05, otherwise N(He)/N(H) = 0.15.

NEUTRAL HELIUM LINES (λ5876)

Table Gives Residual Fluxes, Unit of Flux, and Equivalent Width

θ_e / log g	.28 / 4	.32 / 4	.36 / 4	.40 / 4
$\Delta\lambda$(Å)				
0.0	0.612	0.580	0.555	0.602
0.1	0.612	0.580	0.559	0.626
0.2	0.612	0.583	0.633	0.770
0.3	0.614	0.668	0.812	0.912
0.4	0.712	0.871	0.942	0.976
0.5	0.876	0.938	0.971	0.987
0.6	0.901	0.950	0.977	0.990
0.7	0.914	0.958	0.981	0.992
0.8	0.924	0.964	0.984	0.994
0.9	0.932	0.968	0.987	0.995
1.0	0.939	0.972	0.988	0.996
1.2	0.950	0.978	0.991	0.997
1.4	0.958	0.982	0.993	0.998
1.6	0.965	0.985	0.994	0.998
1.8	0.970	0.987	0.995	0.998
2.0	0.974	0.989	0.996	0.999
2.5	0.982	0.992	0.997	0.999
3.0	0.986	0.994	0.998	0.999
3.5	0.990	0.996	0.998	1.000
4.0	0.992	0.997	0.999	
5.0	0.994	0.998	0.999	
6.0	0.996	0.998		
8.0	0.998	0.999		
Unit of Flux	4.55-4	3.66-4	3.02-4	2.52-4
W(Å)	0.606	0.424	0.305	0.200
log W	-0.217	-0.373	-0.516	-0.698